

Co-evolution of erosion rates, weathering and profile development in soil landscapes of hummocky ground moraines

Francesca Calitri

Univ.-Diss.

**zur Erlangung des akademischen Grades
"doctor rerum naturalium"
(Dr. rer. nat.)
in der Wissenschaftsdisziplin "Geoökologie"**

**eingereicht an der
Mathematisch-Naturwissenschaftlichen Fakultät
Institut für Umweltwissenschaften und Geographie
der Universität Potsdam
und
Leibniz-Zentrum für Agrarlandschaftsforschung (ZALF) e.V.**

Ort und Tag der Disputation

Potsdam, 22nd June 2023

Unless otherwise indicated, this work is licensed under a Creative Commons License Attribution – NonCommercial – NoDerivatives 4.0 International.

This does not apply to quoted content and works based on other permissions.

To view a copy of this licence visit:

<https://creativecommons.org/licenses/by-nc-nd/4.0>

First supervisor: Univ.-Prof. Dr. habil. Michael Sommer

Second supervisor: Prof. Dr. Markus Egli

Reviewer: Prof. Dr. Jerome Poulenard

Published online on the

Publication Server of the University of Potsdam:

<https://doi.org/10.25932/publishup-60138>

<https://nbn-resolving.org/urn:nbn:de:kobv:517-opus4-601387>



πάντα ἰσχύω ἐν τῷ ἐνδυναμοῦντί ᾧ με.

Φιλιππησίους 4:13

Table of Contents

<i>Preface</i>	<i>IX</i>
Summary	IX
Zusammenfassung	XI
Sommario	XIV
Sommaire	XVII
Resumo	XX
Abbreviations	XXII
Academic achievements	XV
Journal articles (peer-reviewed)	XV
Seminars	XVI
Conference contributions	XVII
Thesis supervision	XVII
Chapter 1. Introduction	1
1.1 Soil and its formation	1
1.2 Soil erosion	3
1.3 How to measure erosion on different time ranges	5
1.3.1. Anthropogenic radionuclides – $^{239+240}\text{Pu}$	5
1.3.2. Cosmogenic nuclides – ^{10}Be and ^{14}C	7
1.4 Research Needs and Challenges	10
1.5 Aims and research questions	11
1.6 Thesis Outline	12
Chapter 2. Tracing the temporal evolution of soil redistribution rates in an agricultural landscape using $^{239+240}\text{Pu}$ and ^{10}Be	15
Abstract	15
2.1 Introduction	17
2.2 Study area	20
2.3 Materials and Methods	23

2.3.1 Sampling strategy	23
2.3.2 Soil chemical and physical analyses.....	24
2.3.3 Radiocarbon dating of organic matter fractions	25
2.3.4 ¹⁰ Be analyses.....	25
2.3.5 Determination of ²³⁹⁺²⁴⁰ Pu activities.....	27
2.3.6 Calculation of mass redistribution rates	28
2.3.7 Statistics and trend analyses	32
2.4 Results.....	33
2.4.1 Physical and chemical soil properties.....	33
2.4.2 Meteoric and in situ ¹⁰ Be	36
2.4.3 ²³⁹⁺²⁴⁰ Pu inventory	37
2.4.4 Soil redistribution rates (long- and short-term)	39
2.5 Discussion	43
2.5.1 ¹⁰ Be along the soil profiles	43
2.5.2 Soil redistribution rates (erosion and accumulation).....	47
2.6 Conclusions	52
2.7 Acknowledgements.....	52
References	53
<i>Chapter 3. Soil erosion along a transect in a forested catchment: recent or ancient processes?</i>.....	63
Abstract	63
3.1 Introduction	65
3.2 Study Area.....	67
3.3 Materials and methods.....	70
3.3.1 Soil sampling	70
3.3.2 Soil sample preparation and analysis	70
3.3.3 Sample preparation and measurement for ²³⁹⁺²⁴⁰ Pu activities	71
3.3.4 Conversion of ²³⁹⁺²⁴⁰ Pu activities into soil redistribution rates	71
3.3.5 Radiocarbon dating.....	73

3.3.6 GIS-based terrain analysis	74
3.3.7 Data evaluation and statistical analyses.....	74
3.4 Results.....	76
3.4.1 Soil pattern.....	76
3.4.2 Soil organic carbon (SOC)	78
3.4.3 ²³⁹⁺²⁴⁰ Pu depth functions, inventories and relationship to topographic parameters.....	78
3.4.4 Erosion and deposition rates.....	78
3.5 Discussion	84
3.5.1 ²³⁹⁺²⁴⁰ Pu inventories and depth functions	84
3.5.2 ²³⁹⁺²⁴⁰ Pu spatial distribution and erosion/deposition rates.....	84
3.5.3 Comparison of erosion modelling approaches using ²³⁹⁺²⁴⁰ Pu	85
3.5.4 Terrain attributes and soil depth.....	86
3.5.5 Recent or ancient processes.....	86
3.6 Conclusions	89
3.7 Acknowledgements.....	89
References	90
<i>Chapter 4. ¹⁰Be and ¹⁴C data provide insight on soil mass redistribution along gentle slopes and reveal ancient human impact</i>	<i>99</i>
Abstract.....	99
4.1 Introduction	101
4.2 Study Area.....	103
4.3 Materials and methods.....	105
4.3.1 Sampling strategy	105
4.3.2 Soil chemical and physical analyses.....	105
4.3.3 Radiocarbon dating of organic matter fractions	107
4.3.4 Sample preparation and measurement for ¹⁰ Be analyses.....	108
4.3.5 Calculation of mass redistribution rates	108
4.3.6 Data and statistical analyses.....	111
4.4 Results.....	112

4.4.1 Morphological, physical and chemical soil properties	112
4.4.2 ¹⁴ C dating	112
4.4.3 Meteoric and in situ ¹⁰ Be	117
4.4.4 Soil redistribution rates.....	119
4.5 Discussion	123
4.5.1 Periods of stability and erosion	123
4.5.2 Beryllium-10 (¹⁰ Be) along the soil profile.....	125
4.5.3 Correlation of ¹⁰ Be with soil physical and chemical properties	126
4.5.4 Soil redistribution rates.....	129
4.6 Conclusions	132
Acknowledgements.....	133
References	133
<i>5. Discussion.....</i>	<i>143</i>
5.1 Synthesis of main results.....	143
Constrains of the study results.....	146
5.2 Outlook	148
<i>6. References</i>	<i>149</i>
<i>Appendix.....</i>	<i>I</i>
Supplementary material	I
Acknowledgement	III
<i>Curriculum vitae</i>	<i>V</i>

Preface

Summary

Soil is today considered a non-renewable resource on societal time scale, as the rate of soil loss is higher than the one of soil formation.

Soil formation is complex, can take several thousands of years and is influenced by a variety of factors, one of them is time. Oftentimes, there is the assumption of constant and progressive conditions for soil and/or profile development (i.e., steady-state). In reality, for most of the soils, their (co-)evolution leads to a complex and irregular soil development in time and space characterised by “progressive” and “regressive” phases.

Lateral transport of soil material (i.e., soil erosion) is one of the principal processes shaping the land surface and soil profile during “regressive” phases and one of the major environmental problems the world faces.

Anthropogenic activities like agriculture can exacerbate soil erosion. Thus, it is of vital importance to distinguish short-term soil redistribution rates (i.e., within decades) influenced by human activities differ from long-term natural rates. To do so, soil erosion (and denudation) rates can be determined by using a set of isotope methods that cover different time scales at landscape level.

With the aim to unravel the co-evolution of weathering, soil profile development and lateral redistribution on a landscape level, we used Pluthonium-239+240 ($^{239+240}\text{Pu}$), Beryllium-10 (^{10}Be , in situ and meteoric) and Radiocarbon (^{14}C) to calculate short- and long-term erosion rates in two settings, i.e., a natural and an anthropogenic environment in the hummocky ground moraine landscape of the Uckermark, North-eastern Germany. The main research questions were:

1. How do long-term and short-term rates of soil redistributing processes differ?
2. Are rates calculated from in situ ^{10}Be comparable to those of using meteoric ^{10}Be ?
3. How do soil redistribution rates (short- and long-term) in an agricultural and in a natural landscape compare to each other?
4. Are the soil patterns observed in northern Germany purely a result of past events (natural and/or anthropogenic) or are they imbedded in ongoing processes?

Erosion and deposition are reflected in a catena of soil profiles with no or almost no erosion on flat positions (hilltop), strong erosion on the mid-slope and accumulation of soil material at the toeslope position. These three characteristic process domains were chosen within the CarboZALF-D experimental site, characterised by intense anthropogenic activities. Likewise, a hydrosquence in an ancient forest was chosen for this study and being regarded as a catena strongly influenced by natural soil transport.

The following main results were obtained using the above-mentioned range of isotope methods available to measure soil redistribution rates depending on the time scale needed (e.g., $^{239+240}\text{Pu}$, ^{10}Be , ^{14}C):

1. Short-term erosion rates are one order of magnitude higher than long-term rates in agricultural settings.
2. Both meteoric and in situ ^{10}Be are suitable soil tracers to measure the long-term soil redistribution rates giving similar results in an anthropogenic environment for different landscape positions (e.g., hilltop, mid-slope, toeslope)
3. Short-term rates were extremely low/negligible in a natural landscape and very high in an agricultural landscape – $-0.01 \text{ t ha}^{-1} \text{ yr}^{-1}$ (average value) and $-25 \text{ t ha}^{-1} \text{ yr}^{-1}$ respectively. On the contrary, long-term rates in the forested landscape are comparable to those calculated in the agricultural area investigated with average values of $-1.00 \text{ t ha}^{-1} \text{ yr}^{-1}$ and $-0.79 \text{ t ha}^{-1} \text{ yr}^{-1}$.
4. Soil patterns observed in the forest might be due to human impact and activities started after the first settlements in the region, earlier than previously postulated, between 4.5 and 6.8 kyr BP, and not a result of recent soil erosion.
5. Furthermore, long-term soil redistribution rates are similar independently from the settings, meaning past natural soil mass redistribution processes still overshadow the present anthropogenic erosion processes.

Overall, this study could make important contributions to the deciphering of the co-evolution of weathering, soil profile development and lateral redistribution in North-eastern Germany. The multi-methodological approach used can be challenged by the application in a wider range of landscapes and geographic regions.

Zusammenfassung

Boden wird heute im gesellschaftlichen Zeitmaßstab als nicht erneuerbare Ressource angesehen, da die Geschwindigkeit des Bodenverlusts höher ist als die der Bodenbildung.

Bodenbildung ist komplex, kann mehrere tausend Jahre dauern und wird von einer Vielzahl von Faktoren beeinflusst, unter anderem Zeit. Häufig wird von konstanten und fortschreitenden Bedingungen für die Boden- und/oder Profilentwicklung (d. h. «Steady-State») ausgegangen. Tatsächlich führt ihre (Co-)Evolution bei den meisten Böden zu einer komplexen und zeitlich und räumlich unregelmäßigen Bodenentwicklung, die durch „progressive“ und „regressive“ Phasen gekennzeichnet ist.

Der laterale Transport von Bodenmaterial (d. h. Bodenerosion) ist einer der Hauptprozesse, der die Landoberfläche und das Bodenprofil während „rückläufiger“ Phasen bilden, und eines der größten Umweltprobleme, mit denen die Welt konfrontiert ist.

Anthropogene Aktivitäten wie die Landwirtschaft können die Bodenerosion verstärken. Daher ist es von entscheidender Bedeutung, kurzfristige Bodenumverteilungsraten (d. h. innerhalb von Jahrzehnten), die durch menschliche Aktivitäten beeinflusst werden, von langfristigen natürlichen Raten zu unterscheiden. Zu diesem Zweck können Bodenerosions- (und Denudations-) Raten mithilfe einer Reihe von Isotopenmethoden bestimmt werden, die verschiedene Zeitskalen auf Landschaftsebene abdecken.

Mit dem Ziel, die Co-Evolution von Verwitterung, Bodenprofilentwicklung und lateraler Umverteilung auf Landschaftsebene aufzuklären, verwendeten wir Plutonium-239+240 ($^{239+240}\text{Pu}$), Beryllium-10 (^{10}Be , in situ und meteorisch) und Radiokohlenstoff (^{14}C) zur Berechnung kurz- und langfristiger Erosionsraten in zwei Umgebungen: einer natürlichen und einer anthropogenen Umgebung in der hügeligen Grundmoränenlandschaft der Uckermark in Nordostdeutschland. Die wichtigsten Forschungsfragen waren:

1. Wie unterscheiden sich langfristige und kurzfristige Raten von Bodenumverteilungsprozessen?
2. Sind die aus in situ ^{10}Be berechneten Raten vergleichbar mit denen der Verwendung von meteorischem ^{10}Be ?
3. Wie verhalten sich Bodenumlagerungsraten (kurz- und langfristig) in einer Agrar- und in einer Naturlandschaft zueinander?

4. Sind die in Norddeutschland beobachteten Bodenmuster reine Folge vergangener Ereignisse (natürlich und/oder anthropogen) oder sind sie in laufende Prozesse eingebettet?

Erosion und Ablagerung spiegeln sich in einer Kette von Bodenprofilen mit keiner oder fast keiner Erosion auf flachen Positionen (Hügelkuppe), starker Erosion auf der Hangmitte und Anhäufung von Bodenmaterial am Hangfuss wider. Diese drei charakteristischen Prozessdomänen wurden innerhalb des CarboZALF-D-Versuchsstandorts ausgewählt, der durch intensive anthropogene Aktivitäten gekennzeichnet ist. Ebenso wurde für diese Studie eine Hydrosequenz in einem alten Wald ausgewählt, die als stark vom natürlichen Bodentransport beeinflusste Catena angesehen wird.

Die folgenden Hauptergebnisse wurden unter Verwendung der oben erwähnten Reihe von Isotopenmethoden erzielt, die zur Messung der Bodenumverteilungsraten in Abhängigkeit von der erforderlichen Zeitskala (z. B. $^{239+240}\text{Pu}$, ^{10}Be , ^{14}C) verfügbar sind:

1. Im landwirtschaftlichen Umfeld sind kurzfristige Erosionsraten eine Größenordnung höher als langfristige Raten.
2. Sowohl meteorisches als auch in situ ^{10}Be sind geeignete Bodenindikatoren, um die langfristigen Bodenumverteilungsraten zu messen. Sie liefern ähnliche Ergebnisse in einer anthropogenen Umgebung für verschiedene Landschaftspositionen (z. B. Hügelkuppe, Mittelhang, Hangfuss).
3. Die Kurzzeitraten waren in einer Naturlandschaft extrem niedrig/vernachlässigbar und in einer Agrarlandschaft sehr hoch – $-0,01 \text{ t ha}^{-1} \text{ Jahr}^{-1}$ (Durchschnittswert) bzw. $-25 \text{ t ha}^{-1} \text{ Jahr}^{-1}$. Im Gegensatz dazu sind die langjährigen Belastungen in der Waldlandschaft vergleichbar mit den berechneten in der untersuchten landwirtschaftlichen Fläche mit Durchschnittswerten von $-1,00 \text{ t ha}^{-1} \text{ Jahr}^{-1}$ und $-0,79 \text{ t ha}^{-1} \text{ Jahr}^{-1}$.
4. Die im Wald beobachteten Bodenmuster könnten auf menschliche Einflüsse und Aktivitäten zurückzuführen sein, die nach den ersten Siedlungen in der Region begannen, und nicht auf die jüngste Bodenerosion. Diese Aktivitäten könnten früher als zuvor angenommen, zwischen 2'500 und 4'800 Jahren vor Christus, erfolgt sein.
5. Darüber hinaus sind die langfristigen Bodenumverteilungsraten unabhängig vom Umfeld ähnlich, was bedeutet, dass vergangene natürliche Bodenmassenumverteilungsprozesse immer noch die gegenwärtigen anthropogenen Erosionsprozesse überschatten.

Insgesamt konnte diese Studie wichtige Beiträge zur Entschlüsselung der Co-Evolution von Verwitterung, Bodenprofilentwicklung und lateraler Umverteilung in Nordostdeutschland leisten. Der verwendete multimethodische Ansatz kann durch die Anwendung in einem breiteren Spektrum von Landschaften und geografischen Regionen herausgefordert werden.

Sommario

Il suolo è oggi considerato una risorsa non rinnovabile sulla scala temporale della società, poiché il tasso di perdita di suolo è superiore a quello di formazione del suolo stesso.

La formazione del suolo è complessa, può richiedere diverse migliaia di anni ed è influenzata da una varietà di fattori, uno di questi è il tempo. Spesso si assume l'assunzione di condizioni costanti e progressive per lo sviluppo del suolo e/o del profilo (cioè stato stazionario). In realtà, per la maggior parte dei suoli, la loro (co-)evoluzione porta ad uno sviluppo del suolo complesso e irregolare nel tempo e nello spazio caratterizzato da fasi "progressive" e "regressive".

Il trasporto laterale del materiale del suolo (cioè l'erosione del suolo) è uno dei principali processi che modellano la superficie terrestre e il profilo del suolo durante le fasi "regressive" è uno dei principali problemi ambientali che il mondo deve affrontare.

Le attività antropogeniche come l'agricoltura possono esacerbare l'erosione del suolo. Pertanto, è di vitale importanza distinguere come i tassi di redistribuzione del suolo a breve termine (cioè entro decenni) influenzati dalle attività umane differiscono dai tassi naturali a lungo termine. Per fare ciò, i tassi di erosione (e denudazione) del suolo possono essere determinati utilizzando una serie di metodi isotopici che coprono diverse scale temporali a livello di paesaggio.

Con l'obiettivo di svelare la coevoluzione degli agenti atmosferici, lo sviluppo del profilo del suolo e la redistribuzione laterale a livello paesaggistico, abbiamo utilizzato Plutonio-239+240 ($^{239+240}\text{Pu}$), Berillio-10 (^{10}Be , in situ e meteorico) e Radiocarbonio (^{14}C) per calcolare i tassi di erosione a breve e lungo termine in due contesti, ovvero un ambiente naturale e uno antropogenico nel paesaggio morenico di terreno collinare dell'Uckermark, nella Germania nord-orientale. Le principali domande di ricerca sono state:

1. In che modo differiscono i tassi a lungo termine e a breve termine dei processi di redistribuzione del suolo?
2. I tassi calcolati dal ^{10}Be in situ sono paragonabili a quelli dell'utilizzo del ^{10}Be meteorico?
3. Come sono i tassi di redistribuzione del suolo (a breve e a lungo termine) se mettiamo a confronto un paesaggio agricolo e un paesaggio naturale?

4. Gli schemi del suolo osservati nella Germania settentrionale sono puramente il risultato di eventi passati (naturali e/o antropogenici) o sono coinvolti in processi in corso?

L'erosione e la deposizione si riflettono in una catena di profili del suolo con nessuna o quasi nessuna erosione su posizioni pianeggianti (collina), forte erosione a metà del pendio e accumulo di materiale del suolo in corrispondenza del pendio. Questi tre tipi di processo caratteristici sono stati scelti all'interno del sito sperimentale CarboZALF-D, caratterizzato da intense attività antropogeniche. Allo stesso modo, per questo studio è stata scelta un'idrosequenza in un'antica foresta, considerata come una catena fortemente influenzata dal trasporto naturale del suolo.

I seguenti risultati principali sono stati ottenuti utilizzando la suddetta gamma di metodi isotopici disponibili per misurare i tassi di redistribuzione del suolo in base alla scala temporale necessaria (es. $^{239+240}\text{Pu}$, ^{10}Be , ^{14}C):

1. I tassi di erosione a breve termine sono un ordine di grandezza superiori ai tassi a lungo termine negli ambienti agricoli.
2. Sia il ^{10}Be meteorico che in situ sono tracciatori del suolo adatti per misurare i tassi di redistribuzione del suolo a lungo termine dando risultati simili in un ambiente antropogenico per diverse posizioni paesaggistiche (es. collina, medio pendio, a valle del pendio)
3. I tassi a breve termine erano estremamente bassi/trascurabili in un paesaggio naturale e molto elevati in un paesaggio agricolo – rispettivamente $-0,01 \text{ t ha}^{-1} \text{ anno}^{-1}$ (valore medio) e $-25 \text{ t ha}^{-1} \text{ anno}^{-1}$. Al contrario, i tassi a lungo termine nel paesaggio forestale sono paragonabili a quelli calcolati nella superficie agricola investigata con valori medi di $-1,00 \text{ t ha}^{-1} \text{ anno}^{-1}$ e $-0,79 \text{ t ha}^{-1} \text{ anno}^{-1}$.
4. I modelli del suolo osservati nella foresta potrebbero essere dovuti all'impatto umano e alle attività iniziate dopo i primi insediamenti nella regione, prima di quanto ipotizzato in precedenza, tra 4,5 e 6,8 mila anni fa, e non il risultato della recente erosione del suolo.
5. Inoltre, i tassi di redistribuzione del suolo a lungo termine sono simili indipendentemente dalle impostazioni, il che significa che i passati processi di redistribuzione naturale della massa del suolo oscurano ancora gli attuali processi di erosione antropogenica.

Nel complesso, questo studio potrebbe fornire importanti contributi alla decifrazione della coevoluzione degli agenti atmosferici, dello sviluppo del profilo del suolo e della redistribuzione laterale nella Germania nord-orientale. L'approccio multimetodologico utilizzato può essere messo in discussione dall'applicazione in una più ampia gamma di paesaggi e regioni geografiche.

Sommaire

Le sol est aujourd'hui considéré comme une ressource non renouvelable à l'échelle du temps sociétal, car le taux de perte de sol est supérieur à celui de la formation du sol.

La formation du sol est complexe, peut prendre plusieurs milliers d'années et est influencée par une variété de facteurs parmi lesquels le temps. Souvent, on suppose que les conditions de développement du sol et/ou du profil sont constantes et progressives (c'est-à-dire en régime permanent). En réalité, pour la plupart des sols, leur (co)évolution conduit à un développement complexe et irrégulier du sol dans le temps et l'espace, caractérisé par des phases "progressives" et "régressives".

Le transport latéral des matériaux du sol (c'est-à-dire l'érosion du sol) est l'un des principaux processus qui façonnent la surface et le profil du sol pendant les phases "régressives" et l'un des principaux problèmes environnementaux auxquels le monde est confronté.

Les activités anthropiques comme l'agriculture peuvent exacerber l'érosion des sols. Il est donc vital de distinguer les taux de redistribution des sols à court terme (c'est-à-dire en quelques décennies) influencés par les activités humaines des taux naturels à long terme. Pour ce faire, les taux d'érosion (et de dénudation) des sols peuvent être déterminés en utilisant un ensemble de méthodes isotopiques qui couvrent différentes échelles de temps au niveau du paysage.

Afin d'élucider la coévolution de l'altération, du développement du profil du sol et de la redistribution latérale au niveau du paysage, nous avons utilisé le Pluthonium-239+240 ($^{239+240}\text{Pu}$), le Béryllium-10 (^{10}Be , in situ et météorique) et le Radiocarbone (^{14}C) pour calculer les taux d'érosion à court et long terme dans deux contextes, à savoir un environnement naturel et un environnement anthropique dans le paysage de la moraine de fond bosselée de l'Uckermark au nord-est de l'Allemagne. Les principales questions de recherche étaient les suivantes:

1. Comment les taux à long et court terme des processus de redistribution du sol diffèrent-ils?
2. Les taux calculés à partir du ^{10}Be in situ sont-ils comparables à ceux obtenus à partir du ^{10}Be météorique?
3. Comment se comparent les taux de redistribution du sol (à court et long terme) dans un paysage agricole et dans un paysage naturel?

4. Les modèles pédologiques observés dans le nord de l'Allemagne sont-ils uniquement le résultat d'événements passés (naturels et/ou anthropiques) ou sont-ils intégrés dans des processus en cours?

L'érosion et la déposition sont reflétées dans une catène de profils pédologiques avec une érosion nulle ou presque nulle sur les positions plates (sommet de la colline), une forte érosion sur les pentes moyennes et une accumulation de matériaux pédologiques sur les pentes inférieures. Ces trois domaines de processus caractéristiques ont été choisis au sein du site expérimental CarboZALF-D, caractérisé par d'intenses activités anthropiques. De même, une hydro-séquence dans une forêt ancienne a été choisie pour cette étude étant considérée comme une catène fortement influencée par le transport naturel du sol.

Les principaux résultats suivants ont été obtenus en utilisant la gamme bien mentionnée ci-dessus de méthodes isotopiques disponibles pour mesurer les taux de redistribution du sol selon l'échelle de temps nécessaire (par exemple, $^{239+240}\text{Pu}$, ^{10}Be , ^{14}C):

1. Les taux d'érosion à court terme sont d'un ordre de grandeur supérieur aux taux à long terme dans les milieux agricoles.
2. Les ^{10}Be météorique et in situ sont des traceurs du sol appropriés pour mesurer les taux de redistribution du sol à long terme, donnant des résultats similaires dans un environnement anthropique pour différentes positions du paysage (par exemple, sommet de la colline, mi-pente, bas de la pente).
3. Les taux à court terme étaient extrêmement faibles/négligeables dans un paysage naturel et très élevés dans un paysage agricole - $-0,01 \text{ t ha}^{-1} \text{ an}^{-1}$ (valeur moyenne) et - $25 \text{ t ha}^{-1} \text{ an}^{-1}$ respectivement. A l'opposé, les taux à long terme dans le paysage forestier sont comparables à ceux calculés dans la zone agricole étudiée avec des valeurs moyennes de $-1,00 \text{ t ha}^{-1} \text{ an}^{-1}$ et $-0,79 \text{ t ha}^{-1} \text{ an}^{-1}$.
4. Les caractéristiques du sol observées dans la forêt pourraient être dues à l'impact et aux activités humaines qui ont commencé après les premiers établissements dans la région, plus tôt que ce qui avait été postulé auparavant, entre 4,5 et 6,8 kyr BP, et ne pas être le résultat d'une érosion récente du sol.
5. En outre, les taux de redistribution du sol à long terme sont similaires indépendamment des paramètres, ce qui signifie que les processus naturels passés de redistribution de la masse du sol éclipsent toujours les processus actuels d'érosion anthropique.

Dans l'ensemble, cette étude pourrait apporter des contributions importantes à la compréhension de la coévolution de l'altération, du développement du profil du sol et de la redistribution latérale dans le nord-est de l'Allemagne. L'approche multi-méthodologique utilisée peut être remise en question par l'application dans une gamme plus large de paysages et de régions géographiques.

Resumo

O solo é hoje considerado um recurso não renovável na escala de tempo da sociedade, pois a taxa de perda de solo é maior do que a de formação do solo.

A formação do solo é complexa, pode levar milhares de anos e é influenciada por diversos fatores, um deles é o tempo. Muitas vezes, há a suposição de condições constantes e progressivas para o desenvolvimento do solo e/ou perfil do solo (ou seja, estado estacionário). Na realidade, para a maioria dos solos, a sua (co-)evolução conduz a um desenvolvimento complexo e irregular em tempo e espaço, caracterizados por fases “progressivas” e “regressivas”.

O transporte lateral de material do solo (isto é, a erosão do solo) é um dos principais processos que moldam a superfície da terra e o perfil do solo durante as fases “regressivas” e um dos principais problemas ambientais que o mundo enfrenta.

Atividades antropogênicas como a agricultura podem induzir a erosão do solo. Assim, é de vital importância distinguir as taxas de redistribuição do solo de curto prazo (ou seja, dentro de décadas), influenciadas pelas atividades humanas, das taxas naturais de longo prazo. Para isso, as taxas de erosão do solo (e denudação) podem ser determinadas usando um conjunto de métodos isotópicos que cobrem diferentes escalas de tempo no nível da paisagem.

Com o objetivo de desvendar a co-evolução do intemperismo, desenvolvimento do perfil do solo e redistribuição lateral em nível de paisagem, usamos Plutônio-239+240 ($^{239+240}\text{Pu}$), Berílio-10 (^{10}Be , in situ e meteórico) e Radiocarbono (^{14}C) para calcular as taxas de erosão de curto e longo prazo em duas configurações, ou seja, um ambiente natural e um ambiente antropogênico na paisagem montanhosa do solo de morena de Uckermark, nordeste da Alemanha. As principais questões de pesquisa foram:

1. Como diferem as taxas de longo e curto prazo dos processos de redistribuição do solo?
2. As taxas calculadas a partir do ^{10}Be in situ são comparáveis às do ^{10}Be meteórico?
3. Como se comparam as taxas de redistribuição do solo (curto e longo prazo) em uma paisagem agrícola e uma paisagem natural?
4. Os padrões de solo observados no norte da Alemanha são puramente resultado de eventos passados (naturais e/ou antropogênicos) ou estão embutidos em processos em andamento?

A erosão e a deposição são refletidas em uma cadeia de perfis de solo sem ou quase nenhuma erosão nas posições planas (topo de morro), forte erosão no meio da encosta e acúmulo de material do solo na posição da encosta. Esses três domínios de processo característicos foram escolhidos dentro do sítio experimental CarboZALF-D, caracterizado por intensas atividades antropogênicas. Da mesma forma, uma hidrossequência em uma floresta antiga foi escolhida para este estudo e considerada como uma cadeia fortemente influenciada pelo transporte natural do solo.

Os resultados principais seguintes foram obtidos usando os métodos isotópicos mencionados acima, disponíveis para medir as taxas de redistribuição do solo, dependendo da escala de tempo necessária (por exemplo, $^{239+240}\text{Pu}$, ^{10}Be , ^{14}C):

1. As taxas de erosão de curto prazo são uma ordem de grandeza mais altas do que as taxas de longo prazo em ambientes agrícolas.
2. Tanto o ^{10}Be meteórico quanto o *in situ* são rastreadores de solo adequados para medir as taxas de redistribuição do solo a longo prazo, dando resultados semelhantes em um ambiente antropogênico para diferentes posições da paisagem (por exemplo, topo de colina, meia encosta, e encosta).
3. As taxas de curto prazo foram extremamente baixas/insignificantes em uma paisagem natural, e muito altas em uma paisagem agrícola – $-0,01 \text{ t ha}^{-1} \text{ ano}^{-1}$ (valor médio) e $-25 \text{ t ha}^{-1} \text{ ano}^{-1}$, respectivamente. Ao contrário, as taxas de longo prazo na paisagem florestal são comparáveis às calculadas na área agrícola investigada, com valores médios de $-1,00 \text{ t ha}^{-1} \text{ ano}^{-1}$ e $-0,79 \text{ t ha}^{-1} \text{ ano}^{-1}$.
4. Os padrões de solo observados na floresta podem ser devidos ao impacto humano e atividades iniciadas após os primeiros assentamentos na região, antes do postulado anteriormente, entre 4,5 e 6,8 kyr AP, e não resultado de erosão recente do solo.
5. Além disso, as taxas de redistribuição do solo a longo prazo são semelhantes, independentemente das configurações, o que significa que os processos naturais passados de redistribuição da massa do solo ainda ofuscam os atuais processos de erosão antropogênica.

No geral, este estudo pode trazer contribuições importantes para decifrar a co-evolução do intemperismo, desenvolvimento do perfil do solo, e redistribuição lateral no nordeste da Alemanha. A abordagem multimetodológica utilizada pode ser desafiada pela aplicação em uma ampla gama de paisagens e regiões geográficas.

Abbreviations

σ	Standard deviation
% v/v	volume concentration
°C	degree Celsius
${}^9\text{Be}(\text{NO}_3)_2$	Beryllium nitrate
a	annus=year
a.s.l.	above sea level
$\text{Al}(\text{OH})_3$	Aluminium hydroxide
Al_{ox}	Oxalate-extractable aluminium
AMS	Accelerator Mass Spectrometry
BD	Bulk density
$\text{Be}(\text{OH})_2$	Beryllium hydroxide
BP	Before Present
Bq	becquerel
CaCl_2	Calcium chloride
CaCO_3	Calcium carbonate
CRDS	Cavity Ring-Down System
CO_2	Carbon dioxide
C_{org}	organic Carbon
DIC	Dissolved Inorganic Carbon
DOC	Dissolved Organic Carbon
ED-XRF	Energy Dispersive X-ray Fluorescence
EDTA	Ethylenediaminetetraacetic acid
Fe_{dith}	dithionite-extractable iron
Fe_{ox}	oxalate-extractable iron

FeSO ₄	iron sulphate
FRN	Fallout Radionuclides
H ₂ O ₂	hydrogen peroxide
HCl	hydrochloric acid
HF	hydrofluoric acid
HNO ₃	nitric acid
ICP-MS	inductively coupled plasma mass spectrometry
ka	thousand years
kyr	thousand years
M	molar
m ²	square meter
Mn _{dith}	dithionite-extractable Manganese
N	normal
Na ₄ P ₂ O ₇	tetrasodium pyrophosphate
NaNO ₂	sodium nitrite
NaOH	sodium hydroxide
NH ₄ OH	ammonium hydroxide
pg	picogramme
POM	Particulate Organic Matter
SOC	Soil Organic Carbon
t	tonne
t _{1/2}	half-life
TPI	Topographic Position Index
XRF	X-ray Fluorescence
yr	year

Academic achievements

Journal articles (peer-reviewed)

Calitri F., Sommer M., Norton K., Temme A., Brandová D., Portes R., Christl M., Ketterer M.E., Egli E. (2019): Tracing the temporal evolution of soil redistribution rates in an agricultural landscape using $^{239+240}\text{Pu}$ and ^{10}Be . *Earth Surface Processes and Landform*, 44: 1783-1798. doi: 10.1002/esp.4612

Calitri F., Sommer M., van der Meij M., Egli E. (2020): Soil erosion along a transect in a forested catchment: recent or ancient processes? *Catena*, 194: 104683. doi: 10.1016/j.catena.2020.104683

Lee J., Necpalova M., **Calitri F.**, Six J. (2020) Simulation of regional soil nitrogen balance in Swiss cropland. *Nutrient Cycling in Agroecosystem*, 118: 9-22. doi: 10.1007/s10705-020-10078-6

Loba A., Waroszewski J., Tikhomirov D., **Calitri F.**, Christl M., Sykuła M., Egli M. (2021): Tracing erosion rates in loess landscape of the Trzebnica Hills (Poland) over time using fallout and cosmogenic nuclides. *Journal of Soils and Sediments*, 21: 2952–2968. <https://doi.org/10.1007/s11368-021-02996-x>

Calitri F., Sommer M., van der Meij W.M., Tikhomirov D., Christl M., Egli M. (2021): ^{10}Be and ^{14}C data provide insight on soil mass redistribution along gentle slopes and reveal ancient human impact. *Journal of Soils and Sediments*, 21: 3770–3788. <https://doi.org/10.1007/s11368-021-03041-7>

Table I. Contribution of individual researchers to the following manuscripts.

Task	Calitri et al. 2019	Calitri et al. 2020	Calitri et al. 2021
Fieldwork	Sommer M. Egli M.	Calitri F. Sommer M. Egli M.	Calitri F. Sommer M. Egli M.
Sample Preparation	Calitri F. Brandová D.	Calitri F.	Calitri F. Tikhomirov D.
Sample Measurements	Calitri F. Brandová D. Christl M. Ketterer M.	Calitri F.	Calitri F. Tikhomirov D. Christl M.
Calculations and modelling	Calitri F. Norton K. Egli M.	Calitri F. van der Meij M.	Calitri F. van der Meij M.
Data evaluation and interpretation	Calitri F. Sommer M. Temme A. Portes R. Egli M.	Calitri F. Sommer M. van der Meij M. Egli M.	Calitri F. Sommer M. van der Meij M. Egli M.
Manuscript, tables and figures drafting	Calitri F. Sommer M. Egli M.	Calitri F. Sommer M. Egli M.	Calitri F. Sommer M. Egli M.

Seminars

Calitri F. (25/01/18): Co-evolution of erosion rates, weathering and profile development in soil landscapes of hummocky ground moraines, Soil Science Zvieri seminar series, *University of Zürich, Switzerland*

Calitri F. (18/09/19): Modelling possibilities for $^{239+240}\text{Pu}$ as soil erosion tracer. Seminar series 'Current topics from Accelerator Mass Spectrometry and its applications', *Ion Beam Physics lab, ETH Zürich, Switzerland*

Conference contributions

Calitri F., Necpalova M., Lee J., Zacccone C., Spiess E., Herrera J., Six J. (04/2016): Regional modelling of nitrate leaching from Swiss organic and conventional cropping systems under climate change. *EGU General Assembly 2016*, Vienna, Austria

Calitri F., Egli M., Sommer M., Brandová D., Christl M. (04/2018): Soil erosion and weathering in a hummocky moraine landscape. *EGU General Assembly 2018*, Vienna, Austria

Calitri F., Egli M., Sommer M. (04/2019): Soil erosion rates' assessment of a forested catchment using $^{239+240}\text{Pu}$ and relation to landscape evolution. *EGU General Assembly 2019*, Vienna, Austria

Calitri F., Egli M., Sommer M., Tikhomirov D., Christl M. (05/2020): Complex soil mass redistribution along a catena using meteoric and in-situ ^{10}Be as tracers. *EGU General Assembly 2020*, Vienna, Austria

Short-Course - Visualizing Science. (04/2019) Convener: G. Raab, co-conveners: **F. Calitri**, M. Schiedung, *EGU General Assembly*, Vienna, Austria

Thesis supervision

Amrein, Simon R. (2020): Soil erosion rates caused by tree uprooting in an old-growth temperate forest: Data analysis of Pu- Isotopes from soil sampling in the primeval forest Boubínský prales in south Bohemia, Czech Republic. **Bachelor Thesis** at *Department of Geography, University of Zurich*, Switzerland.

Chapter 1. Introduction

1.1 Soil and its formation

Soil can be defined as “the unconsolidated mineral or organic matter layer on the surface of the Earth that has been subjected to and shows effects of genetic and environmental factors of: climate (including water and temperature effects), and macro- and microorganisms, conditioned by relief, acting on parent material over a period of time. A product-soil differs from the material from which it is derived in many physical, chemical, biological, and morphological properties and characteristics” (Soil Science Society of America, 2008).

Soil is today considered a non-renewable resource on societal time scale, as the rate of soil loss is higher than the one of soil formation (Alewell et al., 2015; Stockmann et al., 2014; Wilkinson, 2005). At the same time, we are observing a general depletion of the quality of our soils, i.e., of their capacity to function, within natural or managed ecosystem boundaries, to sustain plant and animal productivity, maintain or enhance water and air quality, support human health and habitation, and continuous threats to these functions (Karlen et al., 1997; Masson-Delmotte et al., 2019; Montanarella et al., 2016).

Soil formation is complex, can take several thousands of years and is influenced by a variety of factors. It starts with the parent material, e.g. rock or additional material influxes (one of the influencing factor in (Jenny, 1941)’s equation), that evolves into a habitable substrate for organisms by weathering (e.g., physical, chemical and hydrological processes) (Graham et al., 2010). Organisms themselves are responsible for biological activities that can form and transform soils (e.g., chemical transformation of minerals). Other influencing factors are climate (e.g., temperature and precipitation) and relief (e.g., elevation).

Lastly, time is a substantial factor in soil formation and evolution. Since direct observations of pedogenesis are impossible due to the large time scales involved, many pedologists chose to use the so-called “space-for-time approach”. This method compares sequences of soils with different ages to determine the soil production/formation rates, e.g., chronosequences studies. The assumption is that the environmental conditions did not change over the considered period and that soil evolution has been progressive and constant (i.e., steady-state).

This assumption of constant and progressive conditions for soil and/or profile development may lead to unrealistic representations of the dynamics of soil formation and profile evolution

(Phillips, 2010). Steady-state assumptions might be valid only for surfaces that developed on more or less homogeneous bedrock and were not subjected to erosion or deposition in recent times (Phillips, 2010).

The steady-state approach has been challenged due to the low likelihood for forming soils to have stable environmental conditions for the entire period of time of their development. All pedogenic processes, even slow ones, have to be terminated or be in dynamic equilibrium with their environment in order to reach steady state (Targulian and Krasilnikov, 2007). All soil processes take certain ranges of times to change a soil (Brantley, 2008).

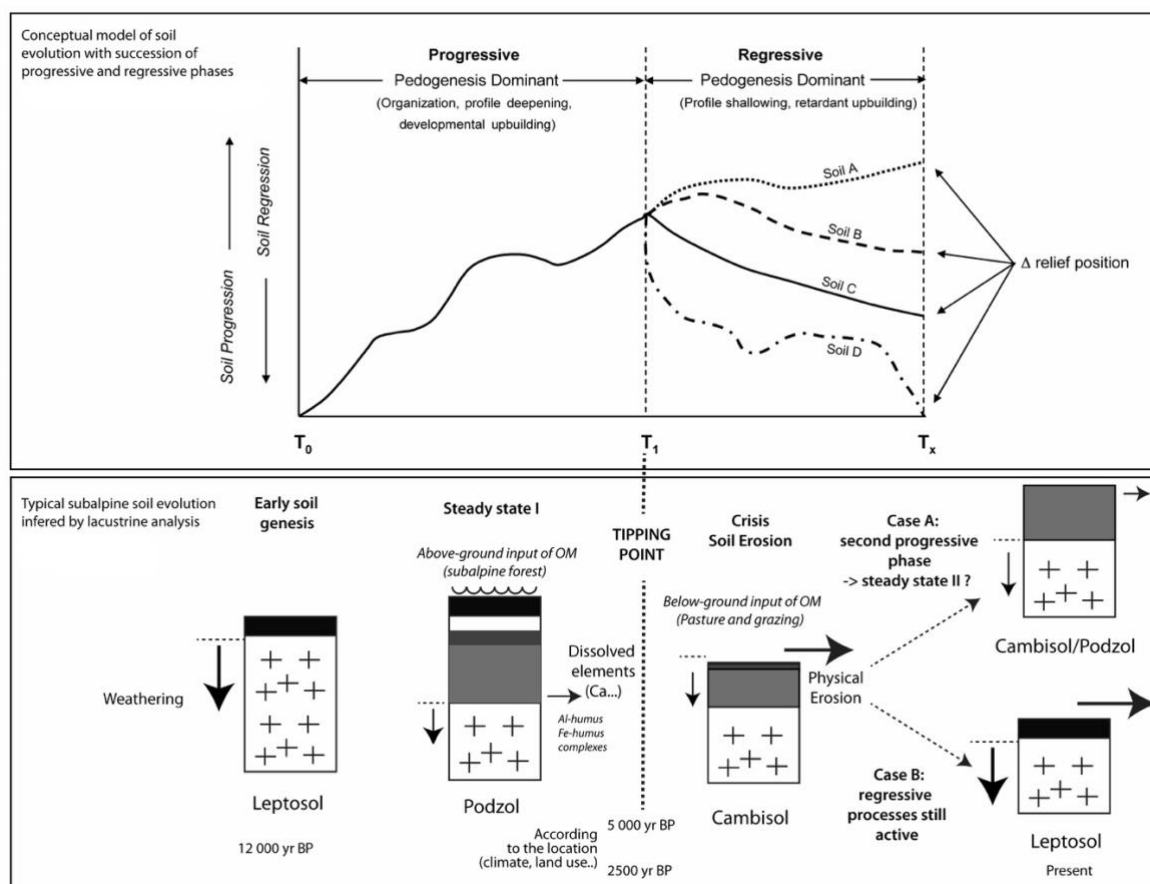


Figure 1.1. A conceptual soil evolution model (upper), showing progressive and regressive phases (with increasing erosion rates from situation A to D), as compared to the dominant soil evolution pathway in the subalpine belt during the Holocene (lower) (Egli and Poulénard, 2016; Johnson and Watson-Stegner, 1987; Sommer et al., 2008).

Changing environmental conditions and soil-landscape development themselves can lead to an acceleration, deceleration or reversal of process rates, which is an example of co-evolution (Phillips, 2015).

Co-evolution can be defined as the intertwined formation of soils and the other aspects of the landscape. In the field of ecology, co-evolution indicates interactive evolution of different species (Ehrlich and Raven, 1964). In soil science, soil-landscape co-evolution is often used to describe and understand simultaneous development of soils and landforms under pedogenic, geomorphic, biotic and hydrologic fluxes and processes (Huggett, 1975; Johnson, 2002; Phillips and Lorz, 2008; Schaetzl and Thompson, 2015; Sommer and Schlichting, 1997; Willgoose, 2018).

This co-evolution lead to a complex and irregular soil development in time and space characterised by “progressive” and “regressive” phases (Figure 1.1; (Johnson and Watson-Stegner, 1987; Sommer et al., 2008). Progressive phases (e.g., profile deepening) occur when soil production exceeds denudation and alternate with regressive phases (e.g., soil erosion through wind and water) that occur when denudation surpasses soil production.

1.2 Soil erosion

One of the principal processes shaping the land surface and soil profile during “regressive” phases is the lateral transport of soil material by erosion.

Soil erosion is a widespread phenomenon, involves different types of ecosystem and is one of the major environmental problems the world faces – as well as population growth, climate change and loss of biodiversity – (Berhe et al., 2018; Lal and Stewart, 1990; Pimentel, 1993; Pimentel et al., 1995; Pimentel and Kounang, 1998). Soil degradation is often caused by soil erosion, that leads to a decrease of soil quality, productivity and diversity of plants, animals and microbes in natural, agricultural and forest ecosystems (Pimentel, 2001; Pimentel et al., 1995; Pimentel and Kounang, 1998).

According to the United Nations, a third of the planet’s land surface, particularly the fertile soil, has already been lost or heavily degraded due to agriculture (United Nations News, 2017). Furthermore, the world population is projected to reach 9.4 billion by 2050 and 10 billion by 2100 (Cohen, 2003), this puts additional stress on soils for rising demand of food (Pimentel, 2006; Pimentel et al., 1995; Richter and Markewitz, 2001).

Despite its importance, there are only few soil erosion records covering the last millennium in favour of data sets dating back millions of years about climate records (Boardman and Poesen, 2006; Poesen, 2018). Other global issues, e.g., climate change, and their correlation with anthropogenic activities are regarded as more concerning, therefore more studied than soil erosion and degradation.

Anthropogenic changes to the surrounding environment, specifically to landscapes, exceed by far those occurring in natural systems (Alewell et al., 2015; Wilkinson, 2005), making humans one of the dominant factors of soil formation (Amundson and Jenny, 1991; Richter et al., 2015). Indeed, human activities can trigger and aggravate erosion processes (Poesen, 2018), contaminate soils (Carré et al., 2017), deplete its resources (Tan et al., 2005) and reduce biodiversity (IPBES, 2019; Van Der Wal et al., 2008).

Agricultural practices in particular, generate changes in soils and landscapes at higher rates than natural processes. Humans caused changes in landscapes for thousands of years (Stephens et al., 2019). Therefore, it is essential to research how natural and anthropogenic processes interact with each other.

There are evidences of erosion corresponding with the first settlers in certain world regions that led to the assumption of water erosion – caused by anthropogenic activities – as the dominant mode of erosion since prehistoric times (Brevik and Hartemink, 2010; Montgomery, 2007; Troeh et al., 1981). In fact, many European landscapes have been altered by anthropogenic activities (e.g. land use change, deforestation, etc.) since the Neolithic and influenced agricultural sustainability (Hughes and Thirgood, 1982; Kappler et al., 2018; Stephens et al., 2019; Vanwalleghem et al., 2017; Wang and Van Oost, 2019). Nonetheless, soil erosion due to tillage, agricultural activities and human influence is even more crucial in recent times (Van Oost et al., 2005; Wilken et al., 2020). Therefore, each human activity, including agriculture, should be carried out in a sustainable way, in order to allow future generations to meet their own needs (World Commission on Environment and Development, 1987).

To tackle these environmental processes, their causes and drivers, they must be looked over larger spatial and longer time scales. To do so, soil erosion (and denudation) rates can be determined by using a set of isotope methods that cover different time scales at landscape level.

1.3 How to measure erosion on different time ranges

A wide range of isotope methods is available to measure soil redistribution rates depending on the time scale needed (Figure 1.2). To decipher whether natural soil redistribution rates (i.e., erosion and accumulation) have changed due to intense agricultural activities in the last decades, there are two main categories in which they are divided: decadal (short-term) erosion rates and millennial (long-term) erosion rates.

Fallout radionuclides (FRNs, e.g. ^{137}Cs , ^7Be , $^{210}\text{Pb}_{\text{ex}}$) have been successfully used to measure short-term erosion rates since 1970s (Zapata, 2003). In particular, Plutonium-239 and -240 ($^{239+240}\text{Pu}$) are the focus in this research study.

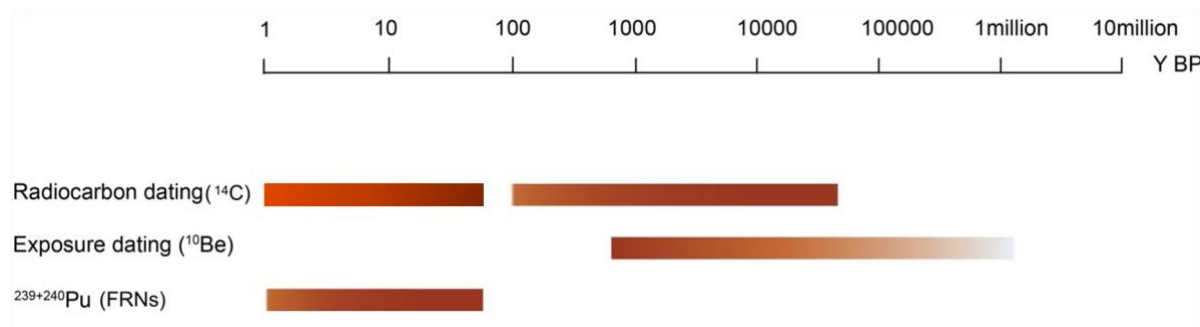


Figure 1.2. Isotope methods available to measure soil erosion rates and the different time ranges covered.

Long-term erosion and denudation rates can be calculated using *meteoric* or *in situ* produced Beryllium-10 (^{10}Be). The difference between these two isotopes is their origin: *meteoric* ^{10}Be is produced in the atmosphere and deposited on Earth's surface; on the contrary, *in situ* ^{10}Be is produced with time in minerals exposed to cosmic rays.

Another possibility is given by radiocarbon dating (^{14}C). ^{14}C is produced in the atmosphere similarly to ^{10}Be and its applications in Quaternary studies are various (Hajdas, 2008).

1.3.1. Anthropogenic radionuclides – $^{239+240}\text{Pu}$

FRNs were dispersed around the globe primarily during the thermonuclear weapon testing between 1952 and 1964, therefore their origin is anthropogenic (Figure 1.3). Other contributions (e.g. nuclear power plant incidents) can spread Pu only locally (Evrard et al.,

2014; Matisoff et al., 2011) unlike in the case of ^{137}Cs . In fact, due to the Chernobyl nuclear accident in 1986, many parts of Europe were contaminated by ^{137}Cs and other fallout nuclides. The Southern Hemisphere is characterised by a lower total fallout of radionuclides than the Northern Hemisphere, because more atmospheric nuclear testing occurred in the latter one.

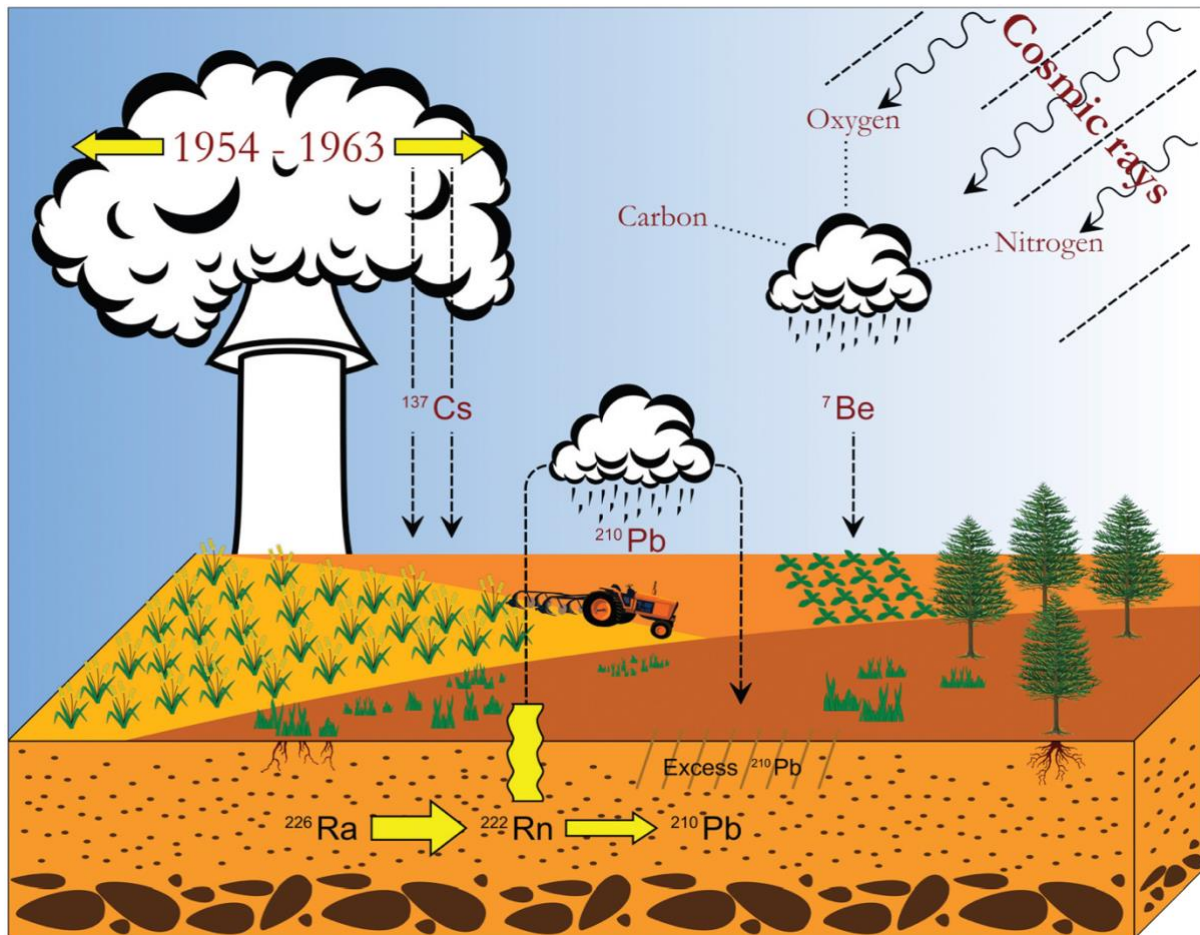


Figure 1.3. Origin of fallout radionuclides (Zupanc and Mabit, 2010).

Pu isotopes have a quite long half-life, i.e., 24,110 y for ^{239}Pu and 6,561 y for ^{240}Pu . This makes them a good replacement for ^{137}Cs that has a half-life of 30.17 y, and already partly disappeared through radioactive decay (ca. 70% of its global fallout; (Xu et al., 2014)).

$^{239+240}\text{Pu}$ was used as soil erosion tracer in different ecosystems: arable land (Schimmack et al., 2001), permanent grasslands (Alewell et al., 2014; Arata et al., 2016; Meusburger et al., 2018; Zollinger et al., 2015) coniferous and evergreen forests (Hoo et al., 2011; Lal et al., 2013; Meusburger et al., 2016; Zollinger et al., 2015).

Through the use of $^{239+240}\text{Pu}$ isotopes as soil erosion tracer is possible to highlight erosion and deposition in the last 60 years, therefore the changes caused by intensive agricultural practices.

1.3.2. Cosmogenic nuclides – ^{10}Be and ^{14}C

Cosmogenic nuclides that are formed in minerals at the Earth's surface (in situ) or in the atmosphere (meteoric) are commonly used for dating and determining physical erosion and denudation rates (Figure 1.4; (Schoonejans et al., 2017).

^{10}Be is the most widely used cosmogenic nuclide for dating in geochronology. It is radioactive and has a half-life of 1.39 million years (Chmeleff et al., 2010; Korschinek et al., 2010).

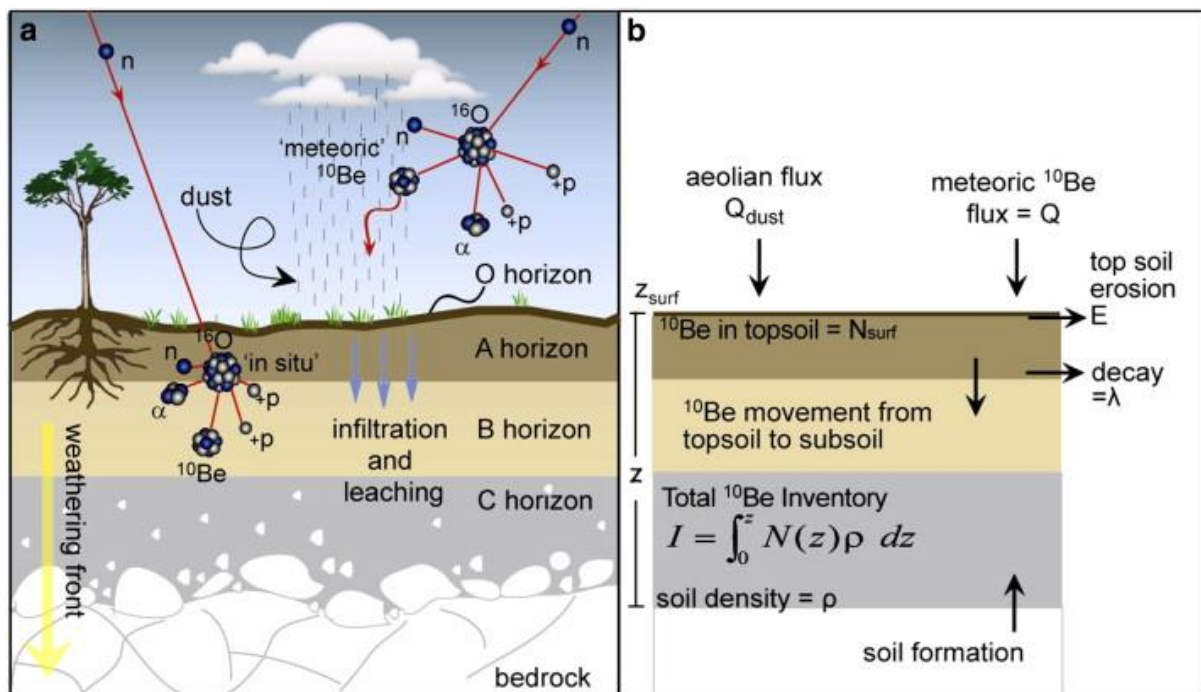


Figure 1.4. Schematic diagram of ^{10}Be production in the atmosphere (meteoric) and at the Earth's surface (in situ) and its interaction and incorporation within a soil profile. (Willenbring and von Blanckenburg, 2010)

Meteoric ^{10}Be is produced constantly by spallation of ^{16}O , ^{14}N and other atmospheric gases, in the upper atmosphere and at the Earth's surface (McHargue and Damon, 1991; Monaghan et al., 1986; Willenbring and von Blanckenburg, 2010). In a spallation reaction, a high energy neutron (or other nucleon) breaks-up a target nucleus to produce several lighter particles (Lal

and Peters, 1967). ^{10}Be produced in the atmosphere is absorbed onto aerosols and is distributed on the Earth's surface by wet and dry deposition (Beer et al., 2012; Graly et al., 2010; Willenbring and von Blanckenburg, 2010). Depending on the latitude and the precipitation rates, the ^{10}Be fluxes can be very different (Graly et al., 2011; Kaste and Baskaran, 2012). At mid-latitudes precipitation tend to be higher than at high latitudes, hence also meteoric ^{10}Be flux/deposition is higher (Beer et al., 2012; Kaste and Baskaran, 2012). Where precipitation is very low, e.g. deserts, dry deposition is more important than wet deposition (Beer et al., 2012; Kaste et al., 2002; Kaste and Baskaran, 2012; Willenbring and von Blanckenburg, 2010).

In situ ^{10}Be is primarily measured in quartz (SiO_2). In quartz at the Earth's surface, ^{10}Be is produced almost exclusively due to spallation reactions with silicon or oxygen. Quartz is almost ubiquitous on Earth and has the advantage that it can be thoroughly chemically cleaned from the much more abundant meteoric ^{10}Be from the atmosphere that could contaminate the in-situ concentrations (Ivy-Ochs and Kober, 2008).

Meteoric ^{10}Be can be used to evaluate both soil erosion and accumulation (Egli et al., 2010; Hidy et al., 2010; Maejima et al., 2005). On the contrary, in situ ^{10}Be has been only used to quantify erosion and denudation rates (Dosseto and Schaller, 2016; Siame et al., 2004).

With the combination of both types of ^{10}Be , the dynamics of soils and related mass transports should be even more traceable.

Radiocarbon, or ^{14}C , is the isotope of carbon produced by cosmic rays (in a similar way to ^{10}Be ; Figure 1.5). The other two stable isotopes of C, ^{12}C and ^{13}C , constitute the 99.9% and 0.1% respectively and originate from the primordial composition of the planet. ^{14}C has a half-life of 5,730 yr (Godwin, 1962) and although ^{14}C is just a minor fraction of the total carbon content, its application are various in geochronological and environmental studies.

^{14}C is incorporated in all organic and inorganic carbon compounds. There is a steady state between the uptake (e.g. photosynthesis, food) and the decay as long as the organism is alive (Libby et al., 1949). After the death of the organism, the steady state is broken, the only remaining process is decay (beta decay in which ^{14}C decays to nitrogen), and the activity begins to decrease with a half-life of 5,730 yr. Measurement of the beta-decay rate (conventional method) or counting the remaining ^{14}C atoms (AMS method) gives a measure of the time that passed since the steady state was broken (Hajdas, 2008). With this method it is possible to date organic samples in soils (e.g., charcoal) of up to 50,000-55,000 yr old.

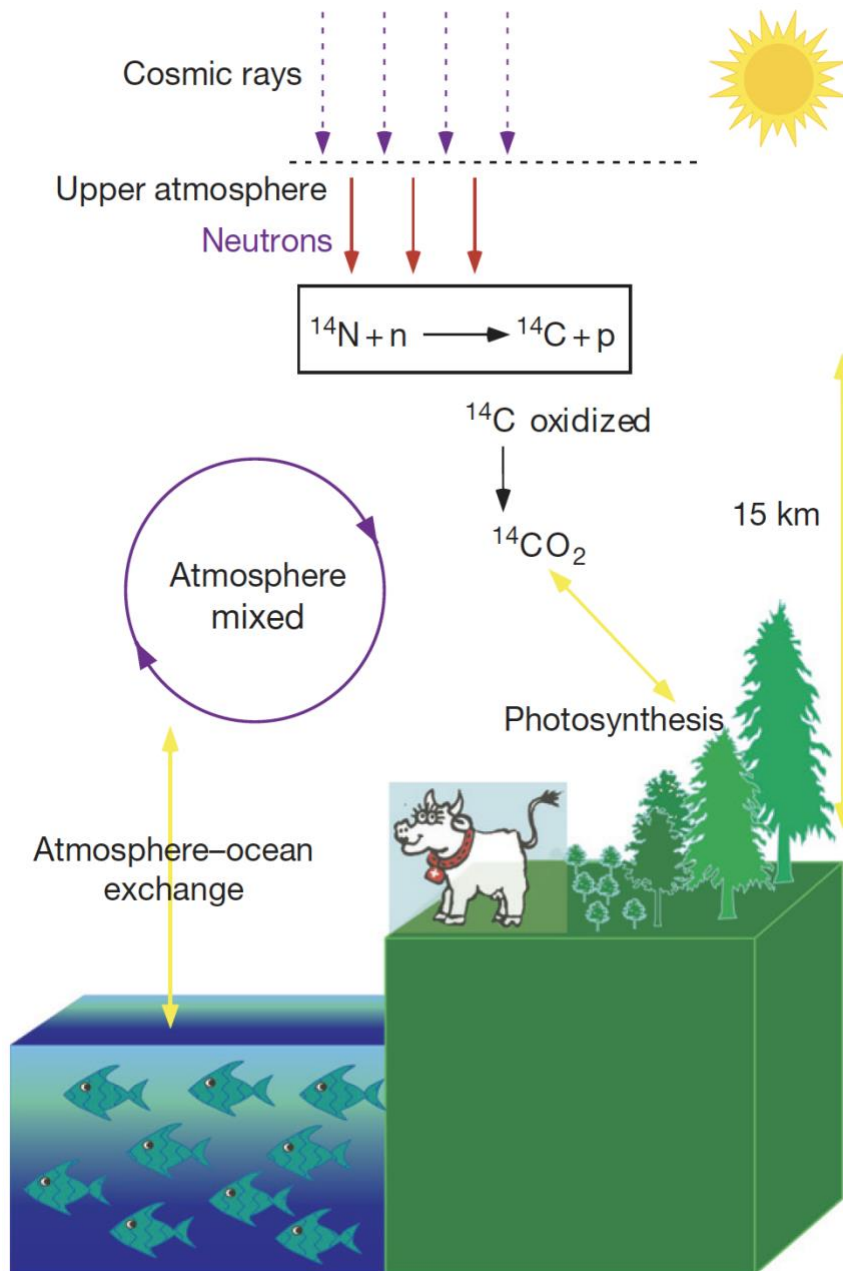


Figure 1.5. Production and distribution of cosmogenic ^{14}C . Produced mainly in the upper atmosphere due to interaction of thermal neutrons with nitrogen, ^{14}C is relatively quickly oxidised and mixed in the atmosphere. Through photosynthesis, it enters the biosphere and through gas exchange, the oceans. (Hajdas, 2008)

1.4 Research Needs and Challenges

Many studies have demonstrated that major land-use changes in the Anthropocene increased soil erosion rates worldwide (Boardman and Poesen, 2006; García-Ruiz et al., 2015; Goudie and Viles, 2016; Hooke, 2000; Maetens et al., 2012; Montgomery, 2007; Tarolli and Sofia, 2016; Vanacker et al., 2014; Vanmaercke et al., 2015; Vanwallegem et al., 2017).

Despite the striking increase in the number of research articles published in ca. 35 years – from 10,000 before 1980 to 69,000 in 2017 (Belpomme, 1980; Poesen, 2018) – there are still major research gaps like the one outlined by Poesen, 2018, i.e., better understand spatial and temporal patterns of soil erosion rates and landscape evolution.

Specifically, there is a need to quantify integrated soil landscape co-evolution by combining different scientific perspectives and human impact on soil-landscape. To do so, methods that can differentiate between natural processes and processes caused by anthropogenic activities are needed. It is essential to gather data on both spatial and temporal scales.

Furthermore, in order to collect data on spatial and temporal scales, there is a need to find a suitable study site/area that can provide the necessary type of data, i.e., areas with current influence of human activities (e.g., agricultural fields) and comparable areas not recently affected by these activities (e.g., forest).

Although the global relevance of this integrated approach is obvious, so far studies of the development of soils under global change have not yet adopted it.

1.5 Aims and research questions

This thesis focused on soil redistribution (erosion and deposition), profile development and weathering to better understand the discontinuous, non-linear and consequently ‘progressive’ and ‘regressive’ soil development of formerly glaciated areas.

The major aim was to unravel the co-evolution of weathering, soil profile development and lateral redistribution on a landscape level. Special focus was given on measuring short- and long-term redistribution rates in order to quantify modern variations from long-term baselines. Short- and long-term processes will be characterized in two settings that experienced a similar geomorphic situation (glaciation during the last ice age; ice-free since about 19-20 ka) but differ in recent geomorphic activities, land use and human impact. Two study sites in the same region of the Uckermark, Northeastern Germany, have been selected (more information about the study area can be found in the paragraphs: 2.2, 3.2 and 4.2): an agricultural landscape, the CarboZALF-D site, and a natural landscape in a forested catchment, the Melzower Forst. The main research questions were:

1. How do long-term and short-term rates of soil redistributing processes differ?
2. Are rates calculated from in situ ^{10}Be comparable to those of using meteoric ^{10}Be ?
3. How do soil redistribution rates (short- and long-term) in an agricultural and in a natural landscape compare to each other?
4. Are the soil patterns observed in northern Germany purely a result of past events (natural and/or anthropogenic) or are they imbedded in ongoing processes?

To answer this question, an innovative multi-methodological approach was used. Long-term soil erosion and weathering rates were quantified using cosmogenic ^{10}Be (*meteoric* and *in situ*). Short-term erosion rates were estimated using $^{239+240}\text{Pu}$ isotopes. Moreover, palaeosurfaces (buried soil horizons) were dated using radiocarbon (^{14}C). Only few studies have used these isotopes to calculate time-trends for a given site and soil profile (O’Farrell et al., 2007; Zollinger et al., 2015).

1.6 Thesis Outline

This thesis is arranged among three research chapters that cover the main objective and multiple research questions, and one chapter in which the main findings are intertwined to answer the research questions.

In the “*Introduction*” (**Chapter 1**), are defined the research objectives and aim. It also provides general information on the scientific background and relevance of this research study.

Chapters 2-4 based on published, internationally peer-reviewed papers.

Chapter 2 “*Tracing the temporal evolution of soil redistribution rates in an agricultural landscape using $^{239+240}\text{Pu}$ and ^{10}Be* ” investigates short- and long-term soil redistribution rates in a hummocky ground moraine landscape with agricultural land use (CarboZALF-D site). This study shows that the short-term mass erosion and accumulation rates – calculated using $^{239+240}\text{Pu}$ – are about one order of magnitude higher than long-term redistribution rates – using both in situ and meteoric ^{10}Be . Moreover, the multi-isotope method used, identifies periods of erosion and deposition, confirming the ‘time-split approach’ of distinct different phases (progressive/regressive) in soil evolution.

Chapter 3 “*Soil erosion along a transect in a forested catchment: recent or ancient processes?*” explores the possible causes responsible for peculiar soil patterns (very shallow thickness on crest positions and buried soils on slope positions) of forest soils in northern Germany (Melzower Forst). No relationship of Pu-based erosion rates to any relief parameter was found. Although, $^{239+240}\text{Pu}$ inventories showed a very high spatial variability, soil erosion and deposition are negligible during the last 55 years. Therefore, the soil patterns are a result of natural events and/or anthropogenic activities during or before medieval times.

Chapter 4 “ *^{10}Be and ^{14}C data provide insight on soil mass redistribution along gentle slopes and reveal ancient human impact*” complements the two previous studies (Chapter 2 and 3) calculating long-term soil redistribution rates on forest soils of Melzower Forst comparing them with those obtained from agricultural soils of CarboZALF-D site. This research shows that a strong erosion impulse or event have occurred between 4.5 and 6.8 kyr BP indicating an earlier human impact on soil erosion than previously postulated (~ 3 kyr earlier). This finding relates with previous studies that report first settlements in the region around 6.8 kyr BP. Furthermore, soil redistribution rates in the forest and in agricultural soils are surprisingly similar.

Chapter 5 “*Conclusions and outlook*” depicts the main findings of the research chapters. It also provides a synthesis of the take-home messages and an outlook on future needs and challenges.

Chapter 2. Tracing the temporal evolution of soil redistribution rates in an agricultural landscape using $^{239+240}\text{Pu}$ and ^{10}Be

Abstract

Two principal groups of processes shape mass fluxes from and into a soil: vertical profile development and lateral soil redistribution. Periods having predominantly progressive soil forming processes (soil profile development) alternate with periods having predominantly regressive processes (erosion). As a result, short-term soil redistribution — years to decades — can differ substantially from long-term soil redistribution; i.e., centuries to millennia. However, the quantification of these processes is difficult and consequently their rates are poorly understood. To assess the competing roles of erosion and deposition we determined short- and long-term soil redistribution rates in a formerly glaciated area of the Uckermark, NE Germany. We compared short-term erosion or accumulation rates using $^{239+240}\text{Pu}$ and long-term rates using both in situ and meteoric cosmogenic ^{10}Be . Three characteristic process domains have been analysed in detail: a flat landscape position having no erosion/deposition, an erosion-dominated mid-slope, and a deposition-dominated lower-slope site. We show that the short-term mass erosion and accumulation rates are about one order of magnitude higher than long-term redistribution rates. Both, in situ and meteoric ^{10}Be provide comparable results. Depth functions, and therefore not only an average value of the topsoil, give the most meaningful rates. The long-term soil redistribution rates were in the range of $-2.1 \text{ t ha}^{-1}\text{yr}^{-1}$ (erosion) and $+0.26 \text{ t ha}^{-1}\text{yr}^{-1}$ (accumulation) whereas the short-term erosion rates indicated strong erosion of up to $25 \text{ t ha}^{-1}\text{yr}^{-1}$ and accumulation of $7.6 \text{ t ha}^{-1}\text{yr}^{-1}$. Our multi-isotope method identifies periods of erosion and deposition, confirming the ‘time-split approach’ of distinct different phases (progressive/regressive) in soil evolution. With such an approach, temporally-changing processes can be disentangled, which allows the identification of both the dimensions of and the increase in soil erosion due to human influence.

Published as: Calitri, F., Sommer, M., Norton, K., Temme, A., Brandová, D., Portes, R., Christl, M., Ketterer, M. E., and Egli, M. (2019) Tracing the temporal evolution of soil redistribution rates in an agricultural landscape using $^{239+240}\text{Pu}$ and ^{10}Be . *Earth Surf. Process. Landforms*, 44: 1783– 1798. <https://doi.org/10.1002/esp.4612>.

2.1 Introduction

Soils are the result of environmental and historical factors (Birkeland et al., 2003; Jenny, 1984). Although it is often not directly perceivable, soils are not static and may be highly dynamic over multi-annual timescales. Three sets of processes shape these dynamics: weathering, soil profile development and lateral redistribution of material (erosion and deposition). It is well-known that these interact strongly (i.e., co-evolve) and affect the soil. The co-evolution and changing drivers, such as climate and land use, lead to complex soil development in time and space. Periods having dominantly progressive processes (e.g., soil deepening, weathering) alternate with periods having dominantly regressive processes (e.g., erosion) due to fast and substantial changes in driving influences. As a result, short-term soil redistribution (years to decades) can differ substantially from long-term soil redistribution (centuries to millennia). Therefore, all three sets of processes must be quantified and understood in relation to each other to provide predictions of soil change due to changing climate and land usage. In landscape evolution studies, soil depth is often considered a function of soil production and denudation (e.g. erosion, leaching and chemical weathering; (Alewell et al., 2014; Egli et al., 2014). The necessary implication is that where soil is present, soil production has been at least equal to or greater than denudation over long timescales. Processes such as clay translocation, bioturbation and gleyzation change soil properties without (necessarily) changing soil thickness.

Owing to an increased disequilibrium in the recent past caused by climate change and land usage, landscapes and soils may change rapidly, but quantitative data are mostly missing. Knowledge about the rates of recent and predominantly anthropogenic processes compared to the ‘natural’ and long-term rates is crucial for prevention and mitigation, because this enables the magnitude of the induced changes to be estimated.

Soil production, formation and/or denudation rates are often obtained by measuring cosmogenic isotopes or by comparing soils having different ages (space-for-time approach). Using these techniques, only a single value can be obtained per site: i.e., the average rate over the entire time of soil evolution. The assumption is that the environmental conditions did not change over the considered period and that soil evolution has been progressive and constant. However, changing environmental conditions and soil-landscape development themselves can lead to an acceleration, deceleration or reversal of process rates, which is an example of co-evolution (Phillips, 2015). For instance, in sensitive alpine environments or in strongly

agriculturally-used areas, a recent acceleration of geomorphic processes can be detected or postulated (Kappler et al., 2018; Sommer et al., 2008). This affects soil profile development.

Erosion and denudation rates can be determined using a set of isotope methods. Because these isotopes cover different time ranges, time-trends for a given site and soil profile can be calculated — something that has not often been undertaken (O’Farrell et al., 2007; Zollinger et al., 2015). Such an approach would enable to decipher whether rates have increased or decreased during the last few decades and to relate this to human impact or climate change. A wide array of methods is available to quantify lateral redistribution of soil material in landscapes over short and long timescales.

A) Decadal (short-term) erosion rates: fallout radionuclides (FRN, e.g., ^{137}Cs , ^7Be , $^{210}\text{Pb}_{\text{ex}}$) have been successfully used for soil redistribution measurements since the 1970s (Zapata, 2003). $^{239+240}\text{Pu}$ was globally dispersed primarily during thermonuclear weapon testing mainly between 1952 and 1964 (Ketterer & Szechenyi, 2008). Relatively few studies have used $^{239+240}\text{Pu}$ as a soil erosion tracer (Alewell et al., 2014; Hoo et al., 2011; Ketterer & Szechenyi, 2008; Schimmack et al., 2001). In Europe, $^{239+240}\text{Pu}$ has advantages over ^{137}Cs in areas where the Chernobyl fallout was detectable and where at the same time a snow-cover was present (Alewell et al., 2014). Moreover, $^{239+240}\text{Pu}$ isotopes have a much longer half-life compared to ^{137}Cs (i.e., ^{239}Pu $t_{1/2} = 24110$ a, ^{240}Pu $t_{1/2} = 6561$ a, ^{137}Cs $t_{1/2} = 30.2$ a) and thus a large part of ^{137}Cs has already decayed in the meantime.

B) Millennial (long-term) erosion rates: long-term soil erosion and denudation rates can be assessed e.g., by using meteoric or in situ produced ^{10}Be (^{10}Be $t_{1/2} = 1.36$ Ma). While meteoric ^{10}Be is produced in the atmosphere and deposited on Earth’s surface, in situ ^{10}Be builds up predictably with time in minerals exposed to cosmic rays: therefore, both deposition and erosion can be assessed from meteoric ^{10}Be (using inventories similar to fallout radionuclide methods). Burial may be apparent from in situ ^{10}Be profiles, but so far it is not possible to derive sedimentation rates from in situ ^{10}Be . The erosion/denudation and soil production rate are preserved in the signal of cosmogenic nuclides in stream sediments (e.g., Norton et al., 2010) or directly in a soil (e.g., Heimsath et al., 1997).

Using cosmogenic nuclides, a positive relationship between physical erosion and chemical weathering has been detected in some landscapes (Dixon et al., 2009; Larsen et al., 2014). Highly eroding soils are continuously rejuvenated and behave like young soils (Alewell et al., 2014) and thus show high soil production rates (Dahms et al., 2012).

Although in situ ^{10}Be is widely used in quantifying erosion or denudation rates, it is still difficult to derive soil redistribution rates. Catchment-wide denudation rates are not only reflecting soil erosion and accumulation, but may also include mass wasting (Norton et al., 2010). Another problem is that often steady-state conditions are assumed to calculate denudation or soil production rates; an assumption that may lead to unrealistic representations of the dynamics of pedogenesis and weathering profile evolution (Phillips, 2010) if the requirements for a steady-state are not fulfilled. Soil denudation rates are rarely estimated from profile data using in situ ^{10}Be (e.g., Hidy et al., 2010; Schaller et al., 2010). With known surface ages, denudation rates can also be calculated using meteoric ^{10}Be (Zollinger et al., 2017) even under a non-steady-state situation. A comparison between these two methods has very rarely been done for the same or similar sites (Schoonejans et al., 2017). Recently, new mathematical approaches were developed to estimate erosion and accumulation rates ('MODERN'; Arata, Alewell, et al., 2016; Arata, Meusburger, et al., 2016). The code MODERN has been tested for short-term rates (^{137}Cs and $^{239+240}\text{Pu}$) and not yet applied for meteoric ^{10}Be : also, these approaches do not require steady-state conditions.

We therefore aim at using and comparing the main results of these methods. This can be done in an area that is known to have experienced recent acceleration of geomorphic processes., The main focus of this paper is consequently threefold, concentrating on the following research questions: 1) How do long-term rates of lateral soil redistribution differ from short-term rates? 2) Are rates calculated from in situ ^{10}Be comparable to those of using meteoric ^{10}Be ? 3) How do the results vary depending on the chosen modelling approach?

2.2 Study area

The investigation area is located in the Uckermark region, NE-Germany, a formerly glaciated, hummocky ground moraine landscape (Figure 2.1). According to Lüthgens et al. (2011), an active ice margin was southwestern of this area between 20.1 (± 1.6) and 19.4 (± 2.4) ka. Hughes et al. (2016) and Stroeven et al. (2016) document that the Uckermark became ice-free about 19 – 20 ka BP. According to the geological map of Brandenburg (<http://www.geo.brandenburg.de/boden/>; Geologische Übersichtskarte, Dezernat Geologische Landesaufnahme/Geoarchiv), the morainic deposits are from the Pleistocene, are Si-rich (granitic material), have a marly character and also contain carbonates. Loess, a particular feature of proglacial areas, does not occur in this region, because it was fully glaciated. Major loess deposits are found south of Berlin (Haase et al., 2007). In the study area, the parent material for soil development is an illitic, calcareous glacial till.

One major characteristic of the ground moraine landscape is the undulating, hummocky topography having kettle holes (Figure 2.2). The altitudinal differences between the hilltops and kettle holes are relatively small (5 to 10 metres). Consequently the altitude ranges between about 40 to 60 m a.s.l. The soil pattern of the region is related to topography and the heterogeneity of Pleistocene deposits. The natural soil pattern has been strongly modified by soil erosion over the past centuries (Deumlich et al., 2010; Kappler et al., 2018; Koszinski et al., 2013; Sommer et al., 2008). Due to the lack of linear drainage patterns, the kettle holes began to be filled in by eroded soil material. Recently, only 20% of the arable land shows non-eroded soils (Albic Luvisols), mainly at lower mid-slopes. Extremely eroded soils (Calcaric Regosols) occur at convex landscape positions as well as steep slopes and strongly eroded soils (Calcic Luvisols) reach from hilltops to upper mid-slopes. Footslopes and closed depressions comprise 20% of the landscape. Here, groundwater-influenced colluvial soils (Gleyic-Colluvic Regosols, partly overlying peat) have developed. Generally, the soil landscape reveals strong local gradients in wetness (< 100m distance). The soil texture is mainly loamy sand to sandy loam.

The area has been used for agriculture since Neolithic times due to its fertile soils (Wetzel, 1996). A strong intensification of land-usage occurred in medieval times, with deforestation accompanied by locally severe water erosion during catastrophic rainfall events (Bork, 2006). More distinct area-wide changes in land-usage occurred after World War II. However, only in the 1970s and 1980s agriculture developed towards an industrial organised production system.

This caused deeper soil tillage practices, enabled by more powerful farm machinery. A reduction of individual field sizes started in the early 80s, but tractor power still continued to increase (Sommer et al., 2008).

The soil profiles were taken at the experimental site ‘CarboZalf-D’ of the Leibniz Centre for Agricultural Landscape Research (ZALF) (Fig.1). This experimental site was established in 2010 to study the dynamics and drivers of the erosion-carbon nexus (Sommer et al., 2016). It is intensively studied in terms of soil thickness (van der Meij et al., 2017), soil organic carbon patterns and short-term erosion rates (Aldana Jague et al., 2016), water and DOC/DIC fluxes (Gerke et al., 2010; Rieckh et al., 2014) as well as CO₂ fluxes (Hoffmann et al., 2017). The climate is sub-continental with a mean annual air temperature of 8.7 °C and an annual precipitation of 483 mm.

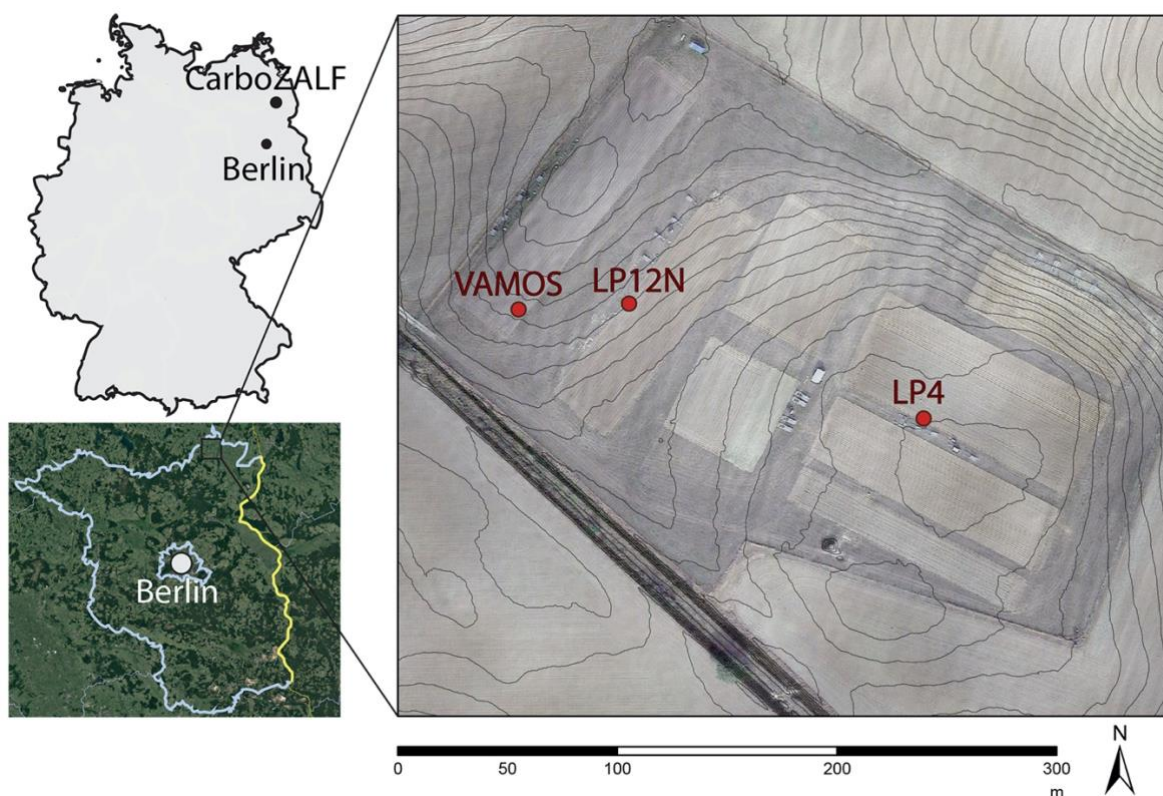


Figure 2.1. Overview of the investigation area and the ZALF experimental site with the location of the sampling sites LP1, LP12 and VAMOS.

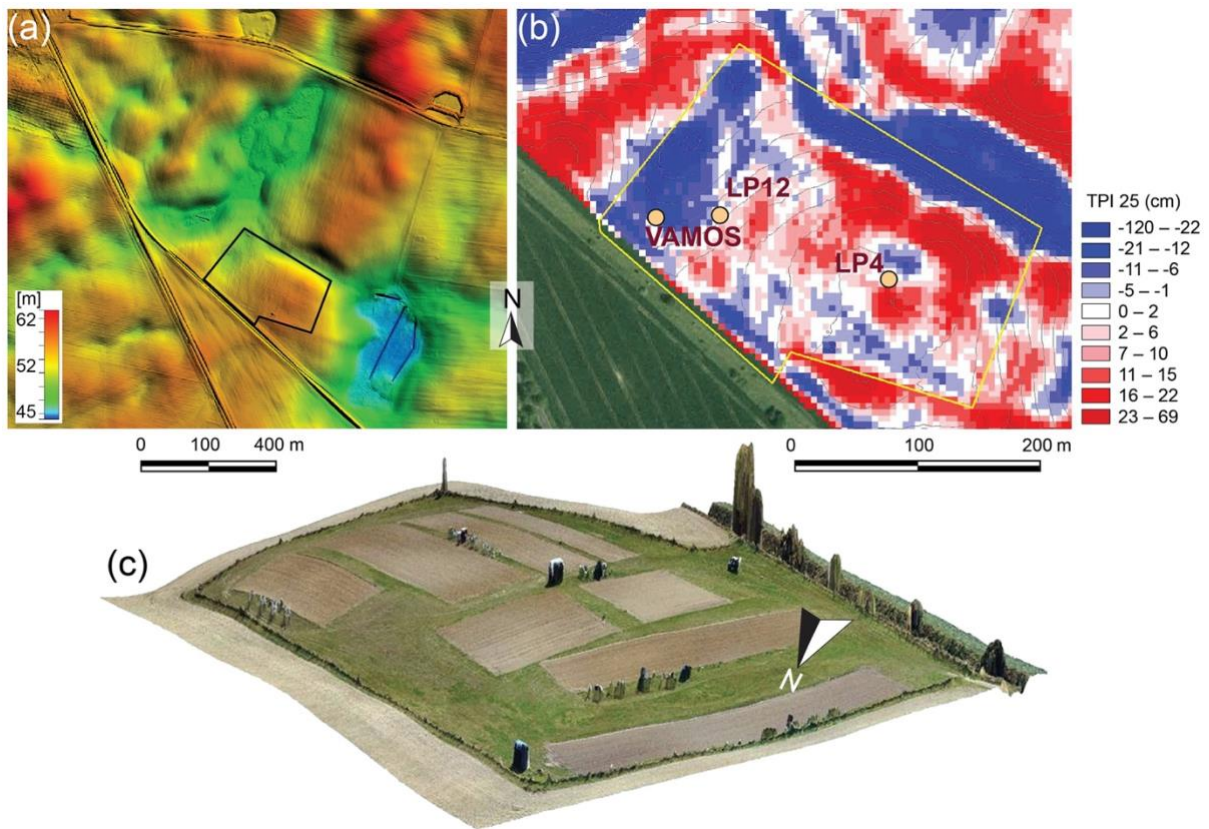


Figure 2.2. Detailed topographic overview showing a) the typical, hummocky ground moraine landscape with kettle holes and b) the topographic position index (TPI; 25m grid; Deumlich et al., 2010). The TPI compares the elevation of each grid cell in a DEM (digital elevation model) with the mean elevation of a neighbourhood defined by circles of arbitrary radius. Positive TPI values represent grid cells higher than their surroundings whereas negative ones are lower than their surroundings. The TPI delineates small depressions (negative values), small hummocks (positive values = slope and summits) and ridges. b) drone image of the CarboZALF experimental site.

2.3 Materials and Methods

2.3.1 Sampling strategy

Erosion and deposition are reflected in a catena of soil profiles (Milne, 1935) with no or almost no erosion on flat positions (hilltop), strong erosion on the mid-slope and accumulation of soil material at the toeslope position. These three characteristic process domains were chosen within the CarboZALF-D experimental site (Table 2.1). The site LP4 is located at a flat landscape position (reference site), LP12N at a mid-slope position (erosion dominated), and VAMOS at the lower part of the mid-slope (deposition dominated, Figures. 2.1 and 2.2). LP4 has an Albic Luvisol, LP12 a Calcic Luvisol and VAMOS a Colluvic Regosol over a buried Gleyic Luvisol.

Table 2.1. Characteristics of the study sites.

Site	Coordinates (° N/E)	Elevation (m asl)	Slope angle (%)	Parent material	Land use	Soil type (IUSS 2014)
LP4	53.379317/ 13.786355	59	0.5	Illitic, calcareous till	Arable land	Albic Luvisol (Cutanic)
LP12N	53.379798/ 13.784539	54	5.7	Illitic, calcareous till	Arable land	Calcic Luvisol (Cutanic)
VAMOS	53.379712/ 13.783665	54	4.1	Sandy colluvium / illitic, calcareous till	Arable land	Colluvic Regosol (Arenic) over Gleyic Luvisol (Loamic)

An average erosion rate since the beginning of soil formation, and thus millennia, can be determined using ^{10}Be . For this purpose, ^{10}Be has to be measured within a soil profile. This will provide information (erosion, accumulation) of a specific topographic position. Principally, both types of ^{10}Be (i.e., in situ and meteoric) should result in similar rates because both started to accumulate since the start of soil formation. Short-term erosion or accumulation rates, i.e., rates of the last 5 – 6 decades, can be detected using $^{239+240}\text{Pu}$ (Alewell et al., 2014; Ketterer & Szechenyi, 2008). Therefore, soil redistribution rates determined using ^{10}Be and $^{239+240}\text{Pu}$ enable a comparison between long-term, average processes and present-day processes.

At each site (LP4, LP12 and VAMOS), three soil cores down to the parent material were taken to i) cover to a certain degree spatial variability and ii) to have enough material for in situ ^{10}Be . To get enough material for in situ ^{10}Be , pooled samples per horizon and depth had to be taken: around 5 – 6 kg of soil material was necessary to obtain enough quartz (obtained from the 0.25 – 0.50 mm fraction; see below). For meteoric ^{10}Be , an aliquot of a few hundred grams was separated.

A different procedure had to be applied for the $^{239+240}\text{Pu}$ that was used to assess the current soil redistribution rates. Since these isotopes were emitted during the nuclear weapon tests of the mid-20th century (maximum in 1963 – 1964), an average soil redistribution rate for the last ~55 years can be obtained (Wallbrink & Murray, 1993). When using $^{239+240}\text{Pu}$ isotopes as tracers for soil redistribution, an undisturbed reference soil — usually having a flat topography — is compared with an erosion/accumulation site. In addition to the previously mentioned soil cores for ^{10}Be measurements, other four to six replicate cores were sampled at all sites down to 60 cm depth. Because the Ap horizon has a homogeneous material due to soil-mixing and ploughing (30 cm), the Pu content was only measured in this horizon and the horizon below to a maximum depth of 60 cm.

2.3.2 Soil chemical and physical analyses

Bulk soil samples were air dried, gently crushed and sieved at 2 mm to separate the fine earth fraction (< 2 mm) from gravel (> 2 mm). The particle size distribution of the fine earth was determined by a combined wet sieving (> 63 μm) and pipette (< 20 μm) method (Schlichting et al., 1995). Pretreatment for particle size analysis was done by (i) wet oxidation of organic matter using H_2O_2 (10 Vol.%) at 80 °C, (ii) carbonate dissolution with 0.5 N HCl (80°C) and (iii) dispersion by shaking the sample end over end for 16 h with a 0.01 M $\text{Na}_4\text{P}_2\text{O}_7$ -solution (Schlichting et al., 1995). Soil pH was measured using a glass electrode in 0.01 M CaCl_2 suspensions at a soil to solution ratio of 1:2.5 (w/v) after a 60 minutes equilibration period (Schlichting et al., 1995). Total carbon and nitrogen contents were analysed by dry combustion using an elemental analyser (Vario EL, Elementar Analysensysteme, Hanau, Germany). Carbonate (CaCO_3) was determined conductometrically using the Scheibler apparatus (Schlichting et al., 1995). Organic carbon (C_{org}) was computed as the difference between total carbon and carbonate carbon. Analyses of basic soil properties were performed in two lab replicates per sample.

Total elemental contents were determined using X-ray fluorescence (XRF). Powder samples (in duplicates) of approximately 5 g material were analysed using an energy dispersive He-flushed X-ray fluorescence spectrometer (ED-XRF, SPECTRO X-LAB 2000, SPECTRO Analytical Instruments, Germany). The quality of the analyses was checked using a soil reference material (Reference Soil Sample CCRMP SO-4, Canada Centre for Mineral and Energy Technology) with certified total element concentrations.

2.3.3 Radiocarbon dating of organic matter fractions

The site VAMOS consists of an older buried soil and a newer soil on top of it. We tried to date when this accumulation occurred on top of the buried soil. To achieve this goal, soil organic matter of the buried soil had to be radiocarbon dated. Soil organic carbon is known to contain several fractions: stable fractions having an old radiocarbon age up to labile fractions having a fast turnover (Eusterhues et al., 2005; Favilli et al., 2009; Helfrich et al., 2007; Kögel-Knabner et al., 2008). To approximately date the fossil A horizon at the site VAMOS, the particulate organic matter (POM) and the H₂O₂-resistant fraction were dated. The date of these two fractions indicates the earliest time that a soil was overridden and approximately when the first organic matter was incorporated into the soil (Favilli et al., 2009). The extraction of the organic matter fractions was done as described in (Favilli et al., 2008).

The carbon ratios were measured by Accelerator Mass Spectrometry (AMS) using 0.2 MV radiocarbon dating facility (MICADAS) of the Ion Beam Physics at the Swiss Federal Institute of Technology Zurich (ETHZ). The calendar ages were obtained using the OxCal 4.3 calibration program (Bronk Ramsey, 2001, 2009) based on the IntCal 13 calibration curve (Reimer et al., 2013). Calibrated ages are reported with their 2 σ error range.

2.3.4 ¹⁰Be analyses

Both meteoric and in situ produced ¹⁰Be were used as a tracer for long-term redistribution processes (Portenga & Bierman, 2011; Zollinger et al., 2017).

Meteoric ¹⁰Be

Meteoric ¹⁰Be was extracted from the soil samples using a modified method from (Horiuchi et al., 1999) and (Egli et al., 2010). In brief, 2 g soil sample (< 2 mm fraction) were needed for meteoric ¹⁰Be. The sample was heated at 550 °C for 3 h to remove organic matter. 1 mg of ⁹Be(NO₃)₂ (carrier) and 8 ml of HCl (16% v/v) were added to the sample and leached overnight in a shaker. The sample was subsequently centrifuged and the liquid collected. Thereafter, 5 ml of HCl were added to the solid part and leached overnight a second time. The liquid was collected together with the first leachate and heated at 80 °C to reduce the volume to ca. 10 ml. In a next step, NaOH (16% v/v) was added until the pH reached the value of 2. To complex metals such as Fe and Mn, 1 ml of 10% EDTA solution was added. The pH value was then increased to 8 by adding NaOH to precipitate the gel containing Be(OH)₂ and Al(OH)₃. NaOH was added to the gel to reach a pH value of 14. Be(OH)₂ and Al(OH)₃ re-dissolved in the solution that was separated from the gel by centrifugation. HCl (to reduce the pH value to 2) and thereafter 1 ml of EDTA were added. The gel containing Be(OH)₂ and Al(OH)₃ was precipitated with NH₄OH and centrifuged. Oxalic acid (0.4 M) was added to the gel to dissolve the sample, and beryllium was separated from Al using cation exchange columns. The sample was heated at 80°C to reduce the volume to about 10 ml and Be(OH)₂ was precipitated using NH₄OH. The gel was then dried in the oven at 70 °C overnight and heated at 200 °C on a heating plate. At the end, the gel was calcinated for 2 h at 850 °C in the oven to obtain BeO. Finally, the BeO was mixed with Nb powder and pressed into a sample holder for accelerator mass spectrometry (AMS).

The ¹⁰Be/⁹Be ratios were measured at the ETH Zurich AMS system Tandy (Christl et al., 2013) and normalised to the ETH Zurich in house AMS standard S2007N (¹⁰Be/Be = 28.1 x 10⁻¹² nominal) which has been calibrated relative to ICN 01-5-1 (¹⁰Be/⁹Be = 2.709 x 10⁻¹¹ nominal) (Nishiizumi et al., 2007) both associated with a ¹⁰Be half-life of 1.387±0.012 My (Chmeleff et al., 2010; Korschinek et al., 2010).

In situ ¹⁰Be

In situ ¹⁰Be was extracted from the soil samples using a modified method from (Kohl & Nishiizumi, 1992). Samples were sieved and the quartz isolated by treating the 0.25 mm – 0.50 mm fraction with *aqua regia* to destroy organic matter contaminations and any calcareous components. After a 1 h treatment with 0.4% HF, we used a floatation system to physically

separate feldspar and mica components from quartz. A soil sample of 100 g for each horizon was leached in 500 ml of 4% hydrofluoric acid (HF) five to six times for seven days each time in a shaker to obtain pure quartz. 0.35 ml of $^9\text{Be}(\text{NO}_3)_2$ (carrier) was added to 40 g of quartz with highly concentrated HF (40% v/v) until the quartz was dissolved. 10 ml of water were added to the dry sample and heated for 3 h at 80 °C. Afterwards, the sample was centrifuged, the liquid part decanted in a centrifuge tube and HCl (37% v/v) was added to reach a concentration of 6 M. Anion exchange columns were used to remove Fe from the solution. The sample was completely dried and oxalic acid (0.4 M) added to separate Al from Be using cation exchange columns. $\text{Be}(\text{OH})_2$ was precipitated using NH_4OH . The same process as for meteoric ^{10}Be was then used to obtain the $^{10}\text{Be}/^9\text{Be}$ ratios.

2.3.5 Determination of $^{239+240}\text{Pu}$ activities

The fallout nuclides $^{239+240}\text{Pu}$ were used to estimate short-term (50 – 55 years) effective soil redistribution.

Pu isotopes measurements were conducted according to (Ketterer et al., 2004). Prior to mass spectrometry analysis, approximately 5 g of milled fine earth were dry-ashed for 18 h at 600 °C to remove the organic matter and spiked with 30 pg (c. 0.0044 Bq) of a ^{242}Pu tracer solution (NIST 4334). The samples were leached with 16 M HNO_3 overnight at 80 °C and subsequently filtered and adjusted to a concentration of 8 M HNO_3 . Pu species were adjusted to the Pu (IV) oxidation state using first an acidified $\text{FeSO}_4 \cdot 7\text{H}_2\text{O}$ solution (2 mg/mL of leached solution) and subsequently a NaNO_2 solution (20 mg/mL of leached solution). The samples were then heated at 75 °C for 2 h. Tetravalent Pu was separated from the leached solution using a Pu-selective TEVA resin (2 mg of TEVA per mL of leached solution). Following occasional agitation for 2 h, the resin was collected in a pipette tip equipped with a glass-wool plug. This disposable column was rinsed with 2 M aqueous HNO_3 to remove unretained matrix elements (e.g., U), then rinsed with 8 M HCl to elute Th and finally rinsed again with 2 M aqueous HNO_3 (rinse volume: 1 ml per 30 mg of TEVA). Pu was eluted using 0.05 M aqueous ammonium oxalate. Data quality was evaluated through the analysis of blanks (soils or rocks devoid of Pu), duplicates and control samples of known $^{239+240}\text{Pu}$ activities (Standard Reference material 4350b — River sediment for radioactivity measurements from NIST). Activities of $^{239+240}\text{Pu}$ were measured using a Thermo X Series II quadrupole ICPMS, located at Northern Arizona University. The ICPMS instrument is equipped with an APEX HF high-efficiency sample

introduction system. The masses of ^{239}Pu and ^{240}Pu in the samples were converted into the summed activity $^{239+240}\text{Pu}$.

2.3.6 Calculation of mass redistribution rates

Several methods were used to calculate soil redistribution rates from ^{10}Be and $^{239+240}\text{Pu}$ measurements.

Long-term rates using meteoric ^{10}Be

Soil erosion rates can be estimated on the basis of meteoric ^{10}Be (Egli et al., 2010; Maejima et al., 2005). Knowing the age of a landform by independent dating, soil erosion can be calculated by comparing the effective abundance of ^{10}Be measured in the soil having the theoretically necessary abundance for the expected age. The soil age, i.e., surface age, of the investigated site was estimated to be 19 to 20 ka based on the timing of deglaciation (Hughes et al., 2016; Lüthgens et al., 2011; Stroeven et al., 2016). Accordingly, the expected abundance of meteoric ^{10}Be was calculated. Considering no erosion, the surface age of a soil is given by:

$$t = -\frac{1}{\lambda} \ln \left(1 - \lambda \frac{N_{exp}}{q} \right) \quad (2.1)$$

and:

$$N_{exp} = q \frac{e^{-\lambda t} - 1}{-\lambda} \quad (2.2)$$

where N_{exp} (atoms cm^{-2}) = expected ^{10}Be inventory in the profile (according to the age of the soil; i.e. accumulated ^{10}Be due to atmospheric deposition in the soil and assuming no erosion), q (atoms $\text{cm}^{-2} \text{yr}^{-1}$) = annual ^{10}Be deposition rate (calculated according to Masarik & Beer, 2009; Willenbring & von Blanckenburg, 2010), λ ($4.997 \times 10^{-7} \text{a}^{-1}$) = decay constant of ^{10}Be and t (a) = surface age. As reported in (Egli et al., 2010), the ^{10}Be deposition rates are mostly unknown for a specific area and have to be estimated. (Masarik & Beer, 2009) showed that the deposition rate of ^{10}Be is primarily a function of the geomagnetic latitude — for the study area, the deposition rate is $\sim 10^6$ atoms $\text{cm}^{-2} \text{yr}^{-1}$. With soil erosion, equation 1 is extended to the following non-steady-state approach (Zollinger et al., 2017):

$$t = -\frac{1}{\lambda} \ln \left(1 - \lambda \frac{N}{q - \rho C_{10\text{Be}} f E_{soil}} \right) \quad (2.3)$$

and:

$$E_{soil} = \frac{1}{\rho f C_{10Be}} \left(\frac{\lambda N}{e^{-\lambda t} - 1} + q \right) \quad (2.4)$$

where C_{10Be} (atoms g^{-1}) = average ^{10}Be in the top eroding horizon, E_{soil} = soil erosion rate (in this equation as cm yr^{-1}), f = fine earth fraction and ρ (g cm^{-3}) = the bulk density of the top horizons. One problem with this approach is that C_{10Be} evolves over time. This can approximately be solved by using an average value of C_{10Be} between $t = 0$ and t (corresponding to $\sim 0.5 \times C_{10Be(\text{today})}$) and by assuming that erosion losses are concentrated on the topsoil horizon (e.g., 0 – 20 cm). We have

$$\frac{N_{exp-N}}{t} = \frac{\Delta N}{t} = E(N) \quad (2.5)$$

where $E(N)$ (atoms $\text{cm}^{-2} \text{yr}^{-1}$) = annually eroded ^{10}Be . The annual erosion rate (E_{soil} ; cm yr^{-1}) is then derived as:

$$E_{soil} = \frac{z_{top} E(N)}{N_{top}} \quad (2.6)$$

where N_{top} = the inventory of ^{10}Be in the topsoil (having the thickness z_{top}). To convert erosion rates from cm/yr to $\text{t km}^{-2} \text{yr}^{-1}$, E_{soil} has to be multiplied by soil density and referred to km^2 . The ^{10}Be content due to pre-exposure was derived from concentrations of ^{10}Be of the C-horizon.

For the purpose of comparison, an additional procedure (Lal, 2001) to estimate erosion rates using meteoric ^{10}Be was used. The soil erosion (E_{soil}) rate is given by:

$$E_{soil} = z_0 K_E \quad (2.7)$$

and:

$$K_E = \frac{N_D}{N_S} \left[\frac{Q + q_a}{N_D} \right] - \lambda \quad (2.8)$$

where z_0 (cm) = thickness of topsoil horizons (comprising O and A horizon), K_E = first-order rate constant for removal of soil from the topsoil layer, N_D (atoms cm^{-2}) = ^{10}Be inventory in the D layer (= remainder of the soil profile comprising B and C horizons), N_S (atoms cm^{-2}) = ^{10}Be inventory in topsoil horizons, Q (atoms $\text{cm}^{-2} \text{yr}^{-1}$) = flux of atmospheric ^{10}Be into the topsoil and q_a (atoms $\text{cm}^{-2} \text{yr}^{-1}$) = flux of meteoric ^{10}Be .

Long-term rates using in situ ¹⁰Be

For sediments that are not vertically mixed, a depth profile can be used to account for a change in the in situ terrestrial cosmogenic nuclides production rate as secondary cosmic ray flux attenuates through the material (Hidy et al., 2010). For nuclides that are produced only from high energy nuclear and muogenic reactions (e.g., ¹⁰Be, ¹⁴C, ²⁶Al, ²¹Ne), the concentration C (atoms g⁻¹) for a specific nuclide m as a function of depth z (cm), erosion rate ε (cm yr⁻¹) and exposure time t can then be written as

$$C_m(z, \varepsilon, t) = \sum_i \frac{P(0)_{m,i}}{\left(\frac{\varepsilon \rho_z}{\Lambda_i} + \lambda_m\right)} \cdot \exp\left(-\frac{z \rho_z}{\Lambda_i}\right) \cdot \left[1 - \exp\left(-t \left(\frac{\varepsilon \rho_z}{\Lambda_i} + \lambda_m\right)\right)\right] + C_{inh,m} \cdot \exp(-\lambda_m t) \quad (2.9)$$

where i represents the various production pathways for nuclide m (neutron spallation, fast muon spallation, and negative muon capture), $P(0)_{m,i}$ is the site-specific surface production rate for nuclide m via production pathway i (in this case 4.29 atoms g⁻¹ yr⁻¹), λ_m is the decay constant for radionuclide m (a⁻¹), ρ_z is the cumulative bulk density at depth z (g cm⁻³), Λ_i is the attenuation length of production pathway i (160 g cm⁻² for neutrons), and $C_{inh,m}$ is the inherited (depositional) concentration of nuclide m (atom g⁻¹). The depth trends were modelled using equation 9 and a Monte Carlo simulation. Each individual, modelled depth trend of the ¹⁰Be content was compared to the observed values and iteratively fitted (using erosion rates and inherited ¹⁰Be) until the differences were minimal. Modelling becomes more difficult when this depth trend has been partially influenced by vertical mixing (e.g., due to ploughing, clay translocation). With enough data points at greater soil depth, the trend can nonetheless be traced.

In the case of well-mixed soils, ¹⁰Be can still be used to determine erosion rates. (i.e., Granger & Riebe, 2007). This is valid at both the landscape scale from streams sediments and at the plot scale for soil production rates (Granger & Riebe, 2014; Norton et al., 2010). As such, we also used the ‘CRONUS’ online calculator for erosion rate estimates (Balco et al., 2008); <http://hess.ess.washington.edu/>) to test the applicability of this simplification in complex agricultural landscapes. Erosion rates were calculated using an average ¹⁰Be concentration of the top ~60cm assuming that these represent an average surface content, as would be the case for complete mixing.

Short-term rates

$^{239+240}\text{Pu}$ inventories (Bq m^{-2}) were calculated based on the following equation:

$$As = \frac{1}{S} \sum_i M_{Ti} C_i \quad (2.10)$$

Where C_i = activity of the i^{th} sub-sample depth increment (Bq kg^{-1}), M_{Ti} = total mass of the i^{th} sample depth increment (kg) and S = area of the horizontal core cross (m^2). Soil redistribution rates were obtained with a comparison of the isotope inventory of an eroding point and a local reference inventory where neither erosion nor soil accumulation is expected. The profile distribution model (PDM) (Walling & Quine, 1990; XINBAO et al., 1990) has been used to convert $^{239+240}\text{Pu}$ inventories into soil redistribution rates (Zollinger et al., 2015):

$$A'(x) = A_{ref} (1 - e^{x/h_0}) \quad (2.11)$$

where $A'(x)$ = amount of isotope inventory above depth x (Bq/m^2), x = depth from soil surface expressed as mass between top and actual depth (kg m^{-2}), A_{ref} = reference inventory as mean of all reference sites (Bq m^{-2}) and h_0 = profile shape factor (kg m^{-2}) that is a coefficient describing the rate of exponential decrease in inventory with depth, for soil profiles in uncultivated sites. The erosion rate Y for a point of interest is calculated as:

$$Y = \frac{10}{t - t_0} \ln \left(1 - \frac{X}{100} \right) h_0 \quad (2.12)$$

Y = erosion rate ($\text{t ha}^{-1} \text{yr}^{-1}$), t = year of sampling, t_0 = '1963' (end of thermonuclear weapon testing), X = % reduction of total inventory (A_u [Bq m^{-2}]) in regard to the local reference value $(A_{ref} - A_u) / A_{ref} \times 100$.

Another possibility to calculate erosion or accumulation rates is an iterative mathematical approach (code MODERN; Arata, Alewell, et al., 2016; Arata, Meusburger, et al., 2016). One key advantage of MODERN is its ability to describe accurately specific depth distribution of any fallout radionuclide (FRN) in the soil, independent of its depth function's shape. The PDM is a very convenient model to estimate erosion rates of unploughed soils. However, as highlighted by (Walling et al., 2014), it involves a number of simplifying assumptions on the depth distribution of FRN in the soil. The underlying idea behind the model is the comparison of the depth profile of the reference site with the total inventory of a sampling site. MODERN returns soil erosion and deposition rates in terms of thickness of the soil layer affected by soil redistribution processes. To estimate the thickness of soil losses/gains, MODERN aligns the total inventory of the sampling site to the depth profile of the reference site (Arata, Alewell, et

al., 2016; Arata, Meusbürger, et al., 2016). Moreover, MODERN can be applied under various land-usage conditions (i.e., ploughed and unploughed soils; Arata, Alewell, et al., 2016; Arata, Meusbürger, et al., 2016). The original code MODERN was developed in Matlab™ and is publicly available. Despite the fact that MODERN has been written for FRN, it can also be applied to cosmogenic radionuclides such as meteoric ^{10}Be . In our case, MODERN could not be applied to Pu owing to the sampling design (too low resolution with soil depth).

2.3.7 Statistics and trend analyses

Linear and multiple linear regressions were carried out to help explain the behaviour of ^{10}Be in the soils and describe it as a function of controlling factors. All data that were considered for this analysis showed a normal distribution (Shapiro-Wilk test). In addition, the best-fit to in situ ^{10}Be concentration profiles were modelled using a time-integrated solution to Eq. 9. A Monte Carlo simulation was conducted for erosion rates varying from 0 to 0.02 cm yr^{-1} , exposure ages from 0 to 100 ka, and inherited nuclide concentration from 0 to $90000\text{ atoms g}^{-1}$ using MatlabR2017b.

2.4 Results

2.4.1 Physical and chemical soil properties

All studied soils have a sandy-loam or loam texture having a low gravel content (Table 2.2). Clay translocation as a main feature of the investigated soils can be easily seen (Figure 2.3). The silt content, as an indicator for loess input, is around 30% and varied insignificantly along the profiles (Table 2.2; Figure 2.3). Loess often also may contain fine sand (0.063 – 0.2 mm in diameter); but also here, no clear sign of a loess input can be detected. The topsoil at the three sites is slightly acidic with pH values ranging between 5.1 and 6.6. In the subsoil and close to the C horizon, both pH values and the content of calcium carbonate increase, with the highest carbonate content in the C horizon of site LP12N ($\text{CaCO}_3 = 14\%$). The soil organic carbon content (SOC) was generally low and ranged from 0.8 to 0.9% in the Ap horizon. Bulk density did not vary greatly along the LP4 profile whereas it increased with profile depth at the sites LP12N and VAMOS.

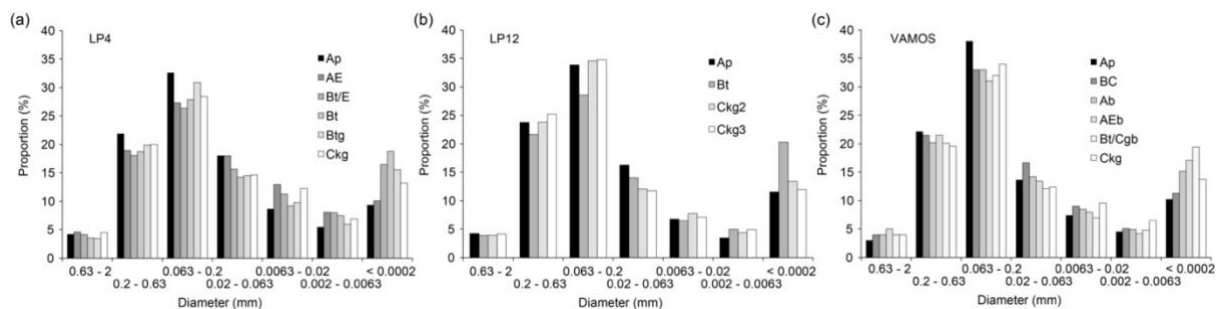


Figure 2.3. Detailed overview of grain sizes as a function of soil horizons for the sites a) LP4, b) LP12 and c) VAMOS.

Table 2.2. Physical and chemical characteristics of the investigated soils.

Site	Soil type (IUSS Working Group WRB, 2015) depth (cm)	Working Soil horizon (IUSS Working Group WRB, 2015)	>2mm (%)	Sand (%)	Silt (%)	Clay (%)	Bulk density (Mg/m ³)	pH (CaCl ₂)	SOC (%)	CaCO ₃ (%)	
LP4	Albic Luvisol (Cutanic)										
	0-30	Ap	3	59	32	9	1.76	5.53	0.78	-	
	30-45	E	3	50	37	13	1.79	6.28	0.30	-	
	45-60	Bt/E	4	49	35	16	1.67	6.37	0.30	-	
	60-95	Bt	2	50	31	19	1.76	6.79	0.29	-	
	95-165	Btg	2	54	30	16	1.73	7.24	0.26	-	
	165-180	Ckg	3	53	34	13	1.79	7.54	0.04	10.4	
LP12N	Calcic Luvisol (Cutanic)										
	0-30	Ap	3	62	27	12	1.48	6.56	0.83	-	
	30-50	Bt	2	54	26	20	1.60	6.98	0.39	1.4	
	50-60	Ckg1	2	54	26	20	1.60	6.98	0.39	10.7	
	60-120	Ckg2	3	62	24	13	1.77	7.66	0.11	14.3	
	120-160	Ckg3	4	64	24	12	1.83	7.76	0.02	14.4	

VAMOS Colluvic Regosol (Arenic) over Gleyic Luvisol (Loamic)										
0-30	Ap	2	63	26	11	1.62	5.05	0.90	-	-
30-70	Ab	2	59	31	11	1.62	5.87	0.44	-	-
70-88	fAh	3	57	28	15	1.65	6.39	0.56	-	-
88-105	AEb	2	58	26	17	1.74	6.66	0.34	-	-
105-147	Bt/Cgb	2	57	24	19	1.81	7.14	0.17	0.5	0.5
147-170	Ckg	3	58	29	14	1.86	7.69	0.01	12.8	12.8

2.4.2 Meteoric and in situ ^{10}Be

Concentrations of meteoric ^{10}Be are given in Figure 2.4 and ranged from 0.15 ± 0.01 to 1.59 ± 0.03 atoms/g $\times 10^8$. The site LP12N has a much lower ^{10}Be inventory than LP4 or VAMOS, which have comparable inventories. The highest concentrations were found in the Bt/E (LP4), Bt (LP12N) and Ab (VAMOS) horizons.

Similar to the meteoric ^{10}Be , the highest content of in situ ^{10}Be was detected in the subsoil (Figure 2.4; Bt/E horizon) of LP4 and VAMOS indicating either a translocation (eluviation/illuviation) or anthropogenic disturbance of the soil. Only at site LP12N was a decrease with increasing depth measured.

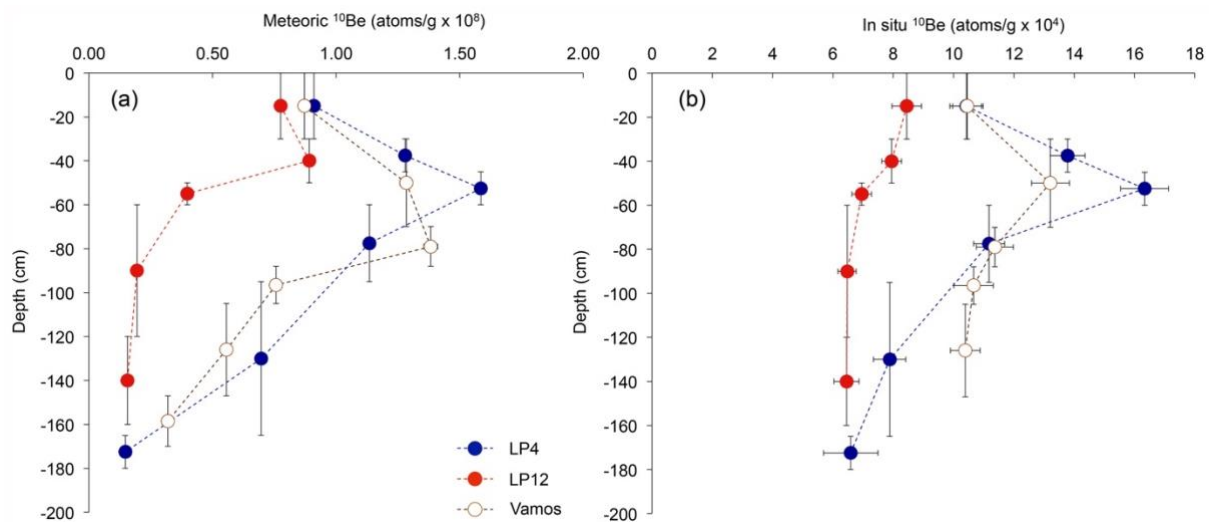


Figure 2.4. Depth trends of a) meteoric ^{10}Be contents and b) in situ ^{10}Be of the sites LP4 (flat position), LP12 (midslope position) and Vamos (footslope position; a profile consisting of two superimposed soils). No in situ ^{10}Be data is available for the lowermost depth of the profile Vamos.

The measured in situ ^{10}Be concentrations were used to model the decrease in ^{10}Be concentration with depth to derive erosion rates using the depth function model (Figure 2.5; Hidy et al. 2010). Due to the clear presence of an overlying soil at VAMOS, the depth function was applied to the whole profile (Figure 2.5c) and to the buried profile only (Figure 2.5d). The production rate parameters were determined in Hidy et al.'s code for site location and muons fit to 5m. Density was allowed to vary uniformly between minimum and maximum values for each profile. The model age was allowed to vary uniformly between 0 and 100ka for all profiles. Erosion rates

were free to vary uniformly between 0 and 20 cm kyr⁻¹, and a threshold of 300 cm total erosion was applied. Inheritance varied uniformly between 0 and 100000 atoms/g and a mean attenuation length of 160 ± 5 g/cm² was used for all models. The model was run 100000 times with a 2 σ threshold. Due to the unusual depth distribution of the ¹⁰Be content, modelling was difficult and resulted in a relatively high variability of possible trends (and thus, erosion rates).

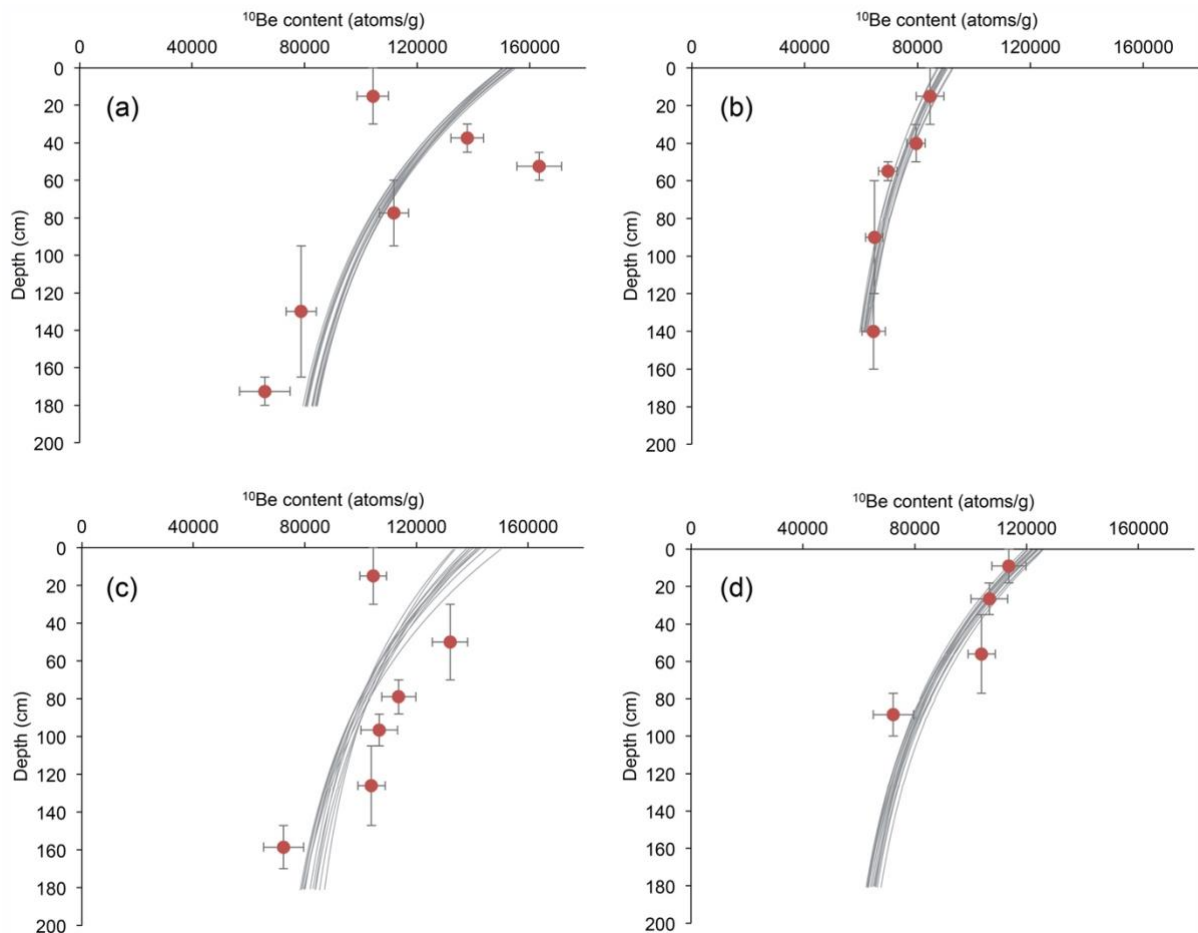


Figure 2.5. In situ ¹⁰Be distribution along the profiles and modelled trend using equation 12. Inherited ¹⁰Be and erosion rates were iteratively obtained by minimising the difference between measured and modelled values. a) LP4, b) LP12, c) Vamos (whole profile) and d) Vamos (buried profile; starting at a depth of 70 cm).

2.4.3 ²³⁹⁺²⁴⁰Pu inventory

The isotope ratio ²⁴⁰Pu/²³⁹Pu was measured alongside the ²³⁹⁺²⁴⁰Pu activities for each sample; for stratospheric global fallout, a ²⁴⁰Pu/²³⁹Pu ratio of 0.180 ± 0.014 is expected (Kelley et al.,

1999). In this study $^{240}\text{Pu}/^{239}\text{Pu}$ ratios are in agreement with a global fallout source and indicate the absence of significant Chernobyl Pu deposition at the study site.

Pu is accumulated at the surface and usually does not migrate deeper than 15 cm (Alewell et al., 2014). At the sites LP4 and LP12N, Pu was indeed concentrated in the first 30 cm (Ap horizon). At the site VAMOS, however, traces of $^{239+240}\text{Pu}$ were detectable down to 60 cm depth. The $^{239+240}\text{Pu}$ inventories varied between 34 and 51 Bq m^{-2} (Figure 2.6). LP4 was used as reference site due to its flat position, soil depth and horizonation assuming neither erosion nor accumulation during the last 50 – 60 years.

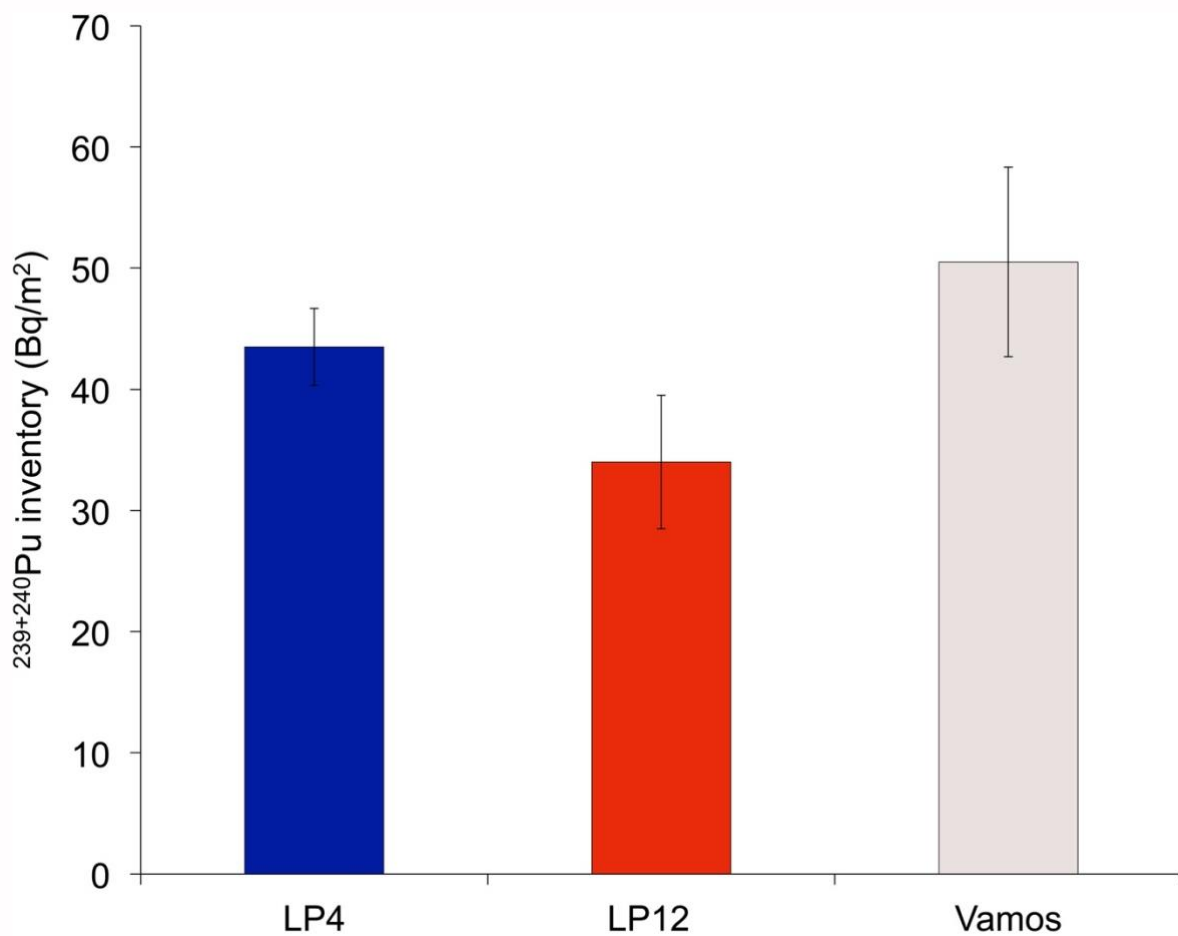


Figure 2.6. $^{239+240}\text{Pu}$ inventory of the investigated three sites (with each having 4 to 6 replicates).

2.4.4 Soil redistribution rates (long- and short-term)

The soil redistribution rates are reported in Table 2.3. Due to the fact that LP4 is considered as the reference site, soil redistribution rates are assumed to be zero for the short-term rates. Consequently, no values are given when using MODERN (^{10}Be) or the PDM model ($^{239+240}\text{Pu}$).

Soil erosion rates calculated using meteoric and in situ ^{10}Be were moderately comparable when employing the approach according to Hidy et al. (2010) or that of Zollinger et al. (2017). The calculations resulted in very low rates for the LP4 site — either very low erosion or a slight accumulation over the entire soil formation period of 19 to 20 ka. At the site LP12N, relatively high long-term erosion rates of 1.6 (Hidy et al., 2010) to 2.1 (Zollinger et al., 2017) $\text{t ha}^{-1} \text{yr}^{-1}$ were measured whereas the footslope site (or lower slope position) exhibited smaller erosion rates when considering the whole soil profile VAMOS; however, this profile however has a buried soil. Before it was overridden by slope deposits, the buried soil exhibited erosion in the range of 0.1 to 1.4 $\text{t ha}^{-1} \text{yr}^{-1}$. The code MODERN was not applicable to LP4 for the long- and short-term soil redistribution rates (because this was the reference site). The values calculated for the other sites using MODERN show similar trends to those when using the approach of (Zollinger et al., 2017) and (Hidy et al., 2010). Considering only the buried soil, the erosion rates were slightly higher compared to the rates of the whole VAMOS profile using the approaches of Lal (2001), Zollinger et al. (2017) and also MODERN. The buried soil had a more or less undisturbed evolution until about 2.1 ka BP. Some of the first organic matter that was incorporated into the soil had an age of about 13.1 ka BP.

The model according to Lal (2001) only results in erosion rates. Also this approach indicates that long-term erosion rates were lower at the LP4 site although the rates are relatively high when compared to the LP12N site. However, the erosion rates calculated for the VAMOS site are higher when compared to those calculated when other approaches are used. The erosion rate calculated using CRONUS also results only in erosion rates.

The models use partially different input parameters. One common parameter is the content of the erosion tracer (i.e., ^{10}Be or $^{239+240}\text{Pu}$). The influence of this parameter on soil erosion was checked by a sensitivity analysis. A convenient way to express the sensitivity of a system to changes in parameters is the normalised sensitivity coefficient, $Q_{i,m}$, that is defined by

$$Q_{i,m} = \frac{\partial \ln C_i}{\partial \ln P_m} \quad (13)$$

where C_i is the dependent variable (erosion) and P is the value of parameter m (Furrer et al., 1990). This formula expresses a partial derivative based on the percentage change in the dependent variable caused by a 1% change in the value of the parameter m . Sensitivity coefficients are negative for parameters in processes that lead to a reduction and positive for parameters that cause an increase in variables of interest (Table 2.3). All models react in a similar range to an increased tracer content (i.e., with a higher content the erosion rate decreases). The PDM approach and the depth function seem to show a slightly higher reactivity and are, thus, more sensitive to changes.

Table 2.3. Short and long-term soil redistribution rates. Negative values indicate soil erosion and positive values indicate soil accumulation.

Site	Long-term rates		In situ ¹⁰ Be		CV (%)	Short-term rates	
	Meteoritic ¹⁰ Be		In situ ¹⁰ Be		²³⁹⁺²⁴⁰ Pu		
	Model used		Depth function	Average			
	(Lal, 2001)	(Zollinger et al., 2017)	(Hidy et al., 2010)	all ¹⁰ Be methods		PDM (Walling & Quine, 1990; XINBAO et al., 1990)	
		MODERN (Arata et al., 2016a; Arata et al., 2016b)					
	t ha ⁻¹ yr ⁻¹	t ha ⁻¹ yr ⁻¹	t ha ⁻¹ yr ⁻¹	t ha ⁻¹ yr ⁻¹	t ha ⁻¹ yr ⁻¹	t ha ⁻¹ yr ⁻¹	
LP4	-1.00	0.26	-	-0.03	-0.34	166	-
LP12N	-1.66	-2.11	-0.67	-1.61	-1.40	42	-25.1
VAMOS (whole)	-1.32	-0.69	-0.28	-0.33	-0.66	63	7.6
VAMOS (buried)	-1.36	-1.13	-0.66	-0.11	-0.79	61	-
$\partial \ln C_i / \partial \ln P_m$ (eq. 13);	-1.00 ± 0.00	-1.04 ± 0.24	-1.22 ± 0.30	-1.36 ± 0.13	-1.01 ± 0.01		-1.42 ± 0.30
sensitivity to a 1% change in content (¹⁰ Be or ²³⁹⁺²⁴⁰ Pu)							

The short-term redistribution rates were considerably higher than the long-term rates (Table 2.3). For the site LP12N, the current erosion rates are $25 \text{ t ha}^{-1} \text{ yr}^{-1}$, one order of magnitude higher than the long-term rates. The erosion rate of $25 \text{ t ha}^{-1} \text{ yr}^{-1}$ equals a local soil truncation of approx. 10 cm over the last 60 years. If continued, such high rates will certainly lead to very shallow soils. In contrast, the site VAMOS exhibits a considerable accumulation with $7.9 \text{ t ha}^{-1} \text{ yr}^{-1}$ during the last 50 years. In general, Pu-based, local erosion and deposition rates are in the range rates inferred from ^{137}Cs inventories at the same investigation area (Aldana Jague et al., 2016). These authors estimated erosion rates up to about $24 \text{ t ha}^{-1} \text{ yr}^{-1}$ and accumulation rates even up to about $53 \text{ t ha}^{-1} \text{ yr}^{-1}$ in the whole area. For the site VAMOS, they calculated an accumulation of about $16 \text{ t ha}^{-1} \text{ yr}^{-1}$ and for site LP12N an erosion rate of about $8 \text{ t ha}^{-1} \text{ yr}^{-1}$.

2.5 Discussion

2.5.1 ^{10}Be along the soil profiles

Surprisingly, both meteoric and in situ ^{10}Be have their maximum content in the subsoil and exhibit similar depth trends (Figure 2.4). The depth trend of ^{10}Be seems, at a first glance, to fit with the general depth trend of the clay content in the soil (Figure 2.7). A similar observation was also made by (Maejima et al., 2005) who found a positive correlation between the clay content and meteoric ^{10}Be in soils. Indeed, in Luvisols and in Podzols, a clay- and podzolisation-mediated transport of ^{10}Be may take place (Egli et al., 2010; Pavich et al., 1984). While the correlation in this case is not significant, it is nonetheless still possible that meteoric ^{10}Be was translocated (via clay eluviation and illuviation) from the topsoil to greater depth. Clay translocation has been confirmed in soils of the study region (Sommer et al., 2008); Figure 2.3; Table 2.2). The distribution pattern of ^{10}Be (in situ and meteoric) seems to correlate moderately well to the soil genetic horizons and the process of clay translocation (Figure 2.7). Clay translocation or translocation of matter in general in soils therefore seem to govern to a certain extent the distribution pattern of ^{10}Be . In situ ^{10}Be however refers to a specific grain size fraction of the soil (see chapter 3.4). To what extent in situ ^{10}Be is now really influenced by clay translocation is difficult to identify. Alternatively, other processes than clay translocation may have influenced both the meteoric and in situ ^{10}Be profiles. The increase in ^{10}Be at the transition from the A to the B horizon might also be due to former deep ploughing. This is a likely explanation for the reversed in situ ^{10}Be concentrations in the upper horizons of LP4. In terms of atomic structure and valence state, Be is affiliated with alkaline earth elements; but geologically and chemically beryllium shows greater affinities to the major cations Al, Si, and Mn, and the lithophile trace-elements Nd and Zr (Ryan, 2002). Dissolved and suspended material in rivers indicate that the geochemistry of ^{10}Be is primarily controlled by two main factors, i) its abundance in the rocks and ii) the extent of its adsorption onto particles (Brown et al., 1992) or re-precipitation with other components. We therefore correlated ^{10}Be with other chemical components in different forms to see which could be the controlling factors of its distribution along the profiles.

Meteoric ^{10}Be shows a weak correlation ($R^2 = 0.36$; $p = 0.05$) to the oxalate-extractable Fe (weakly or non-crystalline forms; Fe_o , Figure 2.7) and to organic carbon ($R^2 = 0.56$; $p < 0.05$), as also found in other investigations (Egli et al., 2010). Visually, the ^{10}Be depth trend also shows similarities to the dithionite-extractable Fe (Fe_d , Figure 2.7). The correlation between

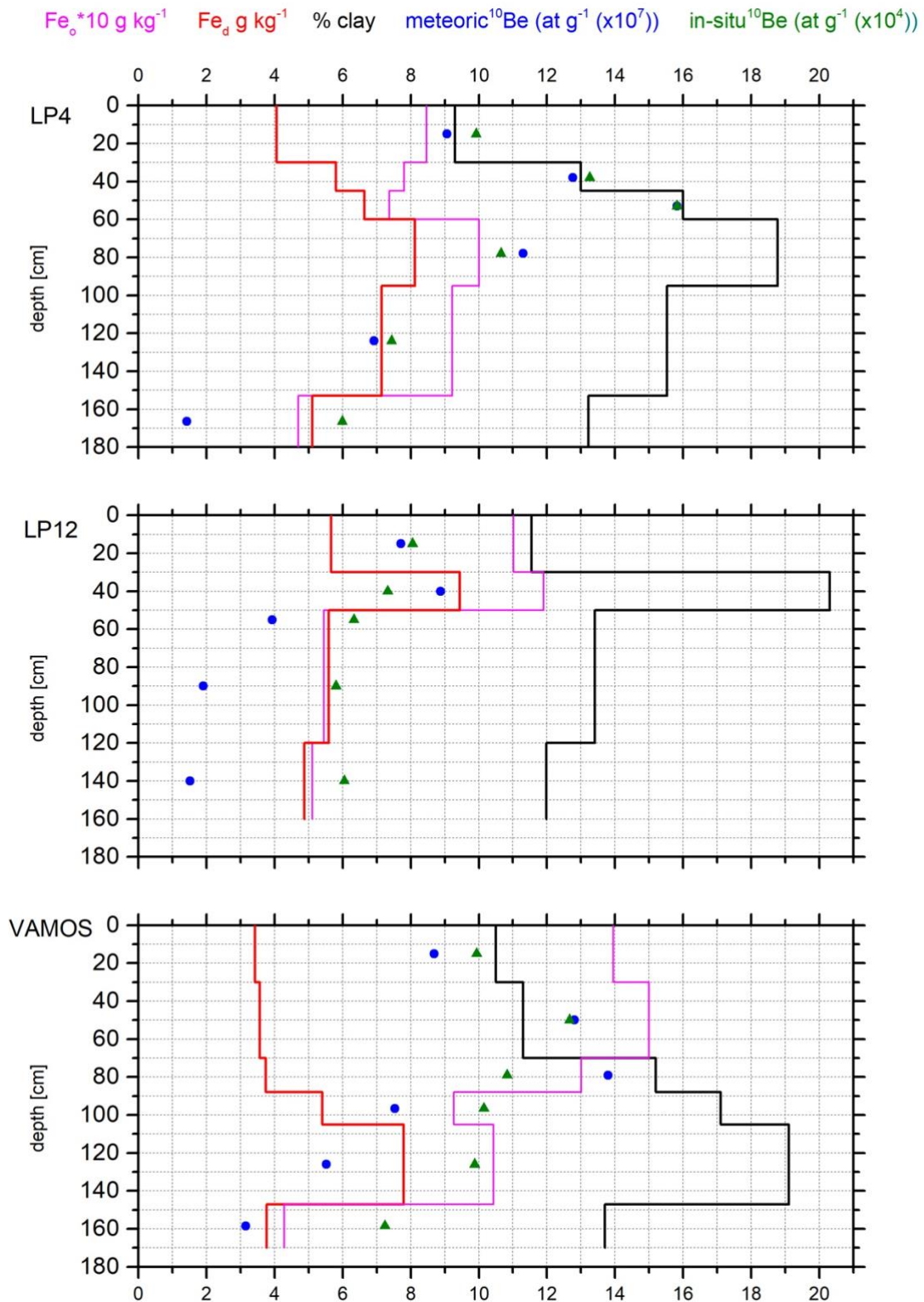


Figure 2.7. Depth trends of meteoric and in situ ^{10}Be of the investigated sites LP4, LP12 and VAMOS in comparison with the clay content, the oxalate-extractable (Fe_0) and dithionite-extractable iron content (Fe_a).

^{10}Be and Fe_a is however not significant. Be has a relatively high affinity to organic ligands that give rise to charged metallo-organic complexes. These complexes easily adsorb on positively charged Fe-oxyhydroxides, Al-oxyhydroxides or clay minerals (Willenbring & von Blanckenburg, 2010). No significant correlation, however, exists between any form of ^{10}Be and Mn or Al. The distribution pattern of meteoric ^{10}Be is therefore governed to a certain extent by soil organic matter and weakly crystalline Fe-oxyhydroxides. However, a relatively good correlation is found between ^{10}Be (in situ and meteoric) and Si ($R^2 = 0.49$, $p < 0.05$): the higher the Si content, the more ^{10}Be . An even better correlation exists with Zr ($R^2 = 0.78$ for in situ ^{10}Be and 0.72 for meteoric ^{10}Be). With increasing weathering, Si and Zr are passively enriched and other cations leached. Zr and Si therefore indicate weathering processes that are most advanced in the uppermost soil horizon where finally also ^{10}Be is accumulated.

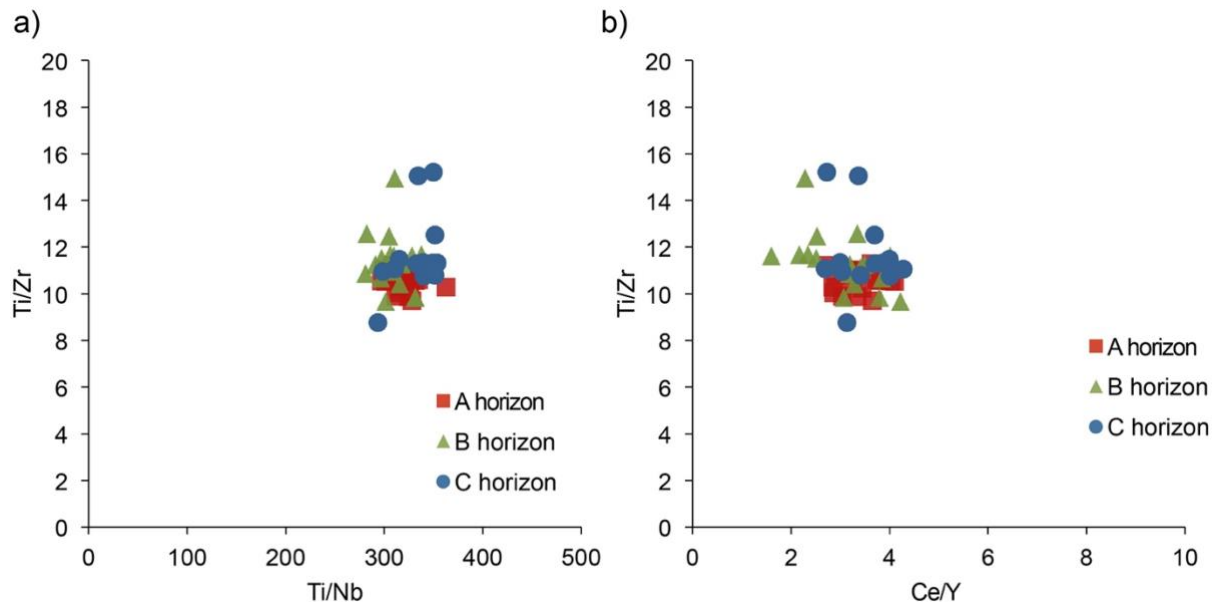


Figure 2.8. Binary diagram of concentration ratios of a) Ti/Zr vs Ti/Nb and b) Ti/Zr vs Ce/Y for samples of the topsoil (A or E horizon), the subsoil (B horizon) and the C horizon from the various sites.

Loess deposition could have affected the profile trend of ^{10}Be (in situ and meteoric) after deglaciation. However, the grain size distribution gives no hint that a major loess contribution has occurred (Table 2.2). This observation fits well with the fact that loess deposits are widespread in Germany, but not in northern Germany close to the Polish border (Haase et al.,

2007; Muhs, 2013). Chemically immobile elements are another method to study potential loess input. We chose the elements Ti, Zr, Nb, Ce, and Y, all of which have a relatively high ionic potential and are considered to be chemically immobile under most near-surface environments (Dahms & Egli, 2016; Muhs & Benedict, 2006). According to (Muhs & Benedict, 2006), Tb and Nb are found in ilmenite, rutile, anatase, titanomagnetite, sphene, and biotite. Zr is mostly present in zircon, although Zr may also be found in other minerals (e.g., zirconolite). The REEs Ce and Y are related to a wide variety of minerals such as phyllosilicates (adsorption on e.g., micas, chlorite, other clay minerals), sphene, amphiboles and apatite (Muhs & Benedict, 2006). Ti/Zr, Ti/Nb and Ce/Y ratios measured in the A, B and C horizons showed a wide overlap (Figure 2.8). The ratios demonstrate that the major chemical background of the various soil horizons does not vary appreciably. Another tracer for aeolian input is the K/Rb ratio: the average ratio is 267 with a very low standard deviation (13). Also here we have no hint that an aeolian input has occurred that would change the main chemistry of the soils (including ^{10}Be). If ever there was an aeolian input, it must have a local source. However, a detectable aeolian input is not confirmed by the grain size analyses.

The in situ ^{10}Be contents in the deepest horizons (C horizon) are still considerably high suggesting a pre-exposure of the parent material to cosmic rays. All model fits of the in situ ^{10}Be along the soil profiles (Figure 2.5) require inherited ^{10}Be due to pre-exposure. The best model fit (minimisation of difference between observed and modelled values) indicates that the inherited content of ^{10}Be is in the range of 50000 – 80000 atoms g^{-1} , which is most likely due to erosion and incorporation of pre-exposed sediment into the glacial moraines. These inherited in situ ^{10}Be concentrations imply at least 10 ka of pre-exposure for all profiles. Stroeve et al. (2016) and Hughes et al. (2016) clearly showed that deglaciation and start of soil formation was c. 19 to 20 ka BP in the investigation area. Best-fit modelled soil ages (1σ error range) for LP12 and VAMOS are at least 10 and 20 ka (Figure 2.9), matching their assumed post-glacial age, with LP4 potentially being formed on older, relict, glacial sediments. In all cases, the long-term erosion rates for allowable ages are less than $\sim 0.005 \text{ cm yr}^{-1}$.

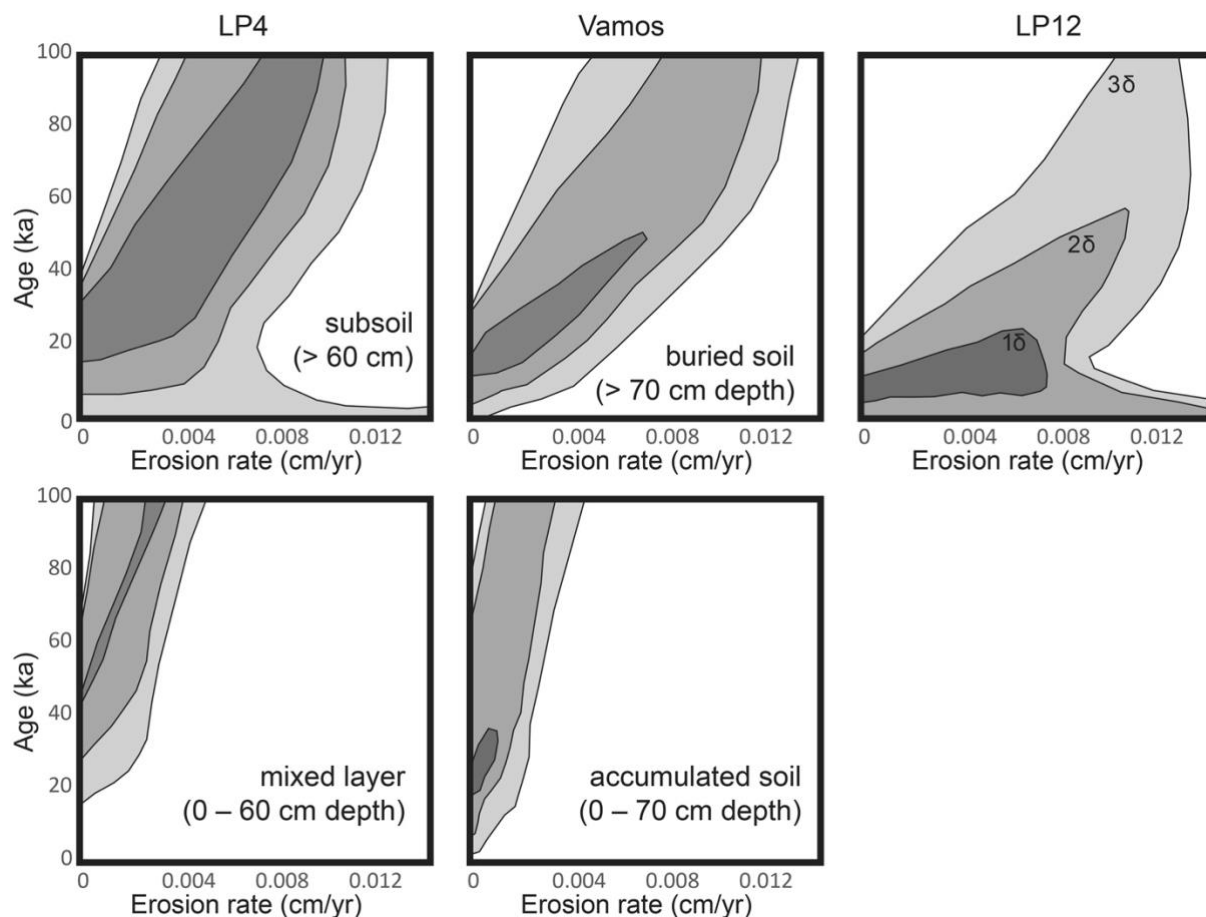


Figure 2.9. Comparison between modelled and measured in situ ^{10}Be contents in the soils as a function of erosion and error minimisation plots for age and erosion rate for 100000 iteration Monte Carlo simulations of in situ ^{10}Be profiles. Erosion rates were allowed to vary between 0 and 0.02 cm/yr, depositional age varied between 0 and 100ka, and inherited nuclide concentration varied between 0 and 90000 atoms/g. The contours show combinations of age and erosion rate that generated 1-, 2-, and 3- σ fits. We define a 1-sigma fit as one in which the total misfit for the modelled profile is smaller than the total 1- σ error on the individual ^{10}Be measurements.

2.5.2 Soil redistribution rates (erosion and accumulation)

Short-term rates

The first study to assess soil redistribution rates (erosion and accumulation) with the use of Pu isotopes was done by (Schimmack et al., 2001, 2002) and focussed on agricultural soils in southern Germany. Since then, only few studies applied Pu isotopes as a soil tracer. During the

last few years a focus using Pu-isotopes has been given to Alpine grassland sites (Alewell et al., 2014; Zollinger et al., 2015) and forest sites in the southern hemisphere (Hoo et al., 2011; R. Lal et al., 2013). The $^{239+240}\text{Pu}$ inventory at the reference site (43 Bq m^{-2}) was slightly under the range of $50 - 100 \text{ Bq m}^{-2}$, which is the expected inventory for the northern hemisphere (Masarik, 2009). The agricultural site studied by (Schimmack et al., 2001, 2002) exhibited soil erosion rates that are comparable to the short-term redistribution rates of the present study. The values determined by these authors ranged from 18 to $44 \text{ t ha}^{-1} \text{ yr}^{-1}$ at erosional sites and $43 \text{ t ha}^{-1} \text{ yr}^{-1}$ for depositional sites at the footslope. Given that soil thickness decreases if soil production is less than the total denudation, the tolerable soil erosion rates will depend strongly on soil age as soil production is dependent on soil age (Alewell et al., 2015). According to (Alewell et al., 2015), tolerable erosion and denudation rates are \leq soil production rates. For soils having a surface age of $> 10 \text{ ka}$ (from temperate to alpine climates), tolerable rates are between c. 0.5 and $1.1 \text{ t ha}^{-1} \text{ yr}^{-1}$. The measured actual erosion rates of $25 \text{ t ha}^{-1} \text{ yr}^{-1}$ at the LP12N site are more than an order of magnitude above these tolerable rates.

The presence of Pu was limited to the Ap horizon, but in some cases, traces of Pu were also found at a slightly greater depth. It is well known that radioisotopes are rapidly adsorbed onto soil particles. $^{239+240}\text{Pu}$ is associated with solid phases and is relatively immobile chemically, being preferentially attached to soil organic matter and sesquioxides (Bunzl et al., 1995). The mobility of Pu in the soil is therefore strongly limited — even more than other FRNs oxides (Bunzl et al., 1992; Lee & Lee, 1999). However, some studies claimed that the association of Pu to organic matter and higher molecular fractions in the soil increases the mobility and potentially leads to an increased downward vertical migration (Alewell et al., 2014).

The highest inventory of $^{239+240}\text{Pu}$ was recorded at the VAMOS site and the lowest at LP12 (Figure 2.6). This fits nicely to the expectancies: VAMOS is a colluvial site, at the topographic lowermost position in a concave footslope depression where under the present-day situation eroded material is accumulated and LP12 on a mid-slope erosion dominated position. LP4 is the highest site and has a flat topography and shows no particular signs of present-day erosion. This all fits well with the catena concept stating that soils along a hillslope are interconnected (Milne, 1935). Hydrology plays the central role: soil profiles changes from point to point are in agreement with conditions of drainage and past history of the land surface (Lin et al., 2005).

Table 2.4. Analysed soil material and related results of radiocarbon dating.

Site/sample	UZH-/ETHZ-code	Material	Treatment ¹	C14 age BP	±1σ	cal age (calBP)	
						1σ	2σ
VAMOS fAh	UZ-6463/ETH-81810	soil	H ₂ O ₂	11282	40	13165 – 13084	13228 – 13061
VAMOS fAh	UZ-6464/ETH-81811	soil	POM	2141	24	2291 – 2066	2300 – 2040

¹ H₂O₂-resistant organic matter fraction (potentially the oldest fraction); POM: particulate organic matter (potentially the youngest fraction).

Long-term rates

Depending on the model approach used and type of ^{10}Be , the soil redistribution rates vary considerably. Some of the models used are not able to detect soil accumulation (e.g., Balco et al., 2008; Lal, 2001). Difficulties in the estimation of erosion rates may particularly then arise when only surface samples (CRONUS) are taken into consideration. Due to pedogenic processes or human impact, the distribution pattern along the profile may be disturbed and, particularly in relatively young soils, far from a state of equilibrium. Nonetheless, the trend of the erosion rates using CRONUS is comparable to Lal (2001), although the obtained rates are in general lower. Furthermore, accumulation rates cannot be calculated from a single surface sample. CRONUS thus has major limitations for soils. Unrealistically high ^{10}Be values in the topsoil are needed to calculate a net accumulation when using the approach of Lal (2001). The approaches of Lal (2001) and Zollinger et al. (2017) achieve quite similar results.

Soil erosion rates calculated with meteoric and in situ ^{10}Be were moderately comparable, with slightly higher erosion rates calculated from the meteoric ^{10}Be data. It is important to remember that these reflect net erosion, i.e., the difference between the gross erosion and accumulation rates that may have occurred at the same site over time. As such, instantaneous rates may have been faster. Some minor loess addition might have taken place during deglaciation giving rise to a lower negative soil material budget. However, any loess addition would have been very low (Haase et al., 2007; Muhs, 2013) and cannot be detected in the grain size distribution of the investigated soils or in their geochemical composition.

Comparison of short- and long-term erosion rates

When using $^{239+240}\text{Pu}$, a clear trend of soil redistribution along the hillslope can be measured for the last decades. Such a trend is not so obvious when using ^{10}Be and calculating long-term rates. LP4 exhibits very low erosion rates and LP12 has high rates on the mid-slope. Due to the fact that VAMOS consists of a buried and a more recent soil, it is difficult to calculate an overall erosion rate. It seems that the buried soil of VAMOS has experience some erosion before the new material was deposited on top of it. This also means that the relief has changed substantially over time.

When comparing short- and long-term soil redistribution rates, it is fairly obvious that the short-term soil redistribution rates are higher. Both erosion and accumulation rates seemed to have distinctly increased during the last few decades. However, the measured present-day rates (i.e., the last 5 – 6 decades) are not responsible for all the material that has been either removed or added since start of soil formation. At site LP12N, for example, 25 t ha⁻¹ are removed annually — giving rise to an amount of 0.15 t over a period of about 60 years that has been removed per m² of surface. The long-term erosion rates lie between 0.7 and 2.1 t ha⁻¹ yr⁻¹. These rates cause a soil loss of 1.3 to 4.2 t m⁻² over a period of 20 ka, which is still considerably more than the 0.15 t m⁻² occurring over the last 60 years.

To a certain extent, erosion seems to have been counterbalanced at the site VAMOS by the deposition of eroded (upslope) soil material about 2.1 ka BP (¹⁴C-dated; Table 2.4). Although numerous archaeological finds in the region were found and, in some cases, traced back to about 4000 BP, (Kappler et al., 2018) show that the main phase of soil erosion can be ascribed to the recent past. Most ages of colluvial sediments that can be attributed to human influence and soil erosion cluster within the last 600 years with a peak during the last 200 years (Kappler et al., 2018).

The present-day erosion rates are substantial in other ways: the approximately ~10 cm erosion in recent years at steep slopes has drastically changed the soil profile, leading to the eroded soils mentioned before (van der Meij et al., 2017).

Formerly glaciated (last glaciation) areas of the lowlands of Middle Europe are considered relatively inactive with respect to tectonics and natural geomorphic processes. However, they are subject to a considerable human impact; e.g., by long-term agricultural land use. The progress in farming technology since World War II has led to accelerated water and tillage erosion (Sommer et al., 2008), hence progressive periods are replaced by regressive periods of soil evolution. Tillage depth and tractor speed are main factors of the magnitude of soil translocation and loss. In some landscapes tillage erosion rates are in the same order of magnitude as water erosion (Van Oost et al., 2009). This type of erosion seems often more than one order of magnitude higher than the long-term rates (averaged over the entire period of soil formation).

2.6 Conclusions

The multi-methodological approach enabled the clear separation of long-term from short-term processes and demonstrated that temporarily-changing processes can be disentangled in their major traits. The long-term soil redistribution rates along slopes were up to one order of magnitude lower than the present-day rates. Both in situ and meteoric ^{10}Be are suitable for use in the measurement of long-term soil redistribution rates and produce comparable results. The ^{10}Be depth profile was in its upper part partially influenced by clay translocation and human impact (ploughing). Due to their relatively young age (19 – 20 ka), the soils do not seem to be in a steady state. Therefore, the most meaningful results were obtained using the depth function model of Hidy et al. (2010) for in situ ^{10}Be , the model of Zollinger et al. (2017) and the code MODERN (Arata et al., 2016a; Arata et al., 2016b) for meteoric ^{10}Be . MODERN was previously only applied for fallout nuclides. Using in situ ^{10}Be , slightly lower rates were obtained but the general soil redistribution pattern corresponds well with meteoric ^{10}Be . The results of all approaches for the determination of long-term erosion rates were all in a relatively narrow range. The short-term erosion rates that were estimated using $^{239+240}\text{Pu}$ are almost an order of magnitude higher. This confirms that industrialised agriculture leaves a clear footprint behind having strong erosion on mid-slope positions and related soil accumulation at the footslope. The multi-method approach (^{10}Be , $^{239+240}\text{Pu}$) seems a promising tool in deciphering time-dependent process rates. In general, our results nicely confirm that distinct different phases (having a progressive/regressive nature) in soil evolution exist as postulated by (Sommer et al., 2008).

2.7 Acknowledgements

This research was supported by a cooperation contract (CORRELATE; F-75113-07-01) between the University of Zurich and the ZALF. We would like to thank one unknown reviewer and A. Heimsath for their helpful comments on an earlier version of the manuscript. We are grateful to Alan Rogers for the English corrections.

References

- Aldana Jague E, Sommer M, Saby NPA, Cornelis J-T, Van Wesemael B, Van Oost K. 2016. High resolution characterization of the soil organic carbon depth profile in a soil landscape affected by erosion. *Soil & Tillage Research* 156: 185–193. <https://doi.org/10.1016/j.still.2015.05.014>.
- Alewell C, Egli M, Meusburger K. 2015. An attempt to estimate tolerable soil erosion rates by matching soil formation with denudation in Alpine grasslands. *Journal of Soils and Sediments* 15(6): 1383–1399. <https://doi.org/10.1007/s11368-014-0920-6>.
- Alewell C, Meusburger K, Juretzko G, Mabit L, Ketterer ME. 2014. Suitability of $^{239+240}\text{Pu}$ and ^{137}Cs as tracers for soil erosion assessment in mountain grasslands. *Chemosphere* 103: 274–280. <https://doi.org/10.1016/j.chemosphere.2013.12.016>.
- Arata L, Alewell C, Frenkel E, A'Campo-Neuen A, Iurian A-R, Ketterer ME, Mabit L, Alewell C. 2016a. Modelling deposition and erosion rates with RadioNuclides (MODERN) – part 2: a comparison of different models to convert $^{239+240}\text{Pu}$ inventories into soil redistribution rates at unploughed sites. *Journal of Environmental Radioactivity* 162–163: 97–106. <https://doi.org/10.1016/j.jenvrad.2016.05.009>.
- Arata L, Meusburger K, Frenkel E, A'Campo-Neuen A, Iurian A-R, Ketterer ME, Mabit L, Alewell C. 2016b. Modelling deposition and erosion rates with RadioNuclides (MODERN) – part 1: a new conversion model to derive soil redistribution rates from inventories of fallout radionuclides. *Journal of Environmental Radioactivity* 162–163: 45–55. <https://doi.org/10.1016/j.jenvrad.2016.05.008>.
- Balco G, Stone JO, Lifton N, Dunai TJ. 2008. A complete and easily accessible means of calculating surface exposure ages or erosion rates from ^{10}Be and ^{26}Al measurements. *Quaternary Geochronology* 3: 174–195. <https://doi.org/10.1016/j.quageo.2007.12.001>.
- Birkeland PW, Shroba RR, Burns SF, Price AB, Tonkin PJ. 2003. Integrating soils and geomorphology in mountains – an example from the Front Range of Colorado. *Geomorphology* 55: 329–344. [https://doi.org/10.1016/S0169-555X\(03\)00148-X](https://doi.org/10.1016/S0169-555X(03)00148-X).
- Bork H-R (ed). 2006. Landscapes of the Earth Under the Influence of Man. Darmstadt; 207 pp: Wissenschaftliche Buchgesellschaft (in German).

- Bronk Ramsey C. 2001. Development of the radiocarbon calibration program. *Radiocarbon* 43: 355–363. <https://doi.org/10.1017/S0033822200038212>.
- Bronk Ramsey C. 2009. Bayesian analysis of radiocarbon dates. *Radiocarbon* 51: 337–360. <https://doi.org/10.1017/S0033822200033865>.
- Brown ET, Edmond JM, Raisbeck GM, Bouchès DL, Yiou F, Measures CI. 1992. Beryllium isotope geochemistry in tropical river basins. *Geochimica et Cosmochimica Acta* 56: 1607–1624. [https://doi.org/10.1016/0016-7037\(92\)90228-B](https://doi.org/10.1016/0016-7037(92)90228-B).
- Bunzl K, Kracke W, Schimmack W. 1992. Vertical migration of Pu-239 + Pu-240, Am-241 and cesium-137 fallout in a forest soil under spruce. *Analyst* 117: 469–474.
- Bunzl K, Flessa H, Kracke W, Schimmack W. 1995. Association of fallout $^{239+240}\text{Pu}$ and ^{241}Am with various soil components in successive layers of a grassland soil. *Environmental Science & Technology* 29:2513–2518.
- Chmeleff J, von Blanckenburg F, Kossert K, Jakob D. 2010. Determination of the ^{10}Be half-life by multicollector ICP-MS and liquid scintillation counting. *Nuclear Instruments and Methods in Physics Research Section B: Beam Interactions with Materials and Atoms* 268: 192–199. <https://doi.org/10.1016/j.nimb.2009.09.012>.
- Christl M, Vockenhuber C, Kubik P, Wacker L, Lachner J, Alfimov V, Synal HA. 2013. The ETH Zurich AMS facilities: performance parameters and reference materials. *Nuclear Instruments and Methods in Physics Research Section B: Beam Interactions with Materials and Atoms* 294: 29–38. <https://doi.org/10.1016/j.nimb.2012.03.004>.
- Dahms D, Favilli F, Krebs R, Egli M. 2012. Soil weathering and accumulation rates of oxalate-extractable phases from alpine chronosequences of up to 1 Ma in age. *Geomorphology* 151–152:99–113. <https://doi.org/10.1016/j.geomorph.2012.01.021>.
- Dahms D, Egli M. 2016. Carbonate and elemental accumulation rates in arid soils of mid-to-late Pleistocene outwash terraces, southeastern Wind River Range, Wyoming, USA. *Chemical Geology* 446:147–162. <https://doi.org/10.1016/j.chemgeo.2015.12.006>.
- Deumlich D, Schmidt R, Sommer M. 2010. A multiscale soil–landform relationship in the glacial-drift area based on digital terrain analysis and soil attributes. *Journal of Plant Nutrition and Soil Science* 173:843–851. <https://doi.org/10.1002/jpln.200900094>.

- Dixon JL, Heimsath AM, Amundson R. 2009. The critical role of climate and saprolite weathering in landscape evolution. *Earth Surface Processes and Landforms* 34: 1507–1521. <https://doi.org/10.1002/esp.1836>.
- Egli M, Brandová D, Böhlert R, Favilli F, Kubik P. 2010. ^{10}Be inventories in Alpine soils and their potential for dating land surfaces. *Geomorphology* 119: 62–73. <https://doi.org/10.1016/j.geomorph.2010.02.019>.
- Egli M, Dahms D, Norton K. 2014. Soil formation rates on silicate parent material in high-mountains: different approaches, different results? *Geoderma* 213: 320–333. <https://doi.org/10.1016/j.geoderma.2013.08.016>.
- Eusterhues K, Rumpel C, Kögel-Knabner I. 2005. Stabilization of soil organic matter isolated via oxidative degradation. *Organic Geochemistry* 36: 1567–1575. <https://doi.org/10.1016/j.orggeochem.2005.06.010>.
- Favilli F, Egli M, Cherubini P, Sartori G, Haeberli W, Delbos E. 2008. Comparison of different methods of obtaining a resilient organic matter fraction in Alpine soils. *Geoderma* 145: 355–369. <https://doi.org/10.1016/j.geoderma.2008.04.002>.
- Favilli F, Egli M, Brandova D, Ivy-Ochs S, Kubik P, Cherubini P, Mirabella A, Sartori G, Giaccai D, Haeberli W. 2009. Combined use of relative and absolute dating techniques for detecting signals of Alpine landscape evolution during the late Pleistocene and early Holocene. *Geomorphology* 112: 48–66. <https://doi.org/10.1016/j.geoderma.2008.04.002>.
- Furrer G, Sollins P, Westall JC. 1990. The study of soil chemistry through quasi-steady-state models: II. Acidity of soil solution. *Geochimica Cosmochimica Acta* 54: 2363–2374. [https://doi.org/10.1016/0016-7037\(90\)90225A](https://doi.org/10.1016/0016-7037(90)90225A).
- Gerke HH, Koszinski S, Kalettka T, Sommer M. 2010. Structures and hydrologic function of soil landscapes with kettle holes using an integrated hydro-pedological approach. *Journal of Hydrology* 393:123–132. <https://doi.org/10.1016/j.jhydrol.2009.12.047>.
- Granger DE, Riebe CS. 2014. Cosmogenic nuclides in weathering and erosion. In *Treatise on Geochemistry, Volume 5: Surface and Ground Water, Weathering, and Soils* (2nd edition), Holland, DH, Turekian KK (eds). 401–436. Elsevier: Amsterdam. DOI: <https://doi.org/10.1016/B978-0-08-095975-7.00514-3>

- Haase D, Fink J, Haase G, Ruske R, Pécsi M, Richter H, Altermann M, Jäger KD. 2007. Loess in Euriope – its spatial distribution based on a European Loess Map, scale 1:2,500,000. *Quaternary Science Reviews* 26: 1301–1312. <https://doi.org/10.1016/j.quascirev.2007.02.003>.
- Heimsath AM, Dietrich WE, Nishiizumi K, Finkel RC. 1997. The soil production function and landscape equilibrium. *Nature* 388:358–361. <https://doi.org/10.1038/41056>.
- Hidy AJ, Gosse JC, Pederson JL, Mattern JP, Finkel RC. 2010. A geologically constrained Monte Carlo approach to modeling exposure ages from profiles of cosmogenic nuclides: an example from Lees Ferry, Arizona. *Geochemistry, Geophysics, Geosystems* 11: Q0AA10. <https://doi.org/10.1029/2010GC003084>.
- Hoffmann M, Jurisch N, Garcia Alba DJ, Albiac Borraz E, Schmidt M, Huth V, Rogasik H, Rieckh H, Verch G, Sommer M, Augustin J. 2017. Detecting small-scale spatial heterogeneity and temporal dynamics of soil organic carbon (SOC) stocks: a comparison between automatic chamber-derived C budgets and repeated soil inventories. *Biogeosciences* 14: 1003–1019. <https://doi.org/10.5194/bg-14-1003-2017>.
- Hoo WT, Fifield LK, Tims SG, Fujioka T, Mueller N. 2011. Using fallout plutonium as a probe for erosion assessment. *Journal of Environmental Radioactivity* 102: 937–942. <https://doi.org/10.1016/j.jenvrad.2010.06.010>.
- Horiuchi K, Minoura K, Kobayashi K, Nakamura T, Hatori S, Matsuzaki H, Kawai T. 1999. Last-glacial to post-glacial ¹⁰Be fluctuations in a sediment core from the Academician Ridge, Lake Baikal. *Geophysical Research Letters* 26: 1047–1050. <https://doi.org/10.1029/1999GL900163>.
- Hughes AL, Gyllencreutz R, Lohne ØS, Mangerud J, Svendsen JJ. 2016. The last Eurasian ice sheets – a chronological database and time-slice reconstruction, DATED-1. *Boreas* 45(1): 1–45. <https://doi.org/10.1111/bor.12142>.
- IUSS. 2014. World Reference Base for Soil Resources 2014. International Soil Classification System for Naming Soils and Creating Legends for Soil Maps, Vol. 106, World Soil Resources Reports No. FAO: Rome.
- Jenny H. 1980. *The Soil Resource-Origin and Behavior*. Springer: New York.
- Kappler C, Kaiser K, Tanski P, Klos F, Füllung A, Mrotzek A, Sommer M, Bens O. 2018. Stratigraphy and age of colluvial deposits indicating Late Holocene soil erosion in

northeastern Germany. *Catena* 170:224–245.
<https://doi.org/10.1016/j.catena.2018.06.010>.

Kelley JM, Bond LA, Beasley TM. 1999. Global distribution of Pu isotopes and ^{237}Np . *Science of the Total Environment* 237(238): 483–500. [https://doi.org/10.1016/S0048-9697\(99\)00160-6](https://doi.org/10.1016/S0048-9697(99)00160-6).

Ketterer ME, Hafer KM, Link CL, Kolwaite D, Wilson J, Mietelski JW. 2004. Resolving global versus local/regional Pu sources in the environment using sector ICP-MS environment using sector ICP-MS. *Journal of Analytical Atomic Spectrometry* 19: 241–245. <https://doi.org/10.1039/B302903D>.

Ketterer ME, Szechenyi SC. 2008. Determination of plutonium and other transuranic elements by inductively coupled plasma mass spectrometry: a historical perspective and new frontiers in the environmental sciences. *Spectrochimica Acta Part B* 63: 719–737. <https://doi.org/10.1016/j.sab.2008.04.018>.

Kögel-Knabner I, Guggenberger G, Kleber M, Kandeler E, Kalbitz K, Scheu S, Eusterhues K, Leinweber P. 2008. Organo-mineral associations in temperate soils: integrating biology, mineralogy, and organic matter chemistry. *Journal of Plant Nutrition and Soil Science* 171:61–82. <https://doi.org/10.1016/j.sab.2008.04.018>.

Kohl CP, Nishiizumi K. 1992. Chemical isolation of quartz for measurement of in-situ produced cosmogenic nuclides. *Geochimica et Cosmochimica Acta* 56: 3583–3587. [https://doi.org/10.1016/0016-7037\(92\)90401-4](https://doi.org/10.1016/0016-7037(92)90401-4).

Korschinek G, Bergmaier A, Faestermann T, Gerstmann U, Knie K, Rugel G, Wallner A, Dillmann I, Dollinger G, Von Gostomski CL, Kossert K, Maiti M, Poutivtsev M, Rimmert A. 2010. A new value for the half-life of ^{10}Be by heavy-ion elastic recoil detection and liquid scintillation counting. *Nuclear Instruments and Methods in Physics Research Section B: Beam Interactions with Materials and Atoms* 268: 187–191. <https://doi.org/10.1016/j.nimb.2009.09.020>.

Koszinski S, Gerke HH, Hierold W, Sommer M. 2013. Geophysicalbased modeling of a kettle hole catchment of the morainic soil landscape. *Vadose Zone Journal* 12: 4. <https://doi.org/10.2136/vzj2013.02.0044>.

Lal D. 2001. New nuclear methods for studies of soil dynamics utilizing cosmic ray produced radionuclides. In: Proceedings, Sustaining the Global Farm-Selected papers from the

- 10th International Soil Conservation Organization Meeting Q, May 24–29, 1999, Purdue University, West Lafayette IN, Stotte DE, Mohr RH, Steinhardt GC (eds). INUSDA-ARS National Soil Erosion Laboratory: West Lafayette, IN; 1044–1052.
- Lal R, Tims SG, Fifield LK, Wasson RJ, Howe D.* 2013. Applicability of ^{239}Pu as a tracer for soil erosion in the wet-dry tropics of northern Australia. *Nuclear Instruments and Methods in Physics Research Section B: Beam Interactions with Materials and Atoms* 294: 577–583. <https://doi.org/10.1016/j.nimb.2012.07.041>.
- Larsen JL, Almond PC, Eger A, Stone JO, Montgomery DR, Malcolm B.* 2014. Rapid soil production and weathering in the Southern Alps, New Zealand. *Science* 343: 637–640. <https://doi.org/10.1126/science.1244908>.
- Lee MH, Lee CW.* 1999. Determination of Cs-137, Sr-90 and fallout Pu in the volcanic soil of Korea. *Journal of Radioanalytical and Nuclear Chemistry* 239: 471–476.
- Lin H, Bouma J, Wilding LP, Richardson JL, Kutilek M, Nielsen DR.* 2005. Advances in Hydropedology. *Advances in Agronomy* 85:1–89. [https://doi.org/10.1016/S0065-2113\(04\)85001-6](https://doi.org/10.1016/S0065-2113(04)85001-6).
- Lüthgens C, Böse M, Preusser F.* 2011. Age of the Pomeranian ice-marginal position in northeastern Germany determined by optically stimulated luminescence (OSL) dating of glaciofluvial sediments. *Boreas* 40: 598–615. <https://doi.org/10.1111/j.1502-3885.2011.00211.x>.
- Maejima Y, Matsuzaki H, Higashi T.* 2005. Application of cosmogenic ^{10}Be to dating soils on the raised coral reef terraces of Kikai Island, southwest Japan. *Geoderma* 126: 389–399. <https://doi.org/10.1016/j.geoderma.2004.10.004>.
- Masarik J.* 2009. Origin and distribution of radionuclides in the continental environment. In *Environmental Radionuclides: Tracers and Timers of Terrestrial Processes*. Radioactivity in the Environment, Froehlich K (ed.). 1–25. Elsevier: Amsterdam. DOI: [https://doi.org/10.1016/S1569-4860\(09\)01601-5](https://doi.org/10.1016/S1569-4860(09)01601-5)
- Masarik J, Beer J.* 2009. An updated simulation of particle fluxes and cosmogenic nuclide production in the Earth's atmosphere. *Journal of Geophysical Research* 114: D11103. <https://doi.org/10.1029/2008JD010557>.
- Milne G.* 1935. Some suggested units for classification and mapping, particularly for East African soils. *Soil Research* 4: 183–198.

- Muhs DR. 2013. The geologic records of dust in the Quaternary. *Aeolian Research* 9: 3–48. <https://doi.org/10.1016/j.aeolia.2012.08.001>.
- Muhs DR, Benedict JB. 2006. Eolian additions to late Quaternary alpine soils, Indian Peaks Wilderness Area, Colorado Front Range. *Arctic Antarctic and Alpine Research* 38(1): 120–130. [https://doi.org/10.1657/1523-0430\(2006\)038\[0120:EATLQA\]2.0.CO;2](https://doi.org/10.1657/1523-0430(2006)038[0120:EATLQA]2.0.CO;2).
- Nishiizumi K, Imamura M, Caffee MW, Southon JR, Finkel RC, McAninch J. 2007. Absolute calibration of ^{10}Be AMS standards. *Nuclear Instruments and Methods in Physics Research Section B: Beam Interactions with Materials and Atoms* 25: 403–413. <https://doi.org/10.1016/j.nimb.2007.01.297>.
- Norton KP, von Blanckenburg F, Kubik PW. 2010. Cosmogenic nuclide-derived rates of diffusive and episodic erosion in the glacially sculpted upper Rhone Valley, Swiss Alps. *Earth Surface Processes and Landforms* 35: 651–662. <https://doi.org/10.1002/esp.1961>.
- O'Farrell CR, Heimsath AM, Kaste JM. 2007. Quantifying hillslope erosion rates and processes for a coastal California landscape over varying timescales. *Earth Surface Processes and Landforms* 32: 544–560. <https://doi.org/10.1002/esp.1407>.
- Pavich MJ, Brown L, Klein J, Middleton R. 1984. ^{10}Be accumulation in a soil chronosequence. *Earth and Planetary Science Letters* 68:198–204. [https://doi.org/10.1016/0012-821X\(84\)90151-1](https://doi.org/10.1016/0012-821X(84)90151-1).
- Phillips JD. 2010. The convenient fiction of steady-state soil thickness. *Geoderma* 156: 389–398. <https://doi.org/10.1016/j.geoderma.2010.03.008>.
- Phillips JD. 2015. The robustness of chronosequences. *Ecological Modelling* 298: 16–23. <https://doi.org/10.1016/j.ecolmodel.2013.12.018>.
- Portenga EW, Bierman P. 2011. Understanding Earth's eroding surface with ^{10}Be . *GSA Today* 21: 4–10. <https://doi.org/10.1130/G1111A.1>.
- Reimer PJ, Bard E, Bayliss A, Beck JW, Blackwell PG, Bronk Ramsey C, Buck CE, Cheng H, Edwards RL, Friedrich M, Grootes PM, Guilderson TP, Haflidason H, Hajdas I, Hatté C, Heaton TJ, Hoffmann DL, Hogg AG, Hughen KA, Kaiser KF, Kromer B, Manning SW, Nui M, Reimer RW, Richards DA, Scott EM, Southon JR, Staff ARA, Turney C, van der Plicht J. 2013. IntCal13 and Marine13 radiocarbon age calibration curves 0–50,000 years cal BP. *Radiocarbon* 55: 1869–1887. https://doi.org/10.2458/azu_js_rc.55.16947.

- Rieckh H, Gerke HH, Siemens J, Sommer M. 2014. Water and dissolved carbon fluxes in an eroding soil landscape depending on terrain position. *Vadose Zone Journal* 13. <https://doi.org/10.2136/vzj2013.10.0173>.
- Ryan JG. 2002. Trace-element systematics of beryllium in terrestrial materials. *Reviews in Mineralogy and Geochemistry* 50: 121–145. <https://doi.org/10.2138/rmg.2002.50.3>.
- Schimmack W, Auerswald K, Bunzl K. 2001. Can $^{239+240}\text{Pu}$ replace ^{137}Cs as an erosion tracer in agricultural landscapes contaminated with Chernobyl fallout? *Journal of Environmental Radioactivity* 53: 41–57. [https://doi.org/10.1016/S0265-931X\(00\)00117-X](https://doi.org/10.1016/S0265-931X(00)00117-X).
- Schaller M, Ehlers TA, Blum JD. 2010. Soil transport on a moraine foreslope. *Geomorphology* 115: 117–228. <https://doi.org/10.1016/j.geomorph.2009.09.040>.
- Schimmack W, Auerswald K, Bunzl K. 2002. Estimation of solid erosion and deposition rates at an agricultural site in Bavaria, Germany, as derived from fallout radiocesium and plutonium as tracers. *Naturwissenschaften* 89: 43–46. <https://doi.org/10.1007/s00114-001-0281-z>.
- Schlichting E, Blume HP, Stahr K. 1995. *Soils Practical*. Blackwell:Berlin (in German).
- Schoonejans J, Vanacker V, Opfergelt S, Christl M. 2017. Long-term soil erosion derived from in-situ ^{10}Be and inventories of meteoric ^{10}Be in deeply weathered soils in southern Brazil. *Chemical Geology* 477:380–388. <https://doi.org/10.1016/j.chemgeo.2017.06.025>.
- Sommer M, Gerke HH, Deumlich D. 2008. Modelling soil landscape genesis – a “time split” approach for hummocky agricultural landscapes. *Geoderma* 145: 480–493. <https://doi.org/10.1016/j.geoderma.2008.01.012>.
- Sommer M, Augustin J, Kleber M. 2016. Feedbacks of soil erosion on SOC patterns and carbon dynamics in agricultural landscapes – the CarboZALF experiment. *Soil & Tillage Research* 156: 182–184. <https://doi.org/10.1016/j.geoderma.2008.01.012>.
- Stroeven AP, Hattestrand C, Kleman J, Heyman J, Fabel D, Fredin O, Goodfellow BW, Harbor JM, Jansen JD, Olsen L, Caffee MW, Fink D, Lundqvist J, Rosqvist GC, Stromberg B, Jansson KN. 2016. Deglaciation of Fennoscandia. *Quaternary Science Reviews* 147: 91–121. <https://doi.org/10.1016/j.quascirev.2015.09.016>.
- van der Meij M, Temme AJAM, Wallinga J, Hierold W, Sommer M. 2017. Topography reconstruction of eroding landscapes – a case study from a hummocky ground moraine

- (CarboZALF-D). *Geomorphology* 295: 758–772.
<https://doi.org/10.1016/j.geomorph.2017.08.015>.
- Wallbrink PJ, Murray AS. 1993. Use of Fallout Radionuclides as indicators of erosion processes. *Hydrological Processes* 7: 297–304. <https://doi.org/10.1002/hyp.3360070307>.
- Walling DE, Quine TA. 1990. Calibration of caesium-137 measurements to provide quantitative erosion rate data. *Land Degradation and Rehabilitation* 2: 161–175. <https://doi.org/10.1002/ldr.3400020302>.
- Walling DE, Zhang Y, He Q. 2014. Conversion models and related software. In Guidelines for Using Fallout Radionuclides to Assess Erosion and Effectiveness of Soil Conservation Strategies. International Atomic Energy Agency Publication: Vienna; 125–148.
- Wetzel G. 1996. The neolithicum in the western Oder region. In Man and Environment in the Middle and Lower Oder Region – Contributions to Prehistory and Early History Settlements, Leciejewicz L, Gringmuth-Dallmer E (eds) Wrocław: Instytut Archeologii i Etnologii Polskiej Akademii Nauk; 61–66 (in German).
- Willenbring JK, von Blanckenburg F. 2010. Meteoric cosmogenic Beryllium-10 adsorbed to river sediment and soil: applications for Earth-surface dynamics. *Earth-Science Reviews* 98: 105–122. <https://doi.org/10.1016/j.earscirev.2009.10.008>.
- Zapata F. 2003. Handbook for the Assessment of Soil Erosion and Sedimentation Using Environmental Radionuclides. Kluwer Academic Publishers: New York.
- Zhang X, Higgitt DL, Walling DE. 1990. A preliminary assessment of the potential for using caesium-137 to estimate rates of soil erosion in the Loess Plateau of China. *Hydrology Sciences Journal* 35:243–252. <https://doi.org/10.1080/02626669009492427>.
- Zollinger B, Alewell C, Kneisel C, Meusburger K, Brandova D, Kubik P, Schaller M, Ketterer M, Egli M. 2015. The effect of permafrost on time-split soil erosion using radionuclides (Cs-137, Pu239 + 240, meteoric Be-10) and stable isotopes (delta C-13) in the eastern Swiss Alps. *Journal of Soils and Sediments* 15: 1400–1419. <https://doi.org/10.1007/s11368-014-0881-9>.
- Zollinger B, Alewell C, Kneisel C, Brandová D, Petrillo M, Plötze M, Christl M, Egli M. 2017. Soil formation and weathering in a permafrost environment of the Swiss Alps: a multi-

parameter and nonsteady-state approach. *Earth Surface Processes and Landforms* 42:814–835. <https://doi.org/10.1002/esp.4040>.

Chapter 3. Soil erosion along a transect in a forested catchment: recent or ancient processes?

Abstract

Forested areas are assumed not to be influenced by erosion processes. However, forest soils of Northern Germany in a hummocky ground moraine landscape can sometimes exhibit a very shallow thickness on crest positions and buried soils on slope positions. The question consequently is: Are these on-going or ancient erosional and depositional processes? Plutonium isotopes act as soil erosion/deposition tracers for recent (last few decades) processes. Here, we quantified the $^{239+240}\text{Pu}$ inventories in a small, forested catchment (ancient forest “Melzower Forst”, deciduous trees), which is characterised by a hummocky terrain including a kettle hole. Soil development depths (depth to C horizon) and $^{239+240}\text{Pu}$ inventories along a catena of sixteen different profiles were determined and correlated to relief parameters. Moreover, we compared different modelling approaches to derive erosion rates from Pu data. We find a strong relationship between soil development depths, distance-to-sink and topography along the catena. Fully developed Retisols (thicknesses $> 1\text{m}$) in the colluvium overlay old land surfaces as documented by fossil Ah horizons. However, we found no relationship of Pu-based erosion rates to any relief parameter. Instead, $^{239+240}\text{Pu}$ inventories showed a very high local, spatial variability ($36 - 70 \text{ Bq m}^{-2}$). Low annual rainfall, spatially distributed interception and stem flow might explain the high variability of the $^{239+240}\text{Pu}$ inventories, giving rise to a patchy input pattern. Different models resulted in quite similar erosion and deposition rates (max: $-5 \text{ t ha}^{-1} \text{ yr}^{-1}$ to $+7.3 \text{ t ha}^{-1} \text{ yr}^{-1}$). Although some rates are rather high, the magnitude of soil erosion and deposition - in terms of soil thickness change - is negligible during the last 55 years. The partially high values are an effect of the patchy Pu deposition on the forest floor. This forest has been protected for at least 240 years. Therefore rather natural events and anthropogenic activities during medieval times or even earlier must have caused the observed soil pattern, which documents strong erosion and deposition processes.

Published as: Calitri, F., Sommer, M., van der Meij, M. W., & Egli, M. (2020). Soil erosion along a transect in a forested catchment: Recent or ancient processes? *Catena*, 194. <https://doi.org/10.1016/j.catena.2020.104683>

3.1 Introduction

Soil erosion is one of the major environmental problem the world has to face, along with population growth, climate change and loss of biodiversity (Berhe et al., 2018). It is a widespread phenomenon and affects any kind of ecosystem (Lal & Stewart, 1990; Pimentel, 1993; Pimentel et al., 1995; Pimentel & Kounang, 1998). Soil erosion gradually leads to soil degradation, causing a decrease of soil quality, productivity and diversity of plants, animals and microbes in natural, agricultural and forest ecosystems (Pimentel, 2001; Pimentel et al., 1995; Pimentel & Kounang, 1998). One usually assumes that soil erosion is a primary concern for arable lands and that no erosion or negligible erosion occurs in forested areas. Erosion and soil formation are over time not constant (Raab et al., 2018; Sommer et al., 2008). Soil erosion is generally driven by tectonic activity, parent material, surface topography, climate, anthropogenic and biotic activity (Smithson et al., 2008) — some of these factors may vary over time. Changing environmental conditions can lead to an acceleration, deceleration or reversal of erosion and soil formation rates: a factor constellation that gives rise to co-evolution (Phillips, 2015). These varying constellations over time are, owing to methodological restrictions, difficult to decipher.

A soil profile with its macromorphological features is the sum of all factors and processes over time that determined its evolution. As a consequence, soil profile thickness stores not only the short-term but also the long-term processes.

Short-term (i.e., over decades) erosion rates can be assessed using fallout radionuclides (FRN, Portes et al., 2018; Raab et al., 2018). Many fallout radionuclides (e.g., ^7Be , $^{210}\text{Pb}_{\text{ex}}$), especially ^{137}Cs , have been successfully used for soil redistribution measurements since the 1970s (Zapata, 2003). Due to the Chernobyl nuclear accident in 1986, a part of Europe has been contaminated by its fallout nuclides (mainly ^{137}Cs). One major weakness of using ^{137}Cs is its short half-life of 30.2 years that makes its detection and consequently the estimation of erosion rates with time more difficult. Therefore, plutonium (Pu) isotopes are an increasingly better alternative. Pu is a well-known FRN and is globally distributed due to thermonuclear weapon testing between 1952 and 1964 (Ketterer & Szechenyi, 2008; Pentreath, 1995). The two major Pu isotopes in the environment are ^{239}Pu ($t_{1/2} = 24,110$ years) and ^{240}Pu ($t_{1/2} = 6,561$ years). They both originate mainly from past nuclear weapon tests, while contributions by other sources, e.g., nuclear power plant incidents, added Pu only locally (Evrard et al., 2014; Matisoff et al., 2011). $^{239+240}\text{Pu}$ may have several advantages over ^{137}Cs particularly there where the

Chernobyl fallout was detectable and where at the same time a snow cover was present (Alewell et al., 2014). With snowmelt on slopes, a distinct part of ^{137}Cs was removed giving rise to a very heterogeneous input into soils.

$^{239+240}\text{Pu}$ can serve as a soil erosion tracer on arable land (Schimmack et al., 2001), permanent grasslands (Alewell et al., 2014; Arata et al., 2016a; Meusbürger et al., 2018; Zollinger et al., 2015) or coniferous and evergreen forests (Hoo et al., 2011; Lal et al., 2013; Meusbürger et al., 2016; Zollinger et al., 2015).

Studies about soil erosion in forests are lacking in most areas worldwide. The forest soils of a hummocky ground moraine landscape in northern Germany sometimes exhibit a very shallow thickness on crest positions (Rüffer, 2018); Calcaric Regosols, Calcaric Cambisols, Nudiargic Luvisols or similar; (Miller et al., 2016) and buried soils on slope positions (Stagnic Albic Retisols, IUSS Working Group WRB, 2015). To understand if recent erosional processes still contribute to the observed soil pattern of the hummocky landscape or if only ancient processes are the main cause, a procedure is needed that enables the discrimination of processes between these two scales. Our main research questions were: Do $^{239+240}\text{Pu}$ isotopes detect any recent erosion in these forest soils? Are the soil patterns observed in northern Germany purely a result of past events (natural and/or anthropogenic) or are they imbedded in on-going processes?

We tried to answer these questions by studying soils of an ancient forest that has not been managed for at least the last 240 years. We hypothesised that even in a forested area soil material may be translocated along slopes and that a corresponding pattern in the spatial distribution of Pu should be detectable.

3.2 Study Area

The study area is located in the Uckermark region, northeast Germany, a formerly glaciated landscape (Figure 3.1). It is characterised by a hummocky terrain with ridges, kettle holes and a series of small lakes. A peculiarity of kettle holes is that the entire history of soil movement is documented in the related small, closed catchment. Hence soil erosion and deposition rates can be quantified by mass balances.

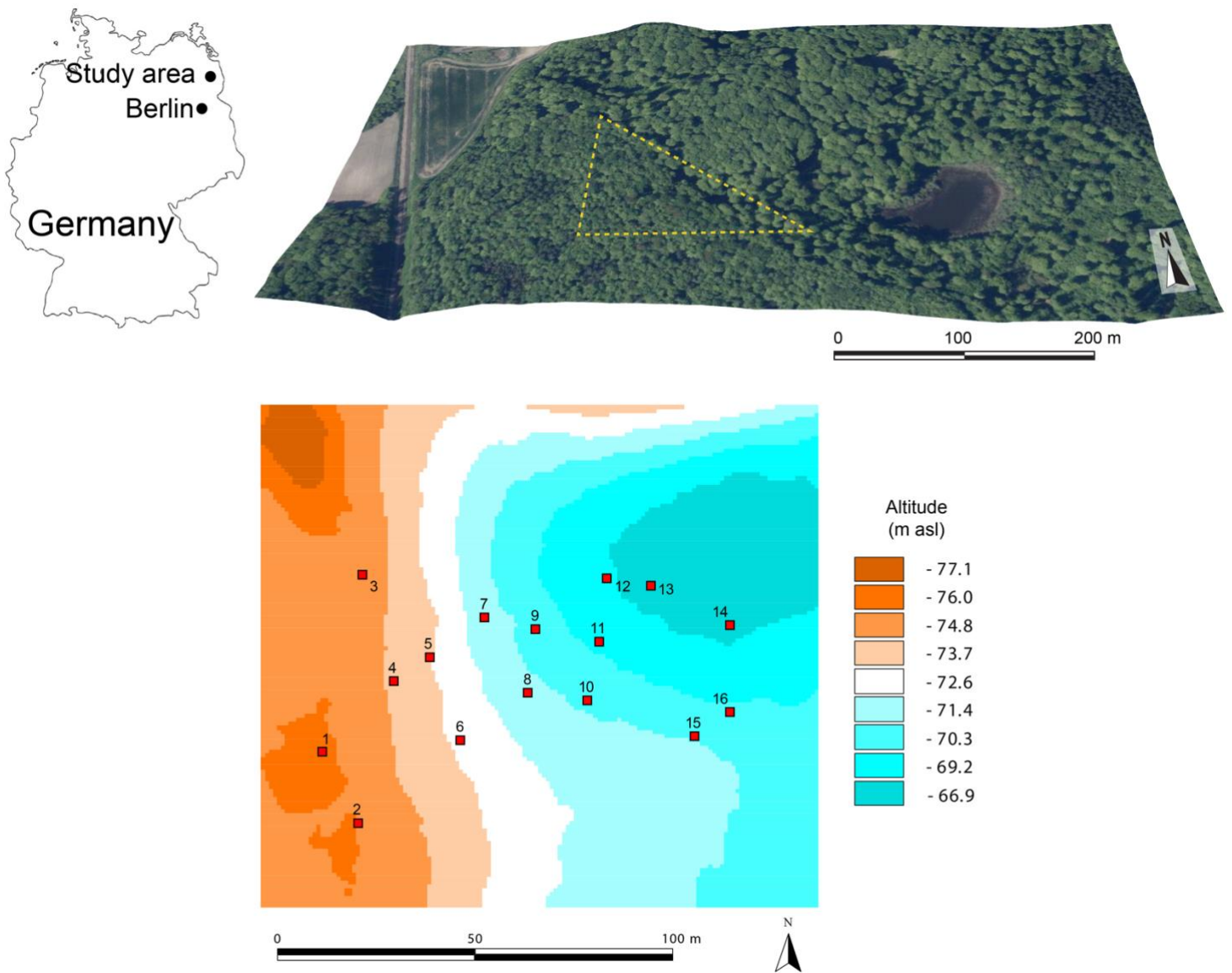


Figure 3.1. Location (yellow triangle), altitude (m a.s.l.) and sampling points of the study area “Melzower Forst”.

Most of the Uckermark region was used for agricultural purposes since Neolithic times due to its fertile soils. Intensification of land use occurred in medieval times by deforestation accompanied by severe water erosion during catastrophic rainfall events and tillage erosion during the last decades (Wetzel, 1996; Bork, 2006; Sommer et al., 2008; Deumlich et al., 2010; Koszinski et al., 2013; Kappler et al., 2018). As a consequence of the hummocky terrain, the soil units of arable land change within short distances as a function of topography, with Calcaric Regosols on ridge positions, Luvisols (partly eroded and influenced by stagnant water; Miller et al., 2016) or Retisols along slopes and Gleysols and Histosols (covered by colluvial soil material) in depressions (former kettle holes). As a consequence, the soil associations within the hummocky ground moraine reveals a pronounced small-scale variation of soil properties (Koszinski et al., 2013; van der Meij et al., 2017).

Our study region is characterised by a subcontinental climate with a mean annual temperature of 8.9 °C and a mean annual precipitation of 540 – 600 mm (Kopp and Schwanecke, 1994; Deutscher Wetterdienst). The climatic water balance is slightly negative (about -25 mm yr⁻¹).

The forested part of the region is characterised by a temperate deciduous forest and is dominated by beech (*Fagus sylvatica* L.). Due to the relatively dry conditions oak (*Quercus robur* and *Quercus petraea*) is widespread. Often also small-leaved lime (*Tilia cordata*), large leaf linden (*Tilia platyphyllos*), European hornbeam (*Carpinus betulus*) and wild cherry (*Prunus avium*) are part of the forest vegetation (Rüffer, 2018).

The majority of the forests grow on soils developed from glaciofluvial deposits, which have been deposited during the last ice age. Only few forested areas are underlain by ground moraines which were deposited during the Pomeranian stages (22 – c. 17 ka BP, MIS 2; (Lüthgens & Böse, 2011) of the Weichselian glaciation (MIS 2 – 4). According to Lüthgens et al. (2011), previous surface exposure dating in the region showed that a first stabilisation of the landscape after melting of dead ice bodies took place around 16.5 ka ago and intensified with the beginning of the Bølling interstadial. Deglaciation and melting of the dead ice left an undulating ground moraine landscape where many kettle holes can be found irregularly distributed (Kalettka et al., 2001).

For comparison with an intensively studied agricultural site on hummocky ground moraines (“CarboZALF-D”, Calitri et al., 2019) we selected the study area “Melzower Forst”, which shows similar soil forming factors (climate, terrain, parent material) except land use. The “Melzower Forst” belongs to an ancient forest complex, which has not been used as arable land

for the last 240 years or more according to historical maps of the late 18th century (Schmettau Map ca. 1790; <https://bb-viewer.geobasis-bb.de>). The study area is part of the Biosphere Reserve Schorfheide-Chorin, which is under full environmental protection since 1938. This natural reserve area was extended in 1990 and is made of an old beech tree forest with some individuals of up to 400 years (Rüffer, 2018).

3.3 Materials and methods

3.3.1 Soil sampling

A first soil survey at the “Melzower Forst” comprised a total of 29 soil corings down to the illitic- calcareous, glacial till (max. 3m) in November 2016. For this purpose we used high-temperature polypropylene (PP) tubes with a nominal diameter of 63 mm (HT DN63) and a length of 2 m (plus 1 m). Each PP tube was inserted in a closed, metal driving core tube (M22; Nordmeyer Geotool, Herne, Germany). The core tube was driven into the soil by a self-propelled vehicle (GTR 790; Nordmeyer Geotool). In addition one soil pit (site 11, Figure 3.1) was opened down to 1.5 m to verify retic properties (IUSS Working Group WRB, 2015). From the 29 sites 16 sites were selected (Figure 3.1) to assess recent soil erosion/deposition rates by Pu inventories. For this purpose a second sampling campaign was carried out in November 2017. We dug one soil pit per site (50 x 50 cm²) and sampled the soil down to 25 cm in 5 cm increments by undisturbed soil cores (100 cm³). At three sites along the catena (8, 11, 16) we sampled and analysed four soil pits for each site separately to quantify local variability (dm-scale).

3.3.2 Soil sample preparation and analysis

Soil samples from cores were air dried, gently crushed and sieved at 2mm to separate the fine earth fraction (<2 mm) from gravel (>2 mm). Aliquots of the fine earth fractions were dried at 105 °C for bulk density (BD) determination. Fine earth masses (kg m⁻² 0.05m⁻¹) were calculated by multiplying bulk densities with 50 and a correction factor for gravel (wt.-% > 2mm).

The C content was measured using a Picarro analyser (G2131-i Picarro) for isotopic CO₂ (Combustion Module-Cavity Ring Down Spectroscopy (CM-CRDS), Sunnyvale, California, USA) with an uncertainty of 0.1%. Fine earth was milled and weighed into tin capsules, then combusted at 950° C. The released CO₂ was measured using a CRDS analyser (Picarro, G2131 type). We used an internal standard (30B00GW9 Chernozem 2013) for the correction of potential drift in the C content values. If top-soils are free of carbonates, total carbon equals soil organic carbon (SOC).

3.3.3 Sample preparation and measurement for $^{239+240}\text{Pu}$ activities

Pu isotopes measurements were performed according to (Ketterer et al., 2004). The samples (5 g of milled fine earth) from the 16 sites were firstly dry-ashed for 18 hours at 600 °C to remove organic matter and subsequently spiked with a ^{242}Pu tracer solution containing ~0.0044 Bq (NIST 4334). Afterwards, the samples were leached overnight with 16 M HNO_3 at 80 °C and successively filtered with an addition of deionized water to reach a concentration of 8 M HNO_3 . Pu species were transformed to the Pu (IV) oxidation state using first an acidified $\text{FeSO}_4 \cdot 7\text{H}_2\text{O}$ solution (2 mg/mL of leached solution) and then a NaNO_2 solution (20 mg/mL of leached solution). The samples were later heated at 75 °C for 2 hours. Pu (IV) was then separated from the leached solution using a Pu-selective TEVA resin (2 mg of TEVA per mL of leached solution) and let it settle for 2 h. The resin was collected in a pipet tip equipped with a glass wool plug. The columns were rinsed with 2 M aqueous HNO_3 to remove unretained matrix elements (e.g., U), then rinsed with 8 M HCl to elute Th and finally rinsed again with 2 M aqueous HNO_3 (rinse volume: 1 ml per 30 mg of TEVA). Pu was eluted using an aqueous solution of 0.05 M ammonium oxalate. Activities of $^{239+240}\text{Pu}$ were measured using an Agilent 8800 Triple Quadrupole ICP-MS with an Apex IR nebulizer (ESI Scientific, Omaha, NE, USA), located at University of Zurich. The masses of ^{239}Pu and ^{240}Pu in the samples were converted into the summed activity $^{239+240}\text{Pu}$. Data quality was evaluated through the analysis of blanks (rocks devoid of Pu), duplicates and control samples of known $^{239+240}\text{Pu}$ activities (Standard Reference material 4350b – River sediment for radioactivity measurements from NIST).

3.3.4 Conversion of $^{239+240}\text{Pu}$ activities into soil redistribution rates

$^{239+240}\text{Pu}$ inventories (Bq m^{-2}) were calculated based on the following equation:

$$As = \frac{1}{S} \sum_i M_{Ti} C_i \quad (3.1)$$

Where C_i = activity of the i^{th} sub-sample depth increment (Bq/kg), M_{Ti} = total mass of the i^{th} sample depth increment (kg) and S = area of the horizontal core cross (m^2). Soil redistribution rates were obtained with a comparison of the isotope inventory of an eroding point and the average inventory within the catchment. In kettle holes, soil material cannot be exported.

Consequently, eroded soil material is deposited in another part of the small catchment. By taking the average value of the Pu inventories, the reference inventory can be calculated.

Three different models were used to convert $^{239+240}\text{Pu}$ inventories into soil redistribution rates (Zollinger et al., 2015). The average values among all the soil profiles for each horizon (0 – 5 cm; 5 – 10 cm; 10 – 15 cm; 15 – 20 cm; 20 – 25 cm) were used as reference values for the calculation of the soil redistribution rates.

1. The profile distribution model (PDM) (Walling & Quine, 1990; XINBAO et al., 1990) is a convenient model to estimate soil erosion rates in unploughed soils. It assumes, among others, an exponential depth distribution:

$$A'(x) = A_{ref}(1 - e^{x/h_0}) \quad (3.2)$$

where $A'(x)$ = amount of isotope inventory above depth x (Bq m^{-2}) x = depth from soil surface expressed as mass between top and actual depth (kg m^{-2}), A_{ref} = reference inventory as mean of all reference sites (Bq m^{-2}) and h_0 = profile shape factor (kg m^{-2}) that is a coefficient describing the rate of exponential decrease in inventory with depth, for soil profiles in uncultivated sites. The erosion rate Y for a point of interest is calculated as:

$$Y = \frac{10}{t - t_0} \ln \left(1 - \frac{X}{100} \right) h_0 \quad (3.3)$$

Y = erosion rate ($\text{t ha}^{-1} \text{a}^{-1}$), t = year of sampling, t_0 = '1963' (end of thermonuclear weapon testing), X = % reduction of total inventory (Au [Bq m^{-2}]) in regard to the local reference value ($(A_{ref} - A_u)/A_{ref} \times 100$).

2. The inventory method (IM) (Lal et al., 2013) has specifically been developed for $^{239+240}\text{Pu}$ and also assumes an exponential depth distribution, but takes a particle size correction factor into account:

$$L = -\frac{1}{\alpha P} \ln \left(1 - \frac{I_{loss}}{I_{Ref}} \right) \quad (3.4)$$

with L = loss of soil, $I_{loss} = I_{ref} - I$, I_{ref} = the local reference inventory as mean of all reference sites (Bq m^{-2}), I = measured total inventory at the sampling point (Bq m^{-2}) and P = particle size correction factor, where $P > 1$. Calculations were done using a P factor of 1, 1.2 (according to Walling & He, 1999) and 1.5 (according to Lal et al.,

2013). Following the approach of (Alewell et al., 2014), the coefficient α was obtained from a least squared exponential fit of $^{239+240}\text{Pu}$ isotopes depth profile.

3. MODERN (Modelling Deposition and Erosion rates with RadioNuclides) (Arata et al. 2016a; Arata et al., 2016b). MODERN has the ability to describe specific depth distribution of any fallout radionuclide (FRN) in the soil, independent of its depth function's shape. A key assumption of MODERN is that the evolution of the depth distribution of the selected FRN is the same at the reference and the sampling sites.

The FRN depth profile of the reference site is modelled as a step function $g(x)$, which at each increment inc returns a value Inv_{inc} , that is the FRN total inventory of a sampling site, measured for the whole depth profile d (cm). The model targets the level x^* (cm) from x^* to x^*+d (cm), where the sum of all Inv_{inc} of the reference site is equal to the total FRN inventory of the sampling site, Inv . MODERN returns the results in cm of soil losses or gains. The conversion to yearly soil losses or gains Y in $\text{t ha}^{-1} \text{yr}^{-1}$ can be calculated using the following equation:

$$Y = 10 \times \frac{x^* \cdot xm}{d \cdot (t_1 - t_0)} \quad (5)$$

where xm is the mass depth (kg m^{-2}) of the sampling site, d is the total depth increment considered at the sampling site, t_1 is the sampling year (yr), and t_0 (yr) is the reference year.

3.3.5 Radiocarbon dating

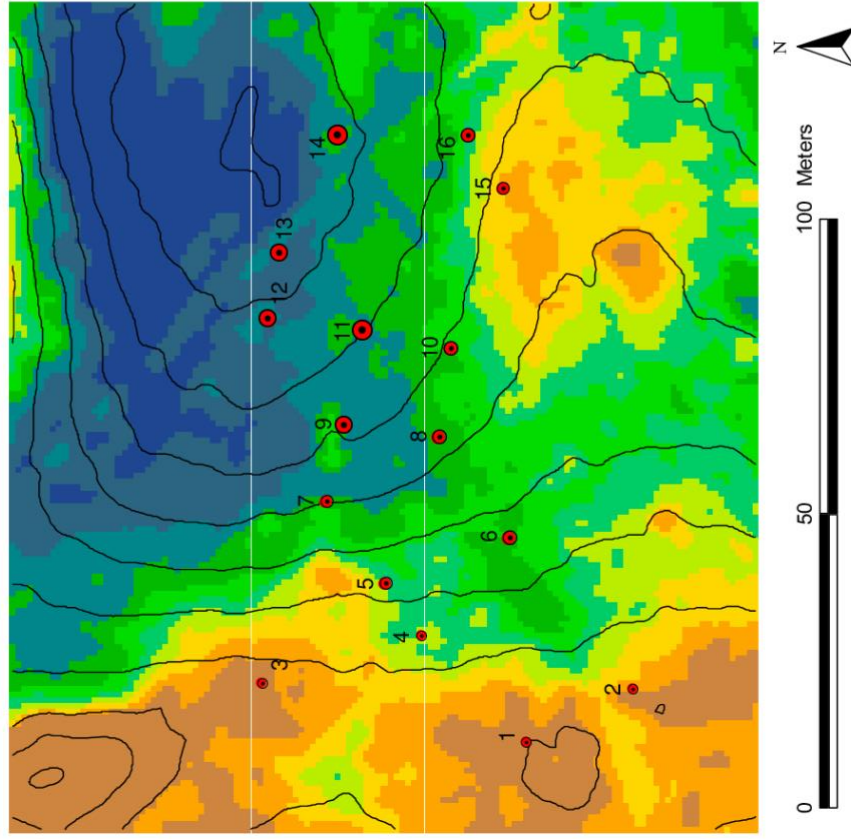
To approximately date the fossil A horizon (Hydro4), the particulate organic matter (POM) was dated. The date of this fractions indicates the time when the soil was overridden (Mirsky et al., 2008; Zollinger et al., 2013). The treated material was combusted at 900°C to produce CO_2 which was then reduced to graphite. The ratios of the carbon isotopes were measured by Accelerator Mass Spectrometry (AMS) using the 0.2 MV MICADAS facility at the Institute of Ion Beam Physics at the Swiss Federal Institute of Technology, Switzerland. The radiocarbon age calibration was done online with the OxCal4.3 tool using IntCal13 for calibration (Reimer et al., 2013).

3.3.6 GIS-based terrain analysis

Based on the official DTM1 for the Federal State of Brandenburg (<https://geobasis-bb.de/geodaten/dgm-laserscan.htm>) we calculated simple terrain parameters using the raster package in statistical software R, like slope angle and aspect. Furthermore, we derived a complex terrain parameter — the Topographic Position Index (TPI) (Weiss, 2001) — using a moving window technique (Figure 3.2). The TPI₂₅ of a grid cell represents the difference in elevation (m asl) between this grid cell and the mean elevation of all neighbouring grid cells in a 25m radius. Positive TPI values indicate grid cells that are higher than the average of their surroundings (crests, small hummocks), while negative TPI values represent cells that are lower than their surroundings (basins, small depressions). Deumlich et al. (2010) showed this approach to be successful in delineating landforms and related soils in agricultural hummock ground moraine landscape. Local distance of each site to the next tree stems was calculated by aerial photograph. Other parameters that we calculated were distance of each site to the sink of the depression and to the nearest trees, and the number of trees in a 10 m radius of each site. The locations of trees were estimated using aerial photography available in Google Earth (earth.google.com).

3.3.7 Data evaluation and statistical analyses

We performed linear and polynomial regressions to describe the distribution of $^{239+240}\text{Pu}$ as a function of controlling, topographic factors as well as for distribution of the trees in the forest (distance to trees, number of trees) using statistical software R and Origin 9.0. All data used for our statistical analysis showed a normal distribution (Shapiro-Wilk test).



Depth-to-C, cm

- 20 - 37
- 42 - 83
- 85 - 154
- 173 - 213
- 214 - 241

TPI 25, cm

- > 42
- 30 - 41
- 19 - 29
- 8 - 18
- 0 - 7
- -9 - -1
- -19 - -10
- -34 - -20
- -52 - -35
- < - 52

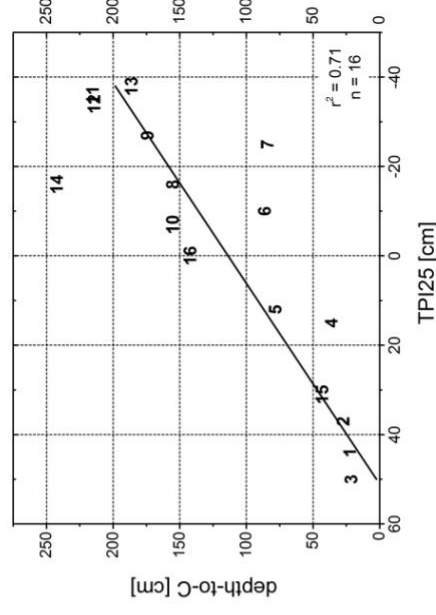
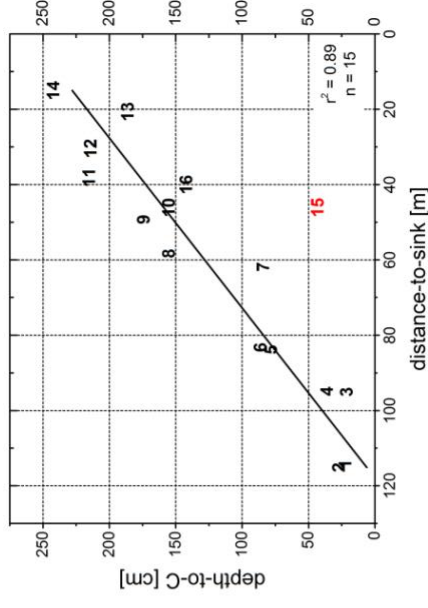


Figure 3.2. Relationship between terrain parameters and soil thickness (depth to C horizons); left: spatial pattern of the TPI (Topographic Position Index); right upper part: regression analysis with depth-to-sink (without site 15 = outside the main catena); right lower part: regression analysis with TPI25.

3.4 Results

3.4.1 Soil pattern

The soils along the catena revealed a regular sequence starting with Calcaric Regosols at the ridge and upslope positions, followed by (eroded) Nudiargic Luvisols and Albic Retisols in the upper half of the slope (Table 3.1). In downslope direction redoximorphism increased, which led to Endostagnic Albic Retisols at lower midslope and Albic Retic Stagnosols at toeslope and in the depression (soil classification according to WRB, IUSS, 2014). Here, buried soils occurred below the recent soils as indicated by several fossil Ah horizons along the catena (85 – 157cm, Table 3.1). The subsoils of the buried soils were either carbonate-free and revealed clay translocations (toeslope) or showed a strong groundwater-related redoximorphism (depression). All recent soils showed an argic B horizon, except for the Calcaric Regosols. Hence, clay translocation is the dominating pedogenic process along the catena. In essence, the catena can be regarded as a hydrosequence, which is strongly influenced by soil transport (erosion, deposition; Figure 3.3).

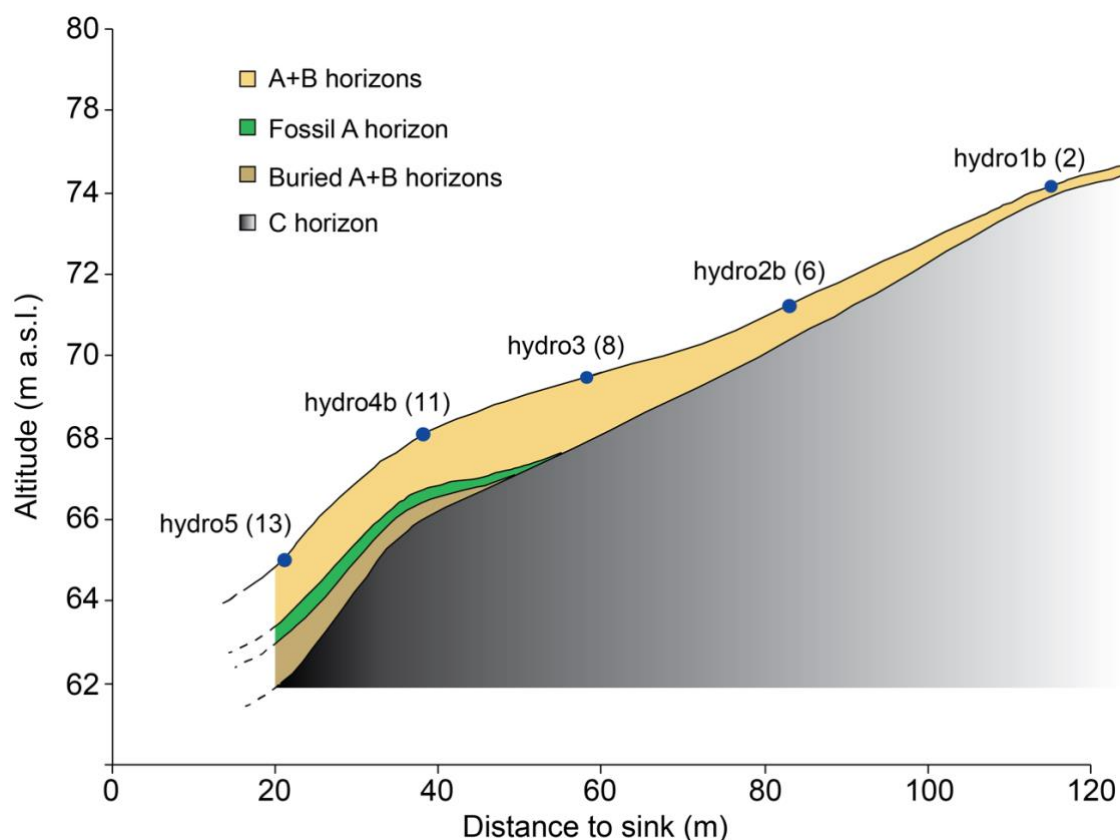


Figure 3.3. Schematic cross-section (using a vertical exaggeration of a factor 3) of the investigated catena (hydro-sequence with sites 2, 6, 8, 11, 13; see Table 3.1).

Table 3.1. Location, landscape attributes and soil characteristics for study site “Melzower Forst”.

Site No.	Site name	Coordinates (°N / °E)	slope °	TPI25 m	dts m	disttree 1 m	disttree 2 m	ntrees	Soil Classification (IUSS, 2014)	depth to C cm	fossile Ah, upper boundary, cm	SOC stock kg m ⁻² 0.2m ⁻¹
1	judge2b	53.151316 / 13.882349	1.8	0.88	114	2.1	3.9	4	Calcaric Regosol (RG-ca)	37	-	6.5
2	hydro1b	53.152938 / 13.883513	4.2	0.79	115	3.6	4.6	6	Nudiaric Luvisol (LV-ng)	26	-	3.5
3	LHS16b	53.153503 / 13.883506	3.9	0.89	95	2.6	3.0	5	Nudiaric Luvisol (LV-ng)	20	-	5.4
4	LHS5b	53.153261 / 13.883627	5.3	0.46	95	1.5	4.5	5	Nudiaric Luvisol (LV-ng)	35	-	2.7
5	LHS11b	53.153320 / 13.883765	6.0	0.25	84	2.6	4.5	7	Albic Retisol (RT-ab)	77	-	2.7
6	hydro2b	53.153126 / 13.883889	4.9	-0.04	83	1.5	6.5	6	Albic Retisol (RT-ab)	85	-	2.6
7	LHS15b	53.153407 / 13.883972	8.4	-0.29	62	5.7	8.1	2	Endostagnic Albic Retisol (RT-stn.ab)	83	-	4.5
8	hydro3	53.153241 / 13.884138	4.4	-0.23	58	2.3	2.8	5	Endostagnic Albic Retisol (RT-stn.ab)	154	-	3.9
9	LHS6b	53.153385 / 13.884173	3.9	-0.36	49	4.9	10.9	1	Endostagnic Albic Retisol (RT-stn.ab)	173	85	4.6
10	LHS7b	53.153224 / 13.884369	4.3	-0.09	46	3.8	5.5	2	Albic Retic Stagnosol (ST-ab.rt)	154	-	4.0
11	hydro4b	53.153361 / 13.884401	4.1	-0.31	38	4.6	6.1	2	Endostagnic Albic Retisol (RT-stn.ab)	214	150	4.2
12	LHS18	53.153507 / 13.884433	3.4	-0.53	30	5.1	9.8	2	Albic Retic Stagnosol (ST-ab.rt)	213	87	4.2
13	hydro5	53.153490 / 13.884591	0.9	-0.62	21	1.9	10.4	1	Albic Retic Stagnosol (ST-ab.rt)	>185	157	4.0
14	LHS20	53.153403 / 13.884898	2.3	-0.38	15	7.5	11.2	1	Albic Retic Stagnosol (ST-ab.rt)	241	107	4.0
15	LHS17	53.153145 / 13.884775	4.4	0.57	46	4.8	5.8	3	Nudiaric Luvisol (LV-ng)	42	-	4.4
16	LHS1	53.153200 / 13.884908	5.8	0.30	40	3.8	9.9	3	Albic Retic Stagnosol (ST-ab.rt)	141	-	3.7

dts = distance to sink, disttree 1 = distance to nearest tree, disttree2 = distance to second nearest tree, ntrees = number of trees in a 10m radius

3.4.2 Soil organic carbon (SOC)

Soil organic matter stocks may reflect average erosional and depositional processes covering a time span that cannot be precisely determined and may vary from decades to millennia. Higher stocks should be related to accumulation and lower stocks to erosional sites. The SOC contents exhibit an exponential decrease with depth in all soil profiles. The SOC stocks were highest at site 1 (6.5 kg SOC m⁻²) and 3 (5.4 kg SOC m⁻²) that also showed the highest TPI25 values (0.88 m; 0.89 m). They are located on the ridge or close to it. The lowest SOC stock was measured at site 6 (2.6 SOC kg m⁻²). In general, SOC stocks were surprisingly high on the ridge, low along the slope and higher again in the former kettle hole. The calculated SOC stocks for the upper 20 cm showed a weak (using a polynomial function) but significant ($p < 0.05$) correlation with the TPI25 (data not shown).

3.4.3 ²³⁹⁺²⁴⁰Pu depth functions, inventories and relationship to topographic parameters

Figure 3.4 displays the depth functions of the ²³⁹⁺²⁴⁰Pu inventories for a catena in straight downslope direction (sites 2-6-8-11-13). In general, the ²³⁹⁺²⁴⁰Pu activity is highest at a depth of 5 – 10 cm and then decreases exponentially with depth, except for the site 2. The ²³⁹⁺²⁴⁰Pu inventories show a very high variability with a minimum value of 36 Bq m⁻² (site 15) and a maximum of 70 Bq m⁻² (site 11) (Table 3.2). We related the ²³⁹⁺²⁴⁰Pu inventory of each site with landscape attributes such as the TPI25 (and also TPI3, 5, 11), slope, aspect, soil depth to the C horizon, distance to the first and second tree and number of trees within a radius of 10 m (Figures 5 and 6). The results showed no correlation between the ²³⁹⁺²⁴⁰Pu inventories and any landscape attributes. There seems a slight tendency (however, not significant) of the Pu stocks with slope (decreasing stocks with increasing slope). Some recent erosion may therefore not be fully excluded. This may also be supported by a slight increase of the Pu stocks from site 2 in direction to site 11 (Table 3.2, Figure 3.4). However, the last site in the kettle hole (site 13) of this sequence has a lower stock.

3.4.4 Erosion and deposition rates

From ²³⁹⁺²⁴⁰Pu inventories we calculated soil erosion and deposition rates per site, using different models (Table 3.2). Positive soil redistribution rates indicate deposition and negative

values stand for erosion. Soil redistribution rates values ranged between $-5.0 \text{ t ha}^{-1} \text{ yr}^{-1}$ (site 16) and $+7.3 \text{ t ha}^{-1} \text{ yr}^{-1}$ (site 11), both calculated with the PDM. The lowest range of values was obtained using MODERN ($-2.3 \text{ t ha}^{-1} \text{ yr}^{-1}$ to $+3.6 \text{ t ha}^{-1} \text{ yr}^{-1}$). Moreover, we compared the soil redistribution rates calculated with MODERN to those obtained from the PDM and the IM (Figure 3.7). The rates obtained from MODERN correlated linearly to the values of the PDM ($R^2 = 0.96$; $p < 0.005$) and the IM ($R^2 = 0.98$; $p < 0.005$). In general, however, the absolute values obtained by using MODERN were smaller than when using the other model approaches.

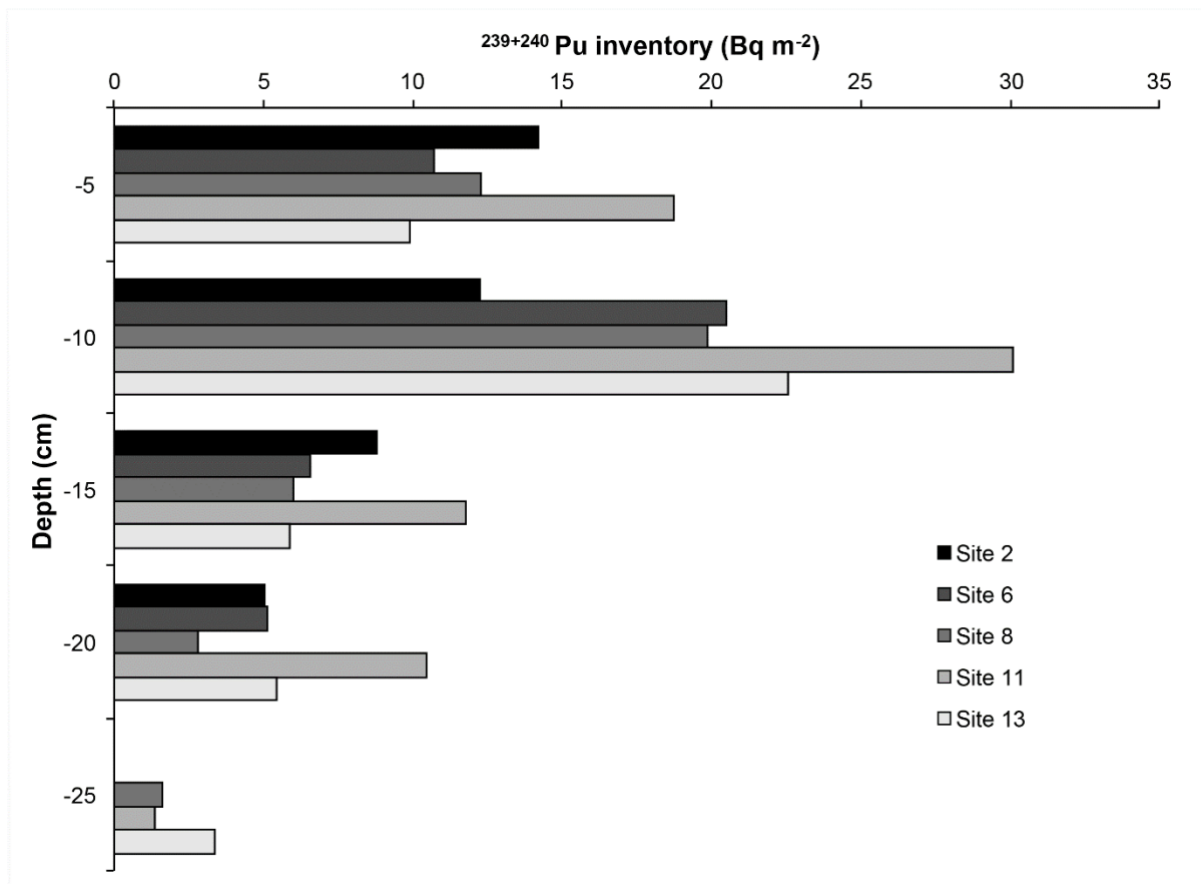


Figure 3.4. ²³⁹⁺²⁴⁰Pu inventories as a function of soil depth of selected soil profiles (hydro-sequence) along the catena.

Table 3.2. $^{239+240}\text{Pu}$ inventories and derived soil redistribution rates. Calculations were done according to the profile distribution model (Walling & Quine, 1990; XINBAO et al., 1990), MODERN (Arata et al., 2016a; Arata et al., 2016b) and the inventory model (Lal et al., 2013). A particle size correction factor (P) of 1.2 (according to Walling & He, 1999) and 1.5 (according to Lal et al., 2013) was applied for the inventory method.

Site No.	Pu inventory Bq m ⁻²	Soil redistribution rates (t ha ⁻¹ yr ⁻¹)				Average	
		PDM	MODERN	IM (P=1)	IM (P=1.2)	IM (P=1.5)	
1	57.8	3.8	2.7	3.2	2.6	2.1	2.9
2	40.4	-2.6	-1.4	-2.6	-2.1	-1.7	-2.1
3	43.9	-1.1	-0.5	-1.0	-0.8	-0.7	-0.8
4	51.4	1.7	1.3	1.6	1.4	1.1	1.4
5	46.0	-0.3	0.0	-0.2	-0.2	-0.2	-0.2
6	42.9	-1.5	-0.8	-1.4	-1.2	-0.9	-1.2
7	36.7	-4.3	-1.6	-3.5	-2.9	-2.3	-2.9
8	41.3 (9.5)	-3.1	-1.2	-2.7	-2.3	-1.8	-2.2
9	40.0	-2.8	-0.8	-2.1	-1.8	-1.4	-1.8
10	55.3	3.0	2.0	2.6	2.1	1.7	2.3
11	71.4 (12.6)	7.3	3.1	6.3	5.2	4.2	5.2
12	63.7	5.6	3.6	4.7	3.9	3.1	4.2
13	47.2	-1.1	-0.5	-1.0	-0.8	-0.7	-0.8
14	61.2	3.2	2.1	3.1	2.6	2.1	2.6
15	36.3	-4.5	-1.7	-3.8	-3.2	-2.5	-3.1
16	37.7 (13.1)	-5.0	-2.3	-4.5	-3.8	-3.0	-3.7

Pu inventories: no. in brackets = std.dev.; rates: negative values = erosion, positive values = deposition

Irrespective of the used model, soil redistribution rates varied distinctly and resulted partially in very high values for forest soils. Transforming the soil redistribution rates ($\text{t ha}^{-1} \text{y}^{-1}$) into soil depth changes (cm) over the last 55 years resulted in a maximum decrease in soil thickness of 3 cm (erosion) and a maximum increase of 4 cm (deposition, mean BD in 0 – 5 cm = 1.07 Mg m^{-3}). We tested a range of landscape attributes (terrain, canopy structure) for explanation of erosion/deposition rates. However, none of these showed any significant correlation (Figure 3.6). This might be due to the very high local variability as can be depicted from the high coefficient of variations (18 – 35% for sites 8, 11, 16, Table 3.2). From our findings we conclude that only a minor recent soil redistribution along the slope must have occurred, although the calculated erosion and accumulation values may appear high. These high values are rather due to an inhomogeneous input of $^{239+240}\text{Pu}$ than due to soil redistribution. Otherwise a correlation to topographic features must exist.

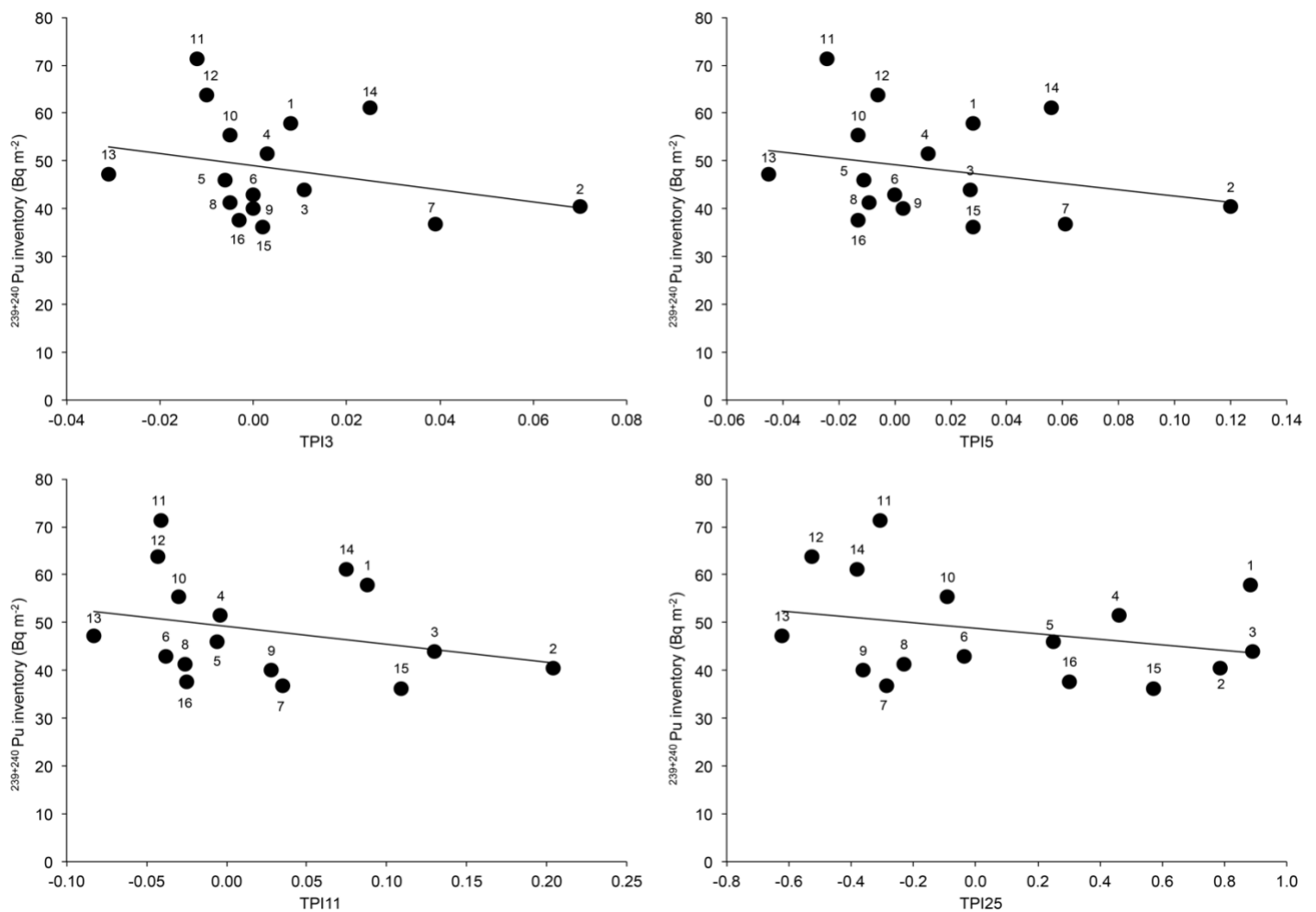


Figure 3.5. Relationship between the $^{239+240}\text{Pu}$ inventories and TPI3, TPI5, TPI11, TPI25.

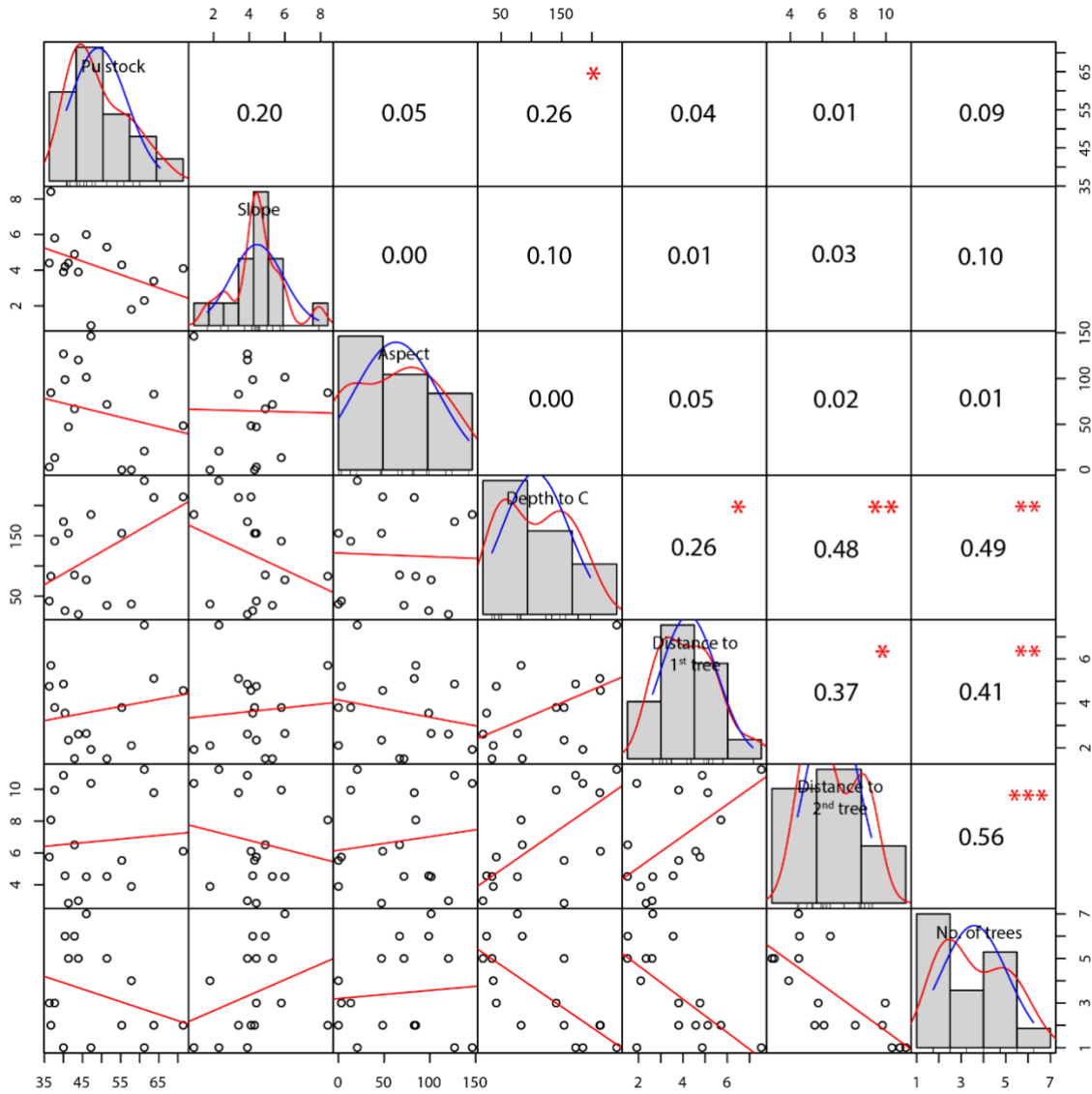


Figure 3.6. Relationship between soil properties and landscape attributes. Depth to C = soil thickness; No. of trees = number of trees within a radius of 10 m.

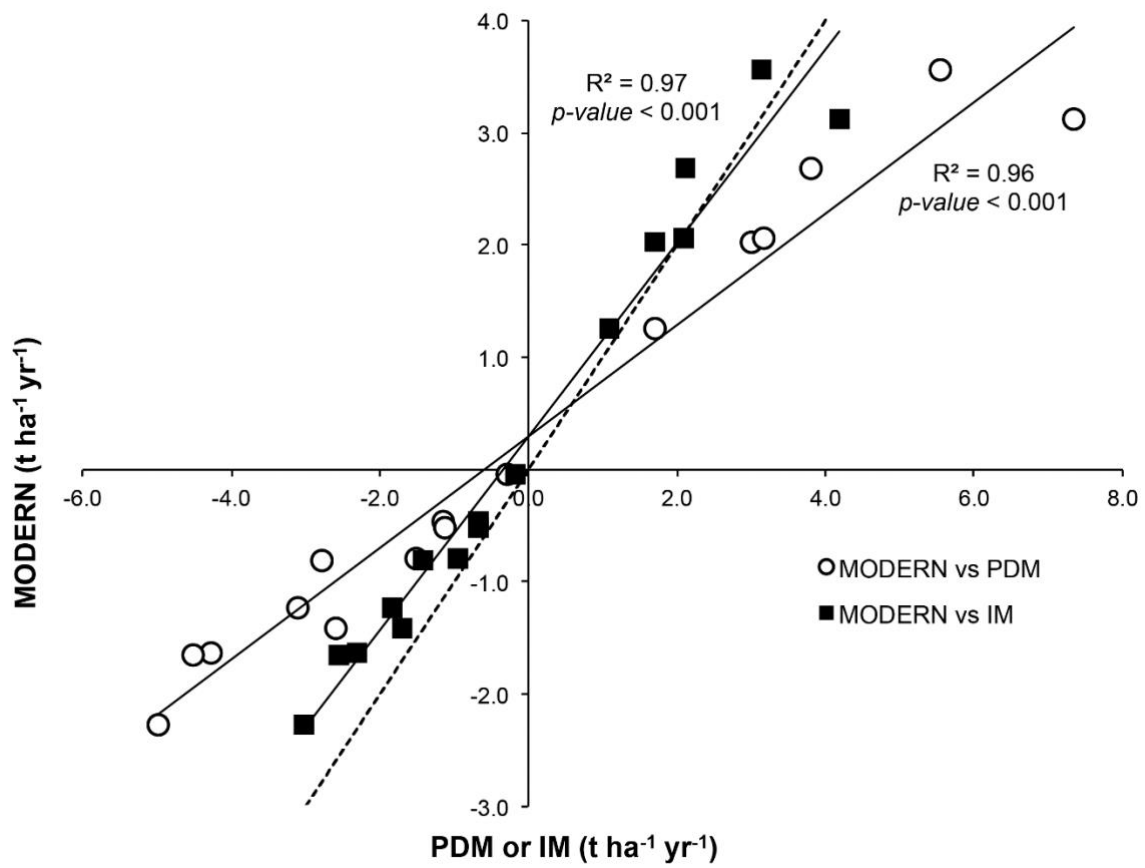


Figure 3.7. Comparison between soil redistribution rates calculated using MODERN, the Inventory Model (IM) and the Profile Distribution Model (PDM).

3.5 Discussion

3.5.1 $^{239+240}\text{Pu}$ inventories and depth functions

The average value of the Pu inventories ($48 \pm 10 \text{ Bq m}^{-2}$) throughout the forest catchment is in quite good agreement with the slightly lower value of $43 \pm 6 \text{ Bq m}^{-2}$ measured in nearby agricultural soils that are not affected neither by erosion nor by deposition (Calitri et al., 2019). Generally, soils under forest should have higher levels of Pu due to the filtration effect of forests for aerosol deposition (interception) when compared to the less specific plant surface area of arable land (Eikenberg et al., 2001).

The mobility of Pu and its behaviour in the soil are still under debate. Pu has four oxidation states in environmental conditions (Pu(III), Pu(IV), Pu(V) and Pu(VI)); (Alewell et al., 2017) and this leads to consider Pu an element with a complex environmental redox chemistry (Xu et al., 2014). Given its complex chemical behaviour in soils we have to assume that Pu, like other FRNs, is attached to fine particles on the soil surface and moves across the landscape mostly through physical processes of soil redistribution rather than chemical (IAEA, 2014).

The $^{240}\text{Pu}/^{239}\text{Pu}$ ratio is in the well-known global fallout range of 0.18 ± 0.014 of the northern hemisphere mid-latitude fallout with reported values varying from 0.14 to 0.24 (Kelley et al., 1999; Mitchell et al., 1997). The average $^{240}\text{Pu}/^{239}\text{Pu}$ ratio within the catchment is 0.21 ± 0.04 . This indicates that there is no contamination from other sources such as the Chernobyl incident, that had a much higher $^{240}\text{Pu}/^{239}\text{Pu}$ ratio (values of 0.37 to 0.41, Boulyga & Becker, 2002; Ketterer et al., 2004; Muramatsu et al., 2000).

3.5.2 $^{239+240}\text{Pu}$ spatial distribution and erosion/deposition rates

In contrast to soil thickness (soil depth down to the C horizon; Figure 3.2), the spatial distribution of the $^{239+240}\text{Pu}$ inventories does not correlate with topography (Figure 3.5). Consequently, we have to assume that during the last 50–60 years only little erosion has occurred and that the spatial behaviour of Pu must be explained by other factors.

The spatial variability of the $^{239+240}\text{Pu}$ inventories in the forest is relatively high. Notably is also that the highest stocks are found at a depth of 5 – 10 cm. The irregular distribution pattern of $^{239+240}\text{Pu}$ in the catchment may be explained by tree uprooting events during the last 55 years. (Šamonil et al., 2017) estimated that 30% of all trees in temperate central European forests are

affected by uprooting. However, we did not observe intense uprooting features in the study area. The interception of contaminants, i.e., FRNs, by the forest canopy strongly depends on the type of forest and the season, and deciduous forests have a much reduced leaf area index compared to coniferous forests. After the deposition (wet or dry) of FRNs, stemflow, throughfall and leaf-fall are the most important input pathways into top-soils in any kind of forest (Shaw, 2007). This set of processes distributes FRNs in an extremely heterogeneous way. Some studies found that the proximity to tree trunks and the species both influence distribution of chemical elements in the soil, and thus also of FRNs (Förster et al., 1991; Fraiture, 1992; Schimmack et al., 1993). In particular, (Förster et al., 1991) compared the activity pattern of ^{137}Cs derived from the Chernobyl fallout under beeches and spruces and found that the amount of ^{137}Cs at the base of the beech trunks was one order of magnitude higher than in areas distant from the trunks. Furthermore, Förster & Schimmack (1992) detected that ^{137}Cs migrated faster into the soil in the stemflow infiltration zone due to intensive water percolation.

Although some authors observed an increasing content in Cs towards the stem of a tree in other forest ecosystem, nothing similar could be measured for Pu in the Melzower Forest. We found no correlation between the $^{239+240}\text{Pu}$ inventory and the distance to the first tree, second tree or any other nearby trees (Figure 3.6).

Garten et al. (1978) studied the distribution and dynamics of $^{239+240}\text{Pu}$ in a deciduous forest and found that the soil accounted for more than 99% of the total Pu inventory, even though transfers between the soil, litter and tree roots were the major driving processes of the redistribution of Pu in the ecosystem. They also predicted through a model based on field data and given $^{239+240}\text{Pu}$ half-life that its uptake, that is particularly low, would increase to a maximum over a period of approximately 100 years in undisturbed deciduous forest.

As a consequence, interception, stemflow and litterfall are probably the factors contributing most to the spatial variability. Litterfall may also dilute the Pu content in the uppermost part of the soil what might explain the slightly higher content at a depth of 5 – 10 cm.

3.5.3 Comparison of erosion modelling approaches using $^{239+240}\text{Pu}$

The PDM is a model that has been first applied to convert ^{137}Cs and lead-210 ($^{210}\text{Pb}_{\text{ex}}$) activities into soil erosion rates (Walling et al., 2003, 2011, 2014). This model was used only later for $^{239+240}\text{Pu}$. The IM, on the contrary, has been used since its first applications to Pu (^{239}Pu , Lal et

al., 2013). For both models, the basic assumption is that the FRN, in our case $^{239+240}\text{Pu}$, has an exponential decreasing function with soil depth.

Unlike the PDM and the IM, MODERN does not take into account a pre-given depth function of FRN (Arata et al., 2016a; Arata et al., 2016b). This can be a key advantage of MODERN in the conversion of $^{239+240}\text{Pu}$ and other FRNs into soil redistribution rates, because FRNs often do not follow an exponential decreasing function with soil depth. For this reason, we might consider the rates obtained by using MODERN as more reliable than values obtained from the PDM and the IM.

3.5.4 Terrain attributes and soil depth

The observed catena in the “Melzower Forst” is similar to catenas from agricultural landscapes. Especially the erosion on crests and deposition in the depression resemble erosion patterns caused by tillage erosion (De Alba et al., 2004). The TPI nicely traces the erosion and deposition (Deumlich et al., 2010) and indicates that the Melzower forest had experienced at least partially similar processes like agricultural landscapes. According to the results obtained from Pu, erosion and deposition can be attributed to older events than those of the last 55 years.

The TPI25 also shows a weak correlation with the C stocks. There is a concave-shaped distribution of the C inventories in the catchment with higher values in the soils on the top-slope and foot-slope and lower values in the soils on a mid-slope position. SOC in the “Melzower Forst” seems partially to be involved in erosion/deposition processes. However, SOC covers in its average mostly a longer time span (century to millennia — however no precise information can be given) of erosion and deposition than $^{239+240}\text{Pu}$.

3.5.5 Recent or ancient processes

The weak relationship between $^{239+240}\text{Pu}$ inventories and terrain characteristics demonstrates that small or negligible erosion and deposition must have occurred during the last few decades, although the calculated erosion or deposition rates seem in some cases high. Some of the calculated erosion rates even would exceed by far tolerable erosion rates. According to Verheijen et al. (2009) and Alewell et al. (2015), tolerable erosion rates lie within about 0.3 to 1.4 t ha⁻¹ yr⁻¹, or for soils having an age of > 10 kyr between 0.5 and 1.1 t ha⁻¹ yr⁻¹, respectively. As previously mentioned, the partially high rates are a product of an inhomogeneous Pu input

onto the forest floor. If the mean of the average erosion/deposition values of the individual investigation sites is calculated, then we obtain $-0.01 \text{ t ha}^{-1} \text{ yr}^{-1}$; a value that definitely does not differ from zero. This stands completely in contrast to agriculture land of the same region. Using $^{239+240}\text{Pu}$ in this agricultural landscape (CarboZALF; Calitri et al., 2019), the recent soil redistribution rates (up to about $25 \text{ t ha}^{-1} \text{ yr}^{-1}$) were up to more than one order of magnitude higher than the long-term rates. Especially the progress in farming technology since World War II has led to accelerated water, wind and particularly tillage erosion (Follain et al., 2006; Sommer et al., 2008). Whereas erosion increases incisions in concavities of landscapes and leads to soil loss in upper and midslope positions, tillage erosion causes soil loss at convex upper slope positions as well as convex hilltops (Lobb et al., 1995). Tillage depth and tractor speed are the main factors for the magnitude of soil translocation and loss. In some landscapes tillage erosion rates are at least in the same order of magnitude or even higher than water erosion (e.g., Van Oost et al., 2009). In the forest, the original landscape is much better preserved compared to the smoothed surfaces (erosion, tillage erosion; van der Meij et al., 2017) of the adjacent agriculture land.

However, the macromorphology of the soils and soil depths trends along the catena clearly show that significant erosion and deposition of soil material must have occurred which is also expressed in the clear correlation to topographic factors (Figure 3.2). Very evidently, these processes must have occurred more than 250 (or most likely > 400) years ago, because this region has not been managed for at least the last 250 years (having oldest trees with an age of 400 years; Ruffer, 2018). Therefore we argue that the present landscape is the result of probably both ancient agricultural and natural (maybe catastrophic) events. These disturbances are likely older than 400 years. The prehistoric landscape of Europe has been overprinted by human activity since the Neolithic and Bronze Age (Birks, 1998; Küster et al., 2012; Ruddiman, 2003). Using lake sediments and pollen analysis, Küster et al. (2012) showed that several phases of erosion must have occurred in the broader region of interest (Müritz region; Mecklenburg Vorpommern). A first phase occurred during the Bronze age. The first cultivation of crops in this region falls into this period together with a distinct clearing of the forest. During the subatlantic period, population density and land use intensity were low. About 1300 BP, land use intensity increased again giving rise to increased erosion. During the Middle Ages and particularly modern era, land use intensity was highest. Since the Middle Ages the most distinct landscape changes have occurred (Küster et al., 2012).

This is in good agreement with findings of van der Meij et al. (2019). Their study of an agricultural kettle hole in the vicinity of the Melzower forest (CarboZALF) showed that the earliest erosion occurred ~ 4500 years ago. Van der Meij et al. (2019) determined several erosional/depositional phases: smaller events 4500 to about 400 yr BP, strongly increased and more frequent events 1795 – 1965 AD and even stronger erosion events during the very recent past due to intensified tillage.

At least part of the erosion events in the “Melzower Forst” fall into prehistoric times, which also explain the fully developed Retisol in the colluvium found at the lower slopes. This assumption is substantiated by a radiocarbon measurement of soil organic matter (particulate organic matter POM) in the fossil A horizon close to site Hydro 4b (site 11; Figures 2 and 3). The erosional event happened about 6.8 ka BP (Table 3.3). We therefore have to assume that ancient (several hundreds up to several millennia) erosion and accumulation events are predominantly responsible for the observed soil pattern. The investigated site was forested for the last 240 years or even longer. The strongest soil erosion events in the region were determined for the last about 230 years that had about one order of magnitude higher intensity than the ancient ones (van der Meij et al., 2019).

Table 3.3. Analysed soil material and related results of radiocarbon dating.

Site/sample	UZH-/ETHZ-code	Material	Treatment ¹	C14 age		cal age (calBP)	
				±1σ	BP	1σ	2σ
Hydro4c fAh	UZ-6516/ETH-96758	soil	POM	5965	27	6845-6747	6885-6731

¹ POM: particulate organic matter (potentially the youngest fraction).

3.6 Conclusions

Soil erosion seems to have been negligible during the last 55 years in the “Melzower Forst”. Although the $^{239+240}\text{Pu}$ inventories indicate for some sites a high erosion and accumulation rates, these values can rather be ascribed to the heterogeneous input of Pu onto the forest floor. The forest area was under severe protection for several hundreds of years. Therefore, major erosion events that were detected in nearby areas and were caused by human impact did not happen in the Melzower forest. Natural events and maybe also anthropogenic activities during the medieval times (or earlier) seem to have caused erosional events, which led to the observed soil pattern. Part of these events happened in the early Holocene (about 6.8 ka BP).

In general, our results show that a combined approach using $^{239+240}\text{Pu}$ and soil morphology is a promising instrument to discriminate between ancient and recent erosional events in forest soils. Due to the relatively dry conditions in the Melzower Forst, the $^{239+240}\text{Pu}$ input to the forest floor is heterogeneous and patchy. A straightforward interpretation of the data is not possible. Therefore, the Pu data needs to be compared to other data such as topography for a more stringent discussion.

3.7 Acknowledgements

This research was supported by a cooperation contract (CORRELATE; F-75113-07-01) between the University of Zurich and the ZALF. We thank Alessandra Musso and Yvonne Forster for the ICP-MS measurements. We are furthermore indebted to two unknown reviewers for their helpful comments on an earlier version of the manuscript.

References

- Alewell C, Meusburger K, Juretzko G, Mabit L, Ketterer ME. 2014. Suitability of $^{239+240}\text{Pu}$ and ^{137}Cs as tracers for soil erosion assessment in mountain grasslands. *Chemosphere* 103, 274–280. <https://doi.org/10.1016/j.chemosphere.2013.12.016>.
- Alewell C, Egli M, Meusburger K. 2015. An attempt to estimate tolerable soil erosion rates by matching soil formation with denudation in Alpine grasslands. *J. Soils Sediments* 15, 1383–1399. <https://doi.org/10.1007/s11368-014-0920-6>.
- Alewell C, Pitois A, Meusburger K, Ketterer M, Mabit L. 2017. $^{239+240}\text{Pu}$ from “contaminant” to soil erosion tracer: Where do we stand? *Earth Sci. Rev.* 172, 107–123. <https://doi.org/10.1016/j.earscirev.2017.07.009>.
- Arata L, Alewell C, Frenkel E, A'Campo-Neuen A, Iurian A-R, Ketterer ME, Mabit L, Meusburger K. 2016a. Modelling Deposition and Erosion rates with RadioNuclides (MODERN) – Part 2: A comparison of different models to convert $^{239+240}\text{Pu}$ inventories into soil redistribution rates at unploughed sites. *J. Environ. Radioact.* 162–163, 97–106. <https://doi.org/10.1016/j.jenvrad.2016.05.009>.
- Arata L, Meusburger K, Frenkel E, A'Campo-Neuen A, Iurian A-R, Ketterer ME, Mabit L, Alewell C. 2016b. Modelling Deposition and Erosion rates with RadioNuclides (MODERN) – Part 1: A new conversion model to derive soil redistribution rates from inventories of fallout radionuclides. *J. Environ. Radioact.* 162–163, 45–55. <https://doi.org/10.1016/j.jenvrad.2016.05.008>.
- Berhe AA, Barnes RT, Six J, Marín-Spiotta E. 2018. Role of soil erosion in biogeochemical cycling of essential elements: carbon, nitrogen, and phosphorus. *Annu. Rev. Earth Planet. Sci.* 46, 521–548. <https://doi.org/10.1146/annurev-earth-082517-010018>.
- Birks HJB. 1998. Numerical tools in palaeolimnology – Progress, potentialities and problems. *J. Paleolimnol.* 20, 307–332.
- Bork H-R (Ed.). 2006. Landscapes of the Earth Under the Influence of Man (in German). Wissenschaftliche Buchgesellschaft, Darmstadt, pp. 207.
- Boulyga SF, Becker JS. 2002. Isotopic analysis of uranium and plutonium using ICPMS and estimation of burn-up of spent uranium in contaminated environmental samples. *J. Anal. At. Spectrom.* 17, 1143–1147. <https://doi.org/10.1039/B202196J>.

- Calitri F, Sommer M, Norton K, Temme A, Brandová D, Portes R, Christl M, Ketterer ME, Egli M. 2019. Tracing the temporal evolution of soil redistribution rates in an agricultural landscape using $^{239+240}\text{Pu}$ and ^{10}Be . *Earth Surf. Proc. Land.* <https://doi.org/10.1002/esp.4612>.
- De Alba S, Lindstrom M, Schumacher TE, Malo DD. 2004. Soil landscape evolution due to soil redistribution by tillage: a new conceptual model of soil catena evolution in agricultural landscapes. *Catena* 58, 77–100. <https://doi.org/10.1016/j.catena.2003.12.004>.
- Deumlich D, Schmidt R, Sommer M. 2010. A multiscale soil-landform relationship in the glacial-drift area based on digital terrain analysis and soil attributes. *J. Plant Nutr. Soil Sci.* 173, 843–851. <https://doi.org/10.1002/jpln.200900094>.
- Deutscher Wetterdienst. https://www.dwd.de/DE/klimaumwelt/klimaatlas/klimaatlas_node.html, accessed March 1, 2020.
- Eikenberg J, Bajo S, Hitz J, Wyer L. 2001. Environmental Radionuclide Analyses around Nuclear Installations in Northern Switzerland 6.
- Evrard O, Pointurier F, Onda Y, Chartin C, Hubert A, Lepage H, Pottin A-C, Lefèvre I, Bonté P, Laceby JP, Ayrault S. 2014. Novel insights into Fukushima nuclear accident from isotopic evidence of plutonium spread along coastal rivers. *Environ. Sci. Technol.* 48, 9334–9340. <https://doi.org/10.1021/es501890n>.
- Follain S, Minasny B, McBratney AB, Walter C. 2006. Simulation of soil thickness evolution in a complex agricultural landscape at fine spatial and temporal scales. *Geoderma* 133, 71–86. <https://doi.org/10.1016/j.geoderma.2006.03.038>.
- Förster H, Schimmack W. 1992. Influence of the stemflow on the depth distribution of radiocesium in the soil under a beech stand. *Naturwissenschaften* 79, 23–24. <https://doi.org/10.1007/BF01132274>.
- Förster H, Schimmack W, Kreuzer KE. 1991. Die horizontale Verteilung von Radiocäsium im Waldboden unter Fichte und Buche. *Zeitschrift für Pflanzenernährung und Bodenkunde* 154, 87–92. <https://doi.org/10.1002/jpln.19911540203>.
- Fraiture A. 1992. Introduction to the Radioecology of Forest Ecosystems and Survey of Radioactive Contamination in Food Products from Forests. Commission of the European Communities, Brussels.

- Garten CT, Gardner RH, Dahlman RC. 1978. A compartment model of plutonium dynamics in a deciduous forest ecosystem. *Health physics* 34, 611–619. doi: 10.1097/00004032-197806000-00009.
- Hoo WT, Fifield LK, Tims SG, Fujioka T, Mueller N. 2011. Using fallout plutonium as a probe for erosion assessment. *J. Environ. Radioact.* 102 (10), 937–942. <https://doi.org/10.1016/j.jenvrad.2010.06.010>.
- IAEA. 2014. Guidelines for Using Fallout Radionuclides to Assess Erosion and Effectiveness of Soil Conservation Strategies, TECDOC Series. INTERNATIONAL ATOMIC ENERGY AGENCY, Vienna.
- IUSS. 2014. World Reference Base for Soil Resources 2014. International Soil Classification System for Naming Soils and Creating Legends for Soil Maps. World Soil Resources Reports No. FAO: Rome.
- Kaletka T, Rudat C, Quast J. 2000. “Potholes” in Northeast German Agro-landscapes: Functions, Land Use Impacts, and Protection Strategies. *Ecological studies*, 147, Chapter: 18, Publisher: Springer, pp. 291–298. Doi:10.1007/978-3-662-04504-6_18.
- Kappler C, Kaiser K, Tanski P, Klos F, Fülling A, Mrotzek A, Sommer M, Bens O. 2018. Stratigraphy and age of colluvial deposits indicating Late Holocene soil erosion in northeastern Germany. *Catena* 170, 224–245. <https://doi.org/10.1016/j.catena.2018.06.010>.
- Kelley JM, Bond LA, Beasley TM. 1999. Global distribution of Pu isotopes and ²³⁷Np. *Sci. Total Environ.* 237–238, 483–500. [https://doi.org/10.1016/S0048-9697\(99\)00160-6](https://doi.org/10.1016/S0048-9697(99)00160-6).
- Ketterer ME, Hafer KM, Mietelski JW. 2004a. Resolving Chernobyl vs. global fallout contributions in soils from Poland using Plutonium atom ratios measured by inductively coupled plasma mass spectrometry. *J. Environ. Radioact.* 73, 183–201. <https://doi.org/10.1016/j.jenvrad.2003.09.001>.
- Ketterer ME, Hafer KM, Link CL, Kolwaite D, Wilson J, Mietelski JW. 2004b. Resolving global versus local/regional Pu sources in the environment using sector ICP-MS. *J. Anal. Atomic Spectrometry* 19, 241–245. doi: 10.1039/B302903D.
- Ketterer ME, Szechenyi SC. 2008. Determination of plutonium and other transuranic elements by inductively coupled plasma mass spectrometry: A historical perspective and new

- frontiers in the environmental sciences. *Spectrochim. Acta, Part B* 63, 719–737. <https://doi.org/10.1016/j.sab.2008.04.018>.
- Kopp D, Schwanecke W. 1994. Standörtlich-naturräumliche Grundlagen ökologiegerechter Forstwirtschaft. Deutscher Landwirtschaftsverlag Berlin GmbH.
- Koszinski S, Gerke HH, Hierold W, Sommer M. 2013. Geophysical-based modelling of a kettle hole catchment of the morainic soil landscape. *Vadose Zone J.* 12. <https://doi.org/10.2136/vzj2013.02.0044>.
- Küster M, Janke W, Meyer H, Lorenz S, Lampe R. 2012. Zur jungquartären Landschaftsentwicklung der Mecklenburgischen Kleinseenplatte. Geomorphologische, bodenkundliche und limnogeologische Untersuchungen am Krummen See bei Blankenförde (Mecklenburg). Müritz Nationalpark, Forschung und Monitoring, Band 3. Nationalparkamt Müritz.
- Lal R, Stewart BA. 1990. *Advances in Soil Science: Soil Degradation*. Springer, New York, New York, NY.
- Lal R, Tims SG, Fifield LK, Wasson RJ, Howe D. 2013. Applicability of ^{239}Pu as a tracer for soil erosion in the wet-dry tropics of northern Australia. *Nucl. Instrum. Methods Phys. Res., Sect. B* 294, 577–583. <https://doi.org/10.1016/j.nimb.2012.07.041>.
- Lobb DA, Kachanoski RG, Miller MH. 1995. Tillage translocation and tillage erosion on shoulder slope landscape positions using ^{137}Cs as a tracer. *Can. J. Soil Sci.* 75, 211–218. <https://doi.org/10.4141/cjss95-029>.
- Lüthgens C, Böse M. 2011. Chronology of Weichselian main ice marginal positions in north-eastern Germany. *E&G Quaternary Sci. J.* 60, 236–247. <https://doi.org/10.3285/eg.60.2-3.02>.
- Lüthgens C, Böse M, Preusser F. 2011. Age of the Pomeranian ice-marginal position in northeastern Germany determined by Optically Stimulated Luminescence (OSL) dating of glaciofluvial sediments. *Boreas* 40, 598–615. <https://doi.org/10.1111/j.1502-3885.2011.00211.x>.
- Matisoff G, Ketterer ME, Rosén K, Mietelski JW, Vitko LF, Persson H, Lokas E. 2011. Downward migration of Chernobyl-derived radionuclides in soils in Poland and Sweden. *Appl. Geochem.* 26, 105–115. <https://doi.org/10.1016/j.apgeochem.2010.11.007>.

- Meusburger K, Mabit L, Ketterer M, Park J-H, Sandor T, Porto P, Alewell C. 2016. A multi-radionuclide approach to evaluate the suitability of $^{239+240}\text{Pu}$ as soil erosion tracer. *Sci. Total Environ.* 566–567, 1489–1499. <https://doi.org/10.1016/j.scitotenv.2016.06.035>.
- Meusburger K, Porto P, Mabit L, La Spada C, Arata L, Alewell C. 2018. Excess Lead-210 and Plutonium-239+240: Two suitable radiogenic soil erosion tracers for mountain grassland sites. *Environ. Res.* 160, 195–202. <https://doi.org/10.1016/j.envres.2017.09.020>.
- Miller BA, Koszinski S, Hierold W, Rogasik H, Schröder B, Van Oost K, Wehrhan M, Sommer M. 2016. Towards mapping soil carbon landscapes: Issues of sampling scale and transferability. *Soil Tillage Res.* 156, 194–208. <https://doi.org/10.1016/j.still.2015.07.004>.
- Mirsky SB, Lanyon LE, Needelman BA. 2005. Evaluating soil management using particulate and chemically labile soil organic matter fractions. *Soil Sci. Soc. Am. J.* 72, 180–185.
- Mitchell PI, Vintró LL, Dahlgard H, Gascó C, Sánchez-Cabeza JA. 1997. Perturbation in the ^{240}Pu ^{239}Pu global fallout ratio in local sediments following the nuclear accidents at Thule (Greenland) and Palomares (Spain). *Sci. Total Environ.* 202, 147–153. [https://doi.org/10.1016/S0048-9697\(97\)00111-3](https://doi.org/10.1016/S0048-9697(97)00111-3).
- Muramatsu Y, Rühm W, Yoshida S, Tagami K, Uchida S, Wirth E. 2000. Concentrations of ^{239}Pu and ^{240}Pu and their isotopic ratios determined by ICP-MS in soils collected from the chernobyl 30-km zone. *Environ. Sci. Technol.* 34, 2913–2917. <https://doi.org/10.1021/es0008968>.
- Pentreath RJ. 1995. The analysis of Pu in environmental samples: A brief historical perspective. *Appl. Radiat. Isot.* 46, 1279–1285. [https://doi.org/10.1016/0969-8043\(95\)00171-9](https://doi.org/10.1016/0969-8043(95)00171-9).
- Phillips JD. 2015. The robustness of chronosequences. *Ecological Modelling, Complexity of Soils and Hydrology in Ecosystems* 298, 16–23. <https://doi.org/10.1016/j.ecolmodel.2013.12.018>.
- Pimentel D. 2001. The limitations of biomass energy. In: *Encyclopedia on Physical Science and Technology*. Academic Press, San Diego. CA, pp. 159–171.
- Pimentel D. 1993. *World Soil Erosion and Conservation*. Cambridge University Press. <https://doi.org/10.1017/CBO9780511735394>.

- Pimentel D, Harvey C, Resosudarmo P, Sinclair K, Kurz D, McNair M, Crist S, Shpritz L, Fitton L, Saffouri R, Blair R. 1995. Environmental and economic costs of soil erosion and conservation benefits. *Science* 267, 1117–1123. <https://doi.org/10.1126/science.267.5201.1117>.
- Pimentel D, Kounang N. 1998. Ecology of soil erosion in ecosystems. *Ecosystems* 1, 416–426. <https://doi.org/10.1007/s100219900035>.
- Portes R, Dahms D, Brandová D, Raab G, Christl M, Kühn P, Ketterer M, Egli M. 2018. Evolution of soil erosion rates in alpine soils of the Central Rocky Mountains using fallout Pu and $\delta^{13}\text{C}$. *Earth Planet. Sci. Lett.* 496, 257–269. <https://doi.org/10.1016/j.epsl.2018.06.002>.
- Raab G, Scarciglia F, Norton K, Dahms D, Brandová D, de Castro Portes R, Christl M, Ketterer ME, Ruppli A, Egli M. 2018. Denudation variability of the Sila Massif upland (Italy) from decades to millennia using ^{10}Be and $^{239+240}\text{Pu}$. *Land Degrad. Dev.* 29, 3736–3752. <https://doi.org/10.1002/ldr.3120>.
- Reimer PJ, Bard E, Bayliss A, Beck JW, Blackwell PG, Bronk Ramsey C, Buck CE, Cheng H, Edwards RL, Friedrich M, Grootes PM, Guilderson TP, Haflidason H, Hajdas I, Hatté C, Heaton TJ, Hoffmann DL, Hogg AG, Hughen KA, Kaiser KF, Kromer B, Manning SW, Nui M, Reimer RW, Richards DA, Scott EM, Southon JR, Staff ARA, Turney C, van der Plicht J. 2013. IntCal13 and Marine13 radiocarbon age calibration curves 0–50,000 years cal BP. *Radiocarbon* 55, 1869–1887. https://doi.org/10.2458/azu_js_rc.55.16947.
- Rüffer O. 2018. Standortsspezifische Entwicklung von Buchenwaldgesellschaften im nordostdeutschen Tiefland, dargestellt am Beispiel des Melzower Buchennaturwaldes. Humboldt-University of Berlin, Germany.
- Ruddiman WF. 2003. The anthropogenic greenhouse era began thousands of years ago. *Clim. Change* 61, 261–293.
- Šamonil P, Daněk P, Adam D, Phillips JD. 2017. Breakage or uprooting: How tree death type affects hillslope processes in old-growth temperate forests. *Geomorphology* 299, 76–84. <https://doi.org/10.1016/j.geomorph.2017.09.023>.
- Schimmack W, Auerswald K, Bunzl K. 2001. Can $^{239+240}\text{Pu}$ replace ^{137}Cs as an erosion tracer in agricultural landscapes contaminated with Chernobyl fallout? *J. Environ. Radioact.* 53, 41–57. [https://doi.org/10.1016/S0265-931X\(00\)00117-X](https://doi.org/10.1016/S0265-931X(00)00117-X).

- Schimmack W, Förster H, Bunzl K, Kreuzer K.* 1993. Deposition of radiocesium to the soil by stemflow, throughfall and leaf-fall from beech trees. *Radiat. Environ. Biophys.* 32, 137–150. <https://doi.org/10.1007/BF01212800>.
- Shaw G.* 2007. Radionuclides in forest ecosystems, in: *Radioactivity in the Environment*. Elsevier, pp. 127–155. doi: 10.1016/S1569-4860(06)10006-6.
- Smithson P, Addison K, Atkinson K.* 2008. *Fundamentals of the Physical Environment*, 4th ed. Routledge, New York.
- Sommer M, Gerke HH, Deumlich D.* 2008. Modelling soil landscape genesis — A “time split” approach for hummocky agricultural landscapes. *Geoderma, Modelling Pedogenesis* 145, 480–493. <https://doi.org/10.1016/j.geoderma.2008.01.012>.
- Verheijen FGA, Jones RJA, Rickson RJ, Smith CJ.* 2009. Tolerable versus actual soil erosion rates in Europe. *Earth Sci. Rev.* 94, 23–38. <https://doi.org/10.1016/j.earscirev.2009.02.003>.
- van der Meij WM, Reimann T, Vornehm VK, Temme AJAM, Wallinga J, Beek R, Sommer M.* 2019. Reconstructing rates and patterns of colluvial soil redistribution in agrarian (hummocky) landscapes. *Earth Surf. Proc. Land.* <https://doi.org/10.1002/esp.4671>.
- van der Meij WM, Temme AJAM, Wallinga J, Hierold W, Sommer M.* 2017. Topography reconstruction of eroding landscapes – A case study from a hummocky ground moraine (CarboZALF-D). *Geomorphology* 295, 758–772. <https://doi.org/10.1016/j.geomorph.2017.08.015>.
- Van Oost K, Cerdan O, Quine TA.* 2009. Accelerated sediment fluxes by water and tillage erosion on European agricultural land. *Earth Surf. Proc. Land.* 34, 1625–1634. <https://doi.org/10.1002/esp.1852>.
- Walling DE, He Q.* 1999. Improved models for estimating soil erosion rates from Cesium-137 measurements. *J. Environ. Qual.* 28, 611. <https://doi.org/10.2134/jeq1999.00472425002800020027x>.
- Walling DE, He Q, Appleby PG.* 2002. Conversion models for use in soil-erosion, soil redistribution and sedimentation investigations. In: *Handbook for the Assessment of Soil Erosion and Sedimentation Using Environmental Radionuclides*. Springer, Dordrecht, pp. 111–164. https://doi.org/10.1007/0-306-48054-9_7.
- Walling DE, He Q, Zhang Y.* 2014. *Conversion Models And Related Software*.

- Walling DE, Quine TA. 1990. Calibration of caesium-137 measurements to provide quantitative erosion rate data. *Land Degrad. Dev.* 2, 161–175. <https://doi.org/10.1002/ldr.3400020302>.
- Walling DE, Zhang Y, He Q. 2011. Models for deriving estimates of erosion and deposition rates from fallout radionuclide (caesium-137, excess lead-210, and beryllium- 7) measurements and the development of user friendly software for model implementation. In: *Impact of Soil Conservation Measures on Erosion Control and Soil Quality*, IAEA-TECDOC-1665, Vienna.
- Weiss AD. 2001. Topographic Position and Landforms Analysis. Conference Poster, ESRI International User Conference, San Diego, CA, USA.
- Wetzel G. 1996. The neolithicum in the western Oder region. In: Leciejewicz, L., Gringmuth-Dallmer, E. (Eds.), *Man and Environment in the Middle and Lower Oder Region - Contributions to Prehistory and Early History Settlements* (in German). Wroclaw, Poland, pp. 61–66.
- Xu C, Athon M, Ho Y-F, Chang H-S, Zhang S, Kaplan DI, Schwehr KA, DiDonato N, Hatcher PG, Santschi PH. 2014. Plutonium immobilization and remobilization by soil mineral and organic matter in the far-field of the savannah river site. *U.S. Environ. Sci. Technol.* 48, 3186–3195. <https://doi.org/10.1021/es404951y>.
- Zapata F. 2003. The use of environmental radionuclides as tracers in soil erosion and sedimentation investigations: recent advances and future developments. *Soil Tillage Res.* 69, 3–13. [https://doi.org/10.1016/S0167-1987\(02\)00124-1](https://doi.org/10.1016/S0167-1987(02)00124-1).
- Zhang X, Higgitt DL, Walling DE. 1990. A preliminary assessment of the potential for using caesium-137 to estimate rates of soil erosion in the Loess Plateau of China. *Hydrol. Sci. J.* 35, 243–252. <https://doi.org/10.1080/02626669009492427>.
- Zollinger B, Alewell C, Kneisel C, Meusburger K, Gärtner H, Brandová D, Ivy-Ochs S, Schmidt MWI, Egli M. 2013. Effect of permafrost on the formation of soil organic carbon pools and their physical-chemical properties in the Eastern Swiss Alps. *Catena* 110, 70–85. <https://doi.org/10.1016/j.catena.2013.06.010>.
- Zollinger B, Alewell C, Kneisel C, Meusburger K, Brandová D, Kubik P, Schaller M, Ketterer M, Egli M. 2015. The effect of permafrost on time-split soil erosion using radionuclides

(^{137}Cs , $^{239+240}\text{Pu}$, meteoric ^{10}Be) and stable isotopes ($\delta^{13}\text{C}$) in the eastern Swiss Alps. *J. Soils Sediments* 15, 1400–1419. <https://doi.org/10.1007/s11368-014-0881-9>.

Chapter 4. ^{10}Be and ^{14}C data provide insight on soil mass redistribution along gentle slopes and reveal ancient human impact

Abstract

Purpose Spatial and temporal patterns of past erosional events are a useful and needed information to explain observed soil patterns in different landscapes. Soil thickness reflects the overall expression of pedogenesis and erosion. Forested soils of Northern Germany exhibit varying soil thicknesses with thin soils on crest positions and buried soils at the footslope. The aim of this study is to reconstruct the complex soil mass redistribution and soil patterns of this forested area due to different periods of erosion and stability.

Methods We explored the explanatory power of both ^{10}Be (in situ and meteoric) on a hillslope and we ^{14}C -dated buried horizons at different depths.

Results The ^{10}Be depth profiles did not show an exponential decrease with depth. They had a 'bulge' shape indicating clay translocation and interaction with oxyhydroxydes (meteoric ^{10}Be), bioturbation and soil mass redistribution (in situ ^{10}Be). The combined application of both ^{10}Be and ^{14}C dating revealed progressive and regressive phases of soil evolution. Although Melzower Forest is protected (same vegetation) since the past 250 years, both ^{10}Be clearly indicated major soil mass redistribution along the investigated catena.

Conclusion A strong erosion impulse must have occurred between 4.5 and 6.8 kyr BP indicating an earlier human impact on soil erosion than previously postulated (~3 kyr earlier). Our findings correlate in fact with the first settlements reported for this region (~6.8 kyr BP) and shows their immediate effect on soils. The overall soil redistribution rates in this forest are surprisingly similar to those obtained from a nearby agricultural area.

Keywords: soil redistribution, erosion, ^{10}Be , forest, catena

Published as: Calitri, F., Sommer, M., van der Meij, W.M., Tikhomirov, D., Christl, M., Egli, M. ^{10}Be and ^{14}C data provide insight on soil mass redistribution along gentle slopes and reveal ancient human impact. *J Soils Sediments* (2021). <https://doi.org/10.1007/s11368-021-03041-7>

4.1 Introduction

Soils are a dynamic system and are the product of environmental and historical factors (Birkeland et al., 2003; Jenny, 1984). Consequently, soil thickness and horizonation at a given time-point in its evolution reflects the overall expression of pedogenesis (progressive evolution) and soil erosion (regressive processes; Sommer et al., 2008).

Soil and landscape heterogeneity is mainly caused by variations of parent material, topography, biota and occurrences of apparently random events (e.g., tree uprooting; Minasny et al., 2015; Šamonil et al., 2017). Differences in soil properties cause variations in hydraulic properties, which influence patterns of surface runoff and subsurface flow and, together with the variation in soil properties, lead to spatially varying rates of mass redistribution across the landscape (van der Meij et al., 2018; van Noordwijk et al., 1997; Van Oost et al., 2007). Humans use soil preferentially based on their assumed and experienced suitability for various purposes (such as pasture, arable land, etc.). This leads to patterns of varied land use and, as a consequence, the formation of heterogeneous landscapes (Minasny et al., 2015).

One of the most important processes shaping the land surface and soil profiles is the lateral transport of soil material by erosion. On agricultural land of mid to high latitudes, water erosion has been assumed to be the dominant mode since prehistoric times, with the first evidence of erosion coinciding with the first settlers (Brevik & Hartemink, 2010; Montgomery, 2007; Troeh et al., 1981). In fact, many European landscapes have been altered by anthropogenic activities (e.g., land use change, deforestation, etc.) since the Neolithic (Kappler et al., 2018). However, the share of soil erosion by tillage and human influence appeared to be even more important in historical and recent times (Van Oost et al., 2005; Wilken et al., 2020). Erosion continuously moves soil material from upslope to downslope (Heimsath et al., 1997) or even the other way round (caused by tree uprooting; Šamonil et al., 2017). From a geomorphological perspective (black box approach) the soil thicknesses are in steady state, when the lowering rate of the soil-bedrock interface, so-called “soil production”, is equivalent to the surface lowering rate, caused by erosion (Heimsath, 2006).

The development of isotopic techniques has facilitated the quantification of long-term geomorphic processes at the Earth’s surface (Banner, 2004; Ivy-Ochs & Kober, 2008; Preusser et al., 2008). Cosmogenic isotopes that are formed in minerals at the Earth’s surface (in situ) or in the atmosphere (meteoric) are now commonly used for dating and determining physical erosion and denudation rates (Schoonejans et al., 2017). Soil production and denudation rates

can be assessed by using meteoric or in situ produced ^{10}Be . Both deposition and soil erosion can be evaluated from meteoric ^{10}Be (using inventories similar to fallout radionuclide methods; Egli et al., 2010; Hidy et al., 2010; Maejima et al., 2005). Burial may also be apparent from in situ ^{10}Be profiles, but so far, in situ ^{10}Be has only been used for the quantification of denudation and erosion.

The depth variations of in situ ^{10}Be concentrations within a weathering profile are a powerful approach to constrain geomorphological parameters, including the mean denudation rate (e.g., Dosseto & Schaller, 2016; Siame et al., 2004). In geochemical studies, meteoric ^{10}Be is often used as a tracer for soil thickness development (Jungers et al., 2009; McKean et al., 1993; West et al., 2013; Willenbring & von Blanckenburg, 2010) and regolith residence time (e.g., Bacon et al., 2012; Pavich, 1989).

With the combination of both types of ^{10}Be , the dynamics of soils and related mass transports should be even more traceable. We explored the explanatory power of both ^{10}Be forms in forested soils along a catena in the hummocky ground moraine landscape of northeastern Germany. These soils have been forested for at least 250 years, but exhibit strongly varying thicknesses with very shallow soils on crest positions (Rüffer, 2018) and soils up to 1.5 m at the footslope, due to (pre-)historical erosion processes (Calitri et al., 2020; Rüffer, 2018). The aim of this study is to reconstruct the complex soil mass redistribution and soil patterns of this forested area due to different periods of erosion and stability. We ^{14}C -dated buried horizons found in five footslope/backslope positions in the catchment to determine erosion periods and we measured both in situ and meteoric ^{10}Be distributions along a soil catena to calculate erosion and deposition rates. With these data, we complement a previous study done in the same region on intensively used agricultural soils to understand what ^{10}Be distributions indicate in terms of soil processes (e.g., erosion, sedimentation) and how and when anthropogenic processes influenced soil mass redistribution and soil patterns (Calitri et al., 2019).

4.2 Study Area

The study area is located in the Uckermark region, northeastern Germany, which is a formerly glaciated landscape (Figure 4.1). The area has a hummocky terrain characterised by knolls, a series of small lakes and kettle holes (Calitri et al., 2019). The kettle holes are closed catchments, which allows quantification of soil erosion and deposition rates by mass balance calculations. The hummocky ground moraine shows a pronounced small-scale variation of soil properties and soil units as a function of topography (Koszinski et al., 2013; van der Meij et al., 2017).

The study region is characterised by a subcontinental climate with a mean annual temperature of 8.9 °C and mean annual precipitation of about 500 mm (Kopp & Schwanecke, 1994). The climatic water balance is slightly negative (with about -25 mm yr⁻¹). We selected the “Melzower Forst” as study area in the region (Calitri et al., 2020). The Melzower Forst is an old forest complex, which has been forested for at least the last 250 years, according to historical maps of the late 18th century. It consists of an old beech tree forest (*Fagus sylvatica* L.) with some individuals having an age of up to 400 years (Rüffer, 2018).

We selected the study area “Melzower Forst” to compare it with an intensively studied agricultural site on hummocky ground moraines (“CarboZALF-D”, Calitri et al., 2019). These sites share similar soil forming factors (e.g., climate, terrain, parent material), except for land use (Calitri et al., 2020). Through this comparison we want to assess the effect of land-use on erosion rates.

The parent material for soil development is an illitic, calcareous glacial till. According to the geological map of Brandenburg (<http://www.geo.brandenburg.de/boden/>; Geologische Übersichtskarte, Dezernat Geologische Landesaufnahme/Geoarchiv), the morainic deposits are from the Pleistocene, have a granitic character (Si-rich), are marly and also contain some carbonates. Loess does not occur in this region, because it was fully glaciated (Calitri et al., 2019). These forest soils exhibit strongly varying thicknesses with very shallow soils, Calcaric Regosols (FAO 2006; IUSS Working Group WRB 2015), on crest positions (Rüffer, 2018) and soils up to 1.5 m at the footslope (Stagnic Albic Retisols, IUSS Working Group WRB 2015) (Calitri et al., 2020).

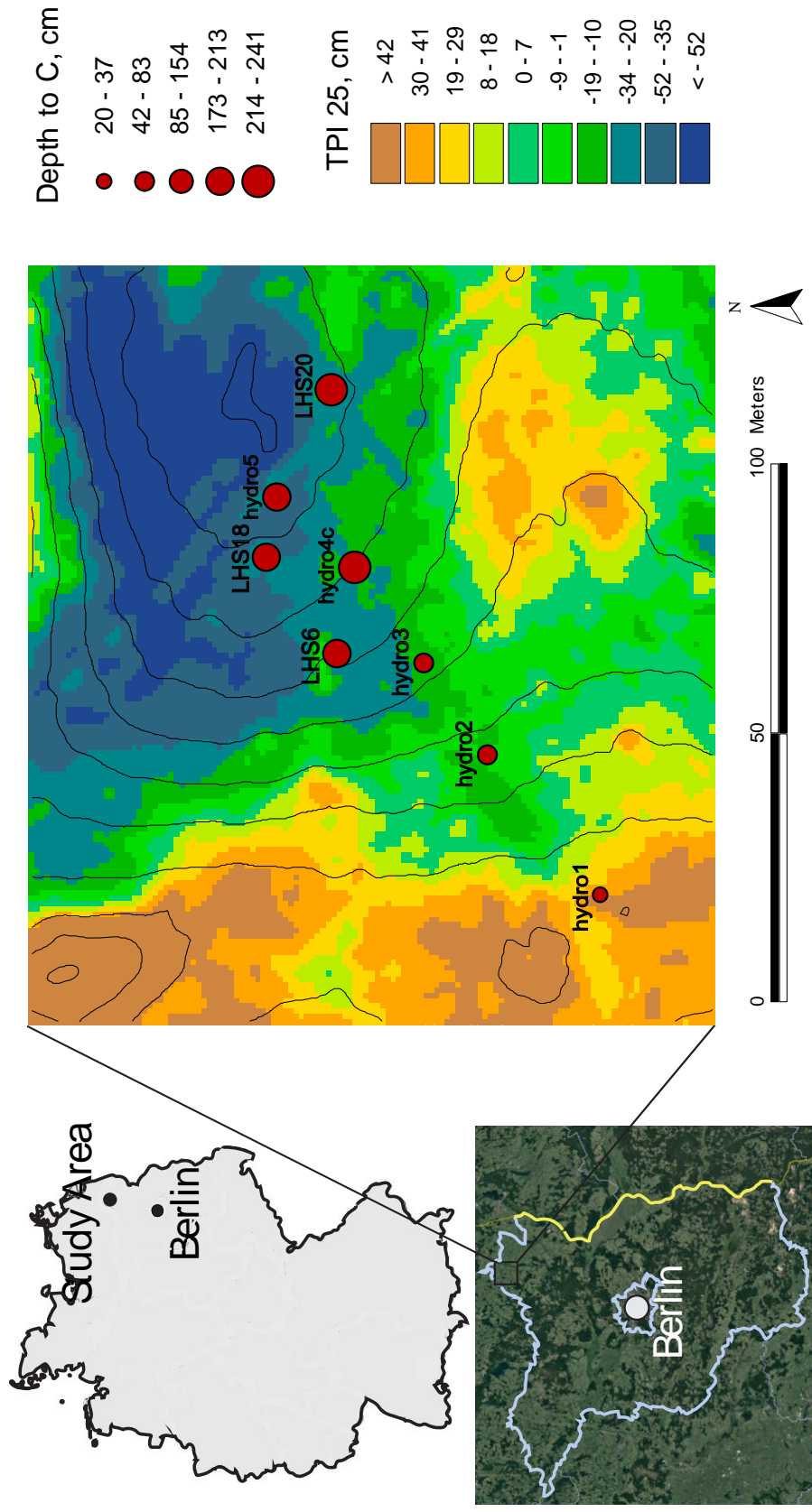


Figure 4.1. Map of Germany and the study area 'Melzower Forst' (left). Relationship between terrain parameters and soil thickness (depth to C horizons) and spatial pattern of the TPI (Topographic Position Index; right).

4.3 Materials and methods

4.3.1 Sampling strategy

A first soil survey at the “Melzower Forst” was completed in November 2016 and consisted of a total of 29 soil corings down to a maximum depth of 3 m. The sampling scheme was designed to select a variety of topographic positions through a conditioned Latin hypercube sampling design (n=20, Minasny & McBratney, 2006), with additional points along a flow path (“hydrosequence”, n=5) and on selected locations based on expert knowledge to cover the full soils’ feature space (n=4). For the sampling, we used polypropylene (PP) tubes with a diameter of 63 mm (HT DN63) and a length of 2+1 m. Each PP tube was inserted in a closed, metal driving core tube (M22; Nordmeyer Geotool, Herne, Germany) that was driven into the soil by a self-propelled vehicle (GTR 790; Nordmeyer Geotool).

From the 29 coring sites, 16 sites were selected to assess recent soil erosion/deposition rates using plutonium (Pu) inventories (Calitri et al., 2020) and three to assess soil redistribution rates along a catena using ^{10}Be (this study). We analysed both types of ^{10}Be : in situ produced and meteoric ^{10}Be in the soils. For this purpose, a second sampling campaign was carried out in November 2017. At the three sites along the catena (Hydro1, crest position; Hydro 3, backslope position; Hydro4c, footslope position; Figure 4.2), we sampled three soil cores down to the parent material (Hydro1 and Hydro3, 45 and 200 cm respectively) and down to a buried horizon (c. 175 cm; Hydro4c). To obtain enough material for in situ ^{10}Be analyses, we combined samples per horizon and depth: around 5 – 6 kg of soil material was necessary to attain enough quartz (extracted from the 0.25 – 0.50 mm fraction; see below). From these samples, an aliquot of a few hundred grams was taken to perform analyses for meteoric ^{10}Be .

For radiocarbon dating of fossil Ah horizons we selected other 4 sites from the first sampling campaign (Hydro5, LHS6, LHS18, LHS20 in Figure 4.1).

4.3.2 Soil chemical and physical analyses

Soil samples from cores were dried at 60 °C in the oven, gently crushed and separated with a 2 mm sieve (fine earth < 2 mm; gravel > 2 mm). To determine the particle size distribution of the fine earth fraction, a combination of wet sieving (> 63 µm) and pipette (< 20 µm) method Schlichting et al. 1995 was used. Particle size analysis pre-treatment consisted of three steps

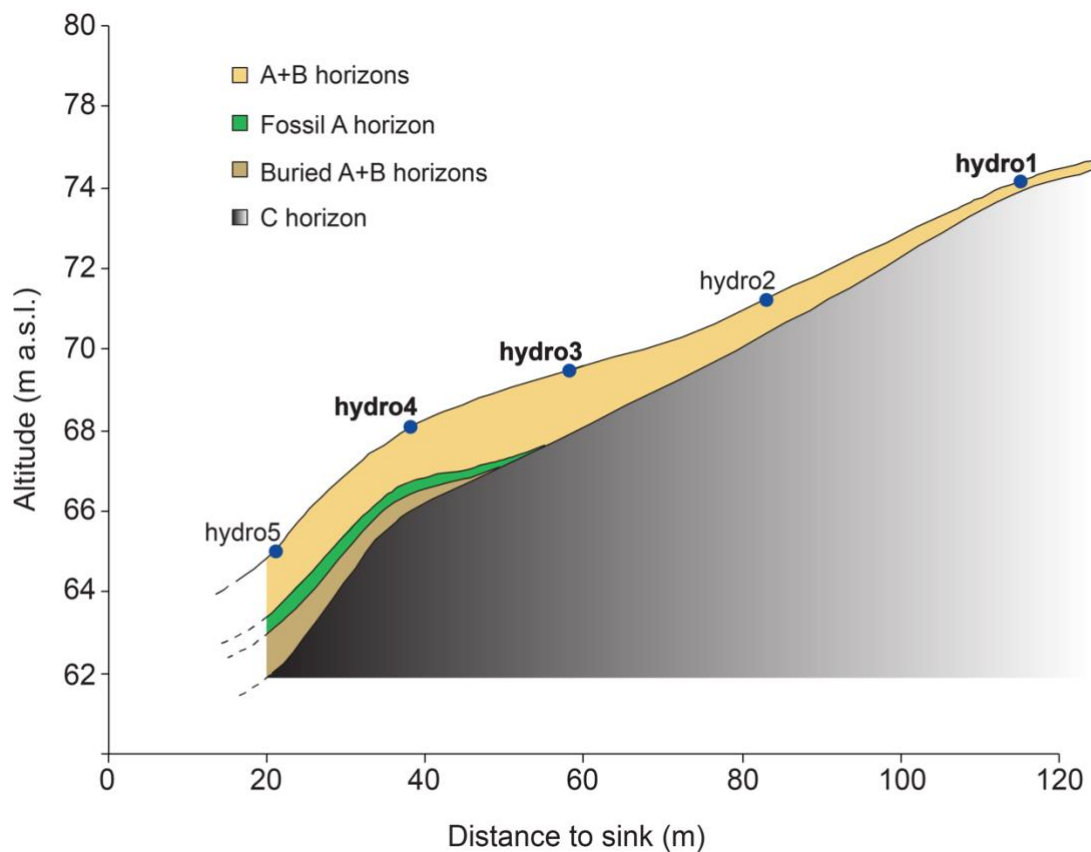
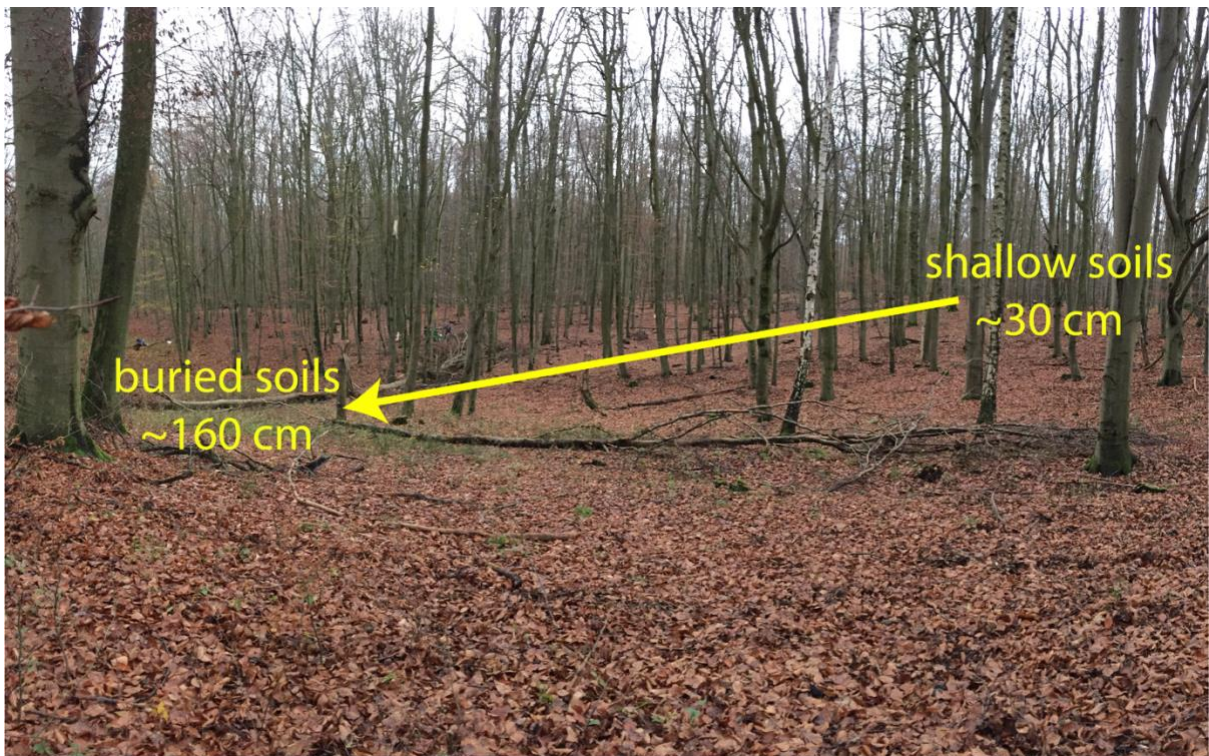


Figure 4.2. Picture of Melzower Forst and schematic cross-section (using a vertical exaggeration of a factor 3) of the investigated catena (hydro-sequence with sites Hydro1, Hydro2, Hydro3, Hydro4c, Hydro5).

(i) oxidation of organic matter using H_2O_2 (10 Vol.%) at 80 °C, (ii) carbonate dissolution with 0.5 N HCl (80°C) and (iii) dispersion by mixing for 16 h with a 0.01 M $\text{Na}_4\text{P}_2\text{O}_7$ -solution (Schlichting et al. 1995). Soil pH was measured using a glass electrode in 0.01 M CaCl_2 suspensions with a soil:solution ratio of 1:2.5 (w/v) after a 60 minutes equilibration period (Schlichting et al. 1995). Samples were combusted in an elemental analyser (Vario EL, Elementar Analysensysteme, Hanau, Germany) to measure total carbon and nitrogen contents. Carbonate (CaCO_3) was determined by electrolytic conductivity using the Scheibler apparatus (Schlichting et al. 1995). Organic carbon (C_{org}) was calculated as the difference between total carbon and inorganic carbon. All the analyses of the soil properties listed above were performed in two lab replicates per sample.

Total elemental contents were determined using X-ray fluorescence (XRF). Finely milled samples of approximately 5 g were analysed using an energy dispersive He-flushed X-ray fluorescence spectrometer (ED-XRF, SPECTRO X-LAB 2000, SPECTRO Analytical Instruments, Germany). The quality of the analyses was checked using a soil reference material with certified total element concentrations (Reference Soil Sample CCRMP SO-4, Canada Centre for Mineral and Energy Technology).

4.3.3 Radiocarbon dating of organic matter fractions

The site Hydro 4c and four other soil profiles (Table 4.5; Figure 4.1) have an older buried soil beneath a more recent soil. To date accumulation, soil organic matter of the buried soil was radiocarbon dated. Soil organic carbon contains several fractions: labile fractions with faster turnover along with more stable fractions having an older radiocarbon age (Eusterhues et al., 2005; Favilli et al., 2009; Helfrich et al., 2007; Kögel-Knabner et al., 2008). Particulate organic matter (POM) was dated to approximately date the burial of the fossil soil at these sites. This organic fraction usually contains the youngest organic compounds and is thus a good indicator of the burial event (Favilli et al., 2009). Furthermore, we dated the H_2O_2 -resistant fraction. This approximately indicates the oldest organic matter and gives an indication about the start of soil development (Favilli et al., 2009). The extraction of the organic matter fractions was done as described in (Favilli et al., 2008).

The carbon ratios were measured by Accelerator Mass Spectrometry (AMS) using the 0.2 MV radiocarbon dating facility (MICADAS) of the Ion Beam Physics at the Swiss Federal Institute of Technology Zurich (ETHZ). The calendar ages were obtained using the OxCal 4.4

calibration program (Bronk Ramsey, 2001, 2009) based on the IntCal 20 calibration curve (Reimer et al., 2020). Calibrated ages are reported with their 2σ error range.

4.3.4 Sample preparation and measurement for ^{10}Be analyses

Sample preparation for meteoric and in situ ^{10}Be is described in detail in (Calitri et al., 2019). In brief: to extract meteoric ^{10}Be , 2 g of soil sample were milled to a fine powder that was spiked with 1 mg of the commercial ^9Be carrier (Flucka 14205) and leached in HCl (16%). Be was extracted from the leachate in the two consecutive steps: hydroxide co-precipitation and chromatographic separation on Bio-Rad AG50-X8 resin.

To obtain in situ ^{10}Be , 30 g of pure quartz were separated from the rest of the soil sample (fraction of 250 – 500 μm) by froth flotation and leached in a HF solution. The quartz was spiked with 0.35 mg of the commercial ^9Be carrier (Scharlau BE3460100) and dissolved in concentrated HF. The resulting fluorides were converted into chlorides and went through a chromatographic separation on Bio-Rad AG1-X8 and AG50-X8 resins.

The purified samples (meteoric and in-situ ^{10}Be) were then precipitated into a hydroxide form, calcinated and mixed with niobium powder prior to accelerator mass spectrometry (AMS) measurement. $^{10}\text{Be}/^9\text{Be}$ ratios were measured with the TANDY AMS system at the Laboratory of Ion Beam Physics, ETH Zurich (Christl et al., 2013). The measured ratios were normalised to the ETH Zurich in-house secondary standards S2007N and/or S2010N.

4.3.5 Calculation of mass redistribution rates

We applied different methods to calculate soil redistribution rates, using both meteoric and in situ ^{10}Be contents.

Long-term redistribution rates using meteoric ^{10}Be

Soils build up ^{10}Be in time by atmospheric deposition (meteoric ^{10}Be). The theoretical abundance of ^{10}Be for a particular site can be calculated by knowing the soil age of that landform by independent dating. Measuring the meteoric ^{10}Be concentrations in the soil allows the estimation of soil redistribution rates (Egli et al., 2010; Maejima et al., 2005). Consequently, soil erosion and deposition can be calculated by comparing the measured ^{10}Be

concentrations with the theoretical concentrations for the expected age. The surface age of the investigated site was estimated to be 19 to 20 ka based on the timing of deglaciation (Hughes et al., 2016; Lüthgens et al., 2011; Stroeven et al., 2016). Considering no erosion, the surface age of a soil is given by:

$$t = -\frac{1}{\lambda} \ln \left(1 - \lambda \frac{N_{exp}}{q} \right) \quad (4.1)$$

and:

$$N_{exp} = q \frac{e^{-\lambda t} - 1}{-\lambda} \quad (4.2)$$

where N_{exp} (atoms cm^{-2}) = calculated theoretical ^{10}Be inventory in the profile based on the soil age assuming no erosion, q (atoms $\text{cm}^{-2} \text{yr}^{-1}$) = annual ^{10}Be deposition rate (calculated according to Masarik & Beer (2009) and Willenbring & von Blanckenburg (2010), λ ($4.997 \times 10^{-7} \text{a}^{-1}$) = decay constant of ^{10}Be and t (a) = soil age. As stated by (Egli et al., 2010), ^{10}Be deposition rates need to be estimated for a specific area. We estimated a deposition rate of ~ 106 atoms $\text{cm}^{-2} \text{yr}^{-1}$ (Masarik & Beer, 2009) for the study area, taking into account the geomagnetic latitude. Considering soil erosion, equation 1 is broadened to a non-steady-state approach (Zollinger et al., 2017):

$$t = -\frac{1}{\lambda} \ln \left(1 - \lambda \frac{N}{q - \rho C_{10\text{Be}} f E_{soil}} \right) \quad (4.3)$$

and:

$$E_{soil} = \frac{1}{\rho f C_{10\text{Be}}} \left(\frac{\lambda N}{e^{-\lambda t} - 1} + q \right) \quad (4.4)$$

where $C_{10\text{Be}}$ (atoms g^{-1}) = average ^{10}Be content in the top eroding soil, E_{soil} = soil erosion rate (cm yr^{-1}), f = fine earth fraction and ρ (g cm^{-3}) = bulk density of the topsoil. Due to the evolution over time of $C_{10\text{Be}}$, we use an average value between $t = 0$ and t of $\sim 0.5 \times C_{10\text{Be}}(\text{today})$ and assume that erosion losses are concentrated on the topsoil (e.g., 0 – 20 cm). We obtain:

$$\frac{N_{exp} - N}{t} = \frac{\Delta N}{t} = E(N) \quad (4.5)$$

where $E(N)$ (atoms $\text{cm}^{-2} \text{yr}^{-1}$) = annually eroded ^{10}Be . As a result, the annual erosion rate (E_{soil} ; cm yr^{-1}) is resulting in:

$$E_{soil} = \frac{z_{top} E(N)}{N_{top}} \quad (4.6)$$

where N_{top} = ^{10}Be content in the topsoil (with the thickness z_{top}). To convert erosion rates to $\text{km}^{-2} \text{yr}^{-1}$, E_{soil} has to be multiplied by soil density and referred to km^2 . The concentrations of ^{10}Be measured in the C-horizon are used to calculate the ^{10}Be content due to pre-exposure.

An additional procedure (Lal, 2001) was applied to estimate erosion rates using meteoric ^{10}Be and compare the different methods. The soil erosion (E_{soil}) rate is calculated as:

$$E_{soil} = z_0 K_E \quad (7)$$

and:

$$K_E = \frac{N_D}{N_S} \left[\frac{Q+q_a}{N_D} - \lambda \right] - \lambda \quad (8)$$

where z_0 (cm) = thickness of topsoil horizons (consist of O and A horizons), K_E = first-order rate constant for removal of soil from the topsoil layer, N_S (atoms cm^{-2}) = ^{10}Be inventory in topsoil horizons, N_D (atoms cm^{-2}) = ^{10}Be inventory in the D layer (usually consists of B and C horizons or the rest of the soil profile), Q (atoms $\text{cm}^{-2} \text{yr}^{-1}$) = flux of meteoric ^{10}Be into the topsoil and q_a (atoms $\text{cm}^{-2} \text{yr}^{-1}$) = flux of meteoric ^{10}Be .

These approaches were suitable only for the sites Hydro1 and Hydro3 as a result of their meteoric ^{10}Be depth trends.

Long-term redistribution rates using in situ ^{10}Be

Hidy et al. (2010) developed a depth profile model for sediments that are not vertically mixed to estimate changes in the in situ terrestrial cosmogenic nuclides production rate considering that secondary cosmic ray flux attenuates through materials. In this case study, the following model was applied to the sites Hydro1 and Hydro3.

The concentration C (atoms g^{-1}) for a specific nuclide m that is produced only from high energy nuclear and muogenic reactions (e.g., ^{10}Be , ^{14}C , ^{26}Al , ^{21}Ne) and is a function of depth z (cm), erosion rate ε (cm yr^{-1}) and exposure time t can be defined as

$$C_m(z, \varepsilon, t) = \sum_i \frac{P(0)_{m,i}}{\left(\frac{\varepsilon \rho_z}{\Lambda_i} + \lambda_m\right)} \cdot \exp\left(-\frac{z \rho_z}{\Lambda_i}\right) \cdot \left[1 - \exp\left(-t \left(\frac{\varepsilon \rho_z}{\Lambda_i} + \lambda_m\right)\right) \right] + C_{inh,m} \cdot \exp(-\lambda_m t) \quad (9)$$

where i stands for the different production pathways for nuclide m (neutron spallation, fast muon spallation, and negative muon capture), $P(0)_{m,i}$ is the site-specific surface production rate for nuclide m via production pathway i (in this case, $4.29 \text{ atoms g}^{-1} \text{yr}^{-1}$), λ_m is the decay constant for nuclide m (a^{-1}), ρ_z is the cumulative bulk density at depth z (g cm^{-3}), Λ_i is the

attenuation length of production pathway i (160 g cm^{-2} for neutrons), and $C_{inh,m}$ is the inherited (depositional) concentration of nuclide m (atom g^{-1}). The depth trends were modelled using equation 9 and a Monte Carlo simulation. Each individual, modelled depth trend of the ^{10}Be content was compared to the observed values and iteratively fitted (using erosion rates and inherited ^{10}Be) until the differences were minimal. In case of vertical mixing, i.e., clay translocation of the depth profile, as observed in our study area, modelling becomes more difficult. Nonetheless, with sufficient data points, the trend can equally be traced.

In the case of well-mixed soils, ^{10}Be can still be used to determine erosion rates at the landscape scale from stream sediments and at the plot scale for soil production rates (i.e., Granger & Riebe, 2007, 2014; Norton et al., 2010). For this purpose, we used the ‘CRONUS’ online calculator for erosion rate estimate (Balco et al., 2008); <http://hess.ess.washington.edu/>. Erosion rates were calculated using an average ^{10}Be concentration of the top ~60cm, assuming that these represent an average surface content due to the complete mixing.

4.3.6 Data and statistical analyses

Linear, multiple linear and polynomial (second order) regressions were carried out to help explain the behaviour of ^{10}Be in the soils and describe it as a function of controlling factors. All data that were considered for this analysis showed a normal distribution (Shapiro-Wilk test).

4.4 Results

4.4.1 Morphological, physical and chemical soil properties

The soil thicknesses as derived from the depth to C-horizons increase along the catena (Table 4.1, 4.2; Figure 4.1; see also Calitri et al., 2020). The intensity of redoximorphism increases towards the lower slope soils but is mostly restricted to subsoil horizons (see horizon designations in Table 4.2). All studied soils have a sandy-loamy to loamy texture and a low gravel content except for a few horizons at the Hydro3 site (Table 4.2). Clay translocation from eluvial to illuvial soil horizons is clearly recognisable as the main pedogenic process along the catena (Figure 4.3). Hydro1 classifies as a Nudiargic Luvisol, Hydro3 as an Endostagnic Albic Retisol, and Hydro4c is a Katostagnic Albic Retisol (IUSS Working Group WRB, 2015; Table 4.1). The clay increase towards the illuvial horizons (Bt) in Hydro3 is almost twice as high as in Hydro4c. Together with the much larger total thickness of Bt horizons (Hydro3: 83 cm, Hydro4c: 30 cm, Table 4.2) this indicates Hydro3 being exposed to a much longer period of progressive soil development (*ceteris paribus*). The topsoil of Hydro4c is acidic with pH ranging between 3.6 and 5.1. Hydro1 and Hydro3 have pH values ranging from strongly acidic (4.0) to neutral (7.0). The C horizon of Hydro1 and Hydro3 are characterised by higher pH values (7.5) due to carbonates (10% CaCO₃). The soil organic carbon content (SOC) in the Ah horizon ranged from 1.6 to 2.8%.

4.4.2 ¹⁴C dating

We analysed soil samples from 5 buried horizons for ¹⁴C dating (Fig. 4.1; Table 4.5). The buried horizons are located at similar depths (ca. 180 – 210 cm) except for the fAh horizon at the LHS6 site (85 – 108 cm). All calibrated ages (POM fraction) are comparable with an age (1- sigma range) spanning from 4607 – 4448 yr cal BP (LHS18) to 6845 – 6745 yr cal BP (Hydro4c). Despite being the most superficially buried horizon (85-108 cm), the fAh horizon at LHS6 is not the youngest (5576–5335 yr cal BP).

Three fossil Ah horizons (Hydro5, LHS18, LHS20) treated with hydrogen peroxide (H₂O₂) treatment showed all comparable ages around 11 kyr cal BP. LHS6 has a slightly younger age 9696 – 9025 yr cal BP. In contrast, Hydro4c is older than the rest of the soil profiles having an age of 17560 – 16161 yr cal BP.

Table 3.1. Location, landscape attributes and soil characteristics for study site “Melzower Forst”.

Site name	Coordinates (°N / °E)	slope °	TPI25 m	dts* m	Soil Classification (IUSS Working Group WRB, 2015)	depth to C cm	fossil Ah, upper boundary, cm
hydro1	53.152938 / 13.883513	4.2	0.79	115	Nudiargic Luvisol (LV-ng)	30	-
hydro3	53.153241 / 13.884138	4.4	-0.23	58	Endostagnic Albic Retisol (RT-stn.ab)	154	-
hydro4c	53.153446 / 13.884194	4.1	-0.31	38	Katostagnic Albic Retisol (RT-stk.ab)	214	170

*dts = distance to sink

Table 3.2. Physical and chemical characteristics of the investigated soils.

Site	Soil type	Soil horizon	>2mm (%)	Sand (%)	Silt (%)	Clay (%)	Bulk density (Mg/m ³)	pH (CaCl ₂)	SOC (%)	CaCO ₃ (%)	Fe _{ox} g kg ⁻¹	Fe _{dith} g kg ⁻¹	Al _{ox} g kg ⁻¹	Mn _{dith} mg kg ⁻¹	
Hydro1	Nudiargic Luvisol														
	0-15	Ah	2	64	21	15	1.32	6.55	2.08	-	0.9	3.5	0.43	242	
	15-30	Bt	3	60	22	18	1.50	6.97	0.69	0.2	1.0	5.5	0.53	216	
	30-45	Ck	3	56	30	14	1.61	7.61	0.46	10.8	0.7	5.2	0.35	140	
Hydro3	Endostagnic Albic Retisol														
	0-15	Ah	5	69	21	10	1.18	4.01	1.59	-	1.6	2.5	0.50	152	
	15-30	AE	2	71	21	8	1.35	4.64	0.70	-	1.5	2.5	0.51	271	
	30-45	EA	3	73	22	5	1.44	4.94	0.37	-	1.4	2.6	0.45	363	
	45-60	E	9	69	21	10	1.45	5.41	0.28	-	1.8	4.0	0.35	306	
	60-75	E/Bht	3	66	22	12	1.49	5.59	0.32	-	2.8	5.7	0.43	251	
	75-90	Bthg1	2	61	25	14	1.65	5.67	0.31	-	2.6	5.4	0.46	217	
	90-105	Bthg2	5	55	28	17	1.63	5.67	0.31	-	2.7	5.7	0.52	157	
	105-120	Btg1	26	50	26	24	1.68	5.84	0.22	-	2.4	6.5	0.54	160	
	120-135	Btg2	6	52	25	23	1.69	6.03	0.23	-	2.3	7.4	0.49	236	
	135-158	Btg3	17	49	29	22	1.64	6.81	0.23	-	2.0	8.7	0.48	256	
	158-165	Ckg	9	51	35	14	1.78	7.24	0.09	3.2	1.3	8.3	0.36	270	

165-185	Ck	2	52	36	12	1.73	7.50	0.02	9.0	0.6	4.4	0.28	153
Hydro4c Katostagnic Albic Retisol													
0-10	Ah	3	69	23	8	0.71	3.64	2.80	-	1.3	2.9	0.43	159
10-20	AE	2	71	22	7	1.13	3.59	1.15	-	1.1	2.7	0.46	121
20-29	EA	2	73	21	6	1.22	3.71	0.90	-	1.0	2.4	0.50	168
29-40	E	3	69	25	6	1.45	3.96	0.48	-	0.9	2.3	0.49	195
40-50	Eg1	3	68	24	8	1.55	4.28	0.21	-	0.8	2.8	0.43	278
50-60	Eg2	3	66	24	10	1.60	4.64	0.20	-	0.8	4.0	0.40	299
60-70	Eg3	3	64	24	12	1.65	4.89	0.22	-	0.9	4.7	0.42	302
70-80	Btg1	3	64	22	14	1.73	4.93	0.22	-	1.0	5.3	0.43	307
80-90	Btg2	4	62	23	15	1.69	4.78	0.23	-	1.1	5.7	0.46	337
90-100	Btg3	3	63	22	15	1.70	4.71	0.24	-	1.2	5.3	0.45	317
100-110	Bg1	6	65	23	12	1.75	4.72	0.23	-	1.3	5.6	0.45	321
110-120	Bg2	4	65	24	11	1.79	4.81	0.25	-	1.3	5.4	0.42	338
120-130	Bg3	5	67	22	11	1.79	4.88	0.27	-	1.3	4.9	0.40	354
130-140	Bg4	3	66	23	11	1.80	4.95	0.21	-	1.3	4.8	0.35	354
140-150	Bg5	3	67	22	11	1.80	5.15	0.21	-	1.4	4.8	0.34	351
150-158	Bg6	1	65	23	12	1.74	5.15	0.32	-	1.3	5.2	0.38	378
158-170	Ab/Bg	2	65	24	11	1.74	5.14	0.47	-	1.4	5.0	0.43	383
170-175	fAh	1	61	26	13	1.75	5.14	0.69	-	1.5	5.6	0.50	418

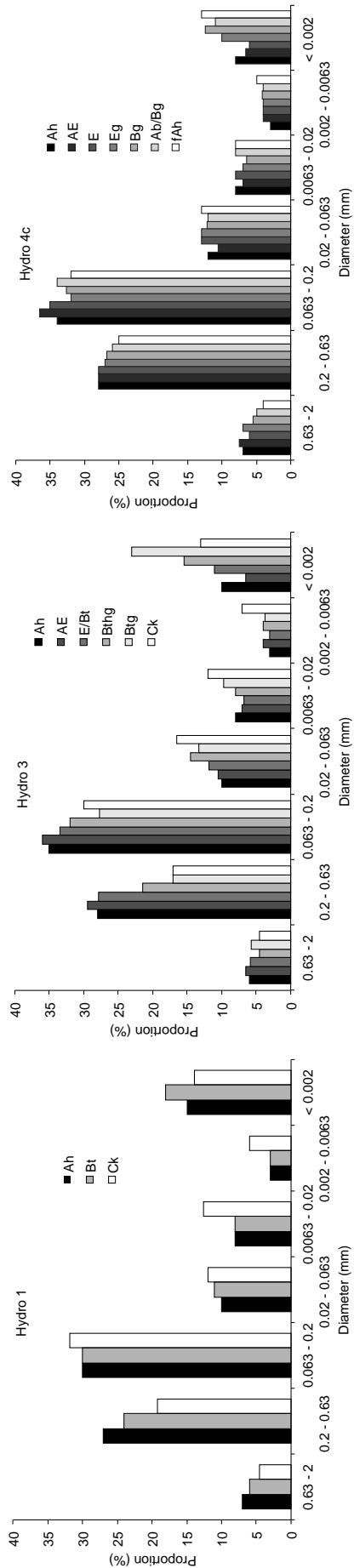


Figure 4.3. Detailed overview of grain sizes as a function of soil horizons for the sites a) Hydro1, b) Hydro3 and c) Hydro4c.

The uncertainty in the ^{14}C measurements of the H_2O_2 treated fraction is relatively high for all the samples - except for the Hydro4c site - due to a too low amount of material for the AMS measurements. The ^{14}C ages of the H_2O_2 -resistant fraction indicates a start of soil development around 17 kyr BP whereas the ^{14}C ages of the POM fraction evidence erosional events between about 4.5 and 6.8 kyr BP.

4.4.3 Meteoric and in situ ^{10}Be

The contents of meteoric ^{10}Be as a function of soil depth are given in Figure 4.4. The original data can be found in the supplementary Table S1. Site Hydro1 has a much lower ^{10}Be content than Hydro3 or Hydro4c. The highest content was usually found in the subsoil (E/Bth-Hydro3). The ^{10}Be contents in Hydro1 match with the profile morphology (Ah, thin Bt and C horizon), which suggests that former E and most of the Bt horizons were removed.

Similar to the meteoric ^{10}Be , the highest content of in situ ^{10}Be was detected in the EA horizon in the Hydro3 profile (Figure 4.4). As in situ ^{10}Be is measured in quartz, it seems unlikely that the ^{10}Be profile primarily reflects clay translocation (eluviation/illuviation). This distribution might also be a result of bioturbation, as intense earthworm and mice activity was observed while sampling.

The profile Hydro4c shows an increase in the meteoric ^{10}Be content with depth and the peak right in the fAh horizon. This might be due to (i) the burial event per se, with the deposition of soil material on the top of an older topsoil and (ii) clay-mediated transport of ^{10}Be (see section 5.2).

Moreover, we compared the ^{10}Be contents of the Melzower Forst (Hydro1, Hydro3, Hydro4c) with ^{10}Be data from an agricultural landscape in a similar geographical setting, the CarboZALF site (with the profiles LP4, LP12N, VAMOS; Figure 4.4; Table 4.1; Calitri et al. 2019). As shown in Figure 4.4, the meteoric ^{10}Be depth profiles of the Melzower Forst are moderately comparable to those at the CarboZALF study site. Both non-eroded soils show similar clay

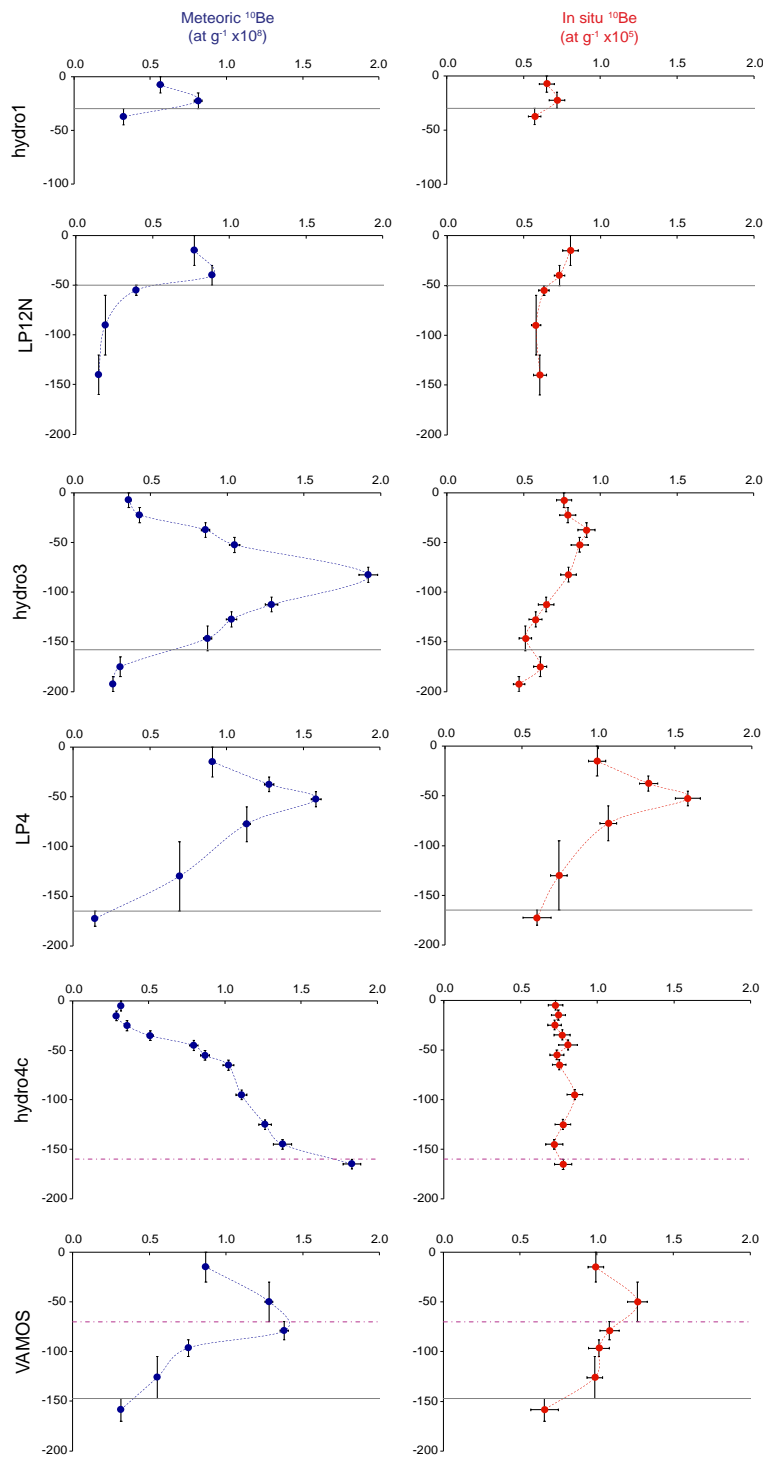


Figure 4.4. Depth trends of meteoric ¹⁰Be (at g⁻¹ fine earth – < 2mm – x10⁸) and in situ ¹⁰Be (at g⁻¹ quartz – 250–500 μm – x10⁵) contents of the forest sites (Melzower Forst) Hydro1 (summit), Hydro3 (backslope) and Hydro4c (footslope) in comparison with depth trends of meteoric and in situ ¹⁰Be of soils in agriculture land (CarboZALF) with the sites LP4, LP12 and VAMOS (Calitri et al., 2019). The grey line represents the C horizon and the dashed magenta line stands for the fossil A horizon.

depth functions and comparable depth profiles for both meteoric and in situ ^{10}Be (Hydro3, backslope position vs. LP4, plateau position). The two eroded soils with remnants of the former Bt (Hydro 1, LP12N) resemble each other in Be depth functions as well.

Table 4.4 shows the relationships between meteoric, in situ ^{10}Be and physical and chemical properties. ^{10}Be and pH exhibit the highest correlation. Although the pattern of clay particles along the soil profile and meteoric ^{10}Be look similar, the correlation between them is not significant.

We found a good correlation of both types of ^{10}Be with pH (Table 4.4). In the case of meteoric ^{10}Be , the correlation has a convex shape with a peak concentration at pH 5.5. Both ^{10}Be showed a statistically significant correlation with pH, Fe_{dith} and Al_{ox} - meteoric ^{10}Be : $R^2 = 0.40$, $p\text{-value} = 0.01$, in situ ^{10}Be $R^2 = 0.43$, $p\text{-value} = 0.004$. Because in situ ^{10}Be is extracted from quartz of the fraction (250 – 500 μm), the relation to pH and pedogenic oxyhydroxides results from similar depth gradients of drivers rather being causal. Furthermore, Be shows affinities to the major cations Al, Si, and Mn, and the lithogenic trace-elements neodymium (Nd) and zirconium (Zr) (Ryan 2002). Although in terms of atomic structure and valence state, it is associated with alkaline earth elements. A multilinear regression highlighted a weak correlation between meteoric ^{10}Be and Nd and Zr ($R^2 = 0.34$; $p\text{-value} = 0.01$; data not shown) for the Melzower Forst.

4.4.4 Soil redistribution rates

The depth function model (Figure 4.5) of Hidy et al. (2010) was used to simulate the in situ ^{10}Be contents along the soil profile and to derive soil erosion rates. This model could be applied successfully to Hydro3 and much less convincingly to profile Hydro1, which had only three data points along the profile. The Hydro4c site exhibited constant in situ ^{10}Be content along the profile; therefore, modelling was not possible.

The soil redistribution rates derived from both meteoric and in situ ^{10}Be are reported in Table 4.3.

The erosion rates calculated for the site Hydro1 (crest position) are always higher than those of the sites Hydro3 and Hydro4c (backslope and footslope position) independent from the method used, except when using the depth function model (Hidy et al., 2010). When using meteoric ^{10}Be , the approach of Lal (2001) does not produce a meaningful sequence. When

using in situ ^{10}Be , the calculated soil erosion rates were usually lower. Independent of the type of nuclide used, erosion rates were much lower at the backslope site (i.e., Hydro4c) than at the other sites.

Moreover, we made an independent estimate of soil erosion using a similar methodology as in van der Meij et al. (2017) (Figure 4.6). We calculated the current soil thickness using linear regression of depth to C horizon using the logarithm of flow accumulation ($R^2 = 0.62$) with 29 soil observations of the study site. We then derived the soil loss by subtracting the current soil depth from the mean depth of undisturbed soils (i.e., soils affected by neither erosion nor deposition; 108 cm). The results show the most soil loss at the crest positions (Figure 4.6). Soil loss decreases towards the centre of the catchment.

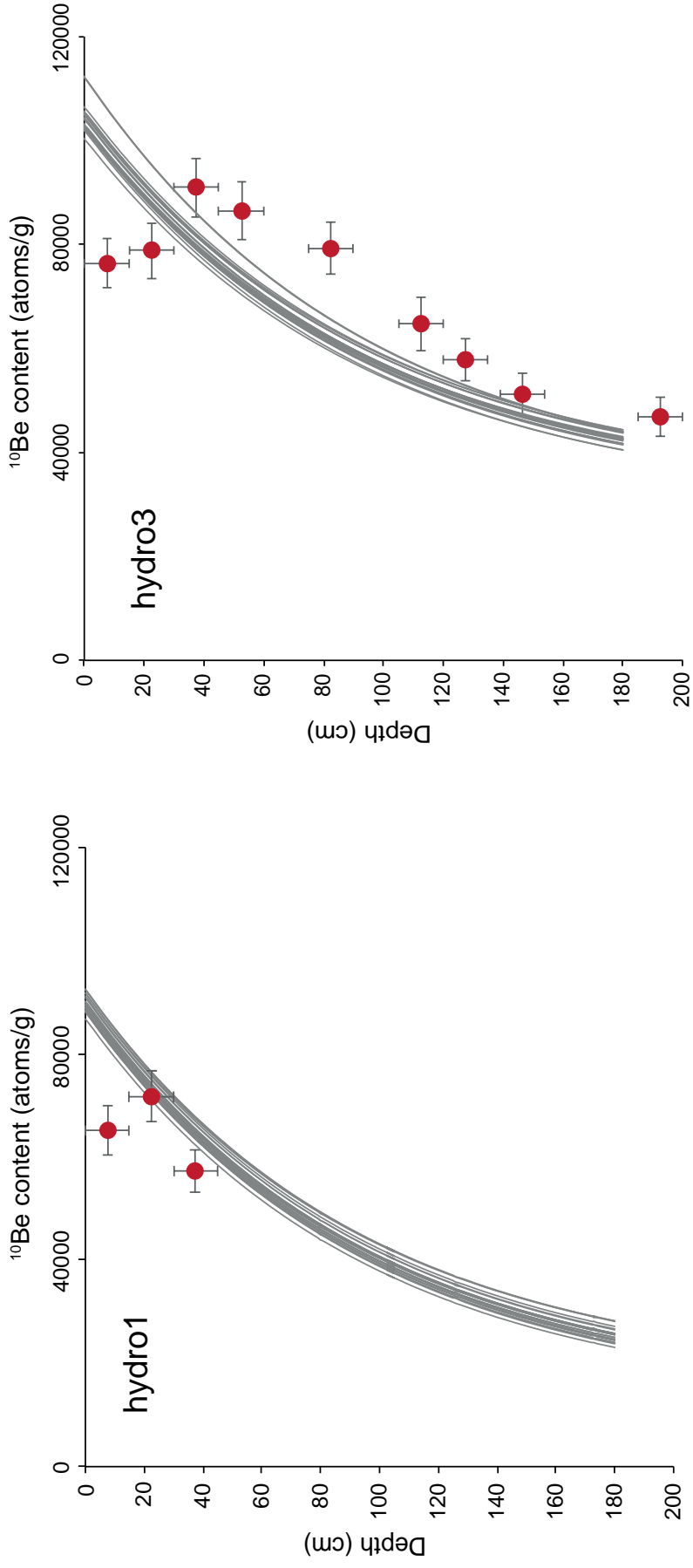


Figure 4.5. In situ ¹⁰Be distribution along the profiles and modelled trend using equation 9. Inherited ¹⁰Be and erosion rates were iteratively obtained by minimising the difference between measured and modelled values. a) Hydro1 and b) Hydro3.

Table 4.3. Long-term soil redistribution rates. Positive values indicate soil erosion/loss.

Site	<i>Meteoric ¹⁰Be</i>		<i>In situ ¹⁰Be</i>	
	Model used			
	Lal (2001)	Zollinger et al. (2017)	Depth function (Hidy et al., 2010)	Cronus (Balco et al., 2008)
	t ha ⁻¹ yr ⁻¹	t ha ⁻¹ yr ⁻¹	t ha ⁻¹ yr ⁻¹	t ha ⁻¹ yr ⁻¹
Hydro1	1.62	3.92	0.11	1.20
Hydro3	2.99	0.47	0.19	0.77
Hydro4c	2.83	-3.88	-	0.81

4.5 Discussion

4.5.1 Periods of stability and erosion

The Melzower Forst has a complex history of varying land-use and land cover, with stable periods with progressive pedogenesis and unstable periods with regressive pedogenesis in the form of soil erosion. The ^{14}C dating helped us identify two of these periods.

The oldest ^{14}C dating of the H_2O_2 -resistant fractions indicate a start of carbon uptake and progressive pedogenesis around 17 to 16 ka BP. This date neatly follows the deglaciation of the area around 19 ka BP (Hughes et al., 2016; Lüthgens et al., 2011; Stroeven et al., 2016).

This stable phase ended around 7 ka BP, as the ^{14}C datings from the POM fractions indicate (Table 4.5). The fAh horizons were all buried about 4.6 to 6.8 ka cal BP. Around this time, the first settlements and agricultural activities started in the region, triggering a regressive phase of soil erosion by deforestation and primitive land management (Schatz 1999; Jahns 2000, 2001; Kulczycka-Leciejewiczowa and Wetzel, 2002; Kappler et al. 2018; van der Meij et al. 2019). Kappler et al. (2018) mention that in spite of numerous Neolithic settlements in the study area no correlative colluvial sediments were detected so far. They attributed first human-induced soil erosion is attributed to the Late Bronze Age, i.e., c. 4000 years ago. With our ^{14}C data we can show that this human induced erosion most likely started earlier than previously thought and that it better matches with the start of the first settlements in that region. The Melzower Forst was probably also affected by these agricultural activities, because deforestation and land management are the main causes of soil disturbance and erosion in such small catchments. This fits well to records of many sedimentary archives globally, where an increase in erosion rates is often observed 6 to 7 ka BP (Owens, 2020). Deforestation and fires can accelerate soil erosion by water distinctly but cannot explain highest erosion at crest position (according to profile truncation). The observed soil patterns, with most erosion on the convex crests and deposition at the footslopes (Figure 4.6), are generally caused by tillage erosion (De Alba et al., 2004; Wilken et al., 2020). The spread in the ^{14}C ages over such small differences in the depression can indicate a gradual infilling of the colluvium. The same was observed at CarboZALF, where the ages of colluvium can vary hundreds to thousands of years of a distance of tens of meters (van der Meij et al., 2019). Charcoal particles and other burnt organic remnants to testify the human presence and deforestation were not found in any of the buried horizons. Nonetheless, we can hypothesise that a change of land use in the Neolithic (4776–2595 BC) triggered a regressive period in the soil development of the area.

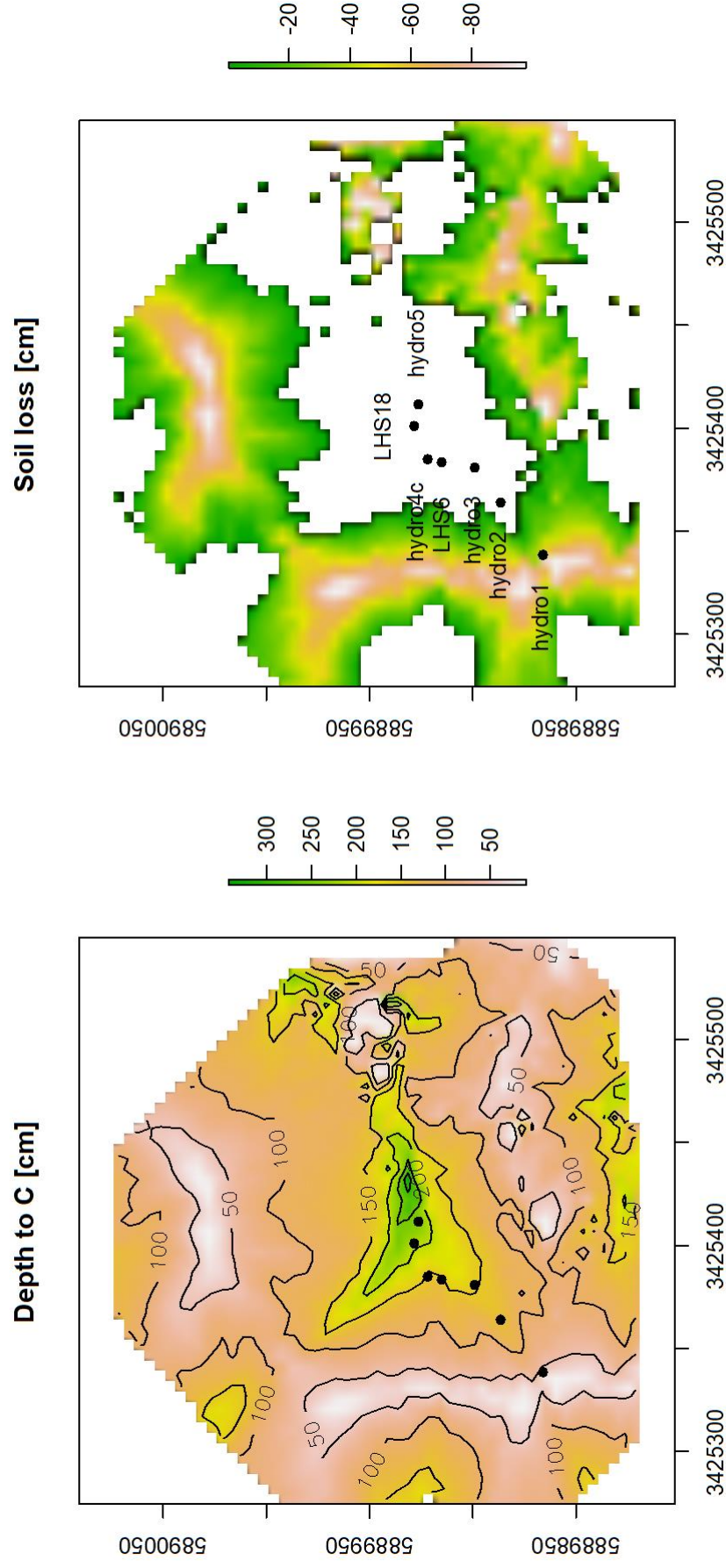


Figure 4.6. Interpolation of the depth to parent material (C horizon; m) and estimation of erosion (soil loss; m).

The current stable phase started at least 250 years ago, according to the historical maps. With reforestation of the catchment, the soil stabilised and progressive pedogenic processes, such as clay translocation, could start again. This especially holds true for Hydro 4c, where distinct E and Bt horizons developed in the colluvial deposits.

With the use of ^{14}C dating and historical maps we could identify these three periods of soil and landscape development in the Melzower Forst. Our findings correlate well with reconstructions of historical land-use in the Uckermark region (Jahns, 2000; Kappler et al., 2018; van der Meij et al., 2019). Since the beginning of agricultural activities, increased erosion events distinctly affected soils and their characteristics giving rise to a landscape with truncated soil profiles and colluviums. However, there might be more periods that we have not yet identified in the deposits at Melzower Forst, such as periods of abandonment and peaks in settlements of the Bronze Age or the Migration Period (Jahns 2000; Schultz, 2009). Additional datings of carbon and sediments throughout the colluvial soil profiles will increase the temporal resolution of the land use reconstruction and can shed light on different periods of landscape stability and instability.

4.5.2 Beryllium-10 (^{10}Be) along the soil profile

The depth trends of meteoric ^{10}Be in the three profiles is classified in literature as a ‘bulge’ type. In these soils, the peak of the meteoric ^{10}Be content can be found in a clay-rich B-horizon layer. Graly et al. (2010) showed in their review that this kind of shape is typical for older and slowly eroding soils. The ‘bulge’-type profile of the investigated soils seems rather due to clay translocation than by age and/or slow erosion (Egli et al., 2010; Pavich et al., 1984). Schaller et al. (2018) investigated the contribution of climate and vegetation cover on hillslope denudation in Chile using in situ ^{10}Be and found ‘bulge’ ^{10}Be depth profiles. In that particular case study, the ‘bulge’-shape was attributed to natural soil mixing (e.g., bioturbation).

We compared the ^{10}Be depth profiles of the present study to ^{10}Be depth profiles from an agricultural landscape (at the CarboZALF research station; see Calitri et al., 2019 in the same research area (Figure 4.4; Table 4.1). Although the quantities of ^{10}Be at Melzower Forst are generally higher than those of CarboZALF but the trends of ^{10}Be along the soil profiles match quite well with each other.

For the erosional site Hydro 1 (Nudiargic Luvisol), the current soil thickness of 30 cm is caused by erosion in the strongly regressive phase that started about 7 ka BP. The soil horizonation of Hydro 1 matches that of profile LP12N at CarboZALF, although the thickness of the Bt is much lower at Hydro 1. Profile morphology corresponds to similar ^{10}Be depth functions in both profiles.

The profile of Hydro3 (Endostagnic Albic Retisol) in a backslope position shows a complete soil profile (Table 2) and resembles LP4 at CarboZALF. Based on the horizonation and the typical bulge shape of the meteoric ^{10}Be , erosion of this profile can be assumed minimal. However, in situ ^{10}Be does not show an increasing content to the soil surface as would be expected from non-eroding soils (Schaller et al., 2018). Instead, the in situ ^{10}Be content is lower in the topsoil (<30 cm) compared to horizons just below. We can explain this depth trend by viewing the topsoil of this backslope position as a transport zone, in which erosion and deposition is balanced. The soil profile Hydro4c (Katostagnic Albic Retisol) has developed at a depositional position. In order for the sediments to reach the depression, they have to be transported along the slope. The ^{10}Be content of the transported material decreases because subsoil material, having a lower ^{10}Be content, has been exposed at the surface of soils at a higher position along the catena. In consequence, the transported material deposited at Hydro4c represents a mixture of differently eroded (top-)soils from the catchment.

The depositional nature of Hydro4c is supported by the presence of a buried topsoil (fAh), just as profile VAMOS at CarboZALF. The meteoric ^{10}Be profiles show a similar trend, with an increasing ^{10}Be content up to the fAh horizon. The in situ ^{10}Be profiles slightly differ, with a constant ^{10}Be content at Hydro4c throughout the profile and a small bulge-shape in the ^{10}Be content at VAMOS.

Although the current land use of Melzower Forst and CarboZALF differ, their ^{10}Be profiles still match fairly well.

4.5.3 Correlation of ^{10}Be with soil physical and chemical properties

The depth distribution of meteoric ^{10}Be is controlled by a wide range of factors. In Luvisols and Podzols, meteoric ^{10}Be may be transported by lessivation and podzolization processes (Egli et al., 2010; Pavich et al., 1984). Despite the documented clay translocation in the region (Calitri et al., 2019; Sommer et al., 2008), which was also observed in the present study (Figure 4.3), the correlation with meteoric ^{10}Be is not significant.

In tropical Oxisols, the meteoric ^{10}Be is primarily in the oxyhydroxide fraction, which allows more transport to depth than simple clay translocation (Barg et al., 1997). Indeed, we found a positive correlation with the oxalate-extractable Fe (weakly or non-crystalline forms; Fe_{ox}), the dithionite-extractable Fe (Fe_{dith}) and dithionite-extractable Mn_{dith} (Table 4.4). Meteoric ^{10}Be can be incorporated as a cation in oxyhydroxide complexes (Barg et al., 1997; Takahashi et al., 1999). Therefore, the distribution pattern of meteoric ^{10}Be is governed to a certain extent by Fe-Mn-oxyhydroxides.

Table 4.4. Relationship between physical/chemical properties and meteoric and in-situ ^{10}Be . Numbers reported refer to R^2 values.

	clay %	pH (CaCl_2)	Fe_{ox} g kg^{-1}	Fe_{dith} g kg^{-1}	Al_{ox} g kg^{-1}	Mn_{dith} mg kg^{-1}
met ^{10}Be	n.s. †	0.67***§	0.35***†	0.26*†	n.s. †	0.37***†
in-situ ^{10}Be	-	0.60***§	0.26**§	0.26*†	0.27*§	0.20*†

n.s.= not significant; * = p-value < 0.05; ** = p-value < 0.01; *** = p-value < 0.001

†=linear regression; §=polynomial regression

Campforts et al. (2016) and Wyshnytzky et al. (2015) identified pH as one of the key variables controlling meteoric ^{10}Be sorption reactions. In contrast, Graly et al. (2010) did not find a statistically significant effect of soil pH on meteoric ^{10}Be . According to Boschi & Willenbring, (2016), the cation exchange capacity and the inverse abundance of quartz best predict Be-sorption. Similarly, Chen et al. (2020) argues that grain size, mineralogy, pH and cation exchange capacity control the ^{10}Be contents in soils. The cation exchange capacity is influenced by soil acidity. In our investigated soils, pH seems to exert an influence on meteoric ^{10}Be (Figure 4.7); the processes or factors that lead to this non-linear pattern, however, seem diverse. In the pH range 3.5 – 5.5, meteoric ^{10}Be decreases with decreasing pH. This effect points to chemical leaching (transport in dissolved forms) and translocation with clay particles. As already pointed out by Heyn (1989) and Keilen et al. (1977), a decreasing pH increases the solubility of Be.

Table 4.5. Analysed soil material and related results of radiocarbon dating.

Site/sample	UZH-/ETHZ-code	Material	Depth (cm)	Treatment ^{1,2}	C14 age BP	$\pm 1\sigma$	cal age (calBP)	1σ	2σ
Hydro4c fAh	UZ-6516/ETH-96758	soil	180-210	POM	5965	27	6845-6745	6888-6731	
Hydro5 fAh	UZ-6518/ETH-96760	soil	185-213	POM	5128	26	5925-5767	5981-5753	
LHS6 fAh	UZ-6515/ETH-96757	soil	85-108	POM	4741	26	5576-5335	5581-5329	
LHS18 fAh	UZ-6517/ETH-96759	soil	180-210	POM	4067	25	4607-4448	4795-4438	
LHS20 fAh	UZ-6519/ETH-96761	soil	170-219	POM	5609	27	6405-6317	6445-6307	
Hydro4c fAh	UZ-6834/ETH-106293.1.1	soil	180-210	H ₂ O ₂	13895	454	17560 - 16161	18177 - 15695	
Hydro5 fAh	UZ-6836/ETH-106295.1.1	soil	185-213	H ₂ O ₂	9567	270	11240 - 10507	11808 - 10225	
LHS6 fAh	UZ-6833/ETH-106292.1.1	soil	85-108	H ₂ O ₂	8440	254	9696 - 9025	10180 - 8774	
LHS18 fAh	UZ-6835/ETH-106294.1.1	soil	180-210	H ₂ O ₂	9762	283	11688 - 10708	12431 - 10300	
LHS20 fAh	UZ-6837/ETH-106296.1.1	soil	170-219	H ₂ O ₂	9551	348	11308 - 10291	12098 - 9999	

¹ POM: particulate organic matter (potentially the youngest fraction).

² H₂O₂: hydrogen peroxide (H₂O₂)-resistant organic matter (potentially the oldest fraction).

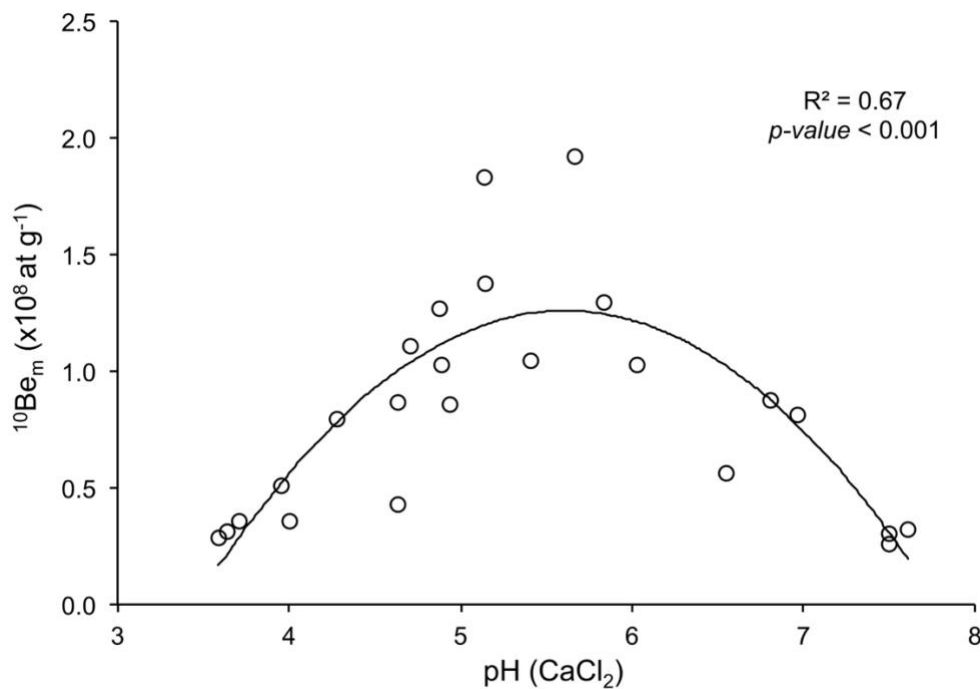


Figure 4.7. Relationship between pH and the meteoric (m) ¹⁰Be content in the fine earth fraction.

The E-horizons often have a pH-value < 5 indicating a leaching of soluble ¹⁰Be and co-translocation with clays. An active clay migration at Hydro4c in the top 40 cm is strongly limited to nonexistent owing to a too low pH. Here, solute transport seems to dominate while at the sites Hydro1 and Hydro4 predominantly clay migration or a combination with solute transport are the determining processes. In the pH range > 6 to 7.7, the contents of meteoric ¹⁰Be decrease with increasing pH. This is due to the fact that high pH values are encountered in the subsoil or parent material where only a small amount of ¹⁰Be accumulated.

4.5.4 Soil redistribution rates

The calculated soil redistribution rates vary substantially, depending on the type of ¹⁰Be and the model that are used to calculate the rates. The calculated erosion rates vary from 0.1 – 3.9 t ha⁻¹ yr⁻¹ (Table 4.3); in some situations, accumulation was determined. The erosion rates correspond to a soil loss of 0.1 to 3.1 m over the entire Holocene. These rates seem too high for (pre-)historic agricultural erosion and would require unrealistic high soil development rates. The measured accumulation rates using meteoric ¹⁰Be for the last 6.8 kyr (Hydro 4c) give a

deposition of about 1.7 m which corresponds quite exactly to the soil layer measured above the buried horizon at this site.

We estimated the spatial pattern of soil loss in Figure 4.6. If we divide the estimated soil loss by the surface age of the investigated site of 19 kyr we obtain an estimate of the spatial variation in long-term soil erosion. The average erosion rate for the entire catchment is $0.3 \pm 0.2 \text{ t ha}^{-1} \text{ yr}^{-1}$. For the Hydro1 site, the long-term erosion rates range from 0.6 to $0.8 \text{ t ha}^{-1} \text{ yr}^{-1}$. These rates are in the same order of magnitude as the soil redistribution rates calculated using in situ ^{10}Be . Based on the estimated soil loss, there was no erosion at the Hydro3 and Hydro4c sites, because their interpolated soil thickness exceeded the reference thickness. The distribution pattern of these calculations match with the results obtained from ^{10}Be (calculate version using the approach of Zollinger et al. (2017)). The absolute values of erosion however differ (with higher values when using ^{10}Be compared to this modelling approach).

The calculated rates are higher than long-term, large scale erosion rates calculated for middle European river catchments ($0.3 - 1.5 \text{ t ha}^{-1} \text{ yr}^{-1}$, Schaller et al. 2001). However, the catchment of the Melzower Forst is much smaller than those of the European rivers studied by Schaller et al. (2001), which would indicate severe erosion and deposition in the Melzower Forst. Also, the calculated erosion rates using in situ ^{10}Be are higher than those at CarboZALF ($0.03 - 1.61 \text{ t ha}^{-1} \text{ yr}^{-1}$, Calitri et al., 2019). This is surprising, because the CarboZALF site has been intensively used in the last centuries, especially since the Second World War, contrary to the Melzower Forst that was forested in that period. This period after the Second World War is generally considered to be the most erosive, due to intensification of agriculture and increase of machine power (Frielinghaus & Vahrson, 1998; Sommer et al., 2008).

Other difficulties may arise in the estimation of erosion rates using in situ ^{10}Be if a model (e.g., CRONUS) considers only the topsoil. The approach according to Zollinger et al. (2017) and Hidy et al., (2010) have problems in solving bulge-shaped ^{10}Be distribution profiles that are due to clay translocation, bioturbation or other processes. An additional error source might be the difficulty in precisely estimating the input rate of meteoric ^{10}Be . The meteoric ^{10}Be flux on Earth's surface is the most critical parameter in estimating soil erosion rates (Chen et al., 2020; Derakhshan-Babaei et al., 2020). Therefore, the calculation of soil erosion or denudation rates using ^{10}Be may be prone to errors depending on the environmental settings. The calculated erosion rates at Melzower Forst using ^{10}Be are higher than expected. An explanation for this can be found in the complex erosion and land use history of Melzower Forst and the limitations

of the applied Beryllium-erosion models to account for different phases of erosion and stability. The soil deposition rates, however, seem to match the conditions.

At Melzower Forst, periods with erosion and deposition alternated with more stable conditions. When calculating erosion rates using in situ or meteoric ^{10}Be , an average value over the entire soil development period (i.e., since the last deglaciation and Holocene) is obtained. This includes therefore also stable periods, where little or no erosion has occurred. Consequently, the erosion rates are underestimated in periods (like 7 kyr BP – 250 yr ago) having instable and regressive conditions and overestimated for stable periods having progressive conditions for soil formation.

Soil removal from eroding positions, transport over the hillslope and deposition in the depression affected the Beryllium profiles differently at different hillslope positions. The current Be-profiles are a product of alternating periods of stability and erosion and landscape position. To disentangle the Be-profiles and reconstruct the erosion history, the used model approaches for ^{10}Be have some difficulties. Numerical process-based models may help in explaining the complex soil mass redistribution (e.g., Campforts et al., 2016).

4.6 Conclusions

The application of meteoric and in situ ^{10}Be and ^{14}C dating along a soil catena in a small forested catchment revealed progressive and regressive phases of soil evolution. Meteoric and in situ ^{10}Be exhibited sometimes depth profiles with a ‘bulge’ shape. Clay translocation can explain in part the profile distribution of meteoric ^{10}Be , but not only. The depth trend of in situ ^{10}Be along the profiles at the mid-slope position is more or less according to the expectancies. In addition, in situ ^{10}Be revealed the different layers and enabled a differentiation between buried horizons, deposited material, biologically reworked and redistributed material. The footslope soil did not show any depth trend and exhibits strongly depositional conditions. The crest position had the lowest ^{10}Be content for both, meteoric and in situ ^{10}Be . Although the Melzower forest is protected and has been a forest since least 250 years, ^{10}Be clearly indicates major soil mass redistribution along the investigated catena. The calculation of soil deposition rates using meteoric ^{10}Be gave realistic values. The determination of meaningful erosion rates was, however, difficult — independent of the type of ^{10}Be and related model for rate calculations. Furthermore, we applied an independent spatial modelling approach where the current soil thickness was related to flow accumulation. Knowing soil depth distribution and their age, the erosion patterns and rates could be calculated. Using this procedure, a quality check with the ^{10}Be results was enabled. The soil redistribution rates (over the entire period of soil formation) were similar to those obtained from a nearby area that is used for intense agriculture (CarboZALF area). This means that the effects of the past, long-term soil mass redistribution still overshadow the present-day erosion.

The ^{14}C ages of buried soil horizons point to strongly regressive soil development phases (with erosion and deposition) that started particularly between about 4.5 and 6.8 kyr BP. Although absolute proofs are lacking, this seems to be due to human impact that started to increasingly affect soil properties at that time. The temporal erosion pattern fits with archaeological finds of first settlement in the region around 7 kyr BP. However, stronger soil erosional signals were so far dated back to about max 5 kyr BP. We show now that strong erosional processes already occurred earlier and seem to coincide with the onset of these settlements.

Acknowledgements

This research was supported by a cooperation contract (CORRELATE; F-75113-07-01) between the University of Zurich and the ZALF.

References

- Bacon AR, Richter D, deB., Bierman PR, Rood DH. 2012. Coupling meteoric ^{10}Be with pedogenic losses of ^9Be to improve soil residence time estimates on an ancient North American interfluvium. *Geology* 40:847–850. <https://doi.org/10.1130/G33449.1>
- Balco G, Stone JO, Lifton NA, Dunai TJ. 2008. A complete and easily accessible means of calculating surface exposure ages or erosion rates from ^{10}Be and ^{26}Al measurements. *Prospects New Front Earth Environ Sci* 3:174–195. <https://doi.org/10.1016/j.quageo.2007.12.001>
- Banner JL. 2004. Radiogenic isotopes: systematics and applications to earth surface processes and chemical stratigraphy. *Earth-Sci Rev* 65:141–194. [https://doi.org/10.1016/S0012-8252\(03\)00086-2](https://doi.org/10.1016/S0012-8252(03)00086-2)
- Barg E, Lal D, Pavich MJ, Caffee MW, Southon JR. 1997. Beryllium geochemistry in soils: evaluation of $^{10}\text{Be}/^9\text{Be}$ ratios in authigenic minerals as a basis for age models. *Chem Geol* 140:237–258. [https://doi.org/10.1016/S0009-2541\(97\)00051-X](https://doi.org/10.1016/S0009-2541(97)00051-X)
- Birkeland PW, Shroba RR, Burns SF, Price AB, Tonkin PJ. 2003. Integrating soils and geomorphology in mountains - an example from the Front Range of Colorado. *Geomorphology* 55:329–344. [https://doi.org/10.1016/S0169-555X\(03\)00148-X](https://doi.org/10.1016/S0169-555X(03)00148-X)
- Boschi V, Willenbring JK. 2021. Chemical and physical drivers of beryllium retention in two soil endmembers. *Sci Total Environ* 754:141591. <https://doi.org/10.1016/j.scitotenv.2020.141591>
- Brevik EC, Hartemink AE. 2010. Early soil knowledge and the birth and development of soil science. *CATENA* 83:23–33. <https://doi.org/10.1016/j.catena.2010.06.011>
- Bronk Ramsey C. 2001. Development of the radiocarbon calibration program. *Radiocarbon* 43:355–363. <https://doi.org/10.1017/S0033822200038212>

- Bronk Ramsey C. 2009. Bayesian analysis of radiocarbon dates. *Radiocarbon* 51:337–360. <https://doi.org/10.1017/S0033822200033865>
- Calitri F, Sommer M, van der Meij MW, Egli M. 2020. Soil erosion along a transect in a forested catchment: Recent or ancient processes? *CATENA* 194:104683. <https://doi.org/10.1016/j.catena.2020.104683>
- Calitri F, Sommer M, Norton K, Temme A, Brandová D, Portes R, Christl M, Ketterer ME, Egli M. 2019. Tracing the temporal evolution of soil redistribution rates in an agricultural landscape using $^{239+240}\text{Pu}$ and ^{10}Be . *Earth Surf Process Landf* 44:1783–1798. <https://doi.org/10.1002/esp.4612>
- Campforts B, Vanacker V, Vanderborght J, Baken S, Smolders E, Govers G. 2016. Simulating the mobility of meteoric ^{10}Be in the landscape through a coupled soil-hillslope model (Be2D). *Earth Planet Sci Lett* 439:143–157. <https://doi.org/10.1016/j.epsl.2016.01.017>
- Chen P, Yi P, Czymzik M, Aldahan A, Ljung K, Yu Z, Hou X, Zheng M, Chen X, Possnert G. 2020. Relationship between precipitation and ^{10}Be and impacts on soil dynamics. *CATENA* 195:104748. <https://doi.org/10.1016/j.catena.2020.104748>
- Christl M, Vockenhuber C, Kubik PW, Wacker L, Lachner J, Alfimov V, Synal H-A. 2013. The ETH Zurich AMS facilities: Performance parameters and reference materials. *Nucl Instrum Methods Phys Res Sect B Beam Interact Mater at* 294:29–38. <https://doi.org/10.1016/j.nimb.2012.03.004>
- De Alba S, Lindstrom M, Schumacher TE, Malo DD. 2004. Soil landscape evolution due to soil redistribution by tillage: a new conceptual model of soil catena evolution in agricultural landscapes. *CATENA* 58:77–100. <https://doi.org/10.1016/j.catena.2003.12.004>
- Derakhshan-Babaei F, Nosrati K, Tikhomirov D, Christl M, Sadough H, Egli M. 2020. Relating the spatial variability of chemical weathering and erosion to geological and topographical zones. *Geomorphology* 363:107235. <https://doi.org/10.1016/j.geomorph.2020.107235>
- Dosseto A, Schaller M. 2016. The erosion response to Quaternary climate change quantified using uranium isotopes and in situ produced cosmogenic nuclides. *Earth-Sci Rev* 155:60–81. <https://doi.org/10.1016/j.earscirev.2016.01.015>
- Egli M, Brandová D, Böhlert R, Favilli F, Kubik PW. 2010. ^{10}Be inventories in Alpine soils and their potential for dating land surfaces. *Geomorphology* 119:62–73. <https://doi.org/10.1016/j.geomorph.2010.02.019>

- Eusterhues K, Rumpel C, Kögel-Knabner I. 2005. Stabilization of soil organic matter isolated via oxidative degradation. *Org Geochem* 36:1567–1575. <https://doi.org/10.1016/j.orggeochem.2005.06.010>
- FAO (Food and Agriculture Organization of the United Nations). 2006. Guidelines for soil description. FAO, Rome
- Favilli F, Egli M, Brandová D, Ivy-Ochs S, Kubik PW, Maisch M, Cherubini P, Haeberli W. 2009. Combination of numerical dating techniques using ^{10}Be in rock boulders and ^{14}C of resilient soil organic matter for reconstructing the chronology of glacial and periglacial processes in a high Alpine catchment during the Late Pleistocene and Early Holocene. *Radiocarbon* 51:537–552. <https://doi.org/10.1017/S0033822200055910>
- Favilli F, Egli M, Cherubini P, Sartori G, Haeberli W, Delbos E. 2008. Comparison of different methods of obtaining a resilient organic matter fraction in Alpine soils. *Model Pedogenesis* 145:355–369. <https://doi.org/10.1016/j.geoderma.2008.04.002>
- Frielinghaus M, Vahrson W-G. 1998. Soil translocation by water erosion from agricultural cropland into wet depressions (morainic kettle holes). *Soil Tillage Res* 46:23–30. [https://doi.org/10.1016/S0167-1987\(98\)80104-9](https://doi.org/10.1016/S0167-1987(98)80104-9)
- Graly JA, Bierman PR, Reusser LJ, Pavich MJ. 2010. Meteoric ^{10}Be in soil profiles - a global meta-analysis. *Geochim Cosmochim Acta* 74:6814–6829. <https://doi.org/10.1016/j.gca.2010.08.036>
- Granger DE, Riebe CS. 2007. 5.19 - cosmogenic nuclides in weathering and erosion. In: Holland HD, Turekian KK (eds) *Treatise on Geochemistry*. Pergamon, Oxford, pp 1–43
- Granger DE, Riebe CS. 2014. 7.12 - cosmogenic nuclides in weathering and erosion. In: Holland HD, Turekian KK (eds) *Treatise on geochemistry (Second Edition)*, 2nd edn. Elsevier, Oxford, pp 401–436
- Heimsath AM. 2006. Eroding the land: steady-state and stochastic rates and processes through a cosmogenic lens. In: Alonso-Zarza AM, Tanner LH (eds) *In Situ-Produced Cosmogenic Nuclides and Quantification of Geological Processes*. Geol Soc Am pp 111-129
- Heimsath AM, Dietrich WE, Nishiizumi K, Finkel RC. 1997. The soil production function and landscape equilibrium. *Nature* 388:358–361. <https://doi.org/10.1038/41056>

- Helfrich M, Flessa H, Mikutta R, Dreves A, Ludwig B.* 2007. Comparison of chemical fractionation methods for isolating stable soil organic carbon pools. *Eur J Soil Sci* 58:1316–1329. <https://doi.org/10.1111/j.1365-2389.2007.00926.x>
- Hey B.* 1989. Elementflüsse und Elementbilanzen in Waldökosystemen der Bärhalde — Südschwarzwald. Freiburger Bodenkundliche Abhandlungen, Heft 23, Institut für Bodenkunde und Waldernährungslehre der Albert-Ludwigs-Universität, Freiburg, Germany
- Hidy AJ, Gosse JC, Pederson JL, Mattern JP, Finkel RC.* 2010. A geologically constrained Monte Carlo approach to modeling exposure ages from profiles of cosmogenic nuclides: an example from Lees Ferry Arizona. *Geochem Geophys Geosystems* 11 <https://doi.org/10.1029/2010GC003084>
- Hughes ALC, Gyllencreutz R, Lohne ØS, Mangerud J, Svendsen JI.* 2016. The last Eurasian ice sheets – a chronological database and time-slice reconstruction, DATED-1. *Boreas* 45:1–45. <https://doi.org/10.1111/bor.12142>
- IUSS Working Group WRB.* 2015. World Reference Base for Soil Resources 2014, update 2015 International soil classification system for naming soils and creating legends for soil maps. FAO, Rome
- Ivy-Ochs S, Kober F.* 2008. Surface exposure dating with cosmogenic nuclides. *EG Quat Sci J* 57:179–209. <https://doi.org/10.3285/eg.57.1-2.7>
- Jahns S.* 2000. Late-glacial and Holocene woodland dynamics and land-use history of the Lower Oder valley, north-eastern Germany, based on two, AMS 14C-dated, pollen profiles. *Veg Hist Archaeobotany* 9:111–123. <https://doi.org/10.1007/BF01300061>
- Jahns S.* 2001. On the Late Pleistocene and Holocene history of vegetation and human impact in the Ücker valley, north-eastern Germany. *Veg Hist Archaeobotany* 10:97–104. <https://doi.org/10.1007/PL00006924>
- Jenny H.* 1984. The soil resource. *Origin and Behavior Vegetatio* 57:102–102. <https://doi.org/10.1007/BF00047304>
- Jungers MC, Bierman PR, Matmon A, Nichols K, Larsen J, Finkel R.* 2009. Tracing hillslope sediment production and transport with in situ and meteoric ^{10}Be . *J Geophys Res Earth Surf* 114:F04020. <https://doi.org/10.1029/2008JF001086>

- Kappler C, Kaiser K, Tanski P, Klos F, Fülling A, Mrotzek A, Sommer M, Bens O. 2018. Stratigraphy and age of colluvial deposits indicating Late Holocene soil erosion in northeastern Germany. *CATENA* 170:224–245. <https://doi.org/10.1016/j.catena.2018.06.010>
- Keilen K, Stahr K, Goltz H, v. d. Zöttl HW. 1977. Zur pedochemie des berylliums — untersuchungen einer bodengesellschaft im gebiet des bärhaldegranits (südschwarzwald). *Geoderma* 17:315–329. [https://doi.org/10.1016/0016-7061\(77\)90092-1](https://doi.org/10.1016/0016-7061(77)90092-1)
- Kögel-Knabner I, Guggenberger G, Kleber M, Kandeler E, Kalbitz K, Scheu S, Eusterhues K, Leinweber P. 2008. Organo-mineral associations in temperate soils: Integrating biology, mineralogy, and organic matter chemistry. *J Plant Nutr Soil Sci* 171:61–82. <https://doi.org/10.1002/jpln.200700048>
- Kopp D, Schwanecke W. 1994. Standortlich-naturräumliche Grundlagen ökologiegerechter Forstwirtschaft. Dtsch Landwirtschaftsverlag Berl GmbH
- Koszinski S, Gerke HH, Hierold W, Sommer M. 2013. Geophysical based nodeling of a kettle hole catchment of the morainic soil landscape. *Vadose Zone J* 12:1–18. <https://doi.org/10.2136/vzj2013.02.0044>
- Kulczycka-Leciejewiczowa A, Wetzel G (2002) Neolithikum im Odergebiet, [w:] E. Gringmuth-Dallmer, L. Leciejewicz (Eds.), Forschungen zu Mensch und Umwelt im Odergebiet in frühgeschichtlicher Zeit. pp. 257–270
- Lal D. 2001. New nuclear methods for studies of soil dynamics utilizing cosmic ray produced radionuclides. In: Stott, D.E., Mohtar, R.H., Steinhardt, G.C.(Eds.) Sustaining the global farm. 10th International Soil Conservation Organization Meeting, Purdue University and USDA-ARS National Soil Erosion Research Laboratory. pp 1044–1052
- Lüthgens C, Böse M, Preusser F. 2011. Age of the Pomeranian ice-marginal position in northeastern Germany determined by Optically Stimulated Luminescence (OSL) dating of glaciofluvial sediments. *Boreas* 40:598–615. <https://doi.org/10.1111/j.1502-3885.2011.00211.x>
- Maejima Y, Matsuzaki H, Higashi T. 2005. Application of cosmogenic ¹⁰Be to dating soils on the raised coral reef terraces of Kikai Island, southwest Japan. *Geoderma* 126:389–399. <https://doi.org/10.1016/j.geoderma.2004.10.004>

- Masarik J, Beer J. 2009. An updated simulation of particle fluxes and cosmogenic nuclide production in the Earth's atmosphere. *J Geophys Res Atmospheres* 114:D11103. <https://doi.org/10.1029/2008JD010557>
- McKean JA, Dietrich WE, Finkel RC, Southon JR, Caffee MW. 1993. Quantification of soil production and downslope creep rates from cosmogenic ^{10}Be accumulations on a hillslope profile. *Geology* 21:343–346. [https://doi.org/10.1130/0091-7613\(1993\)021%3c0343:QOSPAD%3e2.3.CO;2](https://doi.org/10.1130/0091-7613(1993)021%3c0343:QOSPAD%3e2.3.CO;2)
- Minasny B, Finke P, Stockmann U, Vanwalleghem T, McBratney AB. 2015. Resolving the integral connection between pedogenesis and landscape evolution. *Earth-Sci Rev* 150:102–120. <https://doi.org/10.1016/J.EARSCIREV.2015.07.004>
- Minasny B, McBratney AB. 2006. A conditioned Latin hypercube method for sampling in the presence of ancillary information. *Comput Geosci* 32:1378–1388. <https://doi.org/10.1016/j.cageo.2005.12.009>
- Montgomery DR. 2007. Soil erosion and agricultural sustainability. *Proc Natl Acad Sci* 104:13268–13272. <https://doi.org/10.1073/pnas.0611508104>
- Norton KP, von Blanckenburg F, Kubik PW. 2010. Cosmogenic nuclide-derived rates of diffusive and episodic erosion in the glacially sculpted upper Rhone Valley, Swiss Alps. *Earth Surf Process Landf* 35:651–662. <https://doi.org/10.1002/esp.1961>
- Owens PN. 2020. Soil erosion and sediment dynamics in the Anthropocene: a review of human impacts during a rapid global environmental change. *J Soil Sediment* 20:4115–4143. <https://doi.org/10.1007/s11368-020-02815-9>
- Pavich MJ. 1989. Regolith residence time and the concept of surface age of the Piedmont “Peneplain.” *Geomorphology* 2:181–196. [https://doi.org/10.1016/0169-555X\(89\)90011-1](https://doi.org/10.1016/0169-555X(89)90011-1)
- Pavich MJ, Brown L, Klein J, Middleton R. 1984. ^{10}Be accumulation in a soil chronosequence. *Earth Planet Sci Lett* 68:198–204. [https://doi.org/10.1016/0012-821X\(84\)90151-1](https://doi.org/10.1016/0012-821X(84)90151-1)
- Preusser F, Degering D, Fuchs M, Hilgers A, Kadereit A, Klasen N, Krbetschek M, Richter D, Spencer JQG. 2008. Luminescence dating: basics, methods and applications. *EG Quat Sci J* 57:95–149. <https://doi.org/10.3285/eg.57.1-2.5>
- Reimer PJ, Austin WEN, Bard E, Bayliss A, Blackwell PG, Bronk Ramsey C, Butzin M, Cheng H, Edwards RL, Friedrich M, Grootes PM, Guilderson TP, Hajdas I, Heaton TJ, Hogg

- AG, Hughen KA, Kromer B, Manning SW, Muscheler R, Palmer JG, Pearson C, van der Plicht J, Reimer RW, Richards DA, Scott EM, Southon JR, Turney CSM, Wacker L, Adolphi F, Büntgen U, Capano M, Fahrni SM, Fogtmann-Schulz A, Friedrich R, K hler P, Kudsk S, Miyake F, Olsen J, Reinig F, Sakamoto M, Sookdeo A, Talamo S. 2020. The IntCal20 northern hemisphere radiocarbon age calibration curve (0–55 cal kBP). *Radiocarbon* 62:725–757. <https://doi.org/10.1017/RDC.2020.41>
- Rüffer O. 2018. Standortsspezifische Entwicklung von Buchenwaldgesellschaften im nordostdeutschen Tiefland, dargestellt am Beispiel des Melzower Buchennaturwaldes. Humboldt-Univ Berl Gemany
- Ryan JG. 2002. Trace-element systematics of beryllium in terrestrial materials. *Rev Mineral Geochem* 50:121–145. <https://doi.org/10.2138/rmg.2002.50.3>
- Šamonil P, Daněk P, Adam D, Phillips JD. 2017. Breakage or uprooting: how tree death type affects hillslope processes in old-growth temperate forests. *Geomorphology* 299:76–84. <https://doi.org/10.1016/j.geomorph.2017.09.023>
- Schaller M, Ehlers TA, Lang KAH, Schmid M, Fuentes-Espoz JP. 2018. Addressing the contribution of climate and vegetation cover on hillslope denudation, Chilean Coastal Cordillera (26 –38 S). *Earth Planet Sci Lett* 489:111–122. <https://doi.org/10.1016/j.epsl.2018.02.026>
- Schaller M, von Blanckenburg F, Hovius N, Kubik PW. 2001. Largescale erosion rates from in situ-produced cosmogenic nuclides in European river sediments. *Earth Planet Sci Lett* 188:441–458. [https://doi.org/10.1016/S0012-821X\(01\)00320-X](https://doi.org/10.1016/S0012-821X(01)00320-X)
- Schatz T. 1999. Untersuchungen zur holozänen Landschaftsentwicklung Nordost-Deutschlands. Doctoralthesis
- Schlichting E, Blume HP, Stahr K. 1995. Soils practical (in German). Blackwell, Berlin
- Schoonejans J, Vanacker V, Opfergelt S, Christl M. 2017. Long-term soil erosion derived from in-situ ¹⁰Be and inventories of meteoric ¹⁰Be in deeply weathered soils in southern Brazil. *Chem Geol* 466:380–388. <https://doi.org/10.1016/j.chemgeo.2017.06.025>
- Schulz M. 2009. Ur-und Frühgeschichte des Prenzlauer Raumes: von den Anfängen der menschlichen Besiedlung bis zu den Anfängen der Stadt im 13. Jahrhundert. In: Neitmann K, Schich W (eds) Geschichte der Stadt Prenzlau. Geiger-Verlag, Horb am Neckar, pp 15–26

- Siame L, Bellier O, Braucher R, S brier M, Cushing M, Bourl s D, Hamelin B, Baroux E, de Voogd B, Raisbeck G, Yiou F. 2004. Local erosion rates versus active tectonics: cosmic ray exposure modelling in Provence (south-east France). *Earth Planet Sci Lett* 220:345–364. [https://doi.org/10.1016/S0012-821X\(04\)00061-5](https://doi.org/10.1016/S0012-821X(04)00061-5)
- Sommer M, Gerke HH, Deumlich D. 2008. Modelling soil landscape genesis — A “time split” approach for hummocky agricultural landscapes. *Model Pedogenesis* 145:480–493. <https://doi.org/10.1016/j.geoderma.2008.01.012>
- Stroeven AP, H ttestrand C, Kleman J, Heyman J, Fabel D, Fredin O, Goodfellow BW, Harbor JM, Jansen JD, Olsen L, Caffee MW, Fink D, Lundqvist J, Rosqvist GC, Strömberg B, Jansson KN. 2016. Deglaciation of Fennoscandia. *Spec Issue PAST Gatew Palaeo-Arct Spat Temporal Gatew* 147:91–121. <https://doi.org/10.1016/j.quascirev.2015.09.016>
- Takahashi Y, Minai Y, Ambe S, Makide Y, Ambe F. 1999. Comparison of adsorption behavior of multiple inorganic ions on kaolinite and silica in the presence of humic acid using the multitracer technique. *Geochim Cosmochim Acta* 63:815–836. [https://doi.org/10.1016/S0016-7037\(99\)00065-4](https://doi.org/10.1016/S0016-7037(99)00065-4)
- Troeh FR, Hobbs JA, Donahue RL. 1981. Soil and water conservation for productivity and environmental protection. *Soil Sci* 132
- van der Meij WM, Reimann T, Vornehm VK, Temme AJAM, Wallinga J, van Beek R, Sommer M. 2019. Reconstructing rates and patterns of colluvial soil redistribution in agrarian (hummocky) landscapes. *Earth Surf Process Landf* 44:2408–2422. <https://doi.org/10.1002/esp.4671>
- van der Meij WM, Temme AJAM, Lin HS, Gerke HH, Sommer M. 2018. On the role of hydrologic processes in soil and landscape evolution modeling: concepts, complications and partial solutions. *Earth-Sci Rev* 185:1088–1106. <https://doi.org/10.1016/j.earscirev.2018.09.001>
- van der Meij WM, Temme AJAM, Wallinga J, Hierold W, Sommer M. 2017. Topography reconstruction of eroding landscapes – a case study from a hummocky ground moraine (CarboZALF-D). *Geomorphology* 295:758–772. <https://doi.org/10.1016/j.geomorph.2017.08.015>

- van Noordwijk M, Cerri C, Woomer PL, Nugroho K, Bernoux M. 1997. Soil carbon dynamics in the humid tropical forest zone. *Geoderma* 79:187–225. [https://doi.org/10.1016/S0016-7061\(97\)00042-6](https://doi.org/10.1016/S0016-7061(97)00042-6)
- Van Oost K, Quine TA, Govers G, De Gryze S, Six J, Harden JW, Ritchie JC, McCarty GW, Heckrath G, Kosmas C, Giraldez JV, da Silva JRM, Merckx R. 2007. The impact of agricultural soil erosion on the global carbon cycle. *Science* 318:626–629. <https://doi.org/10.1126/science.1145724>
- Van Oost K, Van Muysen W, Govers G, Deckers J, Quine TA. 2005. From water to tillage erosion dominated landform evolution. *Geomorphology* 72:193–203. <https://doi.org/10.1016/j.geomorph.2005.05.010>
- West N, Kirby E, Bierman P, Slingerland R, Ma L, Rood D, Brantley S. 2013. Regolith production and transport at the Susquehanna Shale Hills Critical Zone Observatory, part 2: insights from meteoric ^{10}Be . *J Geophys Res Earth Surf* 118:1877–1896. <https://doi.org/10.1002/jgrf.20121>
- Wilken F, Ketterer M, Koszinski S, Sommer M, Fiener P. 2020. Understanding the role of water and tillage erosion from $^{239+240}\text{Pu}$ tracer measurements using inverse modelling. *SOIL* 6:549–564. <https://doi.org/10.5194/soil-6-549-2020>
- Willenbring JK, von Blanckenburg F. 2010. Meteoric cosmogenic Beryllium-10 adsorbed to river sediment and soil: applications for Earth-surface dynamics. *Earth-Sci Rev* 98:105–122. <https://doi.org/10.1016/j.earscirev.2009.10.008>
- Wyshnytzky CE, Ouimet WB, McCarthy J, Dethier DP, Shroba RR, Bierman PR, Rood DH. 2015. Meteoric ^{10}Be , clay, and extractable iron depth profiles in the Colorado Front Range: implications for understanding soil mixing and erosion. *CATENA* 127:32–45. <https://doi.org/10.1016/j.catena.2014.12.008>
- Zollinger B, Alewell C, Kneisel C, Brandová D, Petrillo M, Plötze M, Christl M, Egli M. 2017. Soil formation and weathering in a permafrost environment of the Swiss Alps: a multi-parameter and non-steady-state approach. *Earth Surf Process Landf* 42:814–835. <https://doi.org/10.1002/esp.4040>

5. Discussion

5.1 Synthesis of main results

The following concluding chapter presents a synthesis of the most important results – already comprehensively discussed within the peer-reviewed papers and their corresponding chapters in this thesis (chapters 2.-4.) – discusses the specific constraints of the methods used and finally outlines potential future perspectives.

The major aim of this thesis was to unravel the co-evolution of weathering, soil profile development and lateral redistribution on a landscape level, specifically in a hummocky ground moraine landscape in Northern Germany. On a regional scale and with a multi-methodological approach (i.e., ^{10}Be , $^{239+240}\text{Pu}$, ^{14}C), the results obtained from the present study contribute to the general knowledge about the geomorphological processes, their timing (i.e., short- and long-term), and their origin (i.e., natural or anthropogenic).

The following results could be achieved:

- By the use of FRNs (i.e., $^{239+240}\text{Pu}$), it was observed and confirmed that short-term erosion rates due to tillage are one order of magnitude higher than long-term soil redistribution rates in an agricultural landscape calculated using ^{10}Be (Wilkinson and McElroy, 2007) (Chapter 2 – Research question 1.)
- Despite the influence of human activities (e.g., ploughing) on the ^{10}Be depth profile, both types of ^{10}Be , *meteoric* and *in situ*, are suitable soil tracers to measure the long-term soil redistribution rates and produce comparable results in agricultural settings – i.e., CarboZALF study site (Chapter 2 – Research question 2.).
- Short-term rates were extremely low/negligible in a natural landscape (i.e., Melzower Forst) and very high in an agricultural landscape. On the contrary, long-term soil redistribution rates in the forested landscape studied, i.e., over the entire period of soil formation, are comparable to those calculated in the nearby agricultural area investigated (Chapters 2-4 – Research question 3.)
- The $^{239+240}\text{Pu}$ distribution was quite heterogenous in the forested area analysed and there was no correlation with topographic features (e.g., slope) indicating no erosional events during the last 55 years. ^{14}C dating of the buried horizons shed light on the start of the carbon uptake and progressive pedogenesis, that started around 16 to 17 ka BP — a

date that follows the estimation of surface ages of the area (Hughes et al., 2016; Lüthgens et al., 2011; Stroeven et al., 2016). Regressive soil development phases happened between 4.5 and 6.8 ka BP, a time where the first settlements in the region were recorded (Jahns, 2000, 2001; Kappler et al., 2018; van der Meij et al., 2019; Schatz, 1999). This leads to the conclusion that the soil patterns observed are often due to human impact. Their activities started after the first settlements in the region, and, thus, earlier than previously postulated (Chapters 3-4 – Research question 4.)

- Finally, considering that soil redistribution rates determined with ^{10}Be , thus from the start of soil formation, are comparable in an agricultural and in a natural site in the same study area, it can be assumed that past natural soil mass redistribution processes still overshadow the present anthropogenic erosion processes (Chapters 2-4).

Table 5.1. Summary of research questions and main results.

Chapters (reference)	Research questions	Main results
2. (Calitri et al. 2019)	1. How do long-term and short-term rates of soil redistributing processes differ?	Short-term erosion rates are one order of magnitude higher than long-term rates in agricultural settings.
2. (Calitri et al. 2019)	2. Are rates calculated from in situ ¹⁰ Be comparable to those of using meteoric ¹⁰ Be?	Both meteoric and in situ ¹⁰ Be are suitable soil tracers to measure the long-term soil redistribution rates giving similar results
2. – 4. (Calitri et al. 2019, 2020, 2021)	3. How do soil redistribution rates (short- and long-term) in an agricultural and in a natural landscape compare to each other?	Short-term rates were extremely low/negligible in a natural landscape and very high in an agricultural landscape (i.e., 25 t ha ⁻¹ yr ⁻¹). On the contrary, long-term rates in the forested landscape are comparable to those calculated in the agricultural area investigated (i.e., -1.00 and -0.79 t ha ⁻¹ yr ⁻¹).
3. – 4. (Calitri et al. 2020, 2021)	4. Are the soil patterns observed in northern Germany purely a result of past events (natural and/or anthropogenic) or are they imbedded in ongoing processes?	Soil patterns observed in the forest might be due to human impact and activities started after the first settlements in the region, earlier than previously postulated, between 4.5 and 6.8 kyr BP, and not a result of recent soil erosion.

2. – 4. (Calitri et al. 2019, 2020, 2021)		Long-term soil redistribution rates are similar independently from the settings, meaning past natural soil mass redistribution processes still overshadow the present anthropogenic erosion processes.
---	--	--

Constrains of the study results

- The biggest constrain was due to the availability of suitable models to convert ^{10}Be (both meteoric and in situ) and $^{239+240}\text{Pu}$ into reasonable soil redistribution rates.
 - Not all models are able to detect accumulation but only erosion (Balco et al., 2008; Lal, 2001). For example, in the case of the approach of Lal (2001), to detect and calculate net accumulation, unrealistically high ^{10}Be values in the topsoil are needed.
 - Few models (e.g. profile distribution model (PDM), (Walling and Quine, 1990; Xinbao et al., 1990) were developed to estimate the activity of different nuclides (e.g. ^{137}Cs instead of $^{239+240}\text{Pu}$). Since every FRN or cosmogenic nuclide has a different behaviour and distribution along the soil profile, it might give a false representation of the processes in which it is involved, thus wrong erosion and accumulation rates.
 - Areas with a complex land use history with alternate regressive and progressive phases like CarboZALF-D and Melzower Forst, cannot be properly represented by most of the models using ^{10}Be .
- Major difficulties arose from the use of *in situ* ^{10}Be to quantify long-term soil redistribution rates compared to *meteoric* ^{10}Be and $^{239+240}\text{Pu}$.
 - Even though *in situ* ^{10}Be is extensively used in quantifying erosion or denudation rates, soil redistribution rates are still difficult to derive. It is laborious to derive sedimentation rates although burial might be apparent. Furthermore, if soil redistribution rates are calculated in a catchment they might also include mass wasting (Norton et al., 2010).

- Often the steady-state conditions to calculate denudation or soil production rates are not fulfilled and this leads to unrealistic representations (i.e., under- or overestimation) of the rates. Soils characterised by human impact like agriculture are quite far from equilibrium and being in a steady-state.
 - Some models (e.g. CRONUS (Balco et al., 2008) consider only surface samples, making them less suitable to soils in general and especially those soils affected by soil disturbance (e.g. bioturbation, ploughing). Furthermore, accumulation rates cannot be calculated from a single surface sample.
 - There was a very high variability of possible erosion rate trends (Hidy et al., 2010). This was due to the unusual distribution of ^{10}Be along the profile (especially in Melzower Forst) and the lack of more data points.
 - Depending on the type of parent material, there might have been a pre-exposure making soil redistribution rates modelling and estimation even more difficult and uncertain.
- Estimation of soil erosion rates using *meteoric* ^{10}Be is subjected to various parameters like annual deposition rate on Earth's surface (Masarik and Beer, 2009; Willenbring and von Blanckenburg, 2010). *Meteoritic* ^{10}Be fluxes are still a critical parameter to estimate (Chen et al., 2020; Derakhshan-Babaei et al., 2020) and soil erosion or denudation rates might contain errors depending on the environmental settings studied.
 - The patchy distribution of $^{239+240}\text{Pu}$ isotopes in the forest made the interpretation of the results difficult and ambiguous, giving space to different explanations and point of views but also scientifically constructive and lively discussions (i.e., with one of the reviewers of Chapter 3).
 - Albeit ^{14}C dated samples in Melzower Forst nicely fit with a possible land use change during the Neolithic (4776-2595 BC) causing a regressive phase in the soil formation, absolute archaeological proofs (e.g., charcoal particles, human artefacts) are missing.
 - Moreover, despite the good fit of the dated soil profiles of Melzower Forst ($^{14}\text{C}+^{10}\text{Be}$) into the bigger land-use history, there might be more periods/phases not yet identified in the analysed samples (e.g., peaks in settlements during the Bronze Age or the Migration Period (Jahns, 2000; Schultz, 2009)).

5.2 Outlook

The planned methodological combination of cosmogenic nuclides like ^{10}Be and ^{14}C , fallout radionuclides like $^{239+240}\text{Pu}$ and physio-chemical aspects to characterise erosion and chemical weathering, allowed to answer satisfactorily the initial research questions. Additionally, new questions arose from those that were answered and can indicate future challenges and research opportunities on the studied topic.

- Some blind spots in the land-use history of the region still exist. Additional dated samples of carbon and sediments throughout the colluvial soil profiles will increase the temporal resolution of the land use reconstruction and can shed light on different periods of landscape stability and instability.
- This study could make important contributions to the deciphering of the co-evolution of weathering, soil profile development and lateral redistribution in North-eastern Germany. However, this study only represents the chronology and land-use history for hummocky ground moraine landscapes of Uckermark's surroundings. The multi-methodological approach used can be challenged by the application in a wider range of landscapes and geographic regions.
- The lack of proper models to convert nuclides concentrations/activities in soil redistribution rates made parts of this study particularly challenging. Numerical process-based models may help in explaining the complexity of soil mass redistribution (e.g., Campforts et al. 2016).
- Investigating in more details the complex ^{10}Be distribution and behaviour in the soil would shed light on the processes behind them. In doing so, better models to convert concentrations/activities in soil redistribution rates can be developed and implemented in the future.
- One of the key winning elements in this study was its study site/area, i.e. the research station CarboZALF-D (Aldana Jague et al., 2016; Hoffmann et al., 2017; Koszinski et al., 2013; van der Meij et al., 2017; Rieckh et al., 2014; Sommer et al., 2016). The effects of anthropogenic activities on soil erosion and landscape patterns could be observed and studied in depth and compared to a natural and preserved landscape like Melzower Forst. Therefore, it is evident the need of such research stations and long-term experiments to expand this kind of research.

6. References

- Aldana Jague E, Sommer M, Saby NPA, Cornelis J-T, Van Wesemael B, Van Oost K.* 2016. High resolution characterization of the soil organic carbon depth profile in a soil landscape affected by erosion. *Soil and Tillage Research* 156:185–193. DOI: 10.1016/j.still.2015.05.014
- Alewell C, Egli M, Meusburger K.* 2015. An attempt to estimate tolerable soil erosion rates by matching soil formation with denudation in Alpine grasslands. *Journal of Soils and Sediments* 15:1383–1399. DOI: 10.1007/s11368-014-0920-6
- Alewell C, Meusburger K, Juretzko G, Mabit L, Ketterer ME.* 2014. Suitability of $^{239+240}\text{Pu}$ and ^{137}Cs as tracers for soil erosion assessment in mountain grasslands. *Chemosphere* 103:274–280. DOI: 10.1016/j.chemosphere.2013.12.016
- Alewell C, Pitois A, Meusburger K, Ketterer M, Mabit L.* 2017. $^{239+240}\text{Pu}$ from “contaminant” to soil erosion tracer: Where do we stand? *Earth-Science Reviews* 172:107–123. DOI: 10.1016/j.earscirev.2017.07.009
- Amundson R, Jenny H.* 1991. The place of humans in the state factor theory of ecosystems and their soils. *Soil Science* 151 [online] Available from: https://journals.lww.com/soilsci/Fulltext/1991/01000/THE_PLACE_OF_HUMANS_IN_THE_STATE_FACTOR_THEORY_OF.12.aspx
- Arata L, Alewell C, Frenkel E, A'Campo-Neuen A, Iurian A-R, Ketterer ME, Mabit L, Meusburger K.* 2016. Modelling Deposition and Erosion rates with RadioNuclides (MODERN) – Part 2: A comparison of different models to convert $^{239+240}\text{Pu}$ inventories into soil redistribution rates at unploughed sites. *Journal of Environmental Radioactivity* 162–163:97–106. DOI: 10.1016/j.jenvrad.2016.05.009
- Balco G, Stone JO, Lifton NA, Dunai TJ.* 2008. A complete and easily accessible means of calculating surface exposure ages or erosion rates from ^{10}Be and ^{26}Al measurements. *Prospects for the New Frontiers of earth and Environmental Sciences* 3:174–195. DOI: 10.1016/j.quageo.2007.12.001

- Beer J, McCracken K, von Steiger R.* 2012. Cosmogenic radionuclides. Theory and Applications in the terrestrial and space environments. Springer: Berlin; Heidelberg [online] Available from: <https://doi.org/10.1007/978-3-642-14651-0>
- Belpomme M.* 1980. For an application of the soil world charter. In Assessment of Erosion, De Boodt M and Gabriels D (eds). John Wiley & Sons: Chichester; 9–22.
- Berhe AA, Barnes RT, Six J, Marín-Spiotta E.* 2018. Role of Soil Erosion in Biogeochemical Cycling of Essential Elements: Carbon, Nitrogen, and Phosphorus. *Annual Review of Earth and Planetary Sciences* 46:521–548. DOI: 10.1146/annurev-earth-082517-010018
- Boardman J, Poesen J.* 2006. Soil Erosion in Europe: Major Processes, Causes and Consequences. In: Soil Erosion in Europe. John Wiley & Sons, Ltd; 477–487. [online] Available from: <https://onlinelibrary.wiley.com/doi/abs/10.1002/0470859202.ch36>
- Brantley SL.* 2008. Understanding Soil Time. *Science* 321:1454–1455. DOI: 10.1126/science.1161132
- Brevik EC, Hartemink AE.* 2010. Early soil knowledge and the birth and development of soil science. *CATENA* 83:23–33. DOI: <https://doi.org/10.1016/j.catena.2010.06.011>
- Campforts B, Vanacker V, Vanderborght J, Baken S, Smolders E, Govers G.* 2016. Simulating the mobility of meteoric ¹⁰Be in the landscape through a coupled soil-hillslope model (Be2D). *Earth and Planetary Science Letters* 439:143–157. DOI: 10.1016/j.epsl.2016.01.017
- Carré F, Caudeville J, Bonnard R, Bert V, Boucard P, Ramel M.* 2017. Soil Contamination and Human Health: A Major Challenge for Global Soil Security. In: Global Soil Security, Field DJ, Morgan CLS, and McBratney AB (eds). Springer International Publishing: Cham; 275–295. [online] Available from: https://doi.org/10.1007/978-3-319-43394-3_25
- Chen P, Yi P, Czymzik M, Aldahan A, Ljung K, Yu Z, Hou X, Zheng M, Chen X, Possnert G.* 2020. Relationship between precipitation and ¹⁰Be and impacts on soil dynamics. *CATENA* 195:104748. DOI: <https://doi.org/10.1016/j.catena.2020.104748>

- Chmeleff J, von Blanckenburg F, Kossert K, Jakob D. 2010. Determination of the ^{10}Be half-life by multicollector ICP-MS and liquid scintillation counting. *Nuclear Instruments and Methods in Physics Research Section B: Beam Interactions with Materials and Atoms* 268:192–199. DOI: 10.1016/j.nimb.2009.09.012
- Cohen JE. 2003. Human Population: The Next Half Century. *Science* 302:1172–1175. DOI: 10.1126/science.1088665
- Derakhshan-Babaei F, Nosrati K, Tikhomirov D, Christl M, Sadough H, Egli M. 2020. Relating the spatial variability of chemical weathering and erosion to geological and topographical zones. *Geomorphology* 363:107235. DOI: 10.1016/j.geomorph.2020.107235
- Dosseto A, Schaller M. 2016. The erosion response to Quaternary climate change quantified using uranium isotopes and in situ-produced cosmogenic nuclides. *Earth-Science Reviews* 155:60–81. DOI: 10.1016/j.earscirev.2016.01.015
- Egli M, Brandová D, Böhlert R, Favilli F, Kubik PW. 2010. ^{10}Be inventories in Alpine soils and their potential for dating land surfaces. *Geomorphology* 119:62–73. DOI: 10.1016/j.geomorph.2010.02.019
- Egli M, Poulénard J. 2016. Soils of Mountainous Landscapes. In *International Encyclopedia of Geography*. John Wiley & Sons, Ltd; 1–10. [online] Available from: <https://onlinelibrary.wiley.com/doi/abs/10.1002/9781118786352.wbieg0197>
- Ehrlich PR, Raven PH. 1964. Butterflies and plants: a study in coevolution. *Evolution* 18: 586-608. <https://doi.org/10.1111/j.1558-5646.1964.tb01674.x>
- Evrard O, Pointurier F, Onda Y, Chartin C, Hubert A, Lepage H, Pottin A-C, Lefèvre I, Philippe B, Laceby JP, Ayrault S. 2014. Novel Insights into Fukushima Nuclear Accident from Isotopic Evidence of Plutonium Spread along Coastal Rivers. *Environmental Science & Technology* 48:9334–9340. DOI: 10.1021/es501890n
- García-Ruiz JM, Beguería S, Nadal-Romero E, González-Hidalgo JC, Lana-Renault N, Sanjuán Y. 2015. A meta-analysis of soil erosion rates across the world. *Geomorphology* 239:160–173. DOI: 10.1016/j.geomorph.2015.03.008
- Godwin H. 1962. Half-life of Radiocarbon. *Nature* 195:984–984. DOI: 10.1038/195984a0

- Goudie AS, Viles HA. 2016. *Geomorphology in the Anthropocene*. Cambridge University Press: Cambridge [online] Available from: <https://www.cambridge.org/core/books/geomorphology-in-the-anthropocene/4BD86845B2D0A864A9BE666A27C30C33>
- Graham RC, Rossi AM, Hubbert RJ. 2010. Rock to regolith conversion: Producing hospitable substrates for terrestrial ecosystems. *GSA Today* 20:4–9. DOI: 10.1130/GSAT57A.1
- Graly JA, Bierman PR, Reusser LJ, Pavich MJ. 2010. Meteoric ¹⁰Be in soil profiles - A global meta-analysis. *Geochimica et Cosmochimica Acta* 74:6814–6829. DOI: 10.1016/j.gca.2010.08.036
- Graly JA, Reusser LJ, Bierman PR. 2011. Short and long-term delivery rates of meteoric ¹⁰Be to terrestrial soils. *Earth and Planetary Science Letters* 302:329–336. DOI: 10.1016/j.epsl.2010.12.020
- Hajdas I. 2008. Radiocarbon dating and its applications in Quaternary studies. *E&G – Quaternary Science Journal* 57(1-2):A.01 DOI: 10.23689/fidgeo-988 [online] Available from: <http://hdl.handle.net/11858/00-1735-0000-0001-B8BE-6>
- Hidy AJ, Gosse JC, Pederson JL, Mattern JP, Finkel RC. 2010. A geologically constrained Monte Carlo approach to modeling exposure ages from profiles of cosmogenic nuclides: An example from Lees Ferry, Arizona. *Geochemistry, Geophysics, Geosystems* 11:Q0AA10 DOI: 10.1029/2010GC003084 [online] Available from: <https://doi.org/10.1029/2010GC003084> (Accessed 19 February 2021)
- Hoffmann M, Jurisch N, Garcia Alba J, Albiac Borraz E, Schmidt M, Huth V, Rogasik H, Rieckh H, Verch G, Sommer M, and Augustin J. 2017. Detecting small-scale spatial heterogeneity and temporal dynamics of soil organic carbon (SOC) stocks: a comparison between automatic chamber-derived C budgets and repeated soil inventories. *Biogeosciences* 14:1003–1019. DOI: 10.5194/bg-14-1003-2017
- Hoo WT, Fifield LK, Tims SG, Fujioka T, Mueller N. 2011. Using fallout plutonium as a probe for erosion assessment. South Pacific Environmental Radioactivity Association: 2008 conference 102:937–942. DOI: 10.1016/j.jenvrad.2010.06.010

- Hooke RLeB. 2000. On the history of humans as geomorphic agents. *Geology* 28:843–846. DOI: 10.1130/0091-7613(2000)28<843:OTHOHA>2.0.CO;2
- Horiuchi K, Minoura K, Kobayashi K, Nakamura T, Hatori S, Matsuzaki H, Kawai T. 1999. Last-Glacial to Post-Glacial ¹⁰Be fluctuations in a sediment core from the Academician Ridge, Lake Baikal. *Geophysical Research Letters* 26:1047–1050. DOI: 10.1029/1999GL900163
- Huggett RJ. 1975. Soil landscape systems: A model of soil Genesis. *Geoderma* 13:1–22. DOI: 10.1016/0016-7061(75)90035-X
- Hughes ALC, Gyllencreutz R, Lohne ØS, Mangerud J, Svendsen JJ. 2016. The last Eurasian ice sheets – a chronological database and time-slice reconstruction, DATED-1. *Boreas* 45:1–45. DOI: 10.1111/bor.12142
- Hughes JD, Thirgood JV. 1982. Deforestation, Erosion, and Forest Management in Ancient Greece and Rome. *Journal of Forest History* 26:60–75. DOI: 10.2307/4004530
- IPBES. 2019. Summary for policymakers of the global assessment report on biodiversity and ecosystem services [online] Available from: <https://doi.org/10.5281/zenodo.3553579>
- Ivy-Ochs S, Kober F. 2008. Surface exposure dating with cosmogenic nuclides. *E&G – Quaternary Science Journal* 57:179–209. DOI: 10.23689/fidgeo-1280
- Jahns S. 2000. Late-glacial and Holocene woodland dynamics and land-use history of the Lower Oder valley, north-eastern Germany, based on two, AMS ¹⁴C-dated, pollen profiles. *Vegetation History and Archaeobotany* 9:111–123. DOI: 10.1007/BF01300061
- Jahns S. 2001. On the Late Pleistocene and Holocene history of vegetation and human impact in the Ücker valley, north-eastern Germany. *Vegetation History and Archaeobotany* 10:97–104. DOI: 10.1007/PL00006924
- Jenny H. 1941. Factors of soil formation: a system of quantitative pedology. McGraw-Hill: New York
- Johnson DL. 2002. Darwin would be proud: Bioturbation, dynamic denudation, and the power of theory in science. *Geoarchaeology*. 17:7-40. <https://doi.org/10.1002/gea.10001>

- Johnson DL, Watson-Stegner D. 1987. Evolution model of pedogenesis. *Soil Science* 143:349-366 [online] Available from: https://journals.lww.com/soilsci/Fulltext/1987/05000/EVOLUTION_MODEL_OF_PEDOGENESIS.5.aspx
- Kappler C, Kaiser K, Tanski P, Klos F, Fülling A, Mrotzek A, Sommer M, Bens O. 2018. Stratigraphy and age of colluvial deposits indicating Late Holocene soil erosion in northeastern Germany. *CATENA* 170:224–245. DOI: 10.1016/j.catena.2018.06.010
- Karlen DL, Mausbach MJ, Doran JW, Cline RG, Harris RF, Schuman GE. 1997. Soil Quality: A Concept, Definition, and Framework for Evaluation (A Guest Editorial). *Soil Science Society of America Journal* 61:4–10. DOI: 10.2136/sssaj1997.03615995006100010001x
- Kaste JM, Baskaran M. 2012. Meteoric ⁷Be and ¹⁰Be as Process Tracers in the Environment. In *Handbook of Environmental Isotope Geochemistry: Vol I*, Baskaran M (ed). Springer Berlin Heidelberg: Berlin, Heidelberg; 61–85. [online] Available from: https://doi.org/10.1007/978-3-642-10637-8_5
- Kaste JM, Norton SA, Hess CT. 2002. Environmental Chemistry of Beryllium-7. *Reviews in Mineralogy and Geochemistry* 50:271–289. DOI: 10.2138/rmg.2002.50.6
- Ketterer ME, Hafer KM, Link CL, Kolwaite D, Wilson J, Mietelski JW. 2004. Resolving global versus local/regional Pu sources in the environment using sector ICP-MS. *Journal of Analytical Atomic Spectrometry* 19:241–245. DOI: 10.1039/B302903D
- Kohl CP, Nishiizumi K. 1992. Chemical isolation of quartz for measurement of in-situ - produced cosmogenic nuclides. *Geochimica et Cosmochimica Acta* 56:3583–3587. DOI: 10.1016/0016-7037(92)90401-4
- Korschinek G, Bergmaier A, Faestermann T, Gerstmann UC, Knie K, Rugel G, Wallner A, Dillmann I, Dollinger G, Lierse von Gostomski Ch, Kossert K, Maiti M, Poutivtsev M, Remmert A. 2010. A new value for the half-life of ¹⁰Be by Heavy-Ion Elastic Recoil Detection and liquid scintillation counting. *Nuclear Instruments and Methods in Physics Research Section B: Beam Interactions with Materials and Atoms* 268:187–191. DOI: 10.1016/j.nimb.2009.09.020

- Koszinski S, Gerke HH, Hierold W, Sommer M.* 2013. Geophysical-Based Modeling of a Kettle Hole Catchment of the Morainic Soil Landscape. *Vadose Zone Journal* 12:1–18. DOI: 10.2136/vzj2013.02.0044
- Lal D.* 2001. New Nuclear Methods for Studies of Soil Dynamics Utilizing Cosmic Ray Produced Radionuclides. In: Stott, D.E., Mohtar, R.H., Steinhardt, G.C.(Eds.) Sustaining the Global Farm. 10th International Soil Conservation Organization Meeting, Purdue University and USDA-ARS National Soil Erosion Research Laboratory. 1044–1052.
- Lal D, Peters B.* 1967. Cosmic Ray Produced Radioactivity on the Earth. In: Kosmische Strahlung II / Cosmic Rays II, Sitte K (ed). Springer Berlin Heidelberg: Berlin, Heidelberg; 551–612. DOI: 10.1007/978-3-642-46079-1_7
- Lal R, Stewart BA.* 1990. Advances in Soil Science. Soil Degradation Volume 11. Springer: New York, NY; XVII, 345. DOI: 10.1007/978-1-4612-3322-0
- Lal R, Tims SG, Fifield LK, Wasson RJ, Howe D.* 2013. Applicability of ²³⁹Pu as a tracer for soil erosion in the wet-dry tropics of northern Australia. Proceedings of the Twelfth International Conference on Accelerator Mass Spectrometry, Wellington, New Zealand, 20-25 March 2011 294:577–583. DOI: 10.1016/j.nimb.2012.07.041
- Libby WF, Anderson EC, Arnold JR.* 1949. Age Determination by Radiocarbon Content: World-Wide Assay of Natural Radiocarbon. *Science* 109:227–228. DOI: 10.1126/science.109.2827.227
- Lüthgens C, Böse M, Preusser F.* 2011. Age of the Pomeranian ice-marginal position in northeastern Germany determined by Optically Stimulated Luminescence (OSL) dating of glaciofluvial sediments. *Boreas* 40:598–615. DOI: 10.1111/j.1502-3885.2011.00211.x
- Maejima Y, Matsuzaki H, Higashi T.* 2005. Application of cosmogenic ¹⁰Be to dating soils on the raised coral reef terraces of Kikai Island, southwest Japan. *Geoderma* 126:389–399. DOI: 10.1016/j.geoderma.2004.10.004
- Maetens W, Poesen J, Vanmaercke M.* 2012. How effective are soil conservation techniques in reducing plot runoff and soil loss in Europe and the Mediterranean? *Earth-Science Reviews* 115:21–36. DOI: 10.1016/j.earscirev.2012.08.003

- Masarik J. 2009. Chapter 1 Origin and Distribution of Radionuclides in the Continental Environment. In *Radioactivity in the Environment*, Froehlich K (ed). Elsevier; 1–25. [online] Available from: <https://www.sciencedirect.com/science/article/pii/S1569486009016015>
- Masarik J, Beer J. 2009. An updated simulation of particle fluxes and cosmogenic nuclide production in the Earth's atmosphere. *Journal of Geophysical Research: Atmospheres* 114:D11103. DOI: 10.1029/2008JD010557
- Masson-Delmotte V, Pörtner H-O, Skea J, Zhai P, Roberts D, Shukla PR, Buendía EC. 2019. Climate change and land: an IPCC special report on climate change, desertification, land degradation, sustainable land management, food security, and greenhouse gas fluxes in terrestrial ecosystems:ix, 896 pp.
- Matisoff G, Ketterer ME, Rosén K, Mietelski JW, Vitko LF, Persson H, Lokas E. 2011. Downward migration of Chernobyl-derived radionuclides in soils in Poland and Sweden. *Applied Geochemistry* 26:105–115. DOI: 10.1016/j.apgeochem.2010.11.007
- McHargue LR, Damon PE. 1991. The global beryllium 10 cycle. *Reviews of Geophysics* 29:141–158. DOI: 10.1029/91RG00072
- van der Meij WM, Reimann T, Vornehm VK, Temme AJAM, Wallinga J, van Beek R, Sommer M. 2019. Reconstructing rates and patterns of colluvial soil redistribution in agrarian (hummocky) landscapes. *Earth Surface Processes and Landforms* 44:2408–2422. DOI: 10.1002/esp.4671
- van der Meij WM, Temme AJAM, Wallinga J, Hierold W, Sommer M. 2017. Topography reconstruction of eroding landscapes – A case study from a hummocky ground moraine (CarboZALF-D). *Geomorphology* 295:758–772. DOI: 10.1016/j.geomorph.2017.08.015
- Meusburger K, Mabit L, Ketterer M, Park J-H, Sandor T, Porto P, Alewell C. 2016. A multi-radionuclide approach to evaluate the suitability of $^{239+240}\text{Pu}$ as soil erosion tracer. *Science of The Total Environment* 566–567:1489–1499. DOI: 10.1016/j.scitotenv.2016.06.035

- Meusburger K, Porto P, Mabit L, La Spada C, Arata L, Alewell C. 2018. Excess Lead-210 and Plutonium-239+240: Two suitable radiogenic soil erosion tracers for mountain grassland sites. *Environmental Research* 160:195–202. DOI: 10.1016/j.envres.2017.09.020
- Monaghan MC, Krishnaswami S, Turekian KK. 1986. The global-average production rate of ^{10}Be . *Earth and Planetary Science Letters* 76:279–287. DOI: 10.1016/0012-821X(86)90079-8
- Montanarella L, Pennock DJ, McKenzie N, Badraoui M, Chude V, Baptista I, Mamo T, Yemefack M, Singh Aulakh M, Yagi K, Young Hong S, Vijarnsorn P, Zhang G-L, Arrouays D, Black H, Krasilnikov P, Sobocká J, Alegre J, Henriquez CR, de Lourdes Mendonça-Santos M, Taboada M, Espinosa-Victoria D, AlShankiti A, AlaviPanah SK, Elsheikh EAEM, Hempel J, Camps Arbestain M, Nachtergaele F, and Vargas R. 2016. World's soils are under threat. *SOIL* 2:79–82. DOI: 10.5194/soil-2-79-2016
- Montgomery DR. 2007. Soil erosion and agricultural sustainability. *Proceedings of the National Academy of Sciences* 104:13268–13272. DOI: 10.1073/pnas.0611508104
- Norton KP, von Blanckenburg F, Kubik PW. 2010. Cosmogenic nuclide-derived rates of diffusive and episodic erosion in the glacially sculpted upper Rhone Valley, Swiss Alps. *Earth Surface Processes and Landforms* 35:651–662. DOI: 10.1002/esp.1961
- O'Farrell CR, Heimsath AM, Kaste JM. 2007. Quantifying hillslope erosion rates and processes for a coastal California landscape over varying timescales. *Earth Surface Processes and Landforms* 32:544–560. DOI: 10.1002/esp.1407
- Phillips JD. 2010. The convenient fiction of steady-state soil thickness. *Geoderma* 156:389–398. DOI: 10.1016/j.geoderma.2010.03.008
- Phillips JD. 2015. The robustness of chronosequences. *Complexity of Soils and Hydrology in Ecosystems* 298:16–23. DOI: 10.1016/j.ecolmodel.2013.12.018
- Phillips JD, Lorz C. 2008. Origins and implications of soil layering. *Earth-Science Reviews* 89:144–155. DOI: 10.1016/j.earscirev.2008.04.003

- Pimentel D (ed).* 1993. *World Soil Erosion and Conservation*. Cambridge University Press: Cambridge [online] Available from: <https://www.cambridge.org/core/books/world-soil-erosion-and-conservation/3836E152D3FB4D90723733B43073B01D>
- Pimentel D, Harvey C, Resosudarmo P, Sinclair K, Kurz D, McNair M, Crist S, Shpritz L, Fitton L, Saffouri R, Blair R.* 1995. Environmental and Economic Costs of Soil Erosion and Conservation Benefits. *Science* 267:1117. DOI: 10.1126/science.267.5201.1117
- Pimentel D.* 2001. The limitations of biomass energy. In *Encyclopedia of Physical Science and Technology*. Academic Press: San Diego, CA; 159–171.
- Pimentel D.* 2006. Soil Erosion: A Food and Environmental Threat. *Environment, Development and Sustainability* 8:119–137. DOI: 10.1007/s10668-005-1262-8
- Pimentel D, Kounang N.* 1998. Ecology of Soil Erosion in Ecosystems. *Ecosystems* 1:416–426. DOI: 10.1007/s100219900035
- Poesen J.* 2018. Soil erosion in the Anthropocene: Research needs. *Earth Surface Processes and Landforms* 43:64–84. DOI: <https://doi.org/10.1002/esp.4250>
- Richter D, Bacon A, Brecheisen Z, Mobley ML.* 2015. Soil in the Anthropocene. IOP Conference Series: Earth and Environmental Science 25:012010. DOI: 10.1088/1755-1315/25/1/012010
- Richter DD, Markewitz D.* 2001. *Understanding soil change: soil sustainability over millennia, centuries, and decades*. University Press, Cambridge
- Rieckh H, Gerke HH, Siemens J, Sommer M.* 2014. Water and Dissolved Carbon Fluxes in an Eroding Soil Landscape Depending on Terrain Position. *Vadose Zone Journal* 13:vzj2013.10.0173. DOI: 10.2136/vzj2013.10.0173
- Rüffer O.* 2018. *Standortspezifische Entwicklung von Buchenwaldgesellschaften im nordostdeutschen Tiefland, dargestellt am Beispiel des Melzower Buchennaturwaldes*. Humboldt-University of Berlin, Germany
- Schaetzl RJ, Thompson ML.* 2015. *Soils*. University Press, Cambridge

- Schatz T. 1999. Untersuchungen zur holozänen Landschaftsentwicklung Nordost-Deutschlands, doctoralthesis
- Schimmack W, Auerswald K, Bunzl K. 2001. Can $^{239+240}\text{Pu}$ replace ^{137}Cs as an erosion tracer in agricultural landscapes contaminated with Chernobyl fallout? *Journal of Environmental Radioactivity* 53:41–57. DOI: 10.1016/S0265-931X(00)00117-X
- Schlichting E, Blume HP, Stahr K. 1995. Soils Practical (in German). Blackwell: Berlin
- Schoonejans J, Vanacker V, Opfergelt S, Christl M. 2017. Long-term soil erosion derived from in-situ ^{10}Be and inventories of meteoric ^{10}Be in deeply weathered soils in southern Brazil. *Chemical Geology* 466:380–388. DOI: 10.1016/j.chemgeo.2017.06.025
- Schultz M. 2009. Ur-und Frühgeschichte des Prenzlauer Raumes: von den Anfängen der menschlichen Besiedlung bis zu den Anfängen der Stadt im 13. Jahrhundert. In Geschichte der Stadt Prenzlau, Neitmann K and Schich W (eds). Geiger-Verlag: Horb am Neckar; 15–26.
- Siame L, Bellier O, Braucher R, Sébrier M, Cushing M, Bourlès D, Hamelin B, Baroux E, de Voogd B, Raisbeck G, Yiou F. 2004. Local erosion rates versus active tectonics: cosmic ray exposure modelling in Provence (south-east France). *Earth and Planetary Science Letters* 220:345–364. DOI: 10.1016/S0012-821X(04)00061-5
- Soil Science Society of America. 2008. Alphabetical Listing of soil terms, A–Z. Soil Science Society of America: Madison, WI
- Sommer M, Augustin J, Kleber M. 2016. Feedbacks of soil erosion on SOC patterns and carbon dynamics in agricultural landscapes—The CarboZALF experiment. *Soil and Tillage Research* 156:182–184. DOI: 10.1016/j.still.2015.09.015
- Sommer M, Gerke HH, Deumlich D. 2008. Modelling soil landscape genesis — A “time split” approach for hummocky agricultural landscapes. *Modelling Pedogenesis* 145:480–493. DOI: 10.1016/j.geoderma.2008.01.012
- Sommer M, Schlichting E. 1997. Archetypes of catenas in respect to matter — a concept for structuring and grouping catenas. *Geoderma* 76:1–33. DOI: 10.1016/S0016-7061(96)00095-X

Stephens L, Fuller D, Boivin N, Rick T, Gauthier N, Kay A, Marwick B, Armstrong CG, Barton CM, Denham T, Douglass K, Driver J, Janz L, Roberts P, Rogers JD, Thakar H, Altaweel M, Johnson AL, Sampietro Vattuone MM, Aldenderfer M, Archila S, Artioli G, Bale MT, Beach T, Borrell F, Braje T, Buckland PI, Jiménez Cano NG, Capriles JM, Diez Castillo A, Çilingiroğlu Ç, Negus Cleary M, Conolly J, Coutros PR, Covey RA, Cremaschi M, Crowther A, Der L, di Lernia S, Doershuk JF, Doolittle WE, Edwards KJ, Erlandson JM, Evans D, Fairbairn A, Faulkner P, Feinman G, Fernandes R, Fitzpatrick SM, Fyfe R, Garcea E, Goldstein S, Goodman RC, Dalpoim Guedes J, Herrmann J, Hiscock P, Hommel P, Horsburgh KA, Hritz C, Ives JW, Junno A, Kahn JG, Kaufman B, Kearns C, Kidder TR, Lanoë F, Lawrence D, Lee GA, Levin MJ, Lindsoug HB, López-Sáez JA, Macrae S, Marchant R, Marston JM, McClure S, McCoy MD, Miller AV, Morrison M, Motuzaitė Matuzevičiūtė G, Müller J, Nayak A, Noerwidi S, Peres TM, Peterson CE, Proctor L, Randall AR, Renette S, Robbins Schug G, Ryzewski K, Saini R, Scheinsohn V, Schmidt P, Sebillaud P, Seitsonen O, Simpson IA, Soltysiak A, Speakman RJ, Spengler RN, Steffen ML, Storzum MJ, Strickland KM, Thompson J, Thurston TL, Ulm S, Ustunkaya MC, Welker MH, West C, Williams PR, Wright DK, Wright N, Zahir M, Zerboni A, Beaudoin E, Munevar Garcia S, Powell J, Thornton A, Kaplan JO, Gaillard MJ, Klein Goldewijk K, Ellis E. 2019. Archaeological assessment reveals Earth's early transformation through land use. *Science* 365:897–902. DOI: 10.1126/science.aax1192

Stockmann U, Minasny B, McBratney AB. 2014. How fast does soil grow? *Geoderma* 216:48–61. DOI: 10.1016/j.geoderma.2013.10.007

Stroeven AP, Hätttestrand C, Kleman J, Heyman J, Fabel D, Fredin O, Goodfellow BW, Harbor JM, Jansen JD, Olsen L, Caffee MW, Fink D, Lundqvist J, Rosqvist GC, Strömberg B, Jansson KN. 2016. Deglaciation of Fennoscandia. *Special Issue: PAST Gateways (Palaeo-Arctic Spatial and Temporal Gateways)* 147:91–121. DOI: 10.1016/j.quascirev.2015.09.016

Tan ZX, Lal R, Wiebe KD. 2005. Global Soil Nutrient Depletion and Yield Reduction. *Journal of Sustainable Agriculture* 26:123–146. DOI: 10.1300/J064v26n01_10

Targulian VO, Krasilnikov PV. 2007. Soil system and pedogenic processes: Self-organization, time scales, and environmental significance. *Rates and Time Scales of Pedogenic*

- Processes in Natural and Man-Affected Soil Systems* 71:373–381. DOI: 10.1016/j.catena.2007.03.007
- Tarolli P, Sofia G. 2016. Human topographic signatures and derived geomorphic processes across landscapes. *Geomorphology* 255:140–161. DOI: 10.1016/j.geomorph.2015.12.007
- Troeh FR, Hobbs JA, Donahue RL. 1981. Soil and Water Conservation for Productivity and Environmental Protection. *Soil Science* 132:189 [online] Available from: https://journals.lww.com/soilsci/Fulltext/1981/08000/Soil_and_Water_Conservation_for_Productivity_and.12.aspx
- United Nations News. 2017. Much of the planet's land severely degraded owing to increased consumption, UN warns. [online] Available from: <https://news.un.org/en/story/2017/09/564752-much-planets-land-severely-degraded-owing-increased-consumption-un-warns>
- Van Der Wal R, Truscott A-M, Pearce ISK, Cole L, Harris MP, Wanless S. 2008. Multiple anthropogenic changes cause biodiversity loss through plant invasion. *Global Change Biology* 14:1428–1436. DOI: 10.1111/j.1365-2486.2008.01576.x
- Van Oost K, Van Muysen W, Govers G, Deckers J, Quine TA. 2005. From water to tillage erosion dominated landform evolution. *Geomorphology* 72:193–203. DOI: 10.1016/j.geomorph.2005.05.010
- Vanacker V, Bellin N, Molina A, Kubik PW. 2014. Erosion regulation as a function of human disturbances to vegetation cover: a conceptual model. *Landscape Ecology* 29:293–309. DOI: 10.1007/s10980-013-9956-z
- Vanmaercke M, Poesen J, Govers G, Verstraeten G. 2015. Quantifying human impacts on catchment sediment yield: A continental approach. *Global and Planetary Change* 130:22–36. DOI: 10.1016/j.gloplacha.2015.04.001
- Vanwallegem T, Gómez JA, Infante Amate J, González de Molina M, Vanderlinden K, Guzmán G, Laguna A, Giráldez JV. 2017. Impact of historical land use and soil management change on soil erosion and agricultural sustainability during the

- Anthropocene. *Anthropocene* 17:13–29. DOI: 10.1016/j.ancene.2017.01.002 [online]
Available from: <https://www.sciencedirect.com/science/article/pii/S2213305417300012>
- Walling DE, Quine TA. 1990. Calibration of caesium-137 measurements to provide quantitative erosion rate data. *Land Degradation & Development* 2:161–175. DOI: 10.1002/ldr.3400020302
- Wang Z, Van Oost K. 2019. Modeling global anthropogenic erosion in the Holocene. *The Holocene* 29:367–379. DOI: 10.1177/0959683618816499
- Wilken F, Ketterer M, Koszinski S, Sommer M, Fiener P. 2020. Understanding the role of water and tillage erosion from ²³⁹⁺²⁴⁰Pu tracer measurements using inverse modelling. *SOIL* 6:549–564. DOI: 10.5194/soil-6-549-2020
- Wilkinson BH. 2005. Humans as geologic agents: A deep-time perspective. *Geology* 33:161–164. DOI: 10.1130/G21108.1
- Wilkinson BH, McElroy BJ. 2007. The impact of humans on continental erosion and sedimentation. *GSA Bulletin* 119:140–156. DOI: 10.1130/B25899.1
- Willenbring JK, von Blanckenburg F. 2010. Meteoric cosmogenic Beryllium-10 adsorbed to river sediment and soil: Applications for Earth-surface dynamics. *Earth-Science Reviews* 98:105–122. DOI: <https://doi.org/10.1016/j.earscirev.2009.10.008>
- Willgoose G. 2018. Principles of Soilscape and Landscape Evolution. University Press, Cambridge
- World Commission on Environment and Development. 1987. Our Common Future . University Press, Oxford, UK
- Xinbao Z, Higgitt DL, Walling DE. 1990. A preliminary assessment of the potential for using caesium-137 to estimate rates of soil erosion in the Loess Plateau of China. *Hydrological Sciences Journal* 35:243–252. DOI: 10.1080/02626669009492427
- Xu C, Athon M, Ho Y-F, Chang H-S, Zhang S, Kaplan DI, Schwehr KA, DiDonato N, Hatcher PG, Santschi PH. 2014. Plutonium Immobilization and Remobilization by Soil Mineral and Organic Matter in the Far-Field of the Savannah River Site, U.S. *Environmental Science & Technology* 48:3186–3195. DOI: 10.1021/es404951y

Zapata F. 2003. Handbook for the Assessment of Soil Erosion and Sedimentation Using Environmental Radionuclides. 1st ed. Springer: Dordrecht [online] Available from: <http://dx.doi.org/10.1007/0-306-48054-9>

Zollinger B, Alewell C, Kneisel C, Meusburger K, Brandová D, Kubik P, Schaller M, Ketterer M, Egli M. 2015. The effect of permafrost on time-split soil erosion using radionuclides (^{137}Cs , $^{239} + ^{240}\text{Pu}$, meteoric ^{10}Be) and stable isotopes ($\delta^{13}\text{C}$) in the eastern Swiss Alps. *Journal of Soils and Sediments* 15:1400-1419 DOI: 10.1007/s11368-014-0881-9

Zupanc V, Mabit L. 2010. Nuclear techniques support to assess erosion and sedimentation processes: preliminary results of the use of ^{137}Cs as soil tracer in Slovenia. *Dela* 33:21–36. DOI: 10.4312/dela.33.21-36

Appendix

Supplementary material

The following Table S1 includes background data of manuscripts III

Supplementary Table S1. Meteoric and in situ ^{10}Be contents of the soil at the “Melzower Forst” and the CarboZALF site.

Location	Profile	Depth	Meteoric ^{10}Be		In situ ^{10}Be	
			^{10}Be atoms per g (1E+8)	error (^{10}Be atoms per g (1E+8))	^{10}Be atoms per g (1E+5)	error (^{10}Be atoms per g (1E+5))
Melzower	Hydro 1	0-15	0.566	0.022	0.651	0.049
Forst		15-30	0.815	0.026	0.718	0.049
		30-45	0.325	0.016	0.572	0.041
	Hydro 3	0-15	0.359	0.004	0.763	0.048
		15-30	0.430	0.006	0.788	0.053
		30-45	0.859	0.019	0.910	0.057
		45-60	1.048	0.026	0.865	0.056
		75-90	1.920	0.053	0.792	0.050
		105-120	1.290	0.033	0.647	0.051
		120-135	1.028	0.026	0.578	0.042
		135-158	0.872	0.020	0.512	0.040
		165-185	0.304	0.002	0.609	0.042
	185-200	0.257	0.000	0.469	0.037	
	Hydro4	0-10	0.317	0.013	0.728	0.047
		10-20	0.288	0.011	0.747	0.045
		20-30	0.357	0.013	0.722	0.044
		30-40	0.510	0.019	0.772	0.052

		40-50	0.796	0.026	0.810	0.062
		50-60	0.869	0.028	0.737	0.047
		60-70	1.022	0.036	0.753	0.045
		90-100	1.109	0.036	0.853	0.052
		120-130	1.264	0.041	0.776	0.050
		140-150	1.378	0.059	0.720	0.055
		160-175	1.833	0.059	0.778	0.056
CarboZALF	LP4	0-30	0.910	0.015	0.992	0.057
		30-45	1.279	0.028	1.326	0.059
		45-60	1.585	0.029	1.582	0.081
		60-95	1.134	0.020	1.065	0.053
		95-165	0.696	0.012	0.743	0.055
		165-180	0.147	0.000	0.599	0.092
	LP12	0-30	0.775	0.012	0.805	0.050
		30-50	0.891	0.015	0.733	0.034
		50-60	0.398	0.007	0.633	0.034
		60-120	0.195	0.001	0.581	0.031
		120-160	0.157	0.000	0.605	0.042
	Vamos	0-30	0.872	0.011	0.984	0.050
		30-70	1.284	0.019	1.254	0.065
		70-88	1.383	0.021	1.073	0.063
		88-105	0.757	0.009	1.005	0.067
		105-147	0.556	0.005	0.978	0.051
		147-170	0.320	0.000	0.665	0.069

Acknowledgement

This PhD taught me that life never goes as planned. And in the space between our plans and reality, Grace creeps in.

All things work together for the good, my good. Philosopher Karl Popper wrote “Alles Leben ist Problemlösen” (all life is problem solving). Hardships and failures mostly perceived as ‘problems’ became ordinary business during these years. So instead of writing a long list of ‘Thank-yous’ I would like to share Abraham Lincoln’s letter to his son’s teacher. Some say it is a fake, some say it is authentic. I think it does not matter. What matters, it is the great lesson we can all learn from the words of a father’s heart.

“My son starts school today. It is all going to be strange and new to him for a while and I wish you would treat him gently. It is an adventure that might take him across continents. All adventures will probably include wars, tragedy and sorrow. To live this life will require faith, love and courage.

So dear Teacher, will you please take him by his hand and teach him things he will have to know, teaching him - but gently, if you can. Teach him that for every enemy, there is a friend. He will have to know that all men are not just, that all men are not true. But teach him also that for every scoundrel there is a hero, that for every crooked politician, there is a dedicated leader.

Teach him if you can that 10 cents earned is of far more value than a dollar found. In school, Teacher, it is far more honourable to fail than to cheat. Teach him to learn how to gracefully lose and enjoy winning when he does win. Teach him to be gentle with gentle people, tough with tough people. Steer him away from envy if you can and teach him the secret of quiet laughter.

Let him learn early that bullies are the easiest to tick. Teach him if you can, how to laugh when he is sad. Teach him there is no shame in tears. Teach him there can be glory in failure and despair in success. Teach him to scoff at cynics and to beware of too much sweetness. Teach him if you can the wonders of books, but also give him time to ponder the extreme mystery of birds in the sky, bees in the sun and flowers on a green hill. Teach him to have faith in his own ideas, even if everyone tells him they are wrong.

Try to give my son the strength not to follow the crowd when everyone else is getting on the bandwagon. Teach him to listen to everyone, but teach him also to filter all that he hears on a screen of truth and take only the good that comes through. Teach him to sell his talents and brains to the highest bidder but never to put a price tag on his heart and soul. Teach him to close his ears to howling mob, and to stand and fight if he thinks he is right.

Treat him gently, but do not coddle him, because only the test of fire makes fine steel. Let him have the courage to be impatient, let him have the patience to be brave. Teach him to have sublime faith in himself, because then he will always have sublime faith in mankind, in God.

This is a big order, Teacher, but see what best you can do. He is such a nice little boy and he is my son.”

Curriculum vitae

Francesca Calitri was born on the 14th of June 1991 in Foggia (Puglia, Italy). She started studying Agricultural Sciences at University of Foggia in 2010. In 2013, she finished a Bachelor of Science degree and started a Master of Science. She completed her Master's Thesis at ETH Zürich in December '15 at the Institute of Agricultural Sciences in Sustainable Agroecosystems – Biogeochemical modelling. She started her PhD at ZALF (Leibniz-Zentrum für Agrarlandschaftsforschung) and University of Potsdam in January '17. From March '21, she works as a senior consultant at PricewaterhouseCoopers (PwC).